J. Bangladesh Acad. Sci. Volume 50, Issue 1, March 2026

ISSN 2224-7270 (Online), 0378-8121 (Print)

Journal of Bangladesh Academy of Sciences is published four times a year (March, June, September and December comprising one volume) in English. Original research articles, review articles, and short communications of all branches of Science and Technology are considered for publication in this journal. Review articles are generally by invitation.

Disclaimer

The opinions, analysis and conclusions expressed or implied in this journal are those of the authors and do not represent the views of Bangladesh Academy of Sciences.

Submission

All correspondence regarding contributions for publication in the journal should be addressed to the *Editor, Journal of Bangladesh Academy of Sciences* <jbas.editor@yahoo.com>. Authors should consult the contributor's guideline at the back of the journal before submitting their manuscripts.

Published by

Bangladesh Academy of Sciences, National Science and Technology Complex, Agargaon, Dhaka-1207.

Design and Printed by

Sucharu Desktop Publishing, 1/E/1, Paribagh, Dhaka-1000, Bangladesh

Annual Subscription: Tk. 500.00 (Bangladesh); US $ 60.00; £ 21.50 plus postage.

Single Copy: Tk. 250.00 (Bangladesh); US $ 30.00; £ 11.25 plus postage.

Obituary

Professor Dr. M. Shamsher Ali (1940–2025)

Professor Dr. M. Shamsher Ali (1940–2025) stands as one of the most towering figures in the scientific and educational backdrop of Bangladesh. Trained as a leading theoretical nuclear physicist, he went beyond the confines of the laboratory to emerge as a visionary academic leader, a pioneer of open education, and an unwavering advocate for the popularization of science. This article explores his early life, his important contributions to nuclear physics, his leadership as the founding Vice-Chancellor of the Bangladesh Open University, and his lifelong mission to harmonize the pursuit of scientific truth with spiritual wisdom.

Introduction

The scientific community of Bangladesh lost one of its brightest personalities with the passing of Professor Dr. M. Shamsher Ali on August 3, 2025. For over six decades, Dr. Ali was synonymous with Physics in Bangladesh. His career was a unique combination of high-level theoretical research and popular science communication. He was not only a rigorous academic who investigated the mysteries of the atomic nucleus but also a charismatic public intellectual who could explain those mysteries to a child. As a founding Vice-Chancellor of two major universities and the President of the Bangladesh Academy of Sciences, he has shaped the nation's educational infrastructure.

Early Life and Academic Brilliance

Professor M. Shamsher Ali was born on November 9, 1940, in Bheramara, Kushtia, located in what was then the Bengal Province of British India. The region of Kushtia was culturally fertile ground. This was the land of Lalon Shah and Rabindranath Tagore, a geography where mysticism and intellect had long connected. Growing up in the twilight of the British Empire, Ali witnessed the shifts of the 1947 partition, which transformed his homeland into East Pakistan. His intellectual promise was evident from his early years. He started his early education with distinction, passing his Matriculation from Jessore Zilla School in 1954 and I. Sc. from Rajshahi Government College in 1956. He then moved to the University of Dhaka, the intellectual hub of the then East Pakistan, where he studied Physics. At that time, the department of physics was still enjoying the long shadow of Satyendra Nath Bose, the theoretical physicist whose collaboration with Einstein had given the world Bose-Einstein statistics. He earned his B.Sc. (Honors) in 1959 and M.Sc. in 1960, with a thesis in nuclear physics. His academic journey continued in the United Kingdom, where he attended the University of Manchester. It was the academic home of Ernest Rutherford, the father of nuclear physics, and was known as a hub for cutting-edge research. Ali arrived in this intense intellectual climate to pursue his doctoral studies. There, he completed a Diploma in Advanced Studies in Science in 1962 and achieved his

Ph.D. in Theoretical Nuclear Physics in 1965. He worked under the supervision of A.R. Bodmer, a distinguished theoretical nuclear physicist. His time in Manchester was the heart of a golden era in nuclear physics research, equipping him with the theoretical tools he would later bring back to his homeland.

Contributions to Theoretical Nuclear Physics

Upon returning to Bangladesh (then East Pakistan), Dr. Ali joined the Atomic Energy Commission (AEC), as a senior scientific officer. In 1970, at the age of 30, he was appointed Director of the Atomic Energy Center, Dhaka (AECD). This period coincided with the most turbulent stage in the nation's history, the 1971 Liberation War. The AECD was a strategic asset, and maintaining its scientific integrity amidst the violence and chaos of the independence struggle was a test of Ali's leadership. Following the independence of Bangladesh, he continued to steer the nation's nuclear research program, serving as Director until 1978 and subsequently as the Chief Scientific Officer of the Bangladesh Atomic Energy Commission (BAEC) from 1975 to 1982. It was during this period that he produced some of his most significant scientific works.

Dr. Ali's research interests were profound and varied. He is best known for his work, 'Ali-Bodmer potential' on the alpha-alpha interaction, a fundamental problem in nuclear physics concerning the forces between alpha particles (helium nuclei). His phenomenological studies in this area provided crucial insights into the structure of light nuclei. Additionally, he made significant developments in the study of hypernuclei - nuclei that contain at least one hyperon (a particle containing a strange quark) in addition to the usual protons and neutrons. His work on lambda-nucleon and lambda-lambda interactions helped expand the understanding of nuclear forces beyond the standard model of nucleonic interactions.

Throughout his career, he has published many research papers in reputed international journals. His work on "Resonating group studies of light nuclei" and "Three-body problems" remains referenced in advanced nuclear physics courses. He was also deeply involved in the International Centre for Theoretical Physics (ICTP) in Trieste, Italy, serving as an Associate and later a Senior Associate, which allowed him to maintain a vibrant connection with the global physics community.

A Visionary Educational Leader

In 1982, Dr. Ali relocated from the Atomic Energy Commission to the University of Dhaka as a Professor of Physics, a role he held until 2006. At the university, he was respected not just for his lectures on Quantum Mechanics and Mathematical Methods, but for his ability to integrate distinct concepts of physics into a unified view.

However, his legacy as an educator extends far beyond the classroom. Dr. Ali was a pioneer in democratizing education in Bangladesh through the Bangladesh Open University (BOU). As the founder Vice-Chancellor of BOU (1992–1996), he commanded the concept of distance learning in a newly independent nation. He understood that traditional brick-and-mortar institutions could not cater to the vast population of Bangladesh. Under his leadership, BOU utilized television, radio, and correspondence to bring education to the doorsteps of the working class, women, and rural populations. Later, he served as the founder Vice-Chancellor of Southeast University (2002–2010), playing a crucial role in the flourishing private university sector, ensuring quality and scientific rigor were maintained in private higher education.

Champion of Popularizing Science

Perhaps Dr. Ali's most beloved role was that of a science communicator. He believed that "science is for everyone," and he spent a lifetime breaking down complex scientific ideas for the public. He delivered over 300 talks on TV and Radio, including appearances on the BBC. His approach was to make science accessible and enjoyable. This philosophy culminated in his book, "Making Math Fun" (2014), which removes the fear

of mathematics from young minds. He also contributed a pivotal chapter titled "Television as a medium of Science Communication" to a Springer publication, highlighting his academic engagement with the very medium he used so effectively.

Whether discussing the Big Bang or the structure of the atom, Dr. Ali had a unique ability to ignite curiosity. He was also deeply interested in the combination of science and religion. Unlike many who view the two as incompatible, Dr. Ali argued for a harmonious coexistence, frequently lecturing on how scientific discovery can be seen as a means of understanding divine creation, a view that resonated deeply in the culturally religious context of Bangladesh.

Awards and Accolades

Dr. Ali's contributions were recognized globally and locally. He was a Fellow of the Bangladesh Academy of Sciences (BAS) since 1978 and served as its President from 2004 to 2012. This role placed him at the apex of the national scientific community. His presidency was marked by an outward-looking strategy. He strengthened Bangladesh's ties with the Inter Academy Partnership (IAP) and the Association of Academies and Societies of Sciences in Asia (AASSA). His international reputation was strengthened by his fellowship at the Third World Academy of Sciences (TWAS) and the Islamic World Academy of Sciences (IAS).

Some of his notable awards include:

- Hari Prasanna Roy Gold Medal (1974): For original contributions to Nuclear Physics.
- Bangladesh Academy of Sciences Gold Medal (1984): In the Physical Sciences (Senior Group).
- Khan Bahadur Ahsanullah Gold Medal (2004).
- Lifetime Achievement Award (2009): By the International Leadership Colloquium in Malaysia for his leadership in higher education.
- TWAS-ROCASA Award (2013): specifically for his work in the "Public Understanding of Science".
- Executive member for Central and South Asia of the TWAS Council (2019–2022)
- Appointed Professor Emeritus at the Bangladesh Open University (2025)

Conclusion

Professor Dr. M. Shamsher Ali was more than a scientist; he was a national institution. He belonged to a generation of nation-builders who used their intellect to lay the foundations of Bangladesh's scientific and educational infrastructure. From the equations of nuclear interactions to the radio signals of national radio, his voice carried the weight of authority and the warmth of a teacher. As Bangladesh continues to modernize its scientific environment, the blueprint left by Dr. Shamsher Ali of open education and public engagement remains its guiding star. August 3, 2025, marked his departure, but his legacy continues to illuminate the classrooms and laboratories he devoted his life to nurturing.

- A.K. M. Akther Hossain

Artificial intelligence was used to assist with writing; the authors reviewed and verified all content.

J. Bangladesh Acad. Sci. 49(2); 157-177: December 2025 DOI: https://doi.org/10.3329/jbas.v49i2.85456

Journal of Bangladesh Academy of Sciences

Journal homepage: http://www.bas.org.bd/publications/jbas.html

Review Article

Arsenic contamination of groundwater and its effects on drinking water, irrigation and public health in Bangladesh

M. Feroze Ahmed*[1] and Tanvir Ahmed[2]

Environmental Engineering Laboratories, BUET, Dhaka, Bangladesh

ARTICLE INFO

Article History

Received: 04 November 2025
Revised: 07 December 2025
Accepted: 09 December 2025

Keywords: Arsenic in drinking water, Arsenic in Agri-environment, Prevalence of arsenicosis, Dose-response relationship and Translocation of Arsenic.

ABSTRACT

Bangladesh is the worst affected country in the world by arsenic contamination of groundwater. The widespread installation of low-cost shallow tubewells, initially intended to control waterborne diseases, has exposed millions to high arsenic concentrations through drinking water. Arsenic (As) in groundwater in the absence of dissolved oxygen is predominantly present as As(III) which is more toxic than As(V). Food, particularly rice, represents another significant pathway of arsenic exposure. Approximately75% of dry-season irrigation relies on groundwater, arsenic accumulation in cropsespecially ricemay substantially contribute to the total body burden in affected areas. The cause, magnitude, and health impacts of arsenic contamination of groundwater have been investigated in many studies. This paper provides an updated synthesis based on available research. The paper also presents a comprehensive analysis of the cause and extent of contamination, andits impacts on drinking water, agro-environment and prevalence of arsenic-related diseases. Arsenic risk management measures implemented in Bangladesh are discussed. The analysis includes estimates of population exposed to varying arsenic concentrations, an assessment of the effects of contaminated irrigation water on soil, paddy plants, and rice grains, and an exploration of the correlation between average drinking water arsenic contents at the Upazila (sub-district) level and the prevalence of arsenic-induced skin lesions in that Upazila..

Introduction

Arsenic is a ubiquitous element, naturally present in the Earth's crust, and biosphere. It is the 20th most abundant element in the Earth's crust and the 12th in the biosphere, and its environmental cycling is governed by both natural processes and anthropogenic activities (Ahmed, 2003). The Department of Public Health Engineering (DPHE), with international support, undertook a massive campaign in the late 1970s and early 1980s to control waterborne diseases such as cholera, typhoid, and dysentery by providing pathogen-free drinking water. Installation of shallow tube wells (STWs) to withdraw groundwater was promoted under this campaign, which is naturally filtered and free of microbial pathogens. The program successfully achieved its immediate goal. An estimated 10 million tube wells were installed in rural Bangladesh (Zahid, 2018), providing what was believed to be safe water to approximately 97% of the rural population, the highest coverage in the region (Ahmed, 2002). However, the potential for elevated arsenic concentrations in groundwater was not anticipated during this expansion of the drinking water supply.

*Corresponding author:<ferozeahmed45@gmail.com>

[1]*Emeritus Professor, Stamford University Bangladesh, Dhaka, Bangladesh*

[2]*Professor, Department of Civil Engineering, Bangladesh University of Engineering & Technology (BUET)*

Subsequent detection of arsenic contamination in many shallow aquifers rendered shallow tube well water unsafe for drinking purposes. The problem is further exacerbated by considerable spatial variability in arsenic concentrations, which vary significantly even within small geographic areas. Bangladesh, situated in the Bengal Basin, became the most severely affected country in terms of population exposure to arsenic.

The problem began to unfold when arsenic contamination was first detected in 1983, but it took nearly a decade to be recognized as a "large-scale public health crisis" (Nordstrom, 2000). The World Health Organization (WHO) declared it the "largest mass poisoning of a population in history" in the late 1990s. This widespread arsenic exposure directly challenged the public health success story of the STW program (Caldwell et al., 2003). Within a few years, the arsenic crisis overshadowed the earlier achievements, thrusting the nation into a desperate nationwide mitigation effort, documented extensively in the national and international literature (Ahmed, 2002; Milon et al., 2012; Sakamoto, 2021).

The nationwide testing revealed that about one-fourth of all shallow tube wells in the country exceeded the national standard of 50 µg/L for arsenic. The test result indicated that the arsenic content of tube wells varied with depth and short horizontal distances. Bangladesh, in terms of population exposure, becomes the most severely affected country in the world.

Arsenic in groundwater is of geological origin, and it has been accepted that arsenic is being dissolute in water from sediment under certain conditions. Arsenic is found in the soils of Bangladesh in concentrations like those in many countries. The average concentration in soils in arsenic affected areas has been found to be approximately 100 times higher than the acceptable concentration in water. The transfer of arsenic from soil to groundwater and vice-versa is dependent on soil-water interaction in the subsoil environment. A clear understanding of origin and mechanism of dissolution of arsenic from soil to water is necessary for mitigation.

The importance of groundwater irrigation increased with the introduction of HYV seeds in the late 1960s to meet the food demand of a growing population (Zahid, 2018). Arsenic contaminated water in the shallow aquifer can be easily abstracted for irrigation by installing of low-cost shallow tube wells. As a result, most irrigation tube wells are shallow and contain higher arsenic concentrations in arsenic-affected areas. In the absence of surface water during the dry season, the future expansion of irrigation depends even more on groundwater. Arsenic withdrawn with groundwater can build up in soil and translocate into irrigated crops. Arsenic intake through food is equally important as arsenic ingestion through drinking water, except that a part of the arsenic intake through food is organic in nature. Arsenic ingestion through both food and water increases the body burden to cause arsenic-related diseases. Phytotoxicity from high concentrations of arsenic in soil and irrigation water, and its long-term impact on crop yield is another primary concern for food security in Bangladesh.

Mechanism of Arsenic Contamination of Groundwater

Many hypotheses have been initially proposed to explain the possible causes of arsenic contamination in Bangladesh. Still, most scientists have settled on oxidation and reduction hypotheses in the absence of adequate evidence for other hypotheses. The most important ores of arsenic are arsenic pyrites, realgar, and orpiment (Yan-Chu, 2004). Mok and Wai (1994) reported arsenic release from these minerals in groundwater by oxidation as shown in the following equations:

$$4\ FeAsS + 13O_2 + 6H_2O \rightarrow 4FeSO_4 + 4H_3AsO_4 \quad (1)$$

$$As_2S_3 + 7\ O_2 + 6\ H_2O = 3H_2SO_4 + 2H_3AsO_4 \quad (2)$$

$$4AsS + 11O_2 + 10H_2O = 4H_2SO_4 + 4H_3AsO_4 \quad (3)$$

In this process, seasonal water-level fluctuations or water-table lowering due to large-scale groundwater withdrawal may expose the aquifer to aeration-induced oxidation. Soils may also be oxidized by infiltration of water saturated with dissolved oxygen.

The intensity of the arsenic problem has not been found to be related to groundwater fluctuations. Similarly, the hot spots in Bangladesh are not located in areas with high groundwater withdrawal for irrigation (Ahmed 2007a and 2007b). A very low sulfate concentration in groundwater is also inconsistent with the pyrite oxidation hypothesis (BGS, DPHE, and MML, 1999; Bhattacharya et al., 1999). The traces of arsenopyrite or arsenic sulfides found in sediments might have formed under conditions of enhanced reduction. Hence, the hypothesis of arsenic release from the oxidation of the top soil layer is not considered a primary mechanism of groundwater contamination in Bangladesh.

According to the reduction hypothesis, arsenic can be mobilized from soil in a reducing environment. In the reducing zone at low redox potential, insoluble ferric iron is partially reduced to soluble ferrous iron, and similarly, manganese is partially reduced to the soluble manganous state. Adsorbed arsenic on dissolution of the minerals is released into pore water. Thus, the reduction and subsequent dissolution of iron, manganese, and other minerals that contribute to the sorption and retention of arsenic can provide a mechanism for arsenic contamination of groundwater. The reduction process also converts precipitated and adsorbed As(V) into more soluble As(III), as shown in the following equation:

$$H_2AsO_4^- + 3\,H^+ + 2\,e^- \rightarrow H_3AsO_3 + H_2O \qquad 4$$

In reducing soil environments, arsenic will predominate in pore water, as As(III). Further reduction of As(III) in the presence of sulfides as reported by Mok and Wai (1994), will immobilize arsenic in soils with the formation of arsenic sulfide precipitates:

$$2\,H_3AsO_3 + 6\,H^+ + 3\,S^{2-} \rightarrow As_2S_3 + 6\,H_2O \qquad 5$$

$$2\,As_2S_3 + 4\,e^- \rightarrow 4\,AsS + 2\,S^{2-} \qquad 6$$

Arsenic from orpiment (As_2S_3) and realgar (AsS) can also be released in water by oxidation, as shown in Equations [2] and [3].

It is generally accepted that arsenic in groundwater is of natural origin and is believed to be released under conditions conducive to the dissolution of arsenic from the solid phase on soil grains into the liquid phase of groundwater. Arsenic occurs in soils at an average concentration of about 5 to 6 mg/l (Bhumbla and Keefer, 1994), but mean arsenic contents in soils as high as 20 ppm in Italy, 14 ppm in Mexico, 11.2 ppm in China, and 11 ppm in Japan have been reported (Yan-Chu, 2004). The average arsenic concentrations in alluvial sand and mud/clay have been reported as 2.9 mg/kg and 6.5 mg/kg, respectively, in Bangladesh (BGS and DPHE, 2001). The presence of high arsenic concentrations in groundwater is not generally dependent on soil arsenic levels. The geochemical and environmental conditions of the soil have a greater influence on arsenic speciation, solubility, and mobility.

The solubility of arsenic in water is usually controlled by redox conditions, pH, biological activity, and reductive dissolution reactions. As(V) is the major arsenic species under oxidative conditions at high Eh values and under reducing conditions at low Eh values, it converts arsenic into a more mobile As(III) form. Arsenic in soil is relatively stable at neutral pH, but exhibits mobility at both higher and lower pH values. Metal ions solubilize at lower pH values from the sediments with concurrent release of arsenic species. The increased hydroxide concentrations at high pH levels displace arsenic species from their binding sites (Mok and Wai, 1994). Desorption of arsenic can also be promoted in the presence of more competing anions, such as phosphate.

The most severely flooded areas are mainly arsenic-contaminated areas of Bangladesh (Ahmed 2000). Reducing the soil environment in most severely flooded areas appears to promote the release of arsenic into groundwater. In these areas, the soils are characterized by paludal deposits of clay, silt and peat and alluvial deposits of silt, and silty clay. The luxuriant vegetation in nutrient-rich floodplains enriches fine-grained soils with organic debris. The anaerobic condition in soils in deeply flooded wetlands is characterized by a gray to blackish color

and the release of methane gas. The dissolved oxygen available in infiltrated floodwater is exhausted in the topsoil, which in rich in biodegradable organic matter. Pore water devoid of dissolved oxygen creates a reducing environment that favors the dissolution of both iron and arsenic (Ahmed 2000).

Rahman and Rahman (1998) collected sediment samples from different arsenic-prone areas, mainly lying in the lower Gangetic plain, and found arsenic-rich iron oxide coatings of varying thickness on sand grains. They concluded that adsorption of arsenic on iron oxide might have occurred during transportation of sand and arsenic-bearing mineral grains by flowing water in open channels. British Geological Survey (BGS), Department of Public Health Engineering (DPHE), Bangladesh, and Mott MacDonald Limited (MML), considered the reductive desorption and dissolution of arsenic adsorbed onto iron oxyhydroxides in recent sediments to be the most probable mechanism of arsenic mobilization in groundwater (BGS, DPHE, and MML, 1999). Moreover, mineralogical examination suggested that the small amount of pyrite present in the sediments had been precipitated since burial.

Bhattacharya et al. (1999) stated that during groundwater development, the flow of reducing groundwater through the aquifers resulted in the dissociation of ferric hydroxides, released the bulk of the arsenic due to the reductive dissolution of ferric oxyhydroxides and the arsenic previously adsorbed onto these minerals. The traces of arsenopyrite or arsenic sulfides found in sediments might have been formed under an enhanced reducing environment, as shown in Equations 5 and 6. Ravenscroft et al (2000) concluded that neither pyrite oxidation nor competitive exchange of fertilizer-phosphate for sorbed arsenic caused arsenic pollution of groundwater in the Bengal basin. Indeed, pyrite in Bangladesh's aquifers is a sink, not a source, of arsenic. Arsenic pollution occurs when FeOOH is microbially reduced, releasing the arsenic it sorbs to groundwater.

Reductive dissolution of iron oxyhydroxides by anaerobic microorganisms has been recognized as a key process governing arsenic mobilization under reducing environments (Ahmann et al., 1997; McCreadie et al., 2000). The arsenic present in these aquifers is thought to have originated from multiple source areas in the upper catchments of the Ganges, Brahmaputra, and Meghna rivers and to have been transported downstream, adsorbed onto colloidal iron oxyhydroxides (Ravenscroft et al., 2005).

In the Bengal Basin of Bangladesh and West Bengal (India), the primary mechanism of groundwater arsenic pollution is the reductive dissolution of iron oxyhydroxides (FeOOH), which releases sorbed arsenic into groundwater (Ahmed, 2007; Nickson et al., 1998; McArthur, 1999; Ravenscroft et al., 2001; Ravenscroft and Ahmed, 2005). Arsenic mobilization occurs under iron-reducing conditions in shallow aquifers (<35 m depth), that are predominantly Holocene in age, where microbial processes drive reduction reactions. The groundwater in these aquifers typically has high concentrations of both arsenic and iron. The sediments of these aquifers are characteristically dark in color, reflecting strongly reducing conditions. The microbial biodegradation of organic matter, mediated by anaerobic iron-reducing bacteria (FeRB) such as *Geobacter* species, facilitates the dissolution of FeOOH and the concomitant release of arsenic (Anawar et al., 2011).

In contrast, oxic to sub-oxic aquifers, which generally correspond to older Pleistocene deposits, produce groundwater with low arsenic concentrations (Ravenscroft and Ahmed, 2005).Arsenic remains mobile under sulfate-reducing conditions, suggesting that authigenic sulfide precipitation is not a significant sink for arsenic in these groundwaters (Zheng et al., 2004). The combined geochemical and microbial evidence supportsthat microbially mediated reductive dissolution of iron oxyhydroxides is the dominant process governing arsenic release in the Bengal Basin aquifers. Chowdhury et al. (2003) confirmed that arsenic was initially transported to the Bengal Basin with sediments from the Ganges,

Brahmaputra, and Meghna (GBM) river systems and subsequently deposited in the basin.

A joint study by the Bangladesh University of Engineering and Technology (BUET), the Massachusetts Institute of Technology (MIT), and the University of Cincinnati (UC) exhibited that arsenic release in aquifers is triggered by the introduction of organic carbon, which serves as a food source for bacteria (Harvey et al, 2002). Evidence of this process includes the presence of methane in groundwater, indicating that anaerobic bacteria are metabolizing organic matter. The resulting anaerobic conditions create a reducing environment that favors arsenic mobilization. This anoxic state, characterized by the absence of dissolved oxygen and very low redox potential, has been confirmed through careful groundwater sampling and field measurement.

The BUET-MIT-UC study observed a positive correlation between arsenic and ammonia and a negative correlation between arsenic and sulfate. These observations are consistent with the mobilization of arsenic through the anoxic degradation of organic matter, rather than the oxidation of sulfide minerals (Harvey et al, 2002). They also indicated that irrigation pumping may facilitate the rapid transport of dissolved organic carbon in the aquifers, thereby triggering anaerobic biochemical reactions. The concept of microbial reductive dissolution of arsenicis further supported by the works of Akai et al. (2001). Their culture experiments using sediments from Bangladesh and Japanese lakes (Sagata and Matarese) showed arsenic elution following a rapid drop in Eh values. This drop was induced by increased bacterial activity after the addition of nutrients (glucose and polypeptone). These experimental results provide findings under reducing conditions created by microbial breakdown of organic matter in aquifers.

Analysis of hydrology, hydrogeology, and soil characteristics of Bangladesh, combined with the distribution and intensity of arsenic contamination, supports the following conceptual model for the origin, transport, deposition, and mobilization of arsenic in Bangladesh:

Origin of Arsenic –The origin of arsenic is arsenic-rich minerals in the upstream basins of the Ganges, Brahmaputra, and Meghna Rivers. Weathering and oxidative processes release arsenic into the river water. The high-energy induced turbulent flow in the upstream reaches saturates the water with oxygen, promoting the oxidation of both arsenic species and suspended sediments. Consequently, arsenic is adsorbed onto suspended particles that are rich in oxidized iron, aluminum, manganese, and other ions.

Transportation - In the middle reaches of the rivers, the arsenic-contaminated suspended sediments are transported downstream. The river velocity at this stage remains too high for significant sediment deposition, though occasional deposition of coarse sand may occur. Due to its relatively small surface area and fewer active sites per unit volume, this sand does not adsorb significant amounts of arsenic. Sediments transported by the Ganges-Brahmaputra-Meghna river system carry arsenic concentrations ranging from 1.002–2.983 mg/kg in sand, 1.858–3.943 mg/kg in silt, and 3.525–6.476 mg/kg in clay, leaving the river water almost free of dissolved arsenic (Chowdhury et al., 2003).

Deposition in Bangladesh –The slope of the rivers is flatter in the lower reaches of Bangladesh. Seasonal floods submerge one-third to one-half of the country each year, depending on their intensity. As water spreads into low-lying floodplains, the water becomes nearly stagnant. This allows arsenic-rich fine-grained silt and clay particles to settle out of suspension. These deposited fine-grained arsenic-rich sediments constitute the primary source of arsenic in Bangladesh.

Mobilization - The aquatic weeds and agricultural residues in nutrient-rich floodplains, mixed with or submerged in sediment, finally decompose an aerobically. A large quantity of organic matter submerged under floodplain sediments forms peat. Anaerobic decay of organic matter in submerged soils creates reducing and low redox conditions, mobilizing arsenic from sediments into groundwater.

Magnitude of the Arsenic Problem in Bangladesh

The World Health Organization Guideline Value (WHO GV) for non-threshold chemicals, such as toxic and carcinogenic substances like arsenic, represents the concentration corresponding to an upper-bound estimate of an excess lifetime cancer risk of 10^{-5}, i.e., one additional cancer case per 100,000 people. The WHO GV is based on 60 kg adult person, drinking 2 liters of water per day, for a lifetime of 70 years. The WHO provisional Guideline Value (WHO GV) of 0.01 mg/L for arsenic in drinking water has been adopted as the national standard in many countries. In comparison, many other countries, including Bangladesh, have retained the earlier WHO Guideline Value of 0.05 mg/L as the national standard or interim target, with the intention of lowering the arsenic standard for drinking water in the future (Ahmed, 2007c).

The disease burdens for arsenic exposure from drinking water, even complying with the WHO GV and Bangladesh Standard (BDS), are comparatively higher (Ahmed et al. 2006b) than the WHO reference disease burden of 1μ DALY per person per year (WHO, 2011). The joint FAO/WHO experts committee on food additives (JECFA) in 1983 derived a value of 0.013 mg/L assuming a 20% allocation to drinking water based on provisional maximum tolerable daily intake (PMTDI) of inorganic arsenic of 0.002 mg/kg of body weight and confirmed as a provisional tolerable weekly intake (PTWI) of 0.015 mg/kg of body weigh in 1988 (FAO/WHO, 1989)

An extensive study on arsenic contamination in Bangladesh was conducted by the British Geological Survey (BGS), the Department of Public Health Engineering (DPHE), and Mott MacDonald Limited (MML) in two phases. The project examined 3534 distributed water samples from 61 districts (excluding 3 hill districts) in an approximate 6x6 km grid. (DPHE, BGS, and MML, 1999; BGS and DPHE, 2001). On average, 58 samples per district and 8 samples per upazila were analyzed. Although the sample size is small, considering the variation in arsenic content over short distances, the study provided a reasonable distribution of arsenic contamination in Bangladesh. The study showed that when shallow tubewells are considered, arsenic concentrations of 46% and 27% exceeded the WHO guideline value of 10μg/L and the Bangladesh Standard of 50μg/L, respectively. In case of deep tubewell samples (>150m depth), arsenic content of only 5% exceeded 10 μg/L and 1% exceeded 50μg/L, indicating that deeper tubewells provide safer drinking water.

Since the variation in arsenic levels in tubewells over short distances is unpredictable, the Government of Bangladesh, in collaboration with partner organizations, implemented a National Screening Program. This program aimed to screen all tubewells in the affected Upazilas identified by the BGS–DPHE study, to delineate contaminated tubewells and identify individuals with arsenic-related skin lesions.

Table 1. Level of Arsenic Contamination in Bangladesh (BAMWSP, 2001).

Percent TW>50 μg/L	Category	Districts	Upazilas	Union	Villages
< = 5 μg/L	Low Risk	7	35	668	22,544
> 5 – 40 μg/L	Moderate Risk	31	145	1,176	14,788
> 40 – 80 μg/L	High Risk	15	65	621	8,331
> 80 – 100 μg/L	Very High Risk	1	23	416	8,378
Total Screened		54	268	2,881	54,041

The National Arsenic Mitigation Information Centre (NAMIC), established under the Bangladesh Arsenic Mitigation Water Supply Project (BAMWSP), compiled the screening results and made the data available to support targeted mitigation efforts. A total of 4.95 million tubewells in arsenic-affected areas were screened, and 1.44 million (29%) were found to be contaminated with arsenic greater than 50 µg/L. The levels of arsenic contamination reported by the National Screening Program are summarized in Table 1(BAMWSP, 2001).

Population Exposure

The population exposed to arsenic concentrations exceeding specific thresholds was estimated by considering the area-wise distribution of shallow tubewells, the percentage of those tubewells exceeding the given concentration, and the population density. Data were compiled from multiple sources, including BGS and DPHE (2001), BAMWSP (2001), DPHE (2000), and BBS (2001). The total exposed population was calculated as the sum of the products of the population in each area and the fraction of contaminated tubewells within that area. Assuming that both contaminated and uncontaminated tubewells were used by an equal number of people within a given geographical unit. The estimated population exposed to various levels of arsenic in drinking water from tubewells is presented in Fig. 1. This estimate showed that 29 million people in Bangladesh in 2001 were exposed to drinking water containing arsenic concentrations exceeding the national standard of 50 µg/L, and 46 million exceed the WHO provisional guideline value of 10 µg/L.

The BGS-DPHE studies finally gave two estimates of population exposure based on a projected population of 125.5 million in 1999 (BGS and DPHE, 2001). The estimates of total population exposed to arsenic concentrations above 50 and 10 µg/L using the kriging method were 35.2 million and 56.7 million, respectively. Based on upazila statistics, the exposure levels to arsenic exceeding 50 and 10 µg/L were 28.1 million and 46.4 million, respectively. School of Environmental Studies, Jadavpur University (SOES, JU), Calcutta, and Dhaka Community Hospital (DCH), Dhaka, estimated that the populations exposed to above 10 µg/L and 50 µg/L in 43 districts of Bangladesh were 51 million and 25 million, respectively (SOES and DCH, 2000).

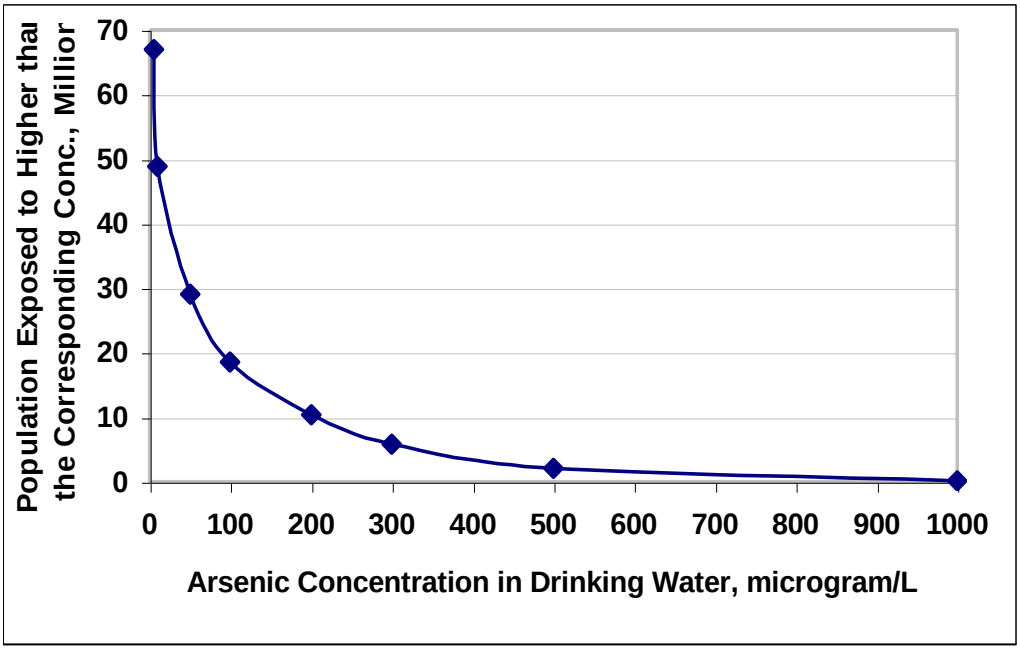

Fig. 1. Population exposed to different levels of arsenic in drinking water.

Arsenic in Agro-environment

Arsenic in Irrigation Water

Arsenic-contaminated water from shallow aquifers is extensively used for irrigation in the dry season in Bangladesh. Dry-season irrigation is needed to increase cropping intensity and produce more food. The percentages of shallow tube well (STW) producing water with arsenic content exceeding the Bangladesh standard of 50 µg/L and the WHO Guideline value of 10 µg/L, and intensity of STW-based irrigation in 8 hydrological regions of Bangladesh are shown in Fig. 2 (WARPO,2001).

The intensity of irrigation using STW is highest (50%) in the northwest region, and fortunately, very few tube wells are contaminated with arsenic there. But groundwater used for irrigation in the southeast regions is significantly elevated, and it is highly contaminated with arsenic. Groundwater-based irrigation in Southcentral, Southeast, and hilly regions is very low. However, the use of groundwater for irrigation in arsenic-contaminated regions will increase in the future for growing more crops to meet the growing demand for food.

Irrigation tube wells operate seasonally for 3-4 months' and a considerable amount of arsenic is withdrawn with groundwater and spread over irrigated land. The highest concentration of arsenic is found around water distribution channels on irrigated lands. Rice crops require about 1000 mm of water, and a concentration of 100 µg/L of arsenic in irrigation water can contribute about 1 kg of arsenic per hectare of irrigated land in each season. If all irrigation wells operate at full capacity, over 900 metric tons of arsenic could recycle each year through irrigation water (Ali et al., 2003a).

Arsenic builds up in the topsoil when irrigated with arsenic-contaminated water, and studies show that the concentration may reach a critical level to affect crop productivity. The results of limited experiments on rice grown with arsenic-contaminated soil and water in pots have demonstrated a decline in yield and accumulation of arsenic in rice grains, as well as high concentrations of arsenic in soils and water (Heikens, 2006).

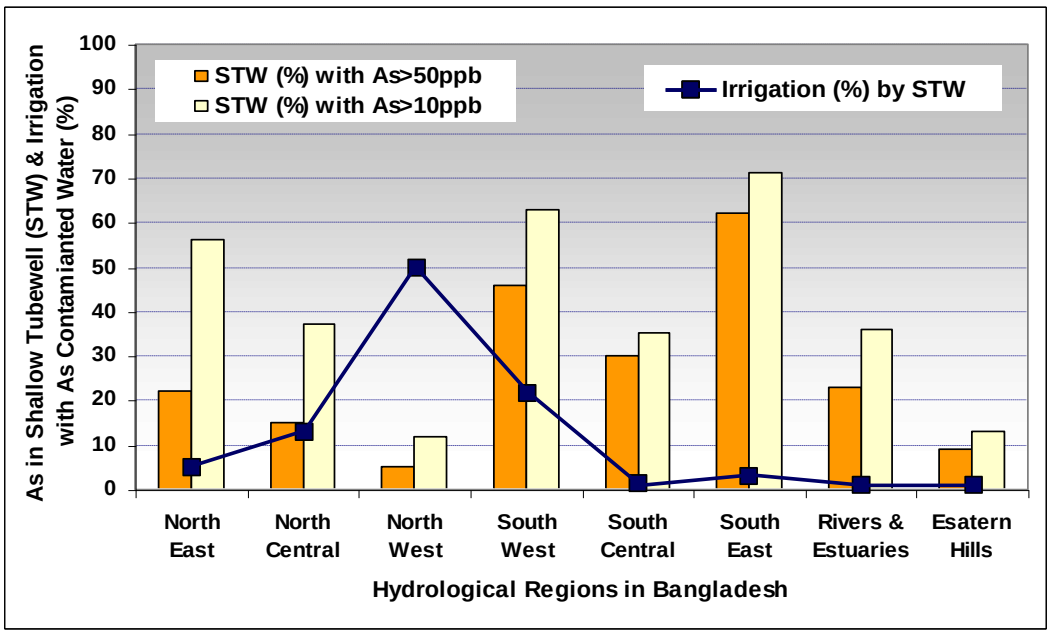

Fig. 2. Irrigation with arsenic contaminated water in Bangladesh.

Arsenic in Soil

Arsenic is a naturally occurring element in soil worldwide. The global average soil arsenic concentration ranges from 5 to 6 mg/kg. In Bangladesh, concentrations vary by soil type, averaging 2.9 mg/kg in alluvial sand and 6.5 mg/kg in mud/clay (DPHE and BGS, 2001). Irrigation dynamics significantly influence soil arsenic levels. As irrigation water evaporates, transpires, or percolates, the arsenic it carries is primarily adsorbed by soil grains containing iron, manganese, and aluminum oxides. Consequently, soil arsenic levels correlate strongly with the arsenic content of irrigation water. However, under certain conditions, this process can reverse, with arsenic dissolving from the solid phase back into the groundwater. Meharg and Rahman (2003) recorded concentrations up to 46 mg/kg in affected areas, compared to less than 10 mg/kg in areas with low-arsenic water. Localized studies have reported even higher levels, such as 51 mg/kg in Faridpur and 83 mg/kg in Comilla (Ullah, 1998). The critical threshold for arsenic in soil is variable, ranging from 21 mg/kg to 51 mg/kg depending on soil type. However, a general acceptable level is considered to be 20 mg/kg (BARI, 2007, citing Yan-Chu, 1994; Wauchope, 1983).

In Bangladesh, irrigation with arsenic-contaminated water results in significant accumulation of arsenic in the soil profile, with the highest concentrations in the top layer. Research indicates a sharply declining gradient with depth. An estimated 90% of the arsenic introduced via irrigation accumulates in the upper 450 mm of soil, with the top 75 mm layer alone retaining approximately 71% of the total (Saha, 2006). At the end of the irrigation season, the average arsenic concentration in this top layer (0-75 mm) was 14.8 mg/kg in arsenic-affected areas, compared to only 1.5 to 3.1 mg/kg in unaffected regions.

The arsenic content of soil during the post-irrigation period decreases significantly, likely due to leaching by monsoon rains, flood water, and microbial methylation processes. Roberts et al. (2010) estimated that between 52 and 250 mg m^{-2} of soil arsenic is released into floodwater during the monsoon season, corresponding to a loss of 13-62% of arsenic added to soil through irrigation each year. The potential for arsenic loss through volatilization—conversion to gaseous forms by arsenic-methylating bacteria—has been quantified. Natural biological gasification rates across Bangladesh range from 0.0003 to 0.014 µg As/kg/day, which can increase to 0.017- 0.679 µg As/kg/day under optimal conditions (Islam et al., 2007). However, in soils with poor drainage and low leaching potential, arsenic can accumulate over time, reaching critical levels that threaten crop productivity.

Excessive soil arsenic accumulation significantly affects rice production, a major concern for food security in Bangladesh. As illustrated in Fig. 3, data from Faridpur shows a negative correlation between soil arsenic and productivity (Panaullah et al., 2009).

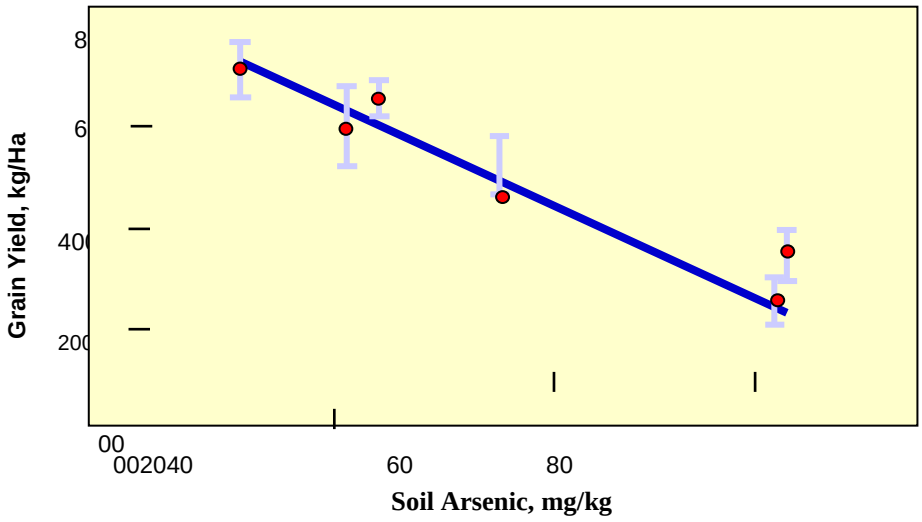

Fig. 3. Loss of Rice Productivity in Arsenic Contaminated Soil.

Arsenic in Paddy Plants

Ali et al. (2003b) found that high arsenic in water resulted in higher concentrations of arsenic in root, stem, and leaf of rice plants, and arsenic in rice grain positively correlated with arsenic in different parts of the rice plant. Saha (2006) established correlations between arsenic concentrations in the top 75 mm of agricultural soil and various parts of the paddy plant, based on approximately 85 samples from across Bangladesh. The study quantified the translocation of arsenic from soil to the root, stem, leaf, and grain, as illustrated in Figs.4 to 8.

The results indicate a strong gradient within the plant. Arsenic concentrations were highest in the roots and decreased progressively through the stem, leaves, and husk. Translocation into the edible rice grain was minimal. Furthermore, arsenic levels in the roots, stems, and leaves demonstrated a strong to moderate correlation with topsoil arsenic concentrations. In contrast, the correlation between arsenic in rice grains and the topsoil was poor, as shown in Fig.7. van Geen et al. (2006), by comparing several rice paddies from Bangladesh, including a control site, have shown that arsenic supplied with irrigation water accumulates in soil and soil-water but much less in rice grain. The observations suggest that exposure of the Bangladesh population to arsenic contained in rice is less of an immediate concern than the continued use of groundwater containing elevated arsenic levels for drinking and cooking.

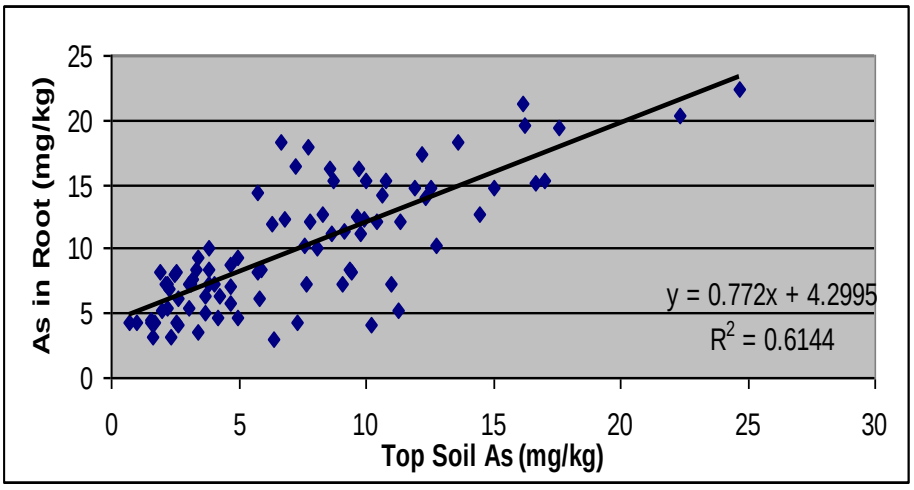

Fig. 4. Relation between As in topsoil & root.

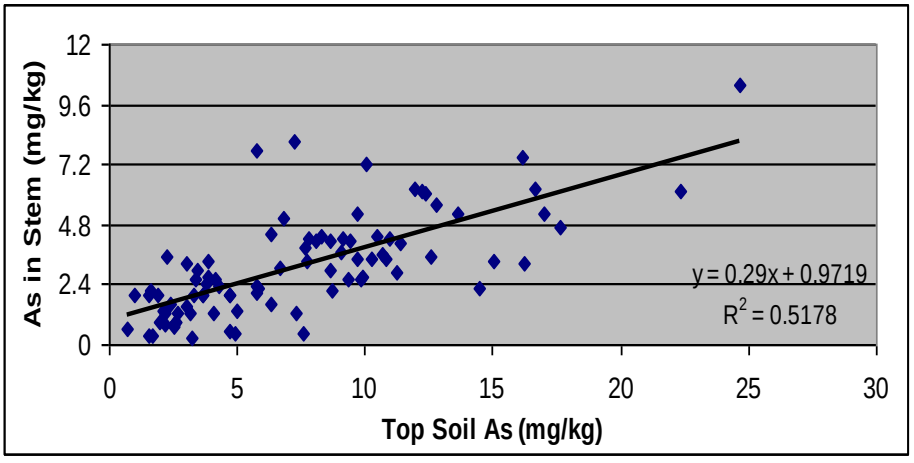

Fig. 5. Relation between As in topsoil & stem.

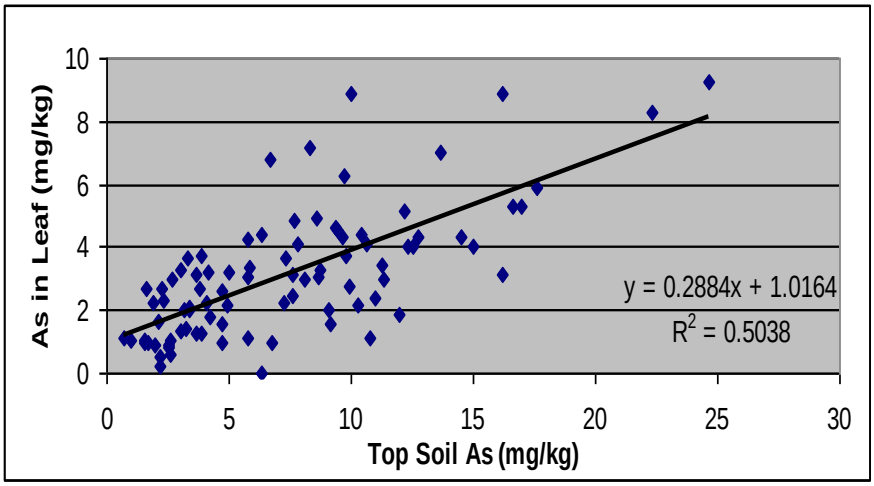

Fig. 6. Relation between As in topsoil & leaf.

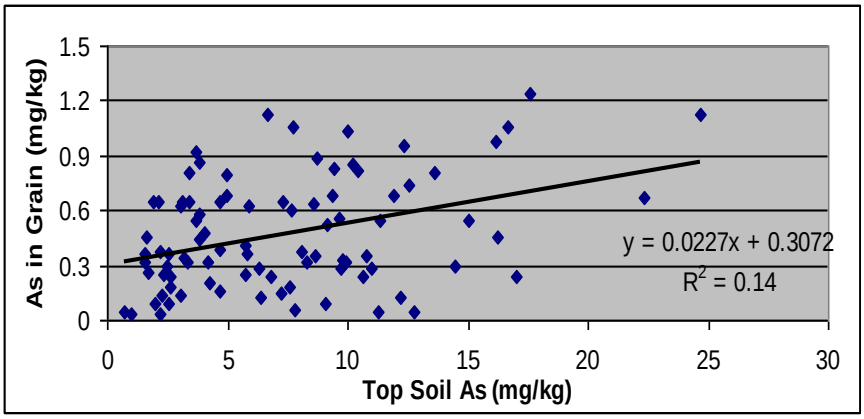

Fig. 7. Relation between As in topsoil & grains.

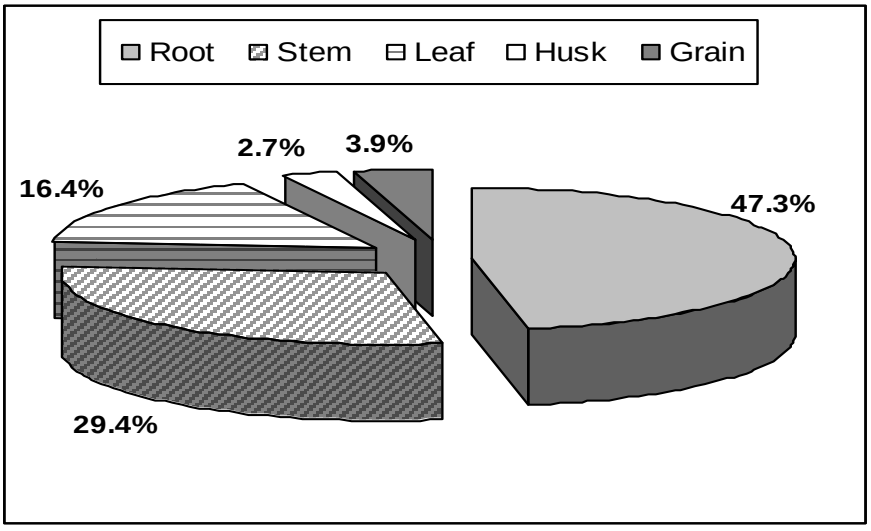

Fig. 8. Arsenic accumulation in different parts of paddy plants in Bangladesh.

Saha (2006) also determined the distribution of arsenic within paddy plants. In a HYV short-stem rice plant, 93.4% of the total arsenic accumulated in the roots, stems, and leaves, leaving only 6.6% in the husk and grains combined (Fig. 7).

A study comparing rice from arsenic-contaminated and uncontaminated regions of Bangladesh found median arsenic concentration of 0.25 ppm and 0.1 ppm, respectively (Hironaka and Ahmad, 2003). Despite levels in contaminated areas being 2.5 times higher, the average arsenic content of Bangladeshi rice was comparable to that of Japanese rice. Subsequent research has established clear links between environmental arsenic and rice grain content. Williams et al. (2006) collected 330 rice samples nationwide and found the highest arsenic levels in the southwestern region. The authors also found a positive correlation between arsenic in irrigation water and rice, noting a stronger relationship for Boro rice grown in the dry season with intensive irrigation than for Aman rice. A similar positive correlation between arsenic in rice and soil was observed by Meharg and Rahman (2003). Empirical data from Duxbury et al. (2003) recorded a wide range of arsenic in Bangladeshi rice, from 10 to 420 µg/kg. The mean concentration in Boro rice was 1.5 times higher than in Aman rice. However, the variation in rice arsenic concentrations was only partially consistent with the spatial pattern of arsenic in drinking water tube wells.

Arsenic Speciation in Rice and Food Safety

Arsenic in foods is present in both inorganic and organic forms. Inorganic arsenic is more toxic than organic arsenic present in food. The chemical form, or speciation, of arsenic in Bangladeshi rice is a critical determinant of its toxicity. Misbahuddin et al. (2007) analyzed rice samples and found the mean concentrations of inorganic arsenic, monomethyl arsenic acid (MMA), and dimethyl arsenic acid (DMA) to be 296.3 µg/kg (33.6%), 222.5 µg/kg (25.2%), and 363.4 µg/kg (41.2%), respectively. Williams et al. (2005) found that inorganic arsenic accounted for about 80% of the total arsenic in Bangladeshi rice, a proportion nearly double that found in U.S. rice (42%). It is a great concern because rice is the staple food in Bangladesh.

The high proportion of inorganic arsenic in Bangladeshi rice may pose a significant food safety risk. Australia's Maximum Permissible Concentration (MPC) for total arsenic in food is 1 mg/kg, but seafood, where arsenic is predominantly organic, the limit is 5 mg/kg. China's food safety standard specifically limits inorganic arsenic in rice to 0.15 mg/kg (Heikens, 2006). Given the high daily rice consumption in Bangladesh, dietary intake of inorganic arsenic is consequently elevated. Therefore, while the total arsenic content in Bangladeshi rice may not appear exceptionally high, its contribution to the total body burden is significant given the prevalence of more toxic inorganic species. Poor translocation of arsenic in rice grain generally leads to a belief that the productivity of rice will be affected before reaching a high level of arsenic in rice grain. If the productivity is affected by high levels of arsenic in irrigation water, it will be equally disastrous for Bangladesh, which depends mostly on rice for food security.

Estimation of Risk and Prevalence of Arsenicosis

Arsenic is naturally found in the atmosphere (0.4–30 ng/m³), food (0.4–120 µg/kg), and water (from undetectable to 12,000 µg/L). Consequently, the global population is routinely exposed to low background levels. While arsenic is considered essential for some animal species, it is non-essential, toxic and carcinogenic to humans. As a known carcinogen and toxin, the ingestion of any amount of arsenic constitutes a potential health risk (Ahmed, 2007b).

Dose-Response Models and Health Effects

Chronic arsenic exposure is associated with a range of symptoms, including melanosis (hyperpigmentation, depigmentation), keratosis, gangrene, peripheral vascular disorders, skin cancer, and various internal cancers. In Bangladesh, skin lesions are the most

commonly manifested symptom. Quantifying the relationship between arsenic ingestion and health effects remains challenging. The U.S. Environmental Protection Agency (USEPA) used a multistsge model in its 1988 assessment, based on epidemiological data from Taiwan. This model estimated that arsenic concentrations in drinking water associated with excess lifetime skin cancer risks of 10^{-4}, 10^{-5}, and 10^{-6} are 1.7 µg/L, 0.17 µg/L, and 0.017 µg/L, respectively. This indicates an approximately linear dose-response relationship at low doses.

Using this linear relationship, the number of additional skin cancer cases (N) can be estimated for a population (P) exposed to a given arsenic concentration (C) with the following equation:

$$N = 5.882 \times 10^{-5} CP \quad (7)$$

It is important to note that these estimates are conservative and may overestimate the actual incidence of skin cancer. At the time of the assessment, data were insufficient to quantitatively define an exposure-response relationship for internal cancers (USEPA, 1988).

Yu et al. (2003) developed dose-response functions for arsenic-induced non-carcinogenic skin lesions in Bangladesh. Using age-adjusted data from a survey by Mazumder et al. (1998) in West Bengal, India, they established quadratic-exponential models of the form:

$$p(c)_{(male/female)} = 1 - exp(-(q_1 c + q_2 c^2)) \quad (8)$$

where $p(c)$ is the prevalence of a specific type of non-carcinogenic arsenicosis within a gender group, c is the arsenic concentration in drinking water (µg/L), q_1 and q_2 are non-negative parameters derived from the survey data. Based on this approach, Ahmed (2007d) developed similar dose-response functions for skin lesions using patient data from 14 Upazilas in Bangladesh. This dataset was compiled by Dhaka Community Hospital through collaborative studies with organizations including BAMWSP, SOES, and UNICEF.

Ahmed et al. (2006b) developed an integrated model for the quantitative health risk assessment of drinking water contaminants. This model takes two primary inputs: Arsenic concentration (µg/L) and Microbial concentration (as TTC or *E. coli* per 100 ml). The output is the total disease burden, quantified in Disability-Adjusted Life Years (DALYs), attributable to arsenic-induced cancers of the skin, lung, and bladder.

The practical difficulty of reliably measuring arsenic at the 0.17 µg/L level (corresponding to a 10^{-5} risk, or ~1 µDALY per person per year) led the World Health Organization (WHO) in 1993 to set a provisional guideline value of 10 µg/L. This concentration is associated with a lifetime excess skin cancer risk of approximately 6 in 10,000 people (WHO, 1993). In contrast, the Bangladesh standard of 50 µg/L, when applied to the same linear model (Equation [7]), is associated with a significantly higher lifetime skin cancer risk of about 29 in 10,000 people.

Empirical Model Based on National Screening Data in Bangladesh

The empirical model is developed based on the relationship between the average arsenic content of tubewells in an Upazila and the number of cases having arsenic-related diseases in that Upazila. A national screening program was conducted from 2001 to 2002 across 268 arsenic-affected Upazilas (sub-districts) to identify contaminated tubewells and arsenicosis cases. Diagnosis was primarily based on visible dermatological manifestations, including melanosis (hyperpigmentation, leukomelanosis), keratosis, hyperkeratosis, gangrene, and skin cancer, following a protocol developed in Bangladesh and later modified by the WHO. This methodology had inherent limitations. The identified cases, while exhibiting arsenic-related skin lesions, were not confirmed through biological sample analysis (e.g., urine, hair, or nail samples). Consequently, the screening may have included non-arsenic-related skin conditions. Furthermore, the survey could not

account for internal cancers and other systemic health effects of arsenic ingestion.

The program tested 4.9 million tube wells and found that 29.12% exceeded the Bangladesh Standard (BDS) limit of 50 µg/L for arsenic. By screening 66 million people in these areas, 38,430 cases of arsenicosis were identified (BAMWSP, 2001). This aligns with the earlier National Hydrochemical Survey (BGS and DPHE, 2001), which found 25% of tube wells nationwide exceeded the BDS. The prevalence of identified arsenicosis cases was significantly lower than expert predictions based on exposure levels. The leading explanation is that the duration of exposure to contaminated water was not sufficient for the full spectrum of health effects to manifest in the exposed population.

Establishing a dose-response relationship

The distribution of patients across Upazilas did not perfectly correlate with the local intensity of tubewell contamination. To analyze this relationship, the average arsenic concentration for each Upazila was computed using BGS and DPHE data. While the sample size is limited, given the high spatial variability, it provides a reasonable estimate. A key methodological consideration was handling samples below the detection limit; following the BGS/DPHE report, these were assigned a value of half the detection limit. Fig.9 plots the number of arsenicosis cases in each Upazila against the average arsenic content of its tubewell water. The result demonstrates an observable dose-response relationship, despite the reliance on clinical diagnosis of skin lesions.

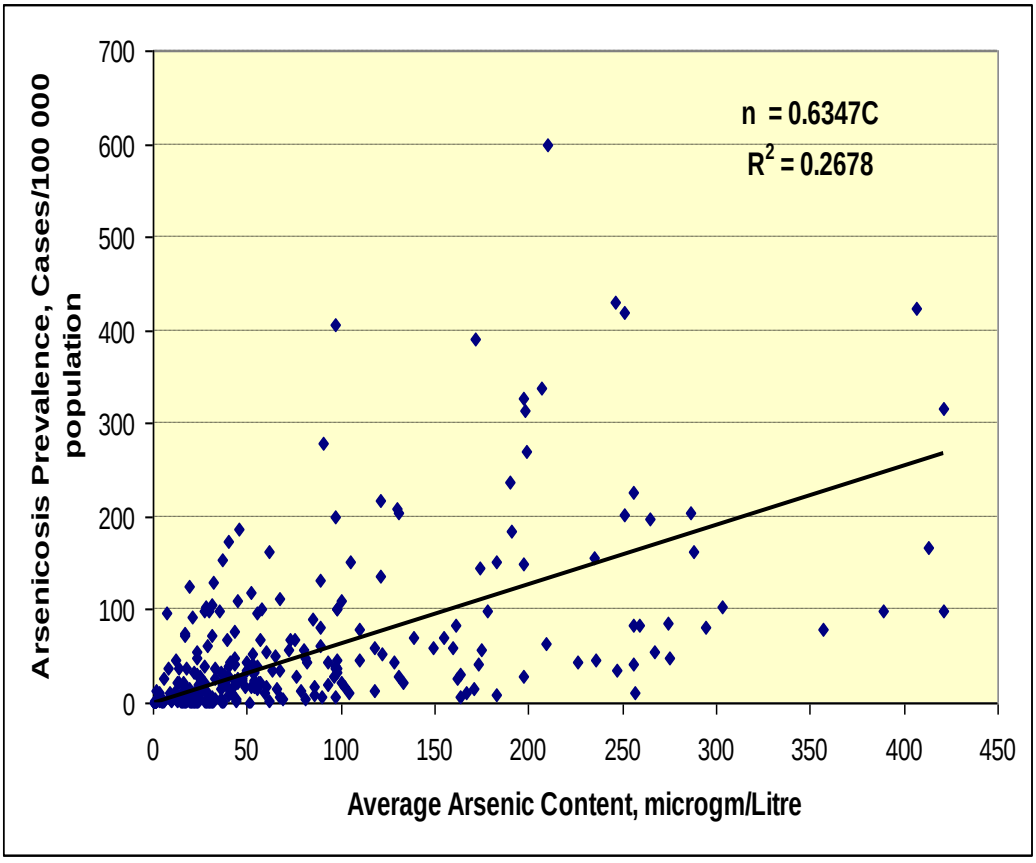

Fig. 9. Relationship between arsenical skin lesion and average arsenic content in drinking water.

A linear fit forced through the origin yields a correlation coefficient (R) of 0.2678, indicating a very weak and poorly defined dose-response relationship, as evidenced by the erratic and scattered data points.

$$n = 0.6347\ C \qquad 8$$

Where n is the total (male + female) cases of arsenic-related skin lesions per 100,000 population, and 'C' is the average arsenic content in µg/L of tubewell water. So Eqn. 8 can be written as:

$$N = 0.6347 \times 10^{-5} CP \qquad 9$$

A comparison of the WHO dose-response [Eqn. 7] and empirical dose-response [Eqn. 9] models reveal a significant discrepancy. The current average prevalence rate of clinical arsenical skin lesions [Eqn. 9] is substantially lower than the excess skin cancer risk predicted by the WHO linear no-threshold model [Eqn. 7]. This is consistent with the age-adjusted skin cancer estimate by Yu et al. (2003), which also falls far below the linear model's prediction.

Applying the empirical model [Eqn. 9] to the national context—using an average arsenic concentration of 55 µg/L (BGS & DPHE, 2001) and a 2001 population of 129 million (BBS, 2001)—yields an estimated 45,032 arsenicosis patients. This figure aligns closely with the 38,430 cases identified in the National Screening Program, validating the empirical model's relevance for the observed clinical presentation.

The Director General of Health Services (DGHS) recorded 38,320 arsenicosis patients in 2009 among those who approached health centers for treatment with skin lesions. These two studies, conducted about 8 years apart, show similar numbers of patients, indicating a stagnation in the prevalence of arsenicosis cases. However, these two sets of data are not comparable because the DGHS recorded cases were medically treated for arsenicosis by qualified medical professionals, but many cases might not have been approached for medical treatment. On the other hand, the national screening compiled by NAMIC and BAMWSP was identified by non-professionals observing skin lesions.

Two key interpretations emerge from this data**.**

First, the prominent regional variability and the lower-than-predicted case numbers suggest that the skin cancer risk of 10^{-5} at 0.17 µg/L, as derived from the linear model, may be a significant overestimate for the Bangladeshi population.

Second, it is equally plausible that the health effects are in a preliminary stage, and the full burden of disease, particularly internal cancers, corresponding to the present contamination level, has yet to manifest, which can only be confirmed by a second round of National screening of arsenicosis cases and levels of contamination of drinking water sources.

Arsenic Risk Mitigation

The Government of Bangladesh embarked on an arsenic mitigation program by developing an arsenic mitigation strategy. In the first phase, Bangladesh has undertaken a program to screen all the tubewells and population in 268 potentially arsenic-affected upazilas to identify contaminated wells and arsenicosis cases. Screening of all tube wells was necessary due to unpredictable variations in arsenic levels in tube well water, even over short distances and at different depths. The contaminated and uncontaminated tube wells are marked red and green respectively. A protocol was developed for diagnosing cases of arsenicosis. The arsenicosis cases are referred to Upazila health centers or specialized hospitals depending on the severity of the cases. An arsenicosis case management protocol was developed to provide health care for affected patients in health centers and hospitals.

Arsenic toxicity has no known effective treatment. Chelating agents used for acute arsenic poisoning have been tested for chronic cases, but the results have generally been unsatisfactory. However,long-term drinking of arsenic-free water has been shown to reverse symptoms in patients at early stages of arsenicosis. Hence, provision of arsenic-safe water to about 30 million people exposed to high levels of arsenic was given priority in arsenic risk mitigation

in Bangladesh. The strategy for providing arsenic-safe water was guided by the principles stated below:

• Alternative technologies are area dependent and cannot be generalized uniformly across the country.

• No single option can serve the needs of people with different social and economic conditions.

• Choice of the community shall be given priority in the selection of technological options.

• Alternative water supplies must comply with the Bangladesh Standard for arsenic in drinking water.

The treatment of arsenic-contaminated groundwater or switching over to arsenic-safe sources like surface water and rainwater are possible alternatives. In some areas, deeper aquifers are found to yield water with low arsenic content and can be used as a source of arsenic-safe water supply. The National Policy and Implementation Plan for Arsenic Mitigation (IPAM), 2004, emphasized that while research to devise appropriate options was ongoing, arsenic mitigation programs shall promote Improved Dug Well, Pond Sand Filters, Deep Tube well, Rainwater Harvesting, Arsenic Treatment Technologies, and Piped Water Supply System for arsenic safe water supply (GoB, 2004).

The possibility of cross-contamination from shallow aquifers due to over pumping of deep aquifers cannot be excluded. Treatment of surface water having low arsenic content by small treatment units, rainwater harvesting and use of dug well water were promoted extensively in arsenic-affected areas of both Bangladesh and India. A risk assessment of arsenic mitigation options revealed that although surface water and rainwater provided arsenic-safe water, consumers in some cases were exposed to a higher microbial health risk from these sources (Ahmed et.al., 2006b).

The approaches outlined in the Bangladesh National Arsenic Mitigation Policy and Implementation Plan were pursued but achieved only partial success. The progress in arsenic mitigation was very slow, and as of 2006, only about 14 percent of the exposed people had access to arsenic-safe water (Ahmed et al., 2006a).

Many units developed for the treatment of arsenic-contaminated water at household and community levels and installed for experimental use in different parts of Bangladesh have shown good potential for arsenic-safe water supply. The Bangladesh Council of Scientific and Industrial Research (BCSIR) conducted an evaluation of prospective arsenic removal technologies in collaboration with the Ontario Centre for Environmental Technology Advancement (OCETA), Canada under the Environmental Technology Verification- Arsenic Mitigation (ETV-AM) program. The performance of the technologies was found to be greatly influenced by the presence of phosphate, silica, pH, and dissolved organic matter, and in some areas with adverse water quality, no technology worked satisfactorily. Only four household and community-based technologies were accepted for deployment in Bangladesh after extensive laboratory and field verification (Ahmed and Ahmed, 2014). All arsenic treatment technologies have their merits and demerits, and require refinements to make them suitable for rural conditions.

BBS and UNICEF (2019) Multiple Indicator Cluster Survey (MICS) study showed that 11.8% water was contaminated with arsenic exceeding Bangladesh standard of 50 μg/L at source, which reduces to 10.6% at the point of consumption. Arsenic contamination, compared with the WHO Guideline value, was higher: 18.6% at the source and 16.7% at the point of contamination. Arsenic reduction over time is due to its coagulation with iron in water and sedimentation in storage containers. The UN Joint Monitoring Program (JMP) estimated that Bangladesh achieved 59 percent coverage of a safe managed water supply, whereas coverage of basic water is 99 percent (WHO/UNICEF, 2000-2024). This wide gap in coverage of drinking water supply was due to microbial and arsenic contamination. Consequently, Bangladesh remains off track in achieving Sustainable Development Goal (SDG) for a safe and managed drinking water supply.

Conclusions

Arsenic contamination of groundwater in Bangladesh is a natural phenomenon triggered by reductive dissolution of sorbed arsenic on oxidized iron, alumina, manganese, and other minerals carried by the fine-grained sediments of the rivers Ganges, Brahmaputra, and Meghna River system. These fine-grained sediments carry arsenic released by the weathering of arsenic-rich minerals in upstream basins and deposit in floodplains, particularly in depressed areas with relatively stagnant water, where reducing conditions with low redox potential are created by the anaerobic decomposition of organic matter. Dissolution and desorption of arsenic from sediments, particularly from arsenic-rich iron oxyhydroxide present on soil grains, and reduction of As(V) to more mobile As(III) appear to be the main mechanisms of groundwater contamination in Bangladesh.

At present, 75% of the areas under irrigation in the dry season use groundwater from shallow aquifers, and fortunately, the levels of arsenic contamination in the areas of intensive irrigation, except the south-west region, are comparatively low. Arsenic content in rice is generally higher in arsenic-contaminated topsoil, but the relationship between arsenic content in rice and arsenic in topsoil is not strong. Although total arsenic content in rice in Bangladesh is not very high, the fraction of inorganic arsenic particularly in Boro rice, appears to be high. High rice consumption and a comparatively higher proportion of inorganic arsenic in rice need to be considered in the estimation of arsenic body burden and revision of national standard for arsenic in Bangladesh.

The National Screening of arsenic-contaminated tubewells and arsenicosis cases in 2001 revealed that the prevalence rate of skin lesions was several times lower than the estimated excess skin cancer risk attributable to arsenic-contaminated drinking water in Bangladesh. Limited data suggest that the skin cancer risk of 10^{-5} for drinking water arsenic content of 0.17 μg/L may be an overestimate. On the other hand, the health effects in Bangladesh might be in the early stages of manifestation; another National Screening is needed to better understand the situation.

The progress in arsenic mitigation in Bangladesh by providing access to arsenic-safe water has been very slow. The UN Joint Monitoring Program (WHO/UNICEF) report 2025 indicated that Bangladesh was out of track in achieving universal access to safely managed water. If the current rate of progress continues, Bangladesh will not meet the Sustainable Development Goal (SDG) for drinking water.

Authors contribution

The corresponding author, M Feroze Ahmed, declares that this paper has been prepared by compiling and analyzing data from relevant sources by me. The co-author, Tanvir Ahmed, has edited the paper and given his consent for the article to be considered by the Editorial Board for publication in the Journal of Bangladesh Academy of Sciences.

Conflict of interest

Regarding publication of this paper, the authors have no conflict of interest.

References

Ahmann D, Krumholz LR, Hemond HF, Lovely DR and Morel FMM. Microbial mobilization of arsenic from sediments of the Aberjona watershed. *Environ. Sci. Technol*. 1997;31: 2923-2930.

Ahmed KM. Geology and hydrogeological controls on the occurrence and distribution of arsenic in Bangladesh groundwater. In: *Arsenic Contamination: Bangladesh perspective*, ITN-BUET Centre for water supply and waste management, BUET, 2nd Ed. 2007a: 136-164.

Ahmed MF and Ahmed T. Status of remediation of arsenic contamination of groundwater in Bangladesh. In: *Comprehensive water quality and purification*, Vol. 1, S Ahuja (ed.). *Elsevier*; 2014: 104-121.

Ahmed MF, Ahuja S, Alauddin M, Hug SJ, Lloyd JR, Pfaff A, Pichler T, Saltikov C, Stute M and Van Geen A. Ensuring safe drinking water in Bangladesh. *Science*, 2006a; 314: 1687-1688.

Ahmed MF, Howard G, Deere D, Mahmud SG and Shamsuddin SAJ. *Quantitative health risk assessment for arsenic and microbial contamination of drinking water*, Arsenic project support unit, Government of the Purple's Republic of Bangladesh; 2006b.

Ahmed MF. Arsenic contamination of groundwater in Bangladesh. In: *Arsenic Contamination: Bangladesh perspective,* ITN-BUET centre for water supply and waste management, BUET, 2nd Ed. 2007b: 42-64.

Ahmed MF. Arsenic. *Chemical & Engineering News (Special Issue Celebrating the Periodic Tables of Elements on the C&EN's the 80th Anniversary), American Chemical Society*, 2003; 81: 92.

Ahmed MF. Drinking water standard and guideline value for arsenic: A critical analysis. In: *Arsenic contamination: Bangladesh perspective,* ITN-BUET centre for water supply and waste management, BUET, 2nd Ed. 2007c: 499-513

Ahmed MF. Theme Paper III: Alternative water supply options for arsenic affected areas of Bangladesh, In: Arsenic Mitigation in Bangladesh, Local Government Division, Ministry of LGRD & Co-operatives, Government of People's Republic of Bangladesh; 2002: 80-174.

Ahmed MF. Soil environment and arsenic contamination of groundwater in Bangladesh. Proceedings International Conference on Geoenvironment *2000*, Sultan Qaboos University, Muscat, Oman, March 4-7, 2000; 1: 256-264.

Ahmed T. Assessment of non-carcinogenic arsenicosis risk in rural Bangladesh, In: *Arsenic contamination: Bangladesh perspective,* ITN-BUET centre for water supply and waste management, BUET, 2nd Ed. 2007d: 326-341.

Akai J, Izumi K and Fukuhara H. Arsenic release experiments using strata model – bacterial activity as a key factor for arsenic dissolution. In: *Arsenic contamination of groundwater-geological, hydrogeological, medical and sociological findings in Bangladesh and inner Mongolia*, Asia Arsenic Network and Research Group for Applied Geology, Japan, 2001.

Ali MA, Badruzzaman ABM, Jalil MA, Hossain MD, Ahmed MF, Al-Masud A, Kamruzzaman M, and Rahman AR. Fate of arsenic extracted with groundwater. In: *Fate of Arsenic in the Environment*, Ahmed MF, Ashraf MA and Adeel Z (eds.), Bangladesh University of Engineering and Technology and United nations University. 2003a: 7-20.

Ali MA, Badruzzaman ABM, Jalil MA, Hossain MD, Ahmed, MF, Al-Masud A, Kamruzzaman M and Rahman, AR. Arsenic in plant-soil environment in Bangladesh. In: *Fate of Arsenic in the Environment*, Ahmed MF, Ashraf MA and Adeel Z. (eds), Bangladesh University of Engineering and Technology and United nations University. 2003b: 85-112.

Anawar HM, Akai J, Mihaljevic M, Sikder AM, Ahmed G, Tareq SM and Rahman MM. *Water* 2011; 3(4):1050-1076.

BAMWSP (Bangladesh Arsenic Mitigation Water Supply Project). Nationwide Screening Program-Tubewell Screening and Arsenicosis Patient Identification, Bangladesh Arsenic Mitigation Water Supply Project: Government of the People's Republic of Bangladesh, 2001.

BARI. Arsenic contamination of soil and crop and remedy. Soil Science Division, Bangladesh Agricultural Research Institute (BARI), Gazipur, Bangladesh. 2007.

BBS and UNICEF. *Progotir Pathey, Bangladesh. Multiple Indicator Cluster Survey (MICS)* – Key Findings, 2019.

BBS (Bangladesh Bureau of Statistics).*Population Census 2001: Preliminary Report*, Statistics

Division, Ministry of Planning, Government of the People's Republic of Bangladesh. 2001.

BGS and DPHE. *Arsenic Contamination of Groundwater in Bangladesh*, Kinniburg DG. and Smedley PL(Eds.), Volume 2: Final Report. *British Geological Survey Report* WC/00/19. 2001.

BGS, DPHE and MML. *Groundwater studies for arsenic contamination*, Department of Public Health Engineering, Government of the People's Republic of Bangladesh; 1999.

Bhattacharya P, Ahmed KM, Hasan MA, Jacks G, Chattergee D, Khan AA, Akhter SH, Imam MB and Sracek A. Groundwater arsenic in the holocene alluvial aquifers in bengal delta plains: petrological, geochemical and isotope geochemical studies. International Conference on Arsenic In Bangladesh Ground Water: World's Greatest Arsenic Calamity, Wagner College, New York, 27-28 February 1999.

Bhumbla DK and Keefer RF Arsenic Mobilization and Bioavailability in Soils, In: *Arsenic in the Environment*, Nriagu JO (Ed.), John Wiley & Sons Inc.1994.

Caldwell BK, Caldwell JC. Mitra SN and Smith W. Tubewells and arsenic in Bangladesh: challenging a public health success story. *Int. J. Popul. Geogr.* 2003.

Chowdhury, M.A.I., Ahmed, M.F. and Ali, M.A. Influence of upstream sediment on arsenic contamination of groundwater in Bangladesh. In: *Fate of Arsenic in the Environment*, M.F. Ahmed et al (eds), Bangladesh University of Engineering and Technology and United nations University. 2003: 21-36.

DGHS. Arseniicosis cases in Bangladesh,

DPHE, *Yearbook (1998-99): Rural Water Supply*, Department of Public Health Engineering (DPHE), Bangladesh; 2000.

Duxbury JM, Mayer AB, Lauren JG and Hassan N. Food chain aspects of arsenic contamination in Bangladesh: Effect on quality of productivity of rice. *J. Environ. Sci. Health*. 2003; A38(1): 61-69.

FAO/WHO Expert Committee. *Toxicological Evaluation of Certain Food Additives an Contaminants*, Cambridge University Press, WHO Food Additive Series No. 24; 1989: 155-162

GoB. *National policy for arsenic mitigation & implementation plan for arsenic mitigation in Bangladesh*. Local Government Division, Ministry of Local Government, Rural Development & Cooperatives, Government of the People's Republic of Bangladesh, 2004.

Harvey CF, Swartz CH, Badruzzaman ABM, Keon-Blute N, Yu W, Ali MA, Jay J, Beckie R, Niedan V, Brabander D, Oates PM, Ashfaque KN, Islam S, Hemond HF and Ahmed MF. Arsenic mobility and groundwater extraction in Bangladesh, *Science*. 2002; 298: 1602-1606.

Heikens A. *Arsenic contamination of irrigation water, soil and crops in Bangladesh: Risk implications for sustainable agriculture and food safety in Asia*. Food and Agricultural Organization, Regional Office in Asia and the Pacific, Bangkok; 2006.

Hironaka H and Ahmad SA. Arsenic concentration of rice in Bangladesh. In: *Fate of Arsenic in the Environment*, Ahmed MF, Ali MA and Adeel Z (eds), Bangladesh University of Engineering and Technology and United nations University. 2003: 123-130.

Islam, SMA, Fukushi K, Yamamoto K and Saha GC. Estimation of biological gasification potential of arsenic from contaminated natural soil by enumeration of arsenic methylating bacterial. *Arch. Environ. Contam. Toxicol.*2007; 52, 332-338.

Mazumder GDN, Haque R, Ghose N, De K, Santra A. Chakraborti D and Smith AH. Arsenic level in drinking water and the prevalence of skin legions in West Bengal, India. *Int. J. Epidemiol*. 1998; 5: 871-877.

McArthur JM. Arsenic poisoning in the ganges delta. *Nature*.1999; 401: 545-547.

McCreadie H, Blowes DW, Ptacek CJ and Jambor JL. Influence of reduction reactions and solid-phase composition on porewater concentrations of arsenic. *Environ. Sci. Technol*. 2000; 34: 3159-3166.

Meharg AA and Rahman MM. Arsenic contamination of Bangladesh paddy field soils: Implications for rice contribution to arsenic consumption. *Environ. Sc. Technol*. 2003; 37: 229-234

Milton AH, Hore, SK, Hossain, MZ and Rahman M. Bangladesh arsenic mitigation programs: lessons from the past. *Emerg. Health Threats J*. 2012: 5(1).

Misbahuddin M, Anjumananara, Liton AK, Khan MAR, Rahman, MS, and Khandker S. Speciation of arsenic in rice and vegetables from arsenic exposed areas of Bangladesh. In: *Applied Research on Arsenic in Bangladesh*, World Health Organization, Dhaka, Bangladesh and Directorate General of Health Services, Govt. of the People's Republic of Bangladesh; 2007.

Mok WM and Wai CM. Mobilization of arsenic in contaminated river water. In: *Arsenic in the Environment*, Nriagu JO, ed., John Wiley & Sons Inc. 1994.

Nickson R, McArthur JM, Burgess W, Ahmed KM, Ravenscroft P and Rahman M. Arsenic poisoning of Bangladesh Groundwater. *Nature*.1998; 395(6700), 338.

Nordstrom DK. An overview of arsenic mass-poisoning in Bangladesh and West Bengal, India, In: *Minor Elements 2000, Processing and Environmental Aspects of As, Sb, Se, Te, and Bi*. Young C. (ed). 2000: 21-30.

Panaullah GM, Alam T, Hossain MB, Loeppert RH, Lauren JG, Meisner CA, Ahmed ZU and Duxbury JM. Arsenic toxicity to rice (Oryza sativa L.) in Bangladesh. Plant Soil, 2009; 317: 31–39.

Rahman MM and Rahman M. Arsenic contamination source detection for hazards mitigation. International Conference on Arsenic Pollution of Groundwater in Bangladesh: Causes, Effects and Remedies, Dhaka, Bangladesh, 1998: 8-12.

Ravenscroft P, Burgess WG, Ahmed KM, Burren M and Perrin J. Arsenic in groundwater of the Bengal basin, Bangladesh: Distribution, field relations, and hydrogeological setting. *Hydrogeol. J*. 2005; 13: 727-751.

Ravenscroft P, McArthur JM and Hoque B. Geochemical and palaeohydrological controls on pollution of groundwater by arsenic. In: *Arsenic Exposure and Health Effects IV*, Chappell WR, Abernathy CO and Calderon R(eds.), *Elsevier Science Ltd., Oxford*; 2001: 53–77.

Roberts LC, Hug SJ, Dittmar J, Voegelin A, Kretzschmar R, Wehrli B, Cirpka OA, Saha GC, Ali MA and Badruzzaman ABM. Arsenic release from paddy soil during monsoon flooding. *Nat. Geosci.* 2010; 3: 53-59.

Saha GC. *Accumulation of Arsenic in Agricultural Soil and Selected Crops*, Ph.D. Thesis, Department of Civil Engineering, BUET, Dhaka. 2006.

Sakamoto M. Revisiting the village where arsenic contamination of underground water was first discovered in Bangladesh: Twenty-Five Years Later. *Int. J. Environ. Res. Public Health.* 2021; 259: 1-18.

SOES and DCH. Groundwater Arsenic Contamination in Bangladesh.(A). Summary of Field Survey from August 1995 to February 2000.(B). Twenty-Seven Days Detailed Field Survey Information from April 1999 to February 2000.

Ullah SM. Arsenic contamination of groundwater in irrigated soils of Bangladesh, International Conference on Arsenic Pollution of Groundwater in Bangladesh: Causes, Effects and Remedies, Dhaka, Bangladesh, 1998; 8-12.

USEPA. Special Report on *Ingested Inorganic Arsenic. Skin Cancer; Nutritional Essentiality*, US Environmental Protection Agency (EPA-625/3-87/013); 1988.

Van Geen A, Zheng Y, Cheng Z, He Y, Dhar RK, Garnier JM, Rose J, Seddique A, Hoque MA and Ahmed KM. Impact of irrigating rice paddies with groundwater containing arsenic in Bangladesh. *Sci. Total Environ*. 2006; 367: 769-777.

WARPO. *National Water Management Plan, Vol. 2 : Main Report*, Water Resources Planning Organization (WARPO), Government of the People's Republic of Bangladesh; 2001.

Wauchope RD. Uptake, translocation and phytotoxicity in plants. In: *Arsenic- Industrial, Biomedical and Environmental Perspectives*, New York; 1983: 348-374.

WHO. Bulletin of the World Health Organization, 2000; 78(9): 1093-1103

WHO. *Guidelines for Drinking-water Quality*, 2nd Edition, World Health Organization, Geneva, Switzerland; 1993.

WHO. *Guidelines for Drinking-water Quality*, 4th Edn. World Health Organization, Geneva, Switzerland; 2011.

WHO/UNICEF. *Progress on household drinking water, sanitation and hygiene.* Joint Monitoring Programme for Water Supply, Sanitation and Hygeia; World Health Organization and United Nations Children Fund, 2000-2024.

WHO/UNICEF. *Progress on household drinking water, sanitation and hygiene 2000–2024: special focus on inequalities.* Geneva: World Health Organization (WHO) and the United Nations Children's Fund (UNICEF), 2025 Licence: CC BY-NC-SA 3.0 IGO.

Williams PN, Islam MR, Adomako EE, Raab A, Hossain SA, Zhu YG and Meharg AA. Increase in rice grain arsenic for regions of Bangladesh irrigating paddies with elevated arsenic in groundwater. *Environ. Sci. Technol*. 2006; 40: 4903-4908.

Williams PN, Price AH, Raab A, Hossain SA, Fieldmann J, Meharg AA. Variation in arsenic speciation and concentration in paddy rice related to dietary exposure. *Environ. Sci. Technol*. 2005; 39: 5531-5540.

Yan-Chu H. Arsenic distribution in soils. In: *Arsenic in the Environment*, Nriagu JO, ed., John Wiley & Sons Inc. 1994: 17-49.

Yu W, Harvey CM and Harvey CF. Arsenic in groundwater in Bangladesh: a geostatistical and epidemiological framework for evaluating health effects and potential remedies. *Wat. Resour. Res.* 2003; 39:1146-1163.

Zahid A. Bangladesh Delta Plan 2100 Baseline Study: 4 Groundwater, 2018: 305-386

Zheng Y, Stute M, Van Geen A, Gavrieli I, Dhar R, Simpson HJ, Schlosser P and Ahmed KM. Redox control of arsenic mobilization in Bangladesh groundwater. *Appl. Geochem.* 2004; 19(2): 201-214.

J. Bangladesh Acad. Sci. 49(2); 179-188: December 2025 DOI:https://doi.org/10.3329/jbas.v49i2.80908

Journal of Bangladesh Academy of Sciences

Journal homepage: http://www.bas.org.bd/publications/jbas.html

Research Article

Genome mining reveals the prevalence of Bsa lantibiotic and its variants in *Staphylococcus aureus* strains

Suvroto Kormokar[1], Md. Amzad Hossain[2], M. Aftab Uddin[1] and Mohammad Riazul Islam[2*]

[1]*Department of Genetic Engineering and Biotechnology, University of Dhaka, Dhaka, Bangladesh*

ARTICLE INFO

Article History

Received: 14 April 2025
Revised: 08 July 2025
Accepted: 19 August 2025

Keywords: Genome mining, Lantibiotic, Class-I lanthipeptide, AntiSMASH, Bsa.

ABSTRACT

With rising antibiotic resistance, the discovery of novel antimicrobial compounds has become increasingly crucial. *In silico* genome mining is widely used to predict secondary metabolite production prior to laboratory testing. In this study, 505 *Staphylococcus aureus* genomes from the NCBI database were analyzed using antiSMASH 7.0, which identified a class I lanthipeptide gene cluster in 206 strains. Although antiSMASH annotated this gene cluster as hyicin 3682 and the RefSeq genome database classified it as a 'gallidermin- or nisin-family lantibiotic', the prepeptide sequence encoded by the cluster is identical to that of the *S. aureus* bacteriocin (Bsa) lantibiotic. Moreover, other genes within the cluster share the same number and orientation as the Bsa loci found in community-acquired *S. aureus* strains. Variations in prepeptide sequences and gene numbers revealed four distinct Bsa variants. Overall, this analysis supports the presence of lantibiotic gene clusters in pathogenic strains and highlights the potential of genome mining to reduce time, cost, and labor in antimicrobial discovery.

Introduction

Scientists have discovered a bunch of new antibiotics, and sooner or later new antibiotic-resistant pathogens have emerged as a result. So, the search for new and novel antibiotics continues from every possible source, e.g., animals, insects, plants, and bacteria. Among several alternative options, lanthipeptides from bacteria show potential as future therapeutic agents due to their ability to kill antibiotic-resistant pathogens and their broad antimicrobial spectrum (van Staden et al., 2021).

Lanthipeptides are ribosomally synthesized and post-translationally modified peptides. They contain specific amino acids, including lanthionine (Lan) and (2S,3S,6R)-3-methyllanthionine (MeLan) (Arnison et al., 2013). The lanthipeptide is produced from a precursor peptide known as LanA, which is then subjected to post-translational changes to yield the mature, bioactive lanthipeptide. After serine (Ser) and threonine (Thr) residues are dehydrated to form dehydroalanine (Dha) and dehydrobutyrine (Dhb), the thiol groups of cysteine (Cys) residues are added to Dha and Dhb to form thioether cross-links, which yield the Lan and MeLan residues, respectively (Arnison et al., 2013). Enzymes responsible for these modifications, lanthipeptide synthetases, show different features that classify the lanthipeptides into 4 subfamilies: class-I – class-IV (Arnison et al., 2013). While Class-I lanthipeptides (such as nisin) have been extensively studied, the prevalence of other classes (III and IV) is gaining attention.

Lantibiotics are produced by the members of the Gram-positive bacteria with a length of usually 19 to 34 amino acids (Willey and van der

*Corresponding author:<mriazulislam@du.ac.bd>

[2]*Department of Biochemistry and Molecular Biology, University of Dhaka, Dhaka, Bangladesh*

Donk, 2007). Some of the reported lantibiotics are Pep5 from *S. epidermidis* 5 (Kaletta et al., 1989), epidermin (Epi) from *S. epidermidis* Tü3298 (Allgaier et al., 1985), gallidermin (Gdm) from *S. gallinarum* DSM 4616 (Kellner et al., 1988), Bsa_{COL} from *S. aureus* COL1881 (Daly et al., 2010), nisin J from *S. capitis* APC2923 (O'Sullivan et al., 2020), homicorcin from *S. hominis* MBL_AB63 (Uddin et al., 2021), etc. Although many lantibiotics are produced by food-grade bacteria or bacteria generally regarded as safe, there have also been a few examples of antibiotic production by pathogens (Cox et al., 2005). One such pathogen is *Staphylococcus aureus*, a frequent opportunistic pathogen of humans and animals. To date, 4 lantibiotics have been reported to be produced by *S. aureus*: Staphylococcin Au-26 (Scott, 1992), Staphylococcin C55 (Navaratna et al., 1998), BacCH91 (Wladyka et al., 2013), and Bsa (bacteriocin of *Staphylococcus aureus*) (Daly et al., 2010). As a member of the *Staphylococcus* genus, the *S. aureus* genome holds the promise of harboring novel antimicrobial compound gene clusters.

Genome mining is a fast, high-throughput technique that exploits genomic information to discover natural products, their biosynthetic pathways, and potential interactions. The possibility of predicting novel putative lanthipeptide gene clusters in bacterial genomes has increased steadily over the last decade, driven by greater genomic data availability and advances in genome-mining tools. One of these tools is antiSMASH (antibiotics and secondary metabolite analysis shell), which analyzes genome sequences, identifies putative lanthipeptide biosynthetic gene clusters, provides information on their post-translational modifications and determines the class of the detected lanthipeptide (Blin et al., 2023). Another one is BAGEL, a web tool that identifies gene clusters in prokaryotic DNA involved in the biosynthesis of Ribosomally synthesized and post-translational modified Peptides (RiPPs) and bacteriocins (van Heel et al., 2018). There are numerous studies on the identification of lanthipeptide gene clusters through *in silico* screening of bacterial genomes, reflecting the growing interest in secondary metabolites (Begley et al., 2009; Singh and Sareen, 2014).

In this study, more than 500 *Staphylococcus aureus* complete genome sequences available in NCBI were screened using antiSMASH 7.0 to examine the pattern of secondary metabolite prediction by *S. aureus*. In 206 strains, a complete lanthipeptide class I gene cluster was identified. Initially, this gene cluster was identified as hyicin 3682 and annotated as a gallidermin or nisin family lantibiotic in the RefSeq genome database. However, analysis of gene arrangement within the cluster and its sequences confirmed that it is a Bsa locus, and its multiple variants were identified. As this is an *in silico* study, this presumption must be validated by experimental analysis.

Methods

Selection of genome sequences and identification of gene clusters using antiSMASH7.0

From the Genome database of NCBI (https://www.ncbi.nlm.nih.gov/genome), the first 505 *S. aureus* complete genome sequences were selected out of 1716 publicly available sequences until October 2023. The accession numbers of these sequences were used as input in 'antibiotics and secondary metabolite analysis shell—antiSMASH' version 7.0 (Blin et al., 2023) (https://antismash.secondarymetabolites.org/) for identification, annotation, and analysis of secondary metabolite biosynthesis gene clusters.

Comparison of the identified lantipeptide cluster genes with corresponding genes of other lantipeptides of the same class

The individual genes of the identified lantipeptide cluster were aligned with corresponding biosynthesis genes of other well-studied class-I lantibiotics using the NCBI Nucleotide BLAST tool (https://www.ncbi.nlm.nih.gov/geo/query/blast.html).

Phylogenetic tree construction

To study the evolutionary relationship among the Seq 1 prepeptide and to compare class I lantipeptides, a phylogenetic tree was constructed in MEGA11 using the neighbour-joining method, with the Poisson model as the substitution model (Tamura et al., 2021). An outgroup sequence of *S. aureus*, glyceraldehyde-3-phosphate dehydrogenase (GPD) was used to determine the root of the sequences.

Results

The lanthipeptide class-I gene cluster was the most prevalent gene cluster in the studied genomes

In the 505 *S. aureus* genomes screened, 7 different types of gene clusters were identified, i.e., lanthipeptide-class-I, non-ribosomal peptide synthetase (NRPS), cyclic lactone autoinducer, siderophore, ribosomally synthesized and post-translationally modified peptides (RiPP) like opine-like-metallophore and terpene. While the other 6 gene clusters were found in more than 500 genomes, the lanthipeptide class I gene cluster was found in only 206 genomes. The most similar gene cluster to this lanthipeptide was predicted to be hyicin 3682. Of these, 161 gene clusters were 100% similar, and 45 were 87% identical to the hyicin 3682 gene cluster.

The lantipeptide cluster identified as the Bsa biosynthesis gene cluster is revealed through gene-by-gene sequence comparison

The identified gene clusters of the class-I lanthipeptide in 206 *S. aureus* strains contain 4 different types of prepeptide sequences at different frequencies, arranged in 5 different arrangements in the clusters. The most prevalent of these types (found in 197 strains out of 206) contains 20 genes of varying lengths in most cases, of which 9 genes (Fig. 1) are supposed to be involved in lantibiotic production and transport according to their annotations by antiSMASH 7.0. Among the 9 genes, two genes code for two different prepeptide sequences (A, A'), three genes code for modification enzymes (B, C, D), one codes for a cleavage enzyme (P), while the other three are involved with transport and immunity (F, E, G). The genes were identified as the most identical genes in the NCBI database, and their roles in lanthipeptide production and transport were determined.

The most prevalent whole gene cluster (Fig. 1) was compared with the other lantibiotic gene clusters to find similarity in terms of gene number, function and orientation (Fig. 2). It is clearly visible that the lanthipeptide class I gene cluster is identical to the Bsa gene cluster (Daly et al., 2010) and hyicin 3682 gene cluster (Carlin et al., 2017) having 8 genes, all of which are in the same orientation. The epidermin gene cluster (Schnell et al., 1992), the 181 allidermin gene cluster (Valsesia et al., 2007), and the nisin A gene cluster (Trmčić et al., 2011) show notable differences in the number of genes (both have 11 genes), their orientation, and their function. Moreover, sequences of all similar genes in the most prevalent cluster were compared (using the NCBI BLAST algorithm) with those of the rest to determine similarity (Table 1). Except for one, all the genes in the identified lanthipeptide gene cluster show significant similarity to the corresponding genes in Bsa.

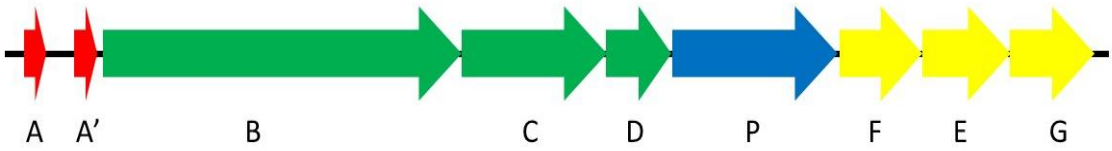

Fig. 1. Arrangement of biosynthetic genes in the most prevalent lanthipeptide class-I gene cluster in *S. aureus*. The function of each gene product is indicated by colors: red, precursor peptide (A, A'); green, modification enzyme (B, C, D); blue, cleavage enzyme (P); and yellow, transport and immunity protein (F, E, G).

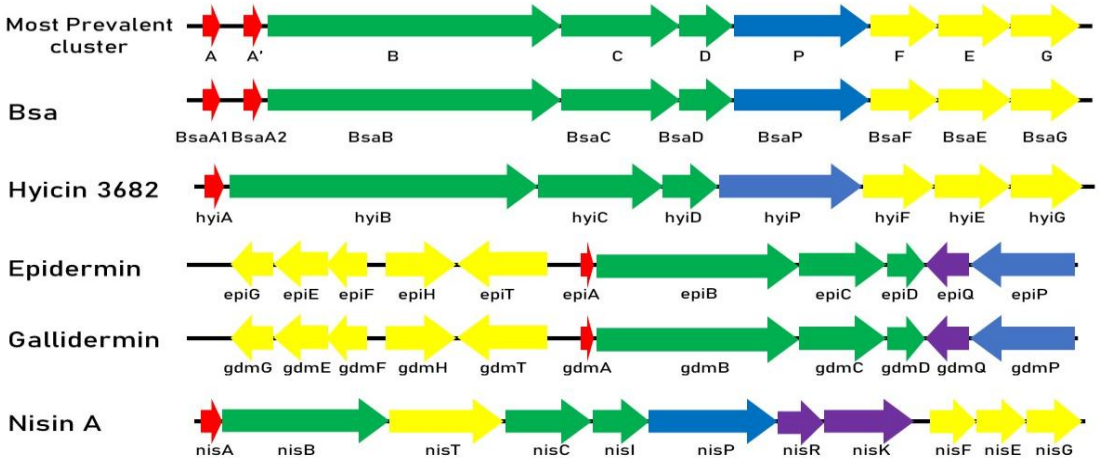

Fig. 2. Comparison of the whole gene cluster of the identified class I lanthipeptide with other lantibiotics. The function of each gene product is indicated by colors: red, precursor peptide; green, modification enzyme; blue, cleavage enzyme; yellow, transport and immunity protein; and purple, response regulator.

Table 1. Sequence comparison (% identity) of different biosynthetic genes of Bsa from different clusters with the corresponding genes of the identified class I lanthipeptide.

	Class-I lanthipeptide genes						
Lantipeptide	**LanB**	**LanC**	**LanD**	**LanP**	**LanF**	**LanE**	**LanG**
Bsa	99.7	100	100	100	100	100	100
Hyicin	60.28	58.21	72.67	64.44	82.46	67.06	56.28
Epidermin	44.87	46.34	53.49	49.34	72.89	50.99	49.34
Gallidermin	43.5	44.47	51.16	46.97	76.37	50.6	48.91
Nisin A	23.08	28.2	...	43.5	46.61	22.12	*

(... indicates absence of corresponding gene and * indicates no significant similarity).

Based on sequence comparisons and gene arrangements within the cluster, it is evident that the identified class-I lanthipeptide gene clusters in 206 *S. aureus* strains are Bsa gene clusters.

Prepeptide sequences in the identified lantipeptide resemble Bsa variants

The 4 different prepeptide sequences have been termed Seq 1, Seq 2, Seq 3, and Seq 4, with frequencies of 197, 194, 8, and 6, respectively, across 206 identified gene clusters.

When the most prevalent prepeptide (Seq 1) of the identified lanthipeptides was aligned with the mentioned lantibiotics (Fig. 3), it showed total identity with Bsa being identical in all 47 residues. Hyicin 3682, a lantibiotic with the same length of prepeptide sequence, is similar to the query and Bsa at 40 positions. The query sequence shows significant dissimilarity to epidermin, gallidermin, and nisin A, with the lengths of the prepeptides also being notably different.

When the structural peptides (without leader sequences) of Seq 1, Seq 2, Seq 3, and Seq 4 were compared with Bsa variants, they showed identity with BsaA2, BsaA1, $BsaA2_{ET3\text{-}1}$, and $BsaA1_{ET3\text{-}1}$, respectively (Fig. 4).

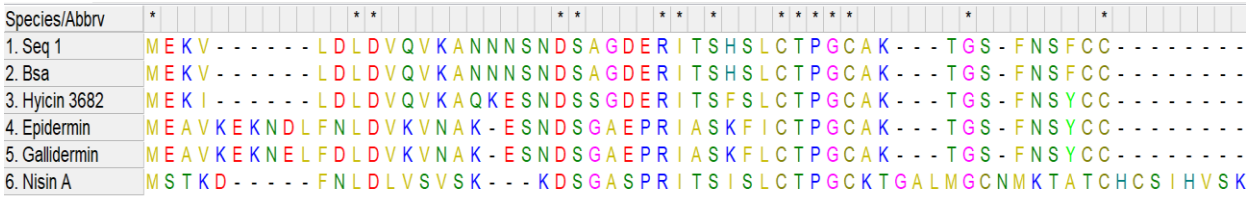

Fig. 3.Amino acid sequence alignment of the prepeptide sequence of Seq 1 with Bsa, Hyicin 3682, Epidermin, Gallidermin and Nisin A. (*) indicates conserved residues. The alignment was performed using MEGA11.

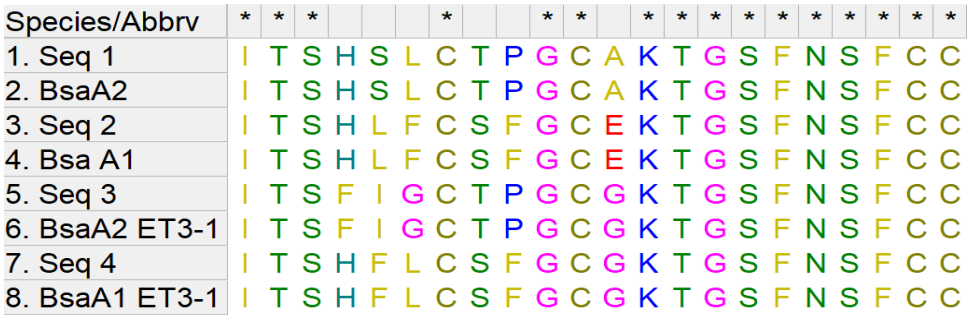

Fig. 4. Amino acid sequence alignment of the 4 different identified structural peptides with different Bsa variants. Seq 1, Seq 2, Seq 3 and Seq 4 are the identified structural peptides with different frequencies. BsaA2, BsaA1, $BsaA2_{ET3-1}$ and $BsaA1_{ET3-1}$ are the 4 variants of Bsa. The alignment was performed using MEGA11.

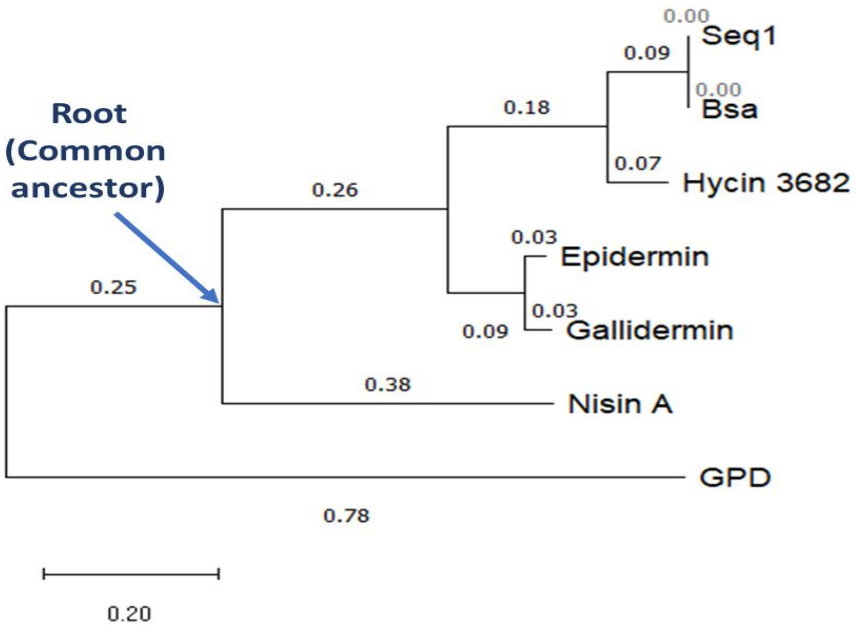

Fig. 5. Phylogenetic tree comprising the most prevalent prepeptide (Seq 1) and other comparable class I lantipeptides. Seq 1 and Bsa are identical showing 0.00 branch length from a common ancestor. Nisin A is the most diverged prepeptide in the group. To identify the common ancestor (root) of the sequences, the glyceraldehyde-3-phosphate dehydrogenase (GPD) sequence of *S. aureus* was used as the outgroup.

Phylogenetic study indicates that Bsa is the most evolved prepeptide within the comparative group

A phylogenetic tree was constructed comprising the most frequent prepeptide (Seq 1) and other class I lantipeptides using the neighbour-joining method (Fig. 5). The *S. aureus* glyceraldehyde-3-phosphate dehydrogenase (GPD) sequence was employed as the outgroup to identify the common ancestor (root) of the sequences. The tree illustrates that Seq 1, identified as Bsa, is the most evolved prepeptide and is significantly closer to hyicin 3682, forming the most divergent clade in the tree. Epidermin and gallidermin constitute an additional clade that has a common ancestor with the previously stated clade. Nisin A is the most divergent prepeptide derived from the root, exhibiting the greatest branch length (0.38) among the comparative group.

Genes from various clusters, aside from prepeptides, also exhibit a notable degree of similarity

The 4 different prepeptide sequences are arranged in 5 different types of biosynthesis gene clusters named CT1 (Cluster type 1), CT2, CT3, CT4 and CT5 having found in 197, 2, 2, 4 and 1 strains respectively (Fig. 6). The most prevalent cluster type (CT1) contains two genes encoding BsaA1 and BsaA2, whereas CT2 only contains $BsaA2_{ET3-1}$ followed by other genes of the clusters for lanthipeptide modification, cleavage and transportation. Like CT1, CT3 contains two successive genes encoding $BsaA1_{ET3-1}$ and $BsaA2_{ET3-1}$. A different picture is seen in CT4, where there are also two genes like CT3 but intervened by a transposase. The transposase gene is also observed in CT5 which separated the gene for BsaA1 and the modifying enzymes.

The genes of the clusters other than the prepeptides were compared with the corresponding genes of the other 5 clusters using the NCBI BLAST algorithm to understand the variability of their roles in producing and transporting the lanthipeptide (Table 2). All genes but one in CT4 and CT5 were identical with the genes of CT1. CT2 shows a little bit of dissimilarity in some of the genes while CT3 shows the most with none of the genes being identical with CT1.

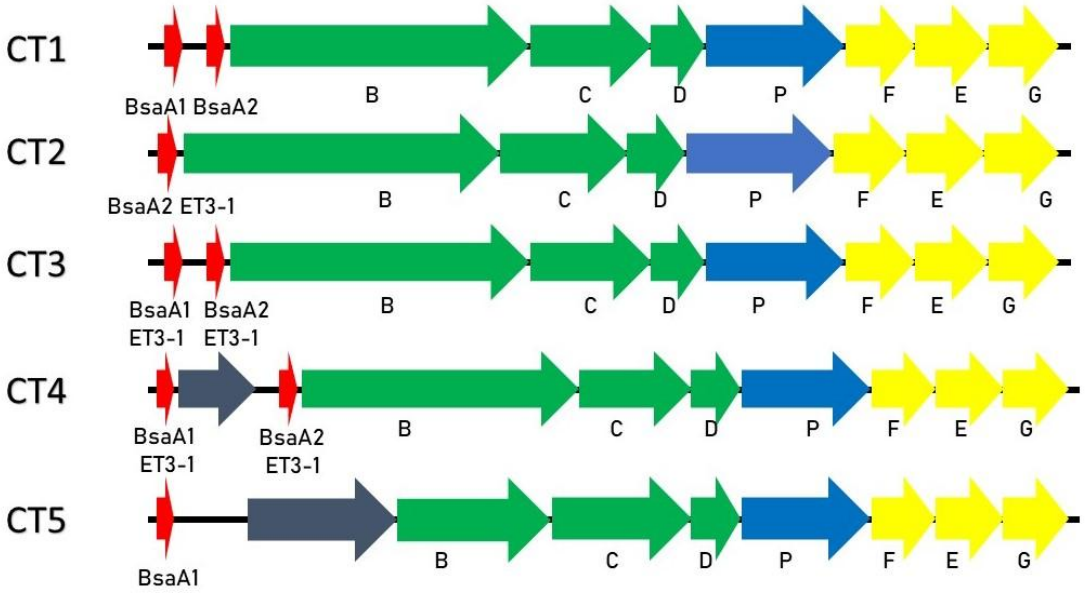

Fig. 6. Variation of Bsa lantibiotic gene clusters identified in *S. aureus* strains. Cluster types (CT) are differentiated by the presence of a single or two genes and a transposase gene. The prepeptide sequences have been labeled by identical matches with various Bsa variants. Functions of the rest of the genes are indicated by colors: red, precursor peptide; green, modification enzyme; blue, cleavage enzyme; yellow, transport and immunity protein; blue gray, uncharacterized protein.

Table 2. Sequence comparison of genes of CT1 with the corresponding genes of other clusters in terms of percentage of identity.

Gene	CT1						
Gene	**LanB**	**LanC**	**LanD**	**LanP**	**LanF**	**LanE**	**LanG**
CT2	93.58	98.07	99.42	94.75	100	100	100
CT3	92.88	88.89	97.67	94.53	97.39	95.26	98.71
CT4	100	99.76	100	100	100	100	100
CT5	98.04	100	100	100	100	100	100

Discussion

Bacterial genome mining is a powerful bioinformatics technique used to identify novel lantibiotics by analyzing bacterial genetic blueprints (Foulston, 2019). This technique involves identifying and characterizing biosynthetic gene clusters (BGCs) in bacterial genomes that encode lantibiotics (Foulston, 2019). Genome mining has identified several bacteriocins, including new variants. Examples include miticin, a leaderless bacteriocin identified in *Streptococcus mitis* (Alkassab et al., 2024). A similar technique was used to identify BGCs for bacillaene, bacillibacin, bacilysin, subtilosin, fengycin and surfactin in *Bacillus subtilis* BDSA1 (Saikat et al., 2024). Furthermore, genome mining has uncovered the prevalent presence of bacteriocin gene clusters in cyanobacteria (Wang et al., 2011). Meanwhile, *in silico* genome mining reveals novel bacteriocins that have not yet been identified in laboratories (Uniacke-Lowe et al., 2023).

The production of lantibiotics is mainly associated with Gram-positive non-pathogenic bacteria (Kashyap, 2019). But with advances in genetic analysis and the purification of compounds from community-acquired microbes, pathogenic species, e.g., *S. mutans*, *S. pyogenes*, and *S. aureus*, are also known to produce lantibiotics (Merritt and Qi, 2012; Biswas and Biswas, 2014; Kawada-Matsuo et al., 2016). To identify additional antimicrobial compound gene clusters, *S. aureus* was selected for analysis in this study, as four lantibiotics have already been reported to be produced by this pathogenic species (Daly et al., 2010).

When the genomes of more than 500 *S. aureus* strains were analyzed with antiSMASH Ver.7 a class I lanthipeptide gene cluster was present in 206 strains, along with other gene clusters for non-ribosomal peptide synthetase (NRPS), autoinducer, siderophore, metallophore, etc. Initially, the lanthipeptide was identified as hyicin 3682 by antiSMASH, as the number of genes in the cluster and their orientation matched almost identically. The prepeptide sequence was annotated as a gallidermin/nisin family lantibiotic (epiA) in both the antiSMASH and RefSeq databases. In this stage, the identified lanthipeptide was thought to be a variant of hyicin 3682, as their prepeptide sequences differ at 7 of 47 residues and at only 2 of 22 residues in the structural peptide. To be further confirmed, when the prepeptide sequence of the identified lanthipeptide was aligned with epidermin, Bsa (an epidermin variant), gallidermin, and nisin, it showed broad identity with Bsa. The results confirmed that the identified class I gene cluster encodes Bsa, which was isolated from a community-acquired *S. aureus* strain (Daly et al., 2010).

The 206 strains of *S. aureus*, in which the Bsa lantibiotic gene cluster was identified, possess 5 different types of arrangements of prepeptide-encoding genes. In contrast, the orientation of other

genes, i.e., modifying enzymes, protease, and immunity protein, remains the same (Fig. 6). In those 5 types of arrangements, prepeptide sequences of four Bsa variants, i.e., BsaA1, $BsaA1_{ET3-1}$, BsaA2, and $BsaA2_{ET3-1}$, were observed. These variants had previously been isolated from different strains of community-acquired *S. aureus* and show very little difference in their structural sequences (Daly et al., 2010). The presence of a transposase gene upstream and between the prepeptide genes indicates different arrangements of prepeptide genes, leading to further evolution of this cluster, and supports the non-production of Bsa by many *S. aureus* isolates despite containing loci that could be due to transposition of mobile DNA (Daly et al., 2010).

The similarity of the Bsa loci's genes has led to the annotation of hyicin 3682, an epidermin or gallidermin family lantibiotic. With the enrichment of microbial genomic data and the improvement of genome mining tools, it is now easier to analyze and annotate unrecognized genes that share identity or similarity with already identified and functional genes. This study further strengthens the effectiveness of genome mining and how it could identify genes encoding compounds of interest with minimal resources and time. Before targeting a microorganism to exploit its potential to synthesize novel compounds, genome sequencing followed by genome analysis would give indications of how that organism will respond during *in vitro* culture. This would surely lessen time and labor. However, this type of predictive analysis does not always guarantee *in vitro* production of antibiotics, as the cellular environment is full of dynamic molecules that can interfere with the production process, as well as genetic modifications.

The presence of the Bsa lantibiotic gene cluster in more than 206 *S. aureus* strains makes it a notable producer of lantibiotics. This might give these strains survival benefits over other closely related organisms. Production and purification are necessary to confirm whether these strains produce Bsa. *S. aureus*, a pathogenic species, has the potential to serve as a commercial producer of antimicrobial compounds.

Acknowledgment

The authors would like to acknowledge Department of Biochemistry and Molecular Biology, University of Dhaka and Department of Genetic Engineering and Biotechnology, University of Dhaka.

Authors contribution

Suvroto Kormokar: Conceptualization, experiment design, experiment conduction, result interpretation and writing draft. Md. Amzad Hossain: Conceptualization, experiment design, experiment conduction, result interpretation, writing draft, review and editing. M. Aftab Uddin: Conceptualization, writing draft, review and editing. Mohammad Riazul Islam: Conceptualization, experiment design, result interpretation, writing draft, review and editing.

Conflict of interest

The authors assert that the research was conducted without any commercial or financial links that could be perceived as a potential conflict of interest.

References

Alkassab D, Sampang J, Budhwani Z, Buragina JT, And Acedo JZ. Discovery of leaderless bacteriocins through genome mining. *Can. J. Chem.* 2024; 102: 533-543.

Allgaier H, Jung G, Werner RG, Schneider U and Zähner H. Elucidation of the structure of epidermin, a ribosomally synthesized, tetracyclic heterodetic polypeptide antibiotic. *Angew. Chemie Int. Ed. Engl.* 1985; 24: 1051-1053.

Arnison PG, Bibb MJ, Bierbaum G, Bowers AA, Bugni TS, Bulaj G, Camarero JA, Campopiano DJ, Challis GL, Clardy J, Cotter PD, Craik DJ, Dawson M, Dittmann E, Donadio S, Dorrestein PC, Entian KD, Fischbach MA, Garavelli JS, Göransson U, Gruber CW, Haft DH, Hemscheidt TK, Hertweck C, Hill C, Horswill AR, Jaspars M, Kelly WL, Klinman JP, Kuipers OP, Link AJ, Liu W, Marahiel MA,

Mitchell DA, Moll GN, Moore BS, Müller R, Nair SK, Nes IF, Norris GE, Olivera BM, Onaka H, Patchett ML, Piel J, Reaney MJT, Rebuffat S, Ross RP, Sahl H-G, Schmidt EW, Selsted ME, Severinov K, Shen B, Sivonen K, Smith L, Stein T, Süssmuth RD, Tagg JR, Tang G-L, Truman AW, Vederas JC, Walsh CT, Walton JD, Wenzel SC, Willey JM and van der Donk WA. Ribosomally synthesized and post-translationally modified peptide natural products: overview and recommendations for a universal nomenclature. *Nat. Prod. Rep* .2013; 30: 108-160.

Begley M, Cotter PD, Hill C and Ross RP. Identification of a novel two-peptide lantibiotic, lichenicidin, following rational genome mining for LanM proteins. *Appl. Environ. Microbiol.* 2009; 75: 5451-5460.

Biswas S and Biswas I. A conserved streptococcal membrane protein, lsrs, exhibits a receptor-like function for lantibiotics. *J. Bacteriol* .2014;196: 1578-1587.

Blin K, Shaw S, Augustijn HE. Reitz ZL, Biermann F, Alanjary M, Fetter A, Terlouw BR, Metcalf WW, Helfrich EJN, van Wezel GP, Medema MH and Weber T. antiSMASH 7.0: new and improved predictions for detection, regulation, chemical structures and visualisation. *Nucleic Acids Res.* 2023; 51: W46-W50.

Carlin FP, Nascimento de Sousa Santos I, Silva Francisco M, Mattos AlbanoR and do Carmo de Freire Bastos M. Genetic and biochemical characterization of hyicin 3682, the first bacteriocin reported for *Staphylococcus hyicus*. *Microbiol. Res.* 2017; 198: 36-46.

Cox C, Coburn P and Gilmore M. Enterococcal cytolysin: A novel two component peptide system that serves as a bacterial defense against eukaryotic and prokaryotic cells. *Curr. protein Pept. Sci.* 2005; 6: 77-84.

Daly KM, Upton M, Sandiford SK, Draper LA, Wescombe PA, Jack RW, O'Connor PM, Rossney A, Götz F, Hill C, Cotter PD, Ross RP and Tagg JR. Production of the Bsa lantibiotic by community-acquired *Staphylococcus aureus* strains. *J. Bacteriol.* 2010; 192: 1131-1142.

Foulston L. Genome mining and prospects for 2019; 51: 1-8.

Kaletta C, Entian K-D, Kellner R, JungG, ReisM and Sahl HG. Pep5, a new lantibiotic: structural gene isolation and prepeptide sequence. *Arch. Microbiol.*1989;152: 16-19.

Kashyap DR. Microbial metabolites: peptides of diverse structure and function. In: *New and future developments in microbial biotechnology and bioengineering,* Gupta VK and Pandey A, eds., Elsevier, 2019; p. 87-101.

Kawada-Matsuo M, Shammi F, Oogai Y, Nakamura N, Sugai M and Komatsuzawa H. C55 bacteriocin produced by ETB-plasmid positive *Staphylococcus aureus* strains is a key factor for competition with *S. aureus* strains. *Microbiol. Immunol.* 2016; 60: 139-147.

Kellner R, Jung G, Horner T, Zähner H, Schnell N, Entian KD and Götz F.Gallidermin: a new lanthionine-containing polypeptide antibiotic. *Eur. J. Biochem.*1988; 177: 53-59.

Merritt J and Qi F. The mutacins of *Streptococcus mutans*: regulation and ecology. *Mol. Oral Microbiol.* 2012; 27: 57-69.

Navaratna MA, Sahl HG and Tagg JR. Two-component anti-*Staphylococcus aureus* lantibiotic activity produced by *Staphylococcus aureus* C55. *Appl. Environ. Microbiol.*1998; 64: 4803-4808.

O'Sullivan JN, O'Connor PM, Rea MC, O'Sullivan O, Walsh CJ, Healy B, Mathur H, Field D, Hill C and Ross RP. Nisin J, a novel natural nisin variant, is produced by *Staphylococcus capitis* sourced from the human skin microbiota. *J. Bacteriol.* 2020; 202(3): e00639-19.

Saikat TA, Sayem Khan MA, Islam MS, TasnimZ and Ahmed S. Characterization and genome mining of *Bacillus subtilis* BDSA1 isolated from

river water in Bangladesh: A promising bacterium with diverse biotechnological applications. *Heliyon*, 2024;10: e34369.

Schnell N, Engelke G, Augustin J, Rosenstein R, UngermannV, Götz F and Entian K-D. Analysis of genes involved in the biosynthesis of lantibiotic epidermin. *Eur. J. Biochem.*1992; 204: 57-68.

Scott J. Lantibiotic-mediated anti-lactobacillus activity of a vaginal *Staphylococcus aureus* isolate. *FEMS Microbiol. Lett.* 1992; 93: 97-102.

Singh M and Sareen D. Novel LanT associated lantibiotic clusters identified by genome database mining. *PLoS One*, 2014; 9: e91352.

Tamura K, Stecher G and Kumar S. MEGA11: Molecular evolutionary genetics analysis version 11. *Mol. Biol. Evol.* 2021; 38: 3022-3027.

Trmčić A, Samelis J, Monnet C, Rogelj I and Matijasic BB**.** Complete nisin A gene cluster from *Lactococcus lactis* M78 (HM219853) — obtaining the nucleic acid sequence and comparing it to other published nisin sequences. *Genes Genom.* 2011; 33: 217-221.

Uddin MA, Akter S, Ferdous M, Haidar B, Al Amin, Molla AHMSI, Khan H and Islam MR. A plant endophyte *Staphylococcus hominis* strain MBL_AB63 produces a novel lantibiotic, homicorcin and a position one variant. *Sci. Rep.* 2021; 11: 11211.

Uniacke-Lowe S, Collins FWJ, Hill C and Ross RP. Bioactivity screening and genomic analysis reveals deep-sea fish microbiome isolates as sources of novel antimicrobials. *Mar. Drugs*, 2023; 21: 444.

Valsesia G, Medaglia G, Held M, Minas W and Panke S. Circumventing the effect of product toxicity: development of a novel two-stage production process for the lantibiotic gallidermin. *Appl. Environ. Microbiol.* 2007; 73: 1635-1645.

van Heel AJ, de Jong A, Song C, Viel JH, Kok J and Kuipers OP. BAGEL4: a user-friendly web server to thoroughly mine RiPPs and bacteriocins. *Nucleic Acids Res.* 2018; 46: W278-W281.

van Staden ADP, van Zyl WF, Trindade M, Dicks LMT and Smith C. Therapeutic application of lantibiotics and other lanthipeptides: old and new findings. *Appl. Environ. Microbiol.* 2021; 87: e0018621.

Wang H, Fewer DP and Sivonen K. Genome mining demonstrates the widespread occurrence of gene clusters encoding bacteriocins in cyanobacteria. *PLoS One* 2011; 6: e22384.

Willey JM and van der Donk WA. Lantibiotics: peptides of diverse structure and function. *Annu. Rev. Microbiol.* 2007; 61: 477-501.

Wladyka B, Wielebska K, Wloka M, Bochenska O, Dubin G, Dubin A and Mak P. Isolation, biochemical characterization, and cloning of a bacteriocin from the poultry-associated *Staphylococcus aureus* strain CH-91. *Appl. Microbiol. Biotechnol.* 2013; 97: 7229-7239.

J. Bangladesh Acad. Sci. 49(2); 189-204: December 2025 DOI:https://doi.org/10.3329/jbas.v49i2.81269

Journal of Bangladesh Academy of Sciences

Journal homepage: http://www.bas.org.bd/publications/jbas.html

Research Article

Environmental and techno-economic feasibility study of photovoltaic systems in Northern Bangladesh

Md. Ahsan Habib*, Md. Masum Billah[1], Jannatun Ferdous[2], Faridul Islam and Rauf Khan[3]

Department of Electrical and Electronic Engineering, Begum Rokeya University, Rangpur, Bangladesh

INFO

Article History

Received: 25 April 2025
Revised: 29 June 2025
Accepted: 19 August 2025

Keywords: Photovoltaic (PV), Emission, Sensitivity analysis, Risk analysis, RETScreen, Homer.

ABSTRACT

The feasibility study for the photovoltaic solar systems in Rajshahi, Bogura, and Sirajganj regarding Bangladesh, comprehensively addresses financial, technical, and environmental factors to attract both the national and international investors. The objective of the analysis is to evaluate photovoltaic (PV) solar systems in northern cities of the Bangladesh; Rajshahi, Bogura, and Sirajganj to minimize the effect of the global warming caused by burning of the fossil fuels as well as to improve region's sustainable development, which was hampered by the factory pollution. To analyze study and the verify its techno-economic and environmental sustainability, RETScreen Expert and Homer software is utilized. Sensitivity analysis emphasizes importance of the considering the diesel prices, inverter efficiency, and interest rates, as these factors significantly impact cost of energy (COE). Among these zones, Rajshahi attitudes out with lowest total emissions and the carbon dioxide levels, making it the furthermost favorable option for the reducing pollution and advancing the sustainable technology in this region.

Introduction

Bangladesh is the developing country that is the almost entirely electrified at this time. Approximately 100% of the Bangladesh's population has access to the electricity from both the renewable and the non-renewable sources. (BPDB, 2021). Electricity demand is constantly increasing due to a rapidly growing population and economic growth. There is always a large gap between electricity supply and demand. In 2041, Bangladesh's total power demand is expected to be around 50,000 megawatts (BER, 2022). To meet this demand, fossil fuels such as coal, gas, and oil are used to generate electricity. To generate electricity (Sarkar et al., 2015), only a limited amount of fossil fuel resources is available. As a result, the storage of fossil fuels has reached an alarming level. The use of fossil fuels has negative effects on the atmosphere and environment. As a result, the demand for alternative energy resources to generate electricity has increased.

Many researchers have examined various renewable energy sources (Rashwan et al., 2017; Hasan and Habib, 2025; Habib and Asgar, 2025), particularly solar energy, to produce environmentally friendly, sustainable electricity. To go for sustainable (Habib et al., 2020a), techno-economic (Noman et al., 2023), and environmentally friendly electricity (Habib et al., 2022), several strategies; decision-making processes (Habib et al., 2020b and Mondal et al., 2009), optimization, etc., are presumed (Habib, 2023) Islam

*Corresponding author:<emonape@gmail.com>

[1]*Department of Physics, Jashore University of Science and Technology, Bangladesh;* [2]*Department of Electronics and Communication Engineering, Hajee Mohammad Danesh Science & Technology University, Dinajpur, Bangladesh;*
[3]*Research Center for Materials Nanoarchitectonics (MANA), National Institute for Materials Science (NIMS), Tsukuba, Japan*

et al. (2022a) suggested multiple optimal fusions to minimize grid dependency and identified the optimum combination of hybrid energy systems comprising nonrenewable and renewable energy for Nilphamari, Bangladesh. Islam et al. (2022b) designed a model using PVsyst software to evaluate and develop a solar photovoltaic rooftop system with a grid-connected system in Bangladesh. Mondol et al. (2009) assessed a 500 kW grid-connected photovoltaic (PV) solar system in southern Bangladesh. Rahman et al. (2018) discussed a hybrid optimization model for obtaining continuous power. Nikita et al. (2016) surveyed several areas in the northwestern region of Bangladesh to assess the viability of PV-based solar electricity generation. Khandelwal and Shrivastava (2017) assessed performance of the 600kW grid-connected photovoltaic system for the Rajasthan village, India. Mehmood et al. (2014) settled the model of the 5kW solar PV stand-alone system to meet the Pakistan's household power demand, for the considering the payback periods, the net present value (NPV), the internal rate of return (IRR), and the greenhouse gas emissions. In the evolutionary game setting, Habib et al. (2022) scrutinized cost-benefit subsidy regarding power generator system, considering rapid growth of global economy and industry. Thevenard et al. (2000) estimated probable potential of the renewable energy system by the providing the initial estimate of size of solar array, pump, or battery. Mirzahosseini and Taheri (2012) projected new electricity tariffs based on the solar photovoltaic power plant's environmental, technical, and economic viability. Mukherjee and Razzak (2017) assessed a 100 kW grid-connected photovoltaic solar system, which has the potential to reduce greenhouse gas emissions by approximately 166 tons per year. Tahera et al. (2019) designed a project to assess the payback period and feasibility of a local grid-connected PV solar project for the residential hall at Bangladesh University of Engineering and Technology. Uddin et al. (2016) surveyed the cost and probable performance of a wind power plant on the Chittagong coastline in Bangladesh. Khan et al. (2009) analyzed the financial and technical information of a photovoltaic system with a small solar grid in the Rangamati district of Bangladesh. Rashid and Habib (2018) presented a Boost converter for solar power control by simulating the system and observing the control mechanism for power-point tracking in Simulink/MATLAB. Habib (2022a) used statistical methods to assess the characteristics of wind speed data from Rangpur, Bangladesh, from 2016 to 2020. The techno-economic feasibility study aimed to optimize the PV-Wind-Hydro hybrid power system in Fukuoka, Japan, as discussed in Habib et al. (2024).

Financial parameters, feasibility analysis, sensitivity analysis, and risk analysis issues were considered on the application of photovoltaic solar energy; Owolabi et al. (2019) established a strategy map for PV solar energy according to Sambo (2009), the investors of the solar energy to make investments in the technology of green energy, such as photovoltaic solar energy, from the underutilization and plentiful of photovoltaic energy in the northern part of Nigeria. This study is only for Nigeria, but almost no similar research has been conducted in the northern part of Bangladesh. So, this research focuses on the northern part; Rajshahi, Bogura, and Sirajganj of Bangladesh, to assess the system.

This paper examines photovoltaic solar systems for producing electricity in the northern regions of Bangladesh: Rajshahi, Bogura, and Sirajganj. This study assesses cost, feasibility, sensitivity, risk, and performance analyses for the RETScreen Expert and Homer software.

The remainder of this paper is organized as follows: Section 2 presents details about the site location. Section 3 establishes the design parameters for a photovoltaic solar system. Section 4 presents results from RETScreen and includes a detailed discussion. Section 5 outlines the materials and methods used for HOMER. Section 6 showcases results and discussion from HOMER. Finally, Section 7 draws the conclusions.

Site location

Bangladesh is almost entirely surrounded by India in the south-subtropics and tropics of Asia, with the only other neighbors being Myanmar to southwest and the Bay of Bengal to the south. The geographical position of Bangladesh extends between latitude: 20°34' to

26°38' and longitude: 88°01' to 92°41' (Bangladesh-An-Introduction). The solar angle of Bangladesh ranges from 40 to 90 degrees due to its location (Mengen et al., 2018). This representsthe study area: Rajshahi (latitude 24.4°, and longitude 88.6°), Bogura(latitude 24.8°, and longitude 89.4°), and Sirajganj (latitude 24.5°, and longitude 89.7°) of Bangladesh.

Design parameters of the PV system

This section discusses the project parameters, technical parameters and methodology of the PV system being measured for the installation of a photovoltaic solar project in the northern region of Bangladesh, specifically Rajshahi, Bogura, and Sirajganj. This includes the PV solar system, the power generation factor, the demand for electricity, the required energy from the PV module size, the inverter size, the battery size, and the capacity factor (Chande et al., 2014). This project is planned for the 100MW solar photovoltaic system.

Panel generating factor

The size of the photovoltaic solar cells is well-defined by the panel generation factor (PGF), which is based on total wattage rating and varies with the solar intensity and length of sunshine [How to Design Solar PV System, 2025]. The PGF for the Bangladesh is calculated as the 2.8, using following formula (Design Solar PV System, 2022).

The Panel Generation Factor = (Solar irradiance × Sunshine hour)/Standard test conditions irradiance (1)

The average solar irradiance = 215 W/m^2 (Owolabi et al., 2019), average sunshine hours = 13 hours (Chande et al., 2014) and standard test conditions irradiance = 1000 W/m^2 (Khan et al., 2015).

Energy of PV modules

The required energy of PV components is calculated using the following formula (Design Solar PV System, 2022) . The total daily electricity demand of the three villages in Rajshahi, Bogura, and Sirajganj, is considered 300 households (an average of 8 people per household) (Standard Test Conditions, 2022). The daily electricity demand in Godagari, Rajshahi, is 35270 kWh/d, in Kahaloo, Bogura, is approximately 31250 kWh/d, and Sadar, Sirajgonj, is approximately 29210 kWh/d. The total daily electricity demand for the three locations is considered 95730 kWh.

The energy loss of the system = 1.3 (Design Solar PV System, 2022).

Energy of PV modules = the requirement of peak energy × energy loss of the system (2)

Energy of PV modules = 95,730×1.3 = 124,449 kWh/d.

Total peak watt rating of PV modules

The total peak watt rating is determined using the following equation (Design Solar PV System, 2022).

Total peak watt rating = Solar PV energy required/ Panel generation factor (3)

Total peak watt standing = (124,449)/2.8 = 44,446.07 kW

PV modules

The mono-silicon China Sunergy CSUN200-72M PV module, with an output power rating of 200W, is chosen for the proposed power plant and photovoltaic solar cell. The technical details of the mono-silicon China Sunergy CSUN200-72M are demonstrated in Table 1.

Required number of PV modules

The following equation computes the total number of PV modules required in the power plant (Design Solar PV System, 2022).

Required number of the PV modules = Total watt peak rating / PV module peak rated output (4)

Required number of PV modules = 44,446.07 / 200 = 222,230.35 ~ 222,231 modules

The size of the inverter

The following formula is used to determine the inverter size.

Inverter size = the requirement of peak energy × safety factor (Design Solar PV System, 2022) (5)

The size of inverter =124,449 kWh × 1.3 = 161783.7 kW

Battery sizing

The following equation determines the battery's size (Design Solar PV System, 2022).

Battery sizing = (Daily power consumption × Days of

autonomy) / (Battery efficiency × Depth of discharge × Battery nominal Voltage) (6)

Battery sizing = (124,449 kW × 3) / (0.85 × 0.6 × 12) = 61004.41 Ah

Daily power consumption = 124,449 kW, days of autonomy = 3, the efficiency of battery = 85%, depth of the discharge = 60%, and battery nominal voltage = 12V (Design Solar PV System, 2022).

Capacity factor

The following formula is used to calculate capacity (Lee et al., 2012).

CF= (Annual kilowatt hours produced per kilowatt AC peak capacity (kWh/kWp))/(8760 h in a year)

The required energy to be produced by the plant = 124,449 kWh/d. Annual energy to be generated from the plant = 124,449 kWh × 365 = 45,423,885 kWh

Peak capacity demand of PV plant=105 kWp CF= (45,423,885/100,000,000)/8760 = 5.18%--

Table 1. Detail of mono-silicon China Sunergy CSUN200-72M.

Parameters	Values
Maximum Power (P_{max})	200 W
Positive Power Tolerance	0-3%
Open Circuit Voltage (V_{OC})	45.3 V
Short Circuit Current (I_{sc})	5.72 A
Maximum Power Voltage (V_{mpp})	37.6 V
Maximum Power Current (I_{mpp})	5.32 A
Module Efficiency	15.67 %
Voltage Temperature Coefficient	−0.307 %/K
Current Temperature Coefficient	+0.039 %/K
Power Temperature Coefficient	−0.423 %/K

Results and Discussion

The financial and environmental parameters, the energy product, and the greenhouse gas (GHG) emissions are used to evaluate the optimization issues of this proposed photovoltaic solar system. The RETScreen expert software produced the result; climate data for the named position, parametric parcels of China surnergy solar PV module, photovoltaic solar energy overview per position, financial input variables, financial output variables, gross GHG emissions, and periodic GHG emissions profit for the three location are represented respectively in Tables 2, 3, 4, 5, 6, 7, and 8. A thorough feasibility study reveals the specialized, profitable, environmental, and risk/sensitivity outcomes.

Technical viability

The ability of any solar photovoltaic module to generate electricity is affected by solar radiation per location as well as the quantity of pure sunny days (Khandelwal and Shrivastava, 2017), the annual electricity exported to the national grid from the capacity utilization factor (CUF) and the panel (Mehmood et al., 2014). As shown in Table 2, the Rajshahi district has the highest monthly average solar radiation of 4.87 kWh/m^2/d and Sirajganj and Bogura districts have the lowest monthly average solar radiation of 4.74 kWh/m^2/d. The properties of the China Sunergy mono-si-CSUN200-72M PV module were determined using the RETScreen Expert software and are shown in Table 3. The mono-silicon China Sunergy CSUN200-72M solar PV module has a 15.67% efficiency. Table 4 displays the overview of photovoltaic solar energy for a specific location. Rajshahi district has the largest annual electricity export to the national grid of 140,155 MWh and the highest capacity factor of 16%. Sirajganj district has the lowest annual electricity export to the national grid of 136,969 MWh and the lowest capacity factor at 15.6%. Bogura district has a capacity factor of 15.7% and an annual energy export to the grid of 137,481 MWh. Fig. 1 shows the monthly variation in daily solar radiation at three locations. The Rajshahi district has the highest daily sun radiation of 6.43 kWh/m^2/d in April, and the Bogura district has the lowest daily solar radiation of 3.91 kWh/m^2/d in September.

Based on the photovoltaic solar system's technological viability, the values are attained as yearly electricity exported to the national grid as well as capacity factors for each of Rajshahi, Bogura, and

Table 2. Climate data of the selected location.

Location	Bogura	Sirajganj	Rajshahi
Latitude	24.8	24.5	24.4
Longitude	89.4	89.7	88.6
Elevation	25	20	22
Heating design temperature (℃)	14	14	13.9
Cooling design temperature (℃)	31.7	31.7	32
Earth temperature amplitude (℃)	15	15	16.9
The monthly average solar radiation kWh/m^2/d)	4.74	4.74	4.87

Table 3. Parametric properties of China surnergy solar module.

Property	Value
PV technology type	mono-Si
Power capacity	100,000 kW
Manufacturer	China Surnergy
Model	mono-Si-CSUN200-72M
Number of units	500,000
Efficiency	15.67%
Nominal operating temperature	45 ℃
Temperature coefficient	0.4%/ ℃
Solar collector area	638162 m^2

Sirajganj in Bangladesh. Therefore, it is technically feasible to construct and operate photovoltaic solar power plants in Rajshahi, Bogura, and Sirajganj using the suggested system.

Economic sustainability

The development of a solar photovoltaic plant requires careful economic analysis. An economic analysis of a solar photovoltaic project establishes its economic

Table 4. Photovoltaic solar energy overview per location.

Locations	Capacity factor	Annual energy exported	Annual electricity exported revenue
Bogura	15.7%	137,481MWh	$ 13,748,101
Sirajganj	15.6%	136,969MWh	$ 13,696,915
Rajshahi	16%	140,155MWh	$ 14,015,512

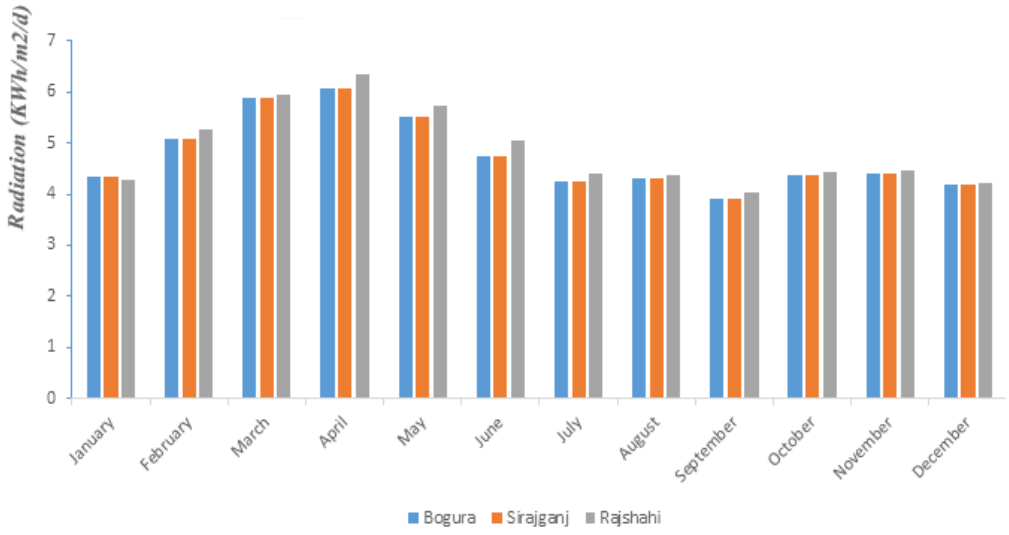

Fig. 1. Monthly variance in daily solar radiation for three different places.

viability and sustainability. As shown in Table 5, the economic analysis worksheet for the software includes financial factors such as escalation rate, fuel, debt term, debt ratio, debt interest rate, electricity export rate, and inflation rate. The software directly obtains the default configuration for the input parameters. Based on the entered inputs, the RETScreen software estimated Net Present Value (NPV), the Internal Rate of Return (IRR), annual life savings, and other economic factors, as shown in Table 6. According to the Table 6, the project in northern cities of Bangladesh; Rajshahi, Bogura, and Sirajganj has a positive net present value (NPV), making it profitable and economically viable (Islam et al., 2022a). In Table 6, the COE (Energy production cost ($/kWh)) for Bogura, Rajshahi and Sirajganj are 0.097$, 0.095$, and 0.097$, respectively.

The period of time required for the planned project to recover its initial cost is called the payback period. Fig. 2 shows the payback period for the northern region Bangladesh, including Rajshahi, Bogura, and Sirajganj. The suggested system's payback duration; simple payback period, and equity payback period were computed based on its 20-year lifespan. Rajshahi district has the lowest payback period at 8.7 years, whereas Bogura district has the greatest payback period of 8.9 years. The district of Bogura and Sirajganj has an 8.9-year payback time. The financial viability of solar PV systems is unaffected by the break-even year. Rajshahi district has the shortest equity payback period at 6.4 years, while Bogura and Sirajganj district has the longest at 6.8 years.

Table 5. Financial input parameters by RETScreen Expert.

Financial parameters	Value
Escalation rate fuel	2%
Inflation rate	2%
Discount rate	9%
Reinvestment rate	9%
Project Life	20
Debt ratio	70%
Debt interest rate	7%
Debt term	15 yr.
Debt payment	$9222748/yr.
Electricity export rate	$0.095/kWh
Electricity export escalation rate	2%
Initial cost	$120,000,000
O & M cost	$1,000,000
Total annual cost	$10,222,748

Table 6. Financial output variables.

Financial viability	Bogura	Sirajganj	Rajshahi
Internal rate of return (%)	17.1	16.9	17.8
Net Present Value (NPV) ($)	32,409,498	31,838,147	35,394,398
Annual life cycle savings ($)	3,550,346	3,487,757	3,877,332
Benefit-cost (B-C) ratio	1.9	1.9	2
Debt service charge	1.5	1.5	1.5
Energy production cost ($/kWh)	0.097	0.097	0.095

Fig. 3 shows the total cash flow of the proposed project after 20 years in three locations in Bangladeshi: Rajshahi, Bogura, and Sirajganj. The project's highest profit is $160,073,300 in Rajshahi district, and its lowest is $151,908,097 in Sirajganj district. In addition, the project profit in the Bogura district is $153,219,926.

Emission reduction assessment

The RETScreen software was used to determine the gross annual greenhouse gas emission reductions of

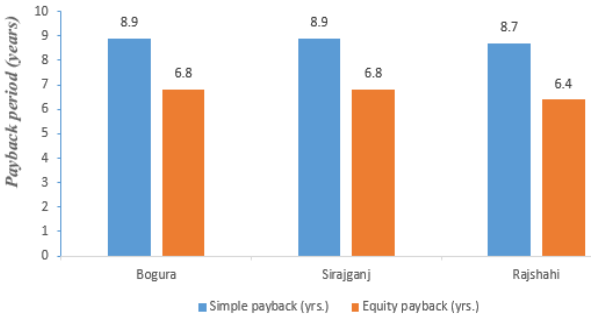

Fig. 2. The payback period for the three locations of proposed project.

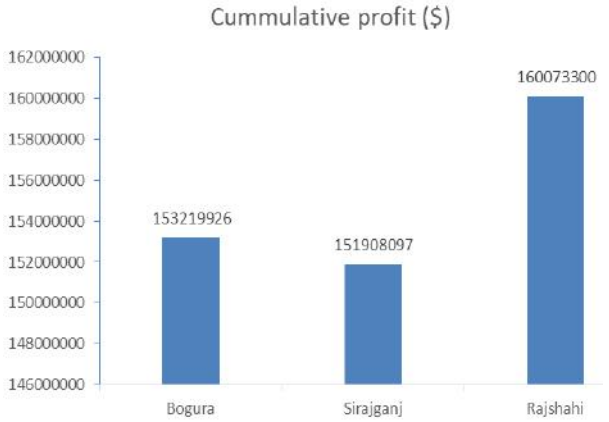

Fig. 3. The total cash flow for the project after 20 years.

the selected locations. The GHG emission reduction is obtained by excluding the determined emission of the proposed case from the determined emission of the baseline case, as shown in Table 7. The GHG emission reduction for the selected locations is illustrated in Fig. 4. Sirajganj district has the lowest GHG emission of 77184.4 tCO2, equivalent to 7,099 hectares of forest absorbing carbon. Rajshahi district has the highest GHG emission of 78979.7 tCO2, which corresponds to 7,264.1 hectares of forest absorbing carbon. Bogura district emits 77472.8 tCO2, which corresponds to 7,125.5 hectares of carbon-absorbing forest.

The software calculated the GHG-emissions-reduction revenue for three locations in Bangladesh: Rajshahi, Bogura, and Sirajganj, as shown in Table 8. Any investor is encouraged to profit from selling GHG emissions reductions rather than carbon trading. The estimated credit rate for GHG emissions

Table 7. Annual GHG emission of the three locations.

Location	Based case (tCO_2)	Proposed case (tCO_2)	Gross annual GHG emission reduction (tCO_2)
Bogura	83304.1	5831.3	77472.8
Sirajganj	82994.0	5809.6	77184.4
Rajshahi	84924.4	5944.7	78979.7

Table 8. Annual GHG emissions revenue for the three locations.

Location	Bogura	Sirajganj	Rajshahi
Net GHG reduction (tCO_2/yr.)	77,473	77,184	78,980
Net GHG reduction for 20 yrs. (tCO_2/yr.)	1,549,457	1,543,688	1,579,595
GHG reduction credit rate ($/($tCO_2$/yr.)	10	10	10
GHG reduction revenue ($)	774,728	771,844	789,797
GHG reduction credit duration (yr.)	15	15	15
Net GHG reduction for 15 yrs. (tCO_2/yr.)	1,162,092	1,157,766	1,184,696

reduction is $10 for a 15-year lifespan with a 2% annual escalation rate. Rajshahi district has the highest net GHG emissions reduction of 1,579,595 tCO2/year, while Sirajganj district has the lowest net GHG emissions reduction of 1,543,688 tCO2/year. Sirajganj has a net GHG emissions reduction of 1,549,457 tCO2/year. This is because Rajshahi district emits the most GHG emissions among the other districts.

Sensitivity analysis

RETScreen software creates the sensitivity analysis worksheet. The sensitivity analysis worksheet reduces uncertainty by comparing two input variables to the calculated financial parameters, as shown in Fig. 5.

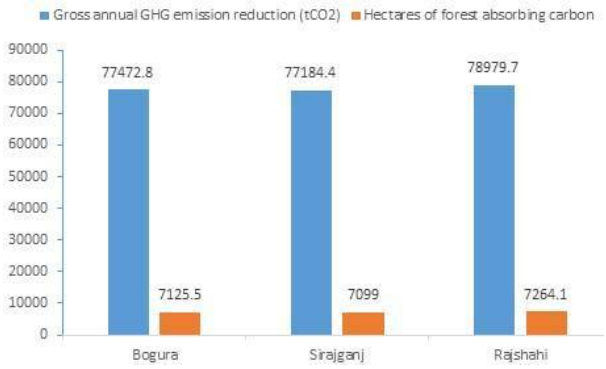

Fig. 4. Gross annual GHG emission and the corresponding hectares of forest absorbing carbon.

The sensitivity analysis is performed only for the photovoltaic solar system in the Rajshahi district because it offers superior technological, economic, and environmental analyses compared to the other regions. The proposed project's net present value (NPV) was subjected to a sensitivity study. Fig. 5 shows the sensitivity analysis worksheet, varying the initial cost in contradiction of the debt interest rate by ±25% for scenario 1 (Fig. 5) and the initial cost in contradiction of the electricity exported to the grid by ±25% for scenario 2 (Fig. 5).

The initial cost in Scenario 1 is calculated to be $120,000,000 with a ±25% discount. The initial costs will be $150,000,000 and $90,000,000, respectively. The original debt interest rate is 7%, but after a ±25% increase, the debt interest rate is 8.75% and 5.25%, respectively. The NPV value and the debt interest rate for the initial cost combination are recalculated while all other parameters remain constant. The software uses orange to identify NPV values less than zero. The project will not be financially profitable with a 25% increase in the starting cost and a 25% decrease in the debt interest rate, since the NPV would be -$2,719,204. If the debt interest rate is raised by 25% while the initial cost is decreased by 25%, the solar PV system project becomes economically viable because the net present value is $ 68,981,014, which is significantly greater than zero. This indicates that the net present value (NPV) is more responsive to the initial cost than the project's debt interest rate. Also, in Scenario 2, the initial cost is measured in terms of electricity exported to the national grid, as shown in Fig. 5.

The proposed project will be economically profitable if the preliminary cost is reduced while increasing the

Sensitivity analysis

Perform analysis on: Net Present Value (NPV)
Sensitivity range: 25%
Threshold: 0 $

- Remove analysis

Debt interest rate		Initial costs: 90,000,000	105,000,000	120,000,000	135,000,000	150,000,000
%		-25.0%	-12.5%	0.0%	12.5%	25.0%
5.25%	-25.0%	68,981,014	56,188,499	43,395,985	30,603,471	17,810,956
6.13%	-12.5%	66,021,315	52,735,518	39,449,720	26,163,923	12,878,126
7.00%	0.0%	62,979,823	49,187,111	**35,394,398**	21,601,685	7,808,972
7.88%	12.5%	59,859,379	45,546,592	31,233,806	16,921,019	2,608,232
8.75%	25.0%	56,662,918	41,817,388	26,971,857	12,126,327	-2,719,204

- Remove analysis

Electricity exported to grid		Initial costs: 90,000,000	105,000,000	120,000,000	135,000,000	150,000,000
MWh		-25.0%	-12.5%	0.0%	12.5%	25.0%
105,116.34	-25.0%	25,460,382	11,667,669	-2,125,043	-15,917,756	-29,710,469
122,635.73	-12.5%	44,220,103	30,427,390	16,634,677	2,841,965	-10,950,748
140,155.12	0.0%	62,979,823	49,187,111	**35,394,398**	21,601,685	7,808,972
157,674.51	12.5%	81,739,544	67,946,831	54,154,119	40,361,406	26,568,693
175,193.90	25.0%	100,499,265	86,706,552	72,913,839	59,121,127	45,328,414

Fig. 5. Sensitivity analysis outcome of the photovoltaic solar project in Rajshahi.

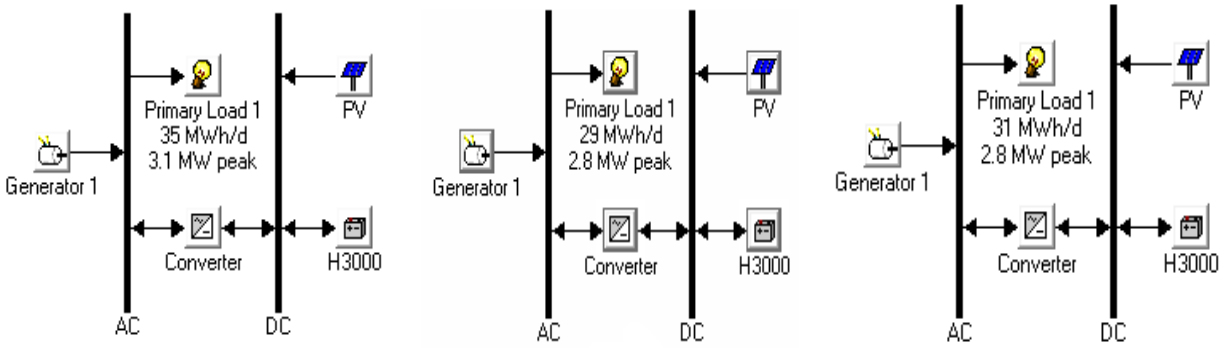

a) Rajshahi **b) Bogura** **c) Sirajganj**

Fig. 6. Configuration of the proposed hybrid system at a) Rajshahi, b) Bogura, and c) Sirajganj, Bangladesh.

value of the electrical energy exported to the national grid. In both scenarios, the initial cost has a greater impact on net present value (NPV) than the debt interest rate and the quantity of electrical energy exported to the national grid.

HOMER simulation methods with materials

This section is essential for researchers seeking to comprehend the study's methodology and for those aiming to extend or confirm its results.

The Configuration of HOMER Simulation

The HOMER software package integrates the simulation, the optimization, and the sensitivity analysis to the accurately assess energy balance across the various seasons. By the modeling energy production and the consumption dynamically, HOMER detects the viable solutions throughout the system's lifecycle. It also computes the levelized cost of energy (LCOE) to evaluate economic viability of energy systems. The next section details the calculation method for Net Present Cost (NPC) as follows:

$$NPC = I + \sum_{i=1}^{n} (C_y)[\frac{1}{(1+d)^i}]$$

I is for initial investment, n is the life span of project, C_y is yearly cost (including O (Operation)) & M (Maintenance) and replacement), and d is discount rate. The levelized cost of energy is expressed as:

$$COE = \frac{NPC}{\sum_{i=1}^{n}(E_y)[\frac{1}{(1+d)^i}]}$$

E_y is the yearly electricity served.

Configuration of the proposed system

The proposed system configuration is shown in Fig.6 and includes a PV source, diesel generator, a converter, and loads. Detailed specifications for each component are provided below.

PV array

The PV array is a crucial component of the energy system, representing the interconnected setup of individual PV modules. The HOMER software evaluates the power output of the PV array using the following equation: $P_{PV} = f_{PV} Y_{PV} \frac{I_T}{I_S}$

Where, f_{PV} is the PV derating factor, Y_{PV} represents the rated capacity of the PV array (KW), I_T introduces the global solar radiation (beam plus diffuse) incident on the surface of the PV array (KW/m^2), and I_S is the standard radiation rate (KW/m^2). Various PV panel sizes, ranging from 0 kW to 4000 kW, were considered for optimization across all sites.

Diesel Generator

To improve system reliability, a 24 kW diesel generator, costing $10,058, has been incorporated into

the energy scheme to provide backup power during periods when renewable sources fall short (Standard Test Conditions (STC) of a Photovoltaic Panel, 2022). This generator consumes 5000 liters of fuel annually and has a lifespan of 15,000 operational hours. The optimization process assesses the range of the diesel generator sizes from the 0 kW to the 500 kW to the guarantee the continuous power supply.

Converter

The converter, which includes both the rectifier and the inverter, is the essential to energy system, dynamically acclimates to the operation of PV system. It efficiently converts the AC to the DC during active the PV power generation and contraries the process for the grid or the off-grid usage. The 2 kW unit, costing $651 and boasting 90% efficiency over the 15-year lifespan, is available in the sizes ranging from the 0 to the 250 kW. This versatility confirms the optimal energy conversion and the system performance (Fig. 7). The converter plays the critical role in the optimizing energy utilization and the ensuring grid compatibility, highlighting its significance in overall system.

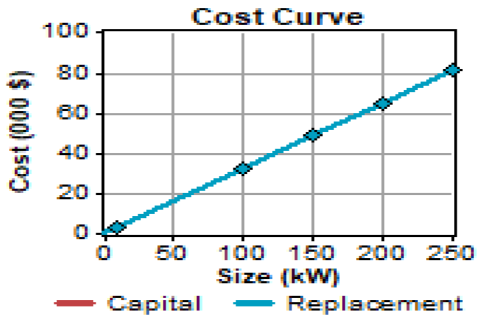

Fig. 7. Cost curve of the converter.

Estimation of the Electrical Loads

The primary load, recognized as electric load, shows total energy demand that the system must meet (Chandel et al., 2014). The daily load demand at Godagari, Rajshahi, is 35 MWh/d, the Kahaloo, Bogura, is the approximately 31 MWh/d, and the Sadar, Sirajgonj, is the approximately 29 MWh/d, which is consistent with the RETScreen.

Resource assessment

The HOMER model shows the crucial role in the study by the enabling of the evaluation of the various energy resource combinations, including the solar energy, to determine most effective system configuration. By systematically evaluating resources as the solar irradiance and reliability of the existing power infrastructure, HOMER classifies the economically viable and the sustainable energy mix that meets demand.

Economics and constraints

The study projects the 25-year lifespan, reflecting the focus on the long-term sustainability and the economic viability. The conservative annual interest rate of 15% is applied in financial analysis to account for time value of the money and the investment risks. Importantly, the system is designed with flexibility, permitting up to the 10% annual capacity shortage, which is acceptable within renewable energy framework.

Results and the discussion by HOMER

The study explores the environmental and the techno-economic feasibility of the implementing photovoltaic (PV) systems in northern areas of the Bangladesh, specifically the Rajshahi, the Bogura, and the Sirajganj. Utilizing the HOMER software, the analysis estimates the various aspects of the PV system performance, including the cost-effectiveness and the environmental impact.

Cost of energy (COE) by HOMER

The simulation in the study goes the beyond merely identifying the optimal solutions by the providing the in-depth sensitivity and the optimization analysis. It clarifies how the various factors influence proposed system's design outcomes. The results, detailed in Table 9, are the crucial for the supporting optimization cases, with discount rate emerging as the significant factor in system's analysis. The simulation proposals valuable insights into dynamics between the factors such as discount rate and the PV capacity, which greatly affect system's reliability and the cost-effectiveness. In the evaluating different power

system combinations with the HOMER, focus is on the economic and the operational characteristics. Among hybrid options, PV-diesel-converter combination is the notable for its versatility, integrating both conventional and non-conventional energy resources. With the calculated cost of the energy (COE) of the $0.329 per kWh for Rajshahi, the $0.351 for Bogura, and the $0.440 for Sirajganj, this configuration displays competitive the affordability and the efficiency. By combining the photovoltaic energy with reliability of the diesel generator and the converter, these configurations proposal the well-balanced approach that boosts their cost-effectiveness. Moreover, systems with the higher proportions of the renewable energy sources, including the PV, are mainly attractive for the environmental sustainability. So, the HOMER simulation results the demonstrate that the PV-diesel-converter combination is the versatile and the efficient solution for the studied areas. Rajshahi's lower COE highpoints its cost-effectiveness, while the ability to the incorporate various energy resources ensures system reliability and the operational flexibility. The findings highlight importance of the considering both the economic and the environmental factors in design and optimization of the energy systems.

Sensitivity analysis

The sensitivity analysis showed the using the HOMER software, as showed in Fig. 8 (a) for the Rajshahi, (b) for the Bogura, and (c) for the Sirajganj, emphases on the diesel price as the important parameter. With the assumed the inverter efficiency of 90% and the interest rate of 15%, the analysis utilizes how the varying diesel prices affect levelized cost of energy (COE) for the hybrid system, which comprises the PV panels, the

Table 9. Cost of energy of the different options with respect to (a) Rajshahi, (b) Bogura, and (c) Sirajganj.

PV (kW)	Label (kW)	H3000	Conv. (kW)	Initial Capital	Operating Cost ($/yr)	Total NPC	COE ($/kWh)	Ren. Frac.	Capacity Shortage	Diesel (L)	Label (hrs)
300...	3000		3000	$ 5,633,750	3,324,830	$ 27,125,942	0.329	0.87	0.00	2,918,423	5,144
300...	3000	1	3000	$ 5,662,272	3,324,446	$ 27,151,984	0.329	0.87	0.00	2,917,958	5,143
	3000			$ 1,257,250	6,031,272	$ 40,244,284	0.488	0.00	0.00	5,339,616	8,759
	3000	1	5	$ 1,287,400	6,031,471	$ 40,275,724	0.488	0.00	0.00	5,339,618	8,759

a) Rajshahi

PV (kW)	Label (kW)	H3000	Conv. (kW)	Initial Capital	Operating Cost ($/yr)	Total NPC	COE ($/kWh)	Ren. Frac.	Capacity Shortage	Diesel (L)	Label (hrs)
300...	3000		3000	$ 5,633,750	3,094,244	$ 25,635,400	0.351	0.89	0.00	2,692,532	5,091
300...	3000	1	3000	$ 5,662,272	3,093,305	$ 25,657,856	0.351	0.89	0.00	2,691,602	5,089
	3000			$ 1,257,250	5,704,492	$ 38,131,936	0.522	0.00	0.00	5,012,836	8,759
	3000	1	5	$ 1,287,400	5,704,690	$ 38,163,360	0.522	0.00	0.00	5,012,836	8,759

b) Bogura

PV (kW)	Label (kW)	H3000	Conv. (kW)	Initial Capital	Operating Cost ($/yr)	Total NPC	COE ($/kWh)	Ren. Frac.	Capacity Shortage	Diesel (L)	Label (hrs)
300...	3000		3000	$ 5,633,750	3,828,930	$ 31,949,706	0.440	0.89	0.00	2,633,217	5,076
300...	3000	1	3000	$ 5,662,272	3,829,115	$ 31,979,498	0.440	0.89	0.00	2,633,217	5,076
	3000			$ 1,257,250	7,071,614	$ 49,859,936	0.687	0.00	0.00	4,906,646	8,759
	3000	1	5	$ 1,287,400	7,071,828	$ 49,891,560	0.687	0.00	0.00	4,906,646	8,759

c) Sirajganj

diesel generator, the battery,the power electronics, and the converter, while allowing for the maximum annual capacity shortage of 10%. As depicted in figure, levelized COE is plotted against the diesel prices ranging from the $1 to the $1.30 per liter. The results display the clear trend: as the diesel prices upsurge, the COE for hybrid option also increases. This trend highpoints system's sensitivity to the fluctuations in the diesel prices and the economic viability. The increase in the diesel prices raises cost of the energy production, emphasizing critical need to the account for such variables in planning and the decision-making processes for the energy projects. This sensitivity analysis emphasizes importance of the considering fuel price volatility and its possible impact on the overall system costs.

The sensitivity analysis conducted using the HOMER software, shown in the Fig. 9 (a) for the Rajshahi, (b) for the Bogura, and (c) for the Sirajganj, efforts on the inverter efficiency as primary parameter. With the presumed interest rate of 15%, the analysis assesses how varying the inverter efficiency moves levelized cost of energy (COE) for hybrid system, which includes the PV panels, the diesel generator, the battery, the power electronics, and the converter, while allowing for the maximum annual capacity shortage of the 10%. The figure shows the COE plotted against different the inverter efficiency values ranging from the 70% to the 90%. The results reveal that the higher inverter efficiency leads to lower COE, indicating the lower energy production costs. This tendency highlights sensitivity of hybrid system's economic viability to change in the inverter efficiency, highlighting significance of the accounting for the factors in planning and the decision-making processes for the energy projects.

The sensitivity analysis conducted by the using HOMER software, exposed in Fig. 10 (a) for the Rajshahi, (b) for the Bogura, and (c) for the Sirajganj, emphases on the interest rate as important parameter. With the presumed inverter efficiency of the 90%, the analysis explores how the varying interest rates influence levelized cost of energy (COE) for hybrid system, which includes the PV panels, the diesel generator, the battery, the power electronics, and the converter, while allowing for the maximum annual capacity shortage of the 10%. The figure depicts COE plotted against the interest rate values ranging from the 13% to the 15%. The results show that the increasing interest rates generally lead to the rise in COE, though in the several cases, energy production costs may decrease. This trend underlines sensitivity of hybrid system's economic viability to change in the interest rates, the highlighting the critical need to consider these factors in planning and decision-making for the energy projects.

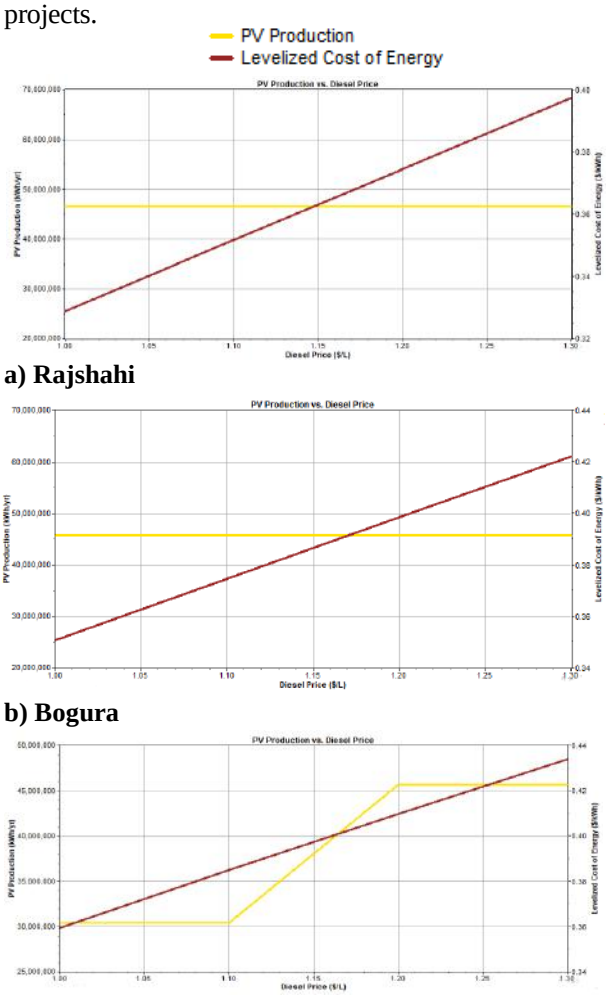

a) Rajshahi

b) Bogura

c) Sirajganj

Fig. 8. The sensitivity analysis is driven for (a) the Rajshahi, (b) the Bogura, and (c) the Sirajganj focuses on relationship between PV production, diesel price, and levelized cost of energy (COE).

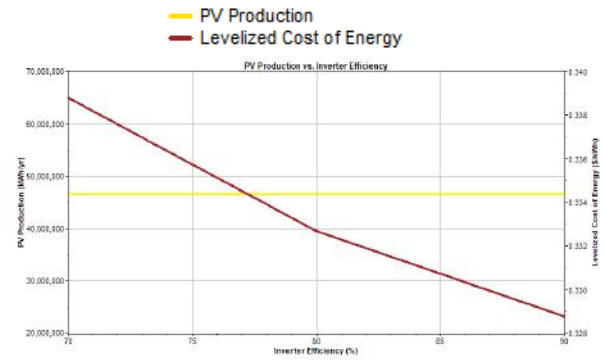

a) Rajshahi

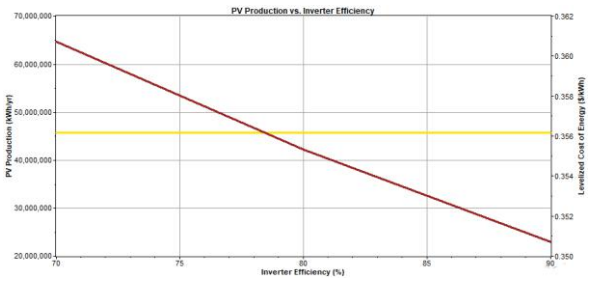

b) Bogura

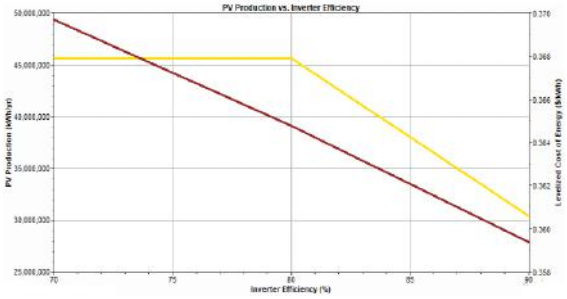

c) Sirajganj

Fig. 9. The sensitivity analysis is conducted for (a) Rajshahi, (b) Bogura, and (c) Sirajganj focuses on the relationship between PV production, inverter efficiency, and levelized cost of energy (COE).

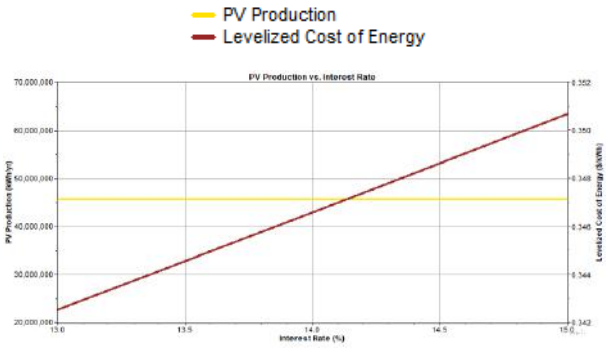

a) Rajshahi

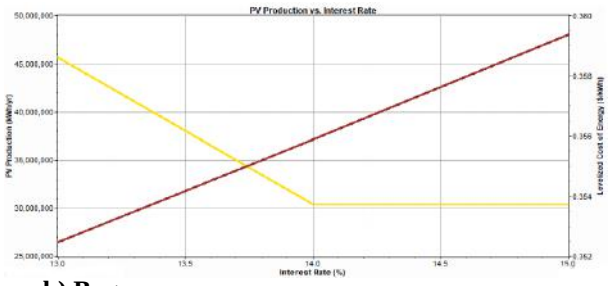

b) Bogura

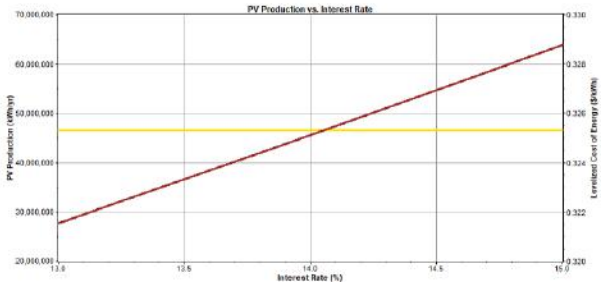

c) Sirajganj

Fig. 10. The sensitivity analysis is conducted for (a) Rajshahi, (b) Bogura, and (c) Sirajganj emphases on the relationship between PV production, interest rate, and levelized cost of energy (COE).

Table 10. The emission analysis is driven for (a) Rajshahi, (b) Bogura, and (c) Sirajganj.

Rajshahi	
Pollutant	**Emissions (kg/yr)**
carbon dioxide	768943
carbon monoxide	18967
sulfur dioxide	15431
Nitrogen oxides	169242

Bogura	
Pollutant	**Emissions (kg/yr)**
carbon dioxide	7087875
carbonmonoxide	17495
sulfur dioxide	14234
Nitrogen oxides	156113

Sirajganj	
Pollutant	**Emissions (kg/yr)**
carbon dioxide	6934126
carbon monoxide	17116
sulfur dioxide	13925
Nitrogen oxides	152727

emissions. Here's a breakdown: the Rajshahi has lowest carbon dioxide emissions, while the Bogura and the Sirajganj have the much higher emissions. Sirajganj has the lowest carbon monoxide emissions, followed closely by the Bogura. Sirajganj has the lowest sulfur dioxide emissions. Sirajganj has the lowest nitrogen oxides emissions. Regarding the overall emissions comparison: the Rajshahi has the lowest total emissions, and the Bogura has the highest. Based on the providing data, Rajshahi is the better option owing to its lower overall pollution levels. It has the lowest carbon dioxide and total emissions, suggesting a lower environmental impact than the Bogura and the Sirajganj.

Conclusion

The viability study for applying the photovoltaic solar system in the Rajshahi, the Bogura, and the Sirajganj, Bangladesh, addresses financial, technical, and environmental issues. Its aim is to attract both the national and the international investors by highlighting potential for the clean energy in the Bangladesh. The study considered the effect of sensitivity, risk, technical, financial, and environmental factors. This was established to the develop the photovoltaic solar energy strategy that will attract the PV solar energy investors from the national and the international administrations to fund Bangladesh's abundant and underutilized the clean energy. This will reduce overall warming and the advance the region's sustainable technological development.

RETScreen Expert software responses the lower energy production costs for Bogura, Sirajganj, and Rajshahi ($0.097, ($0.097, and $0.095 per kWh), HOMER's calculations display the higher costs of energy (COE) for these regions, with $0.329 per kWh for the Rajshahi, $0.351 for the Bogura, and $0.440 for the Sirajganj. Despite the discrepancies, HOMER's results reveal that the hybrid configurations are still competitively affordable and the efficient, reflecting the robust energy solution for the regions.

The sensitivity analysis discloses that rising diesel prices pointedly increase levelized cost of energy (COE), emphasizing the need to account for the fuel price volatility in the energy planning. Higher inverter efficiency reduces COE, representing its importance in the improving economic viability. Conversely, increasing the interest rates generally raise COE, highlighting the impact of the financial factors on project costs. These findings highlight the need to carefully consider the fuel prices, the inverter performance, and the interest rates in development and the decision-making processes for the hybrid energy systems.

Based on the emissions data, Rajshahi is the best option for pollution levels, as it has the lowest total emissions and the lowest carbon dioxide emissions. Sirajganj, while having the lowest emissions of carbon monoxide, sulfur dioxide, and nitrogen oxides, still falls behind Rajshahi in overall emissions. As a result, the effects of global warming will be greatly reduced.

Acknowledgment

Dedicated to the great kind hearted person, Professor Jun Tanimoto, Dr., Kyushu University, Japan, a very special person in my life who inspired me to take the challenge.

Authors contribution

All authors contributed equally to the conception, design, data collection, analysis, and writing of the manuscript.

Conflict of interest

There is no conflict of interest.

References

Bangladesh-An-Introduction. *https://mofa.gov.bd/site/page/6dde350b-1ca6-4c69-becd-a3f12cf14ac1/Bangladesh*

Bangladesh Economic Review (BER). Bangladesh Economic Review, 2022. Finance Division, Ministry of Finance, Government of the People's Republic of Bangladesh, Dhaka

Bangladesh Power Development Board (BPDB). *Annual report*, 2020-2021. Ministry of Power, Energy & Mineral Resources, Government of the People's Republic of Bangladesh, Dhaka.

Chande M, Agrawal GD, Mathur S andMathur A. Techno-economic analysis of solar photovoltaic power plant for garment zone of Jaipur city. *Case Stud Therm Eng*. 2014; 2:1-7.

Habib MA and Asgar MA. Analyzing wind speed trends and statistical insights for Panchagarh District, Bangladesh. *Int J EngComput Sci*. 2025;14(4):27040-27052.

Habib MA, Debnath SK, Parvej MS, Ferdous J, Asgar MA, Habib MA and Jemy MA. Evaluating the feasibility of a photovoltaic-fuel cell hybrid energy system for the ice cream factory in fukuoka city, Japan: An economic and technical analysis. *Int J Educ Manag Eng*. 2024;14(4):23-35.

Habib MA, Kabir KMA and Tanimoto J. Do humans play according to the game theory when facing the social dilemma situation? A survey study. *Evergreen*. 2020a ;7(1):7-14.

Habib MA, Tanaka M and Tanimoto J. How does conformity promote the enhancement of cooperation in the network reciprocity in spatial prisoner's dilemma games? *Chaos Solitons Fractals.* 2020b; 138:109997.

Habib MA, Kabir MA and Tanimoto J. Evolutionary game analysis for sustainable environment under two power generation systems. *Evergreen*, 2022; 09(02):323-41.

Habib MA. Game theory, electrical power market and dilemmas. *J. Electr. Eng. Electron. Control. Comput. Sci.* 2022a; 8(29):33-42.

Habib MA. Wind speed data and statistical analysis for Boguradistrict in Bangladesh. *J.Electr. Eng. Electron. Control.Comput. Sci.* 2022b; 8(30):1-10.

Habib MA. The application of asymmetric game in the electrical power market. *J. Electr. Eng. Electron. Control.Comput. Sci.* 2023; 9(31): 1-10.

Hasan MM and Habib MA. Wind speed analysis and its implications for Muktagacha, Mymensingh, Bangladesh. *J. Bangladesh Acad. Sci.* 2025; 49(1):123-35.

How to Design Solar PV System - Guide for sizing your solar photovoltaic system, 2025. https://www.leonics.com/support/article2_12j/articles2_12j_en.php

Islam MS, Islam F and Habib MA. Feasibility analysis and simulation of the solar photovoltaic rooftop system using PV systsoftware. *Int. J. Educ. Manag. Eng.* 2022a;12(6):21-32.

Islam MS, Noman NA and Habib MA. The Best techno-economic aspects of the feasibility study concerning the proposed PV-Wind-hydro hybrid system in Nilphamari, Bangladesh. *Int. J. Educ. Manag. Eng.* 2022b;12(5):24-37.

Khan M, Khan M and Khan M. Solar power irrigation towards saving energy for agricultural production: A feasibility study. *J. Environ. Sci. Nat. Resour.* 2015;8(1):125-128.

Khan SI, Kashem MA and Hoque MA. Design and analysis of a mini solar grid in remote area of Bangladesh. In: *41st North American Power Symposium.* 2009. p. 1-5.

Khandelwal A and Shrivastava V. Viability of grid-connected solar PV system for a village of Rajasthan. In: *2017 International Conference on Information, Communication, Instrumentation and Control (ICICIC).* 2017. p. 1-6.

Lee KH, Lee DW, Baek NC, Kwon HM and Lee CJ. Preliminary determination of optimal size for renewable energy resources in buildings using RETScreen. *Energy*, 2012;47(1): 83-96.

Mehmood A, Shaikh FA and Waqas A. Modeling of the solar photovoltaic systems to fulfill the energy demand of the domestic sector of Pakistan using RETSCREEN software. In: Conference: IEEE-Xplore_International Conference and Utility Exhibition 2014 on Green Energy for Sustainable Development (ICUE 2014), Pattaya City, Thailand, 19-21 March, 2014. pp. 1-7.

Mirzahosseini AH and Taheri T. Environmental, technical and financial feasibility study of solar power plants by RETScreen, according to the

targeting of energy subsidies in Iran. *Renew Sustain Energy Rev*. 2012; 16(5): 2806-11.

Mondal MAH and Islam AKMS. Techno-economic feasibility of grid connected solar PV system in Bangladesh. In: *1st International Conference on the Developments in Renewable Energy Technology (ICDRET)*. 2009. p. 1-4.

Mukherjee S and Razzak MA. Analysis of 100 kW grid-connected solar photovoltaic system developed on the river deltas of eight divisions of Bangladesh using RETScreen. In: *International Conference on Electrical, Computer and Communication Engineering (ECCE),* 2017. p. 350-355.

Nikita KN, Islam SN, Islam MS, Saha M and Khan MF. Prospect of solar PV based power generation in the marshy lands of Bangladesh: An analysis through RETScreen software. In: *4th International Conference on the Development in Renewable Energy Technology (ICDRET),* 2016. p. 1-6.

Noman NA, Islam MS, Habib MA and Debnath SK. The techno-economic feasibility serves to optimize the pv-wind-hydro hybrid power system at Tangail in Bangladesh. *Int. J. Educ. Manag. Eng*. 2023; 13(3): 19-32.

Owolabi AB, Nsafon BEK, Roh JW, Suh D and Huh JS. Validating the techno-economic and environmental sustainability of solar PV technology in Nigeria using RETScreen Experts to assess its viability. *Sustain Energy Technol Assess.* 2019; 36: 100542.

Rahman M, Habib MA, Rashid MMU and Hasan MM. Study and analysis of hybrid energy options for electricity production in Bogura, Bangladesh. *Asian J. Curr. Res.* 2018; 3(1): 9-14.

Rashid MMU and Habib MA. Design and construction of the solar photovoltaic simulation system with the implementation of mppt and boost converter using Matlab/Simulink. *Asian J. Curr. Res*. 2018; 3(1): 27-36.

Rashwan SS, Shaaban AM and Al-Suliman F. A comparative study of a small-scale solar PV power plant in Saudi Arabia. *Renew. Sustain. Energy Rev*. 2017; 80:313-318.

RETScreen, 2025. https://www.nrcan.gc.ca/maps-tools-and-publications/tools/modellingtools/ retscreen /7465.

Sambo A. Strategic developments in renewable energy in Nigeria energy demand and supply projections for Nigeria. *Int. Assoc. Energy Econ.* 2009;16: 15-19.

Sarkar MR, Rabbani MG, Khan AR and Hossain MM. Electricity demand forecasting of Rajshahi City in Bangladesh using fuzzy linear regression model. In: *International Conference on Electrical Engineering and Information Communication Technology (ICEEICT),* 2015. p. 1-3.

Standard Test Conditions (STC) of a Photovoltaic Panel, 2025. https://www.alternative-energy-tutorials.com/photovoltaics/standard-test-conditions.html

Tahera KU, Fabiha R and Khan MZR. Solar photovoltaic system design for a residential hall in BUET. In: *ICECE 2018 - 10th International Conference on Electrical and Computer Engineering*. 2019. pp. 437-440.

Thevenard D, Leng G and Martel S. The RETScreen model for assessing potential PV projects. In: *Conference Record of the Twenty-Eighth IEEE Photovoltaic Specialists Conference – 2000.* pp. 1626-1629.

Uddin SMN, Bodrudduza M, Rahman BKMM and Khan MF. RETScreen based feasibility study on the prospect of wind power generation along the coastal region of Chittagong, Bangladesh. In: *4th International Conference on the Development in Renewable Energy Technology (ICDRET),* 2016. p. 1-5.

J. Bangladesh Acad. Sci. 49(2); 205-214: December 2025 DOI:https://doi.org/10.3329/jbas.v49i2.76778

Journal of Bangladesh Academy of Sciences

Journal homepage: http://www.bas.org.bd/publications/jbas.html

Research Article

Spectrophotometric analysis of caffeine and sugar content in energy drinks commonly consumed in Dhaka City, Bangladesh: A public health concern

Othai Saha, Md. Mazharul Islam* and Mohammad Shoeb

Department of Chemistry, University of Dhaka, Dhaka, Bangladesh

ARTICLE INFO

Article History

Received: 09 October 2024
Revised: 20 August 2025
Accepted: 20 August 2025

Keywords: Caffeine, Carbohydrate, Energy drinks, Solid mass, UV-Visible spectrometer.

ABSTRACT

Energy drink consumption has escalated, especially among the younger generation, credited to their stimulating properties, mainly because of their caffeine and carbohydrate contents. Given the potential health risks associated with excessive consumption of these substances, it is imperative to examine the composition of energy drink products on the market. This study used an analytical quantitative method to determine the mass concentrations of total solids, caffeine, and carbohydrates in eight brands of energy drink on sale in Dhaka, Bangladesh, using a composite, cost-effective experimental design. Total solid mass contents were 10.30 to 13.13 g per 100 mL of drinks, caffeine was found 233.30 to 546.48 mgL^{-1}, and carbohydrates were found 7.09 to 11.15 g per 100 mL energy drink using the double beam UV-visible spectrophotometer. The accuracy of the results was also indicated by the low standard deviation values of 1.04 to 4.39 for caffeine and 0.08 to 0.23 for carbohydrate, and the relative standard deviation of 0.26 to 1.75% for caffeine and 0.54 to 2.72% for carbohydrate. There was a need for proper health, legal, and standard considerations in energy drink manufacturing, given the results.

Introduction

Caffeine has long been used for thousands of years and is currently one of the most widely used active food compounds. Caffeine (1,3,7-trimethylxanthine; $C_8H_{10}N_4O_2$) is an organic xanthine alkaloid compound that occurs naturally (Committee on Military Nutrition Research, 2001; Heckman et al., 2010) and has mainly been discovered in coffee (*Coffea arabica*), tea (*Thea sinensis*), and cocoa (*Theobroma cacao*) plants. Due to its stimulant, antioxidant, anti-inflammatory, and analgesic effects (Cappelletti et al., 2015; Vieira et al., 2020), it has long been used as a vital compound for the formulation of over-the-counter medicines. Caffeine has remained a primary energetic compound, widely present in tea, soft drinks, chocolates, confectionery, and energy drinks, thereby making it one of the most commonly used substances worldwide (Błaszczyk-Bębenek et al., 2021; Saraiva et al., 2023). Recent health suggestions from administrations emphasize the health risks associated with the consumption of this stimulant for pregnant, lactating women; teenagers; children; youth; as well as those experiencing health conditions like cardiovascular disease (Wikoff et al., 2017). Such guidelines highlight significant differences in physiological responses to regular and excessive caffeine doses (Temple et al., 2017). The exact amount of caffeine needed to elicit adverse responses also varies from person to person, depending on body weight and caffeine sensitivity (Higdon & Frei, 2006). Sensitive persons are suggested to restrict their caffeine intake to less than 400mg daily to remain unaffected by the adverse responses of caffeine, including drowsiness, headaches, nausea, and anxiety (Smith, 2002). Caffeine works as an antagonist of adenosine receptors, resulting in the facilitation of the discharge of neurotransmitter chemicals like dopamine, noradrenaline, and acetylcholine, responsible for several psychoactive responses, including peripheral vasoconstriction, hypertension, thermogenesis, and augmentation of the functions of the kidneys and

*Corresponding author:<mazharulchdu@gmail.com>

stomach, respectively (Benowitz, 1990; Riksen et al., 2009).

Confirming the solid mass of an energy drink is vital for evaluating its nutritional profile and quality. Quantifying the total mass will give manufacturers a means to determine the amounts of each carbohydrate, vitamin, mineral, and herbal supplement they have added for dietary improvement, and to enhance their ability to maintain product formulation and comply with regulations. Consumers also benefit from this determination, as they can make more informed decisions about what they consume and how the nutritional components of an energy drink will affect their dietary requirements. Carbohydrates are the primary organic compounds and the most significant energy source, and all carbohydrates, including non-digestible carbohydrates, are considered fundamental elements of a healthy diet (Grosch et al., 2008; Belitz et al., 2009). Most energy beverages contain a large percentage of carbohydrates, along with caffeine and various other stimulants in chocolates and candies (Campos et al., 2022), thus resulting in an increasing amount of research conducted to determine how these different ingredients may affect cognitive function (Seifert et al., 2011; Boyle et al., 2018). Studies have indicated that the combined effect of caffeine and carbohydrates is a positive influence on both sustained attention (over 30 minutes) and short-term attention (less than 30 minutes) (Kennedy and Scholey, 2004; Aniţei et al., 2011). Not only do caffeine and glucose improve mental energy by relaying an increase in mental alertness, achievement of mood elevation, and motivation to perform tasks (described as effective mental energy) (Childs and De Wit, 2008; Gorby et al., 2010), but the consumption of caffeine with glucose has been shown to enhance perceptions of alertness, stimulation, and arousal (Smit et al., 2006; Howard et al., 2010). This quantifiable energy correlate is essential for evaluating energy, creating nutrition labels, and identifying adulterations. Additionally, by understanding the composition of carbohydrates consumed, one is better positioned to correlate the carbohydrate intake with health outcomes (Menezes et al., 2004).

Energy drinks are distinguished from conventional soft drink products because they are generally formulated with significantly higher concentrations of both caffeine and sugar, and their contents have been analyzed. Researchers have specifically examined the total solid mass of energy drinks and the amounts of caffeine and carbohydrates in each drink to evaluate the health risks associated with their consumption. Energy drinks are marketed to give users an energy boost by containing a combination of caffeine, the natural stimulant, sugars, glucuronolactone, amino acids, herbs, and vitamins, and most contain very high levels of caffeine and sugar (O'Brien et al., 2008). The growth rate of caffeine-based energy drinks globally has been extremely rapid since the start of the millennium (Spaeth et al., 2014). The energy drink market in Bangladesh is projected to grow from USD 128.5 million in 2024 to USD 185.40 million in 2029. The increased sales of energy drinks in Bangladesh are primarily due to rising demand for ready-to-drink beverages, particularly among working-class individuals with busy schedules. Due to the widespread availability of energy drinks through convenience stores, supermarkets, and local retailers in Bangladesh, there is a greater demand and increased consumer acceptance of these products (Bangladesh Energy Drinks Market Insights, 2023). The primary purpose of this research project is to develop a low-cost, easy-to-use, and quick method for measuring caffeine and carbohydrate (sugar) levels in energy drinks sold in Bangladesh. The objective of this project is to determine the caffeine and carbohydrate content of energy drinks and to educate consumers about the limits of daily energy drink consumption without adverse health effects.

Materials and Methods

Chemicals, glassware, and instruments

Deionized water was used for all analyses carried out throughout the project. The glassware used included micropipettes (1-1000 µL), pipettes (5-10 mL), volumetric flasks (5, 10, 20, 50, and 100 mL), funnels, beakers, spatulas, and vials. This glassware was cleaned with detergent and water, rinsed 3 times with distilled water, then rinsed with acetone, and finally baked in an oven set to 60 ^{0}C. The baked glassware was wrapped in aluminum foil, and Mini-uniprep™ vials were used to store standard and sample preparations. For the experimental examination, the equipment used included an electrical balance (ATY124, SHIMADZU), an oven (GSM 11/8, Hope Valley, S336RB, England), a UV-visible spectrophotometer (UV-1800, SHIMADZU), a vortex mixer (Stuart), and a rotary vacuum evaporator (VP30, Lab Tech).

Sample collection and storage

Energy drink samples of different brands (n=8) were Braver, Fighter, Power, Oscar, Royal Tiger, Speed, Red Bull, and Bull Dozer, collected from other areas of Dhaka city for analysis (Table 1). The sample collection was conducted from April 2023 to August 2023. All collected samples were refrigerated to preserve their chemical composition without degradation or alteration (Ouhakki et al., 2024). Each sample was procured and analyzed within the recommended time for consumption to ensure the accuracy and relevance of the analytical results.

Determination of solid mass

To quantify the solid mass of energy drink samples, an aliquot of 10 mL was accurately measured with a volumetric flask and transferred into a cleaned, dried, and pre-weighed 100 mL round-bottom flask (RBF). The RBF was then attached to a rotary evaporator at a temperature setting of 35-40 °C. The liquid fraction was considered to have evaporated when it left only a viscous solid residue adhering to the walls of the RBF; the RBF was then transferred to a freeze dryer. Once the solid mass in the RBF was arid, it was weighed along with the final weight of the RBF holding the solid residue. The mass of the solid was measured and expressed in grams per 100 grams of sample.

Preparation of a standard solution of caffeine

Caffeine standards were kept in a vial wrapped and stored in a refrigerator at 0 °C. To make the stock solution, 0.01 g of the caffeine standard was dissolved in deionized water in a 100 mL volumetric flask to yield a solution at 100 mgL^{-1}. This solution was assigned the name of the standard used and the concentration. It was stored in the refrigerator at 0 °C. Subsequent concentrations of 60.0, 40.0, 20.0, 10.0, 4.0, 2.0, and 1.0 mgL^{-1} were obtained after the serial dilution process. The absorbance of these solutions was measured using a double-beam UV spectrophotometer to construct a calibration curve. The UV-Visible spectrum of standard caffeine was recorded at λmax 273 nm (Bhawani et al., 2015; Habtamu and Belay, 2020). The calibration curves were obtained by serially diluting working standard solutions of caffeine and plotting absorbance against concentration in Microsoft Excel. The calibration curve is shown in Fig. 1.

Sample preparation for the determination of caffeine

At first, 20 mL of an energy drink was transferred to a cleaned volumetric flask, filtered, and degassed

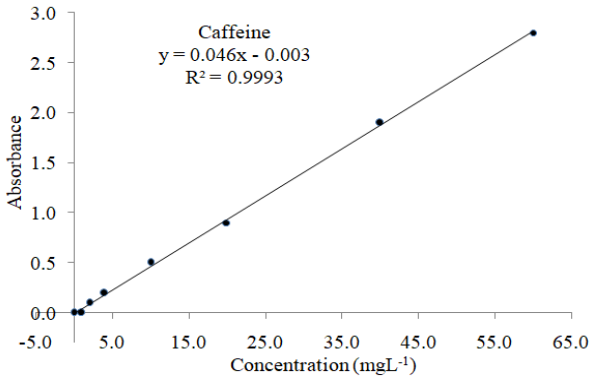

Fig. 1. Standard Calibration Curve of Caffeine

over about 10-15 min. A known volume (5 mL) of this degassed sample was transferred to a volumetric flask for dilution. This sample was diluted several times with deionized water. All sample solutions were prepared similarly, and absorbance was measured for each solution using a UV-Visible spectrophotometer (Amos-Tautua et al., 2014).

The UV spectrometer was initially run with a blank solution (deionized water) for caffeine determination. A wavelength range of 240-350 nm was used for caffeine determination. At these fixed wavelengths, the absorbance of each sample solution was measured at λmax = 273 nm. Absorbance spectra of two samples are shown in Fig. 2.

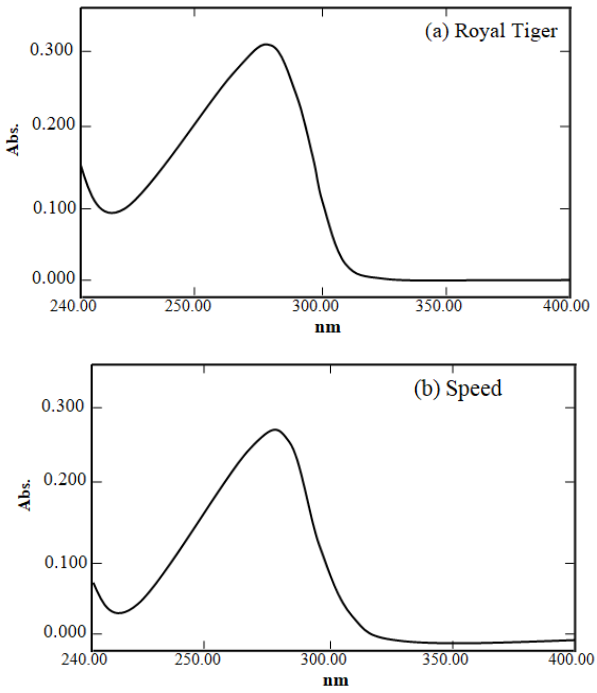

Fig. 2. UV-spectrum of sample solutions (a) Royal Tiger and (b) Speed energy drinks

Preparation of a standard solution of carbohydrate

Exactly 2.0 mg of standard glucose was weighed into a 100 mL volumetric flask to prepare a standard solution. Different concentrations of solution, such as 12.5, 60, 100, 150, and 200 mgL^{-1}, were prepared from the standard solution. For each experiment, 3 mL of each solution was collected, and 50 µL of phenol was added. Then, 3.0 mL of H_2SO_4 was carefully added. A reddish-brown colored solution was obtained, and the absorbance was measured at 489 nm (Sultana et al., 2012; Gerwig, 2021). The calibration curve (Fig. 3) was obtained by measuring the absorbance of serially diluted glucose standards and plotting absorbance against concentration in Microsoft Excel.

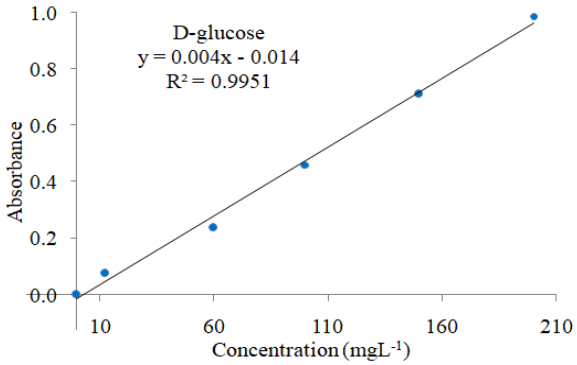

Fig. 3. Calibration curve for standard D-glucose

Sample preparation for the determination of total carbohydrate

Exactly 20 mg of the solid mash from each sample was dissolved in 100 mL of water, and the mixture was homogenized using a vortex mixer. From this solution, 3 mL was taken in a test tube. Then 50 µL phenol (80 %) and 3 mL H_2SO_4 (con.) solution were added to the test tube. All of the sample solutions were prepared similarly, and the absorbance of each solution was measured in a UV-Visible spectrophotometer using a 1 cm quartz cell (Albalasmeh et al., 2013).

The UV spectrometer was initially run with a blank solution of sulfuric acid for carbohydrate determination. The wavelength range of 400-600 nm was used for carbohydrate determination. At these fixed wavelengths, the absorbance of each sample solution was taken at λmax 489 nm. Absorbance spectra of two samples are shown in Fig. 4.

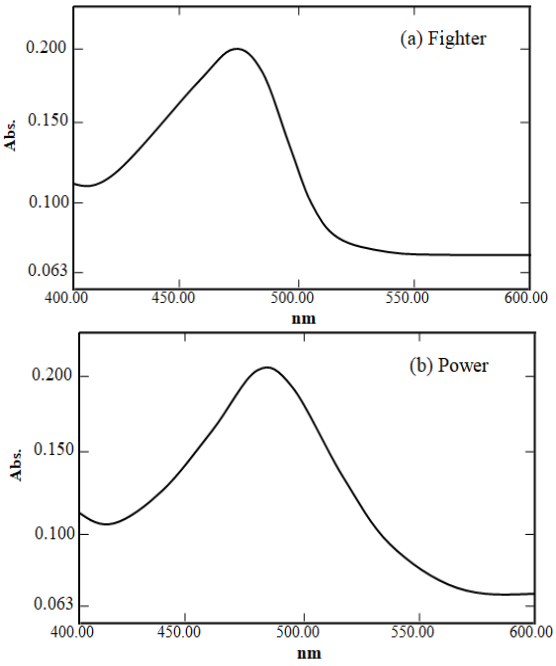

Fig. 4. UV-spectrum of sample solutions (a) Fighter and (b) Power energy drinks

By comparing the absorbance at specific λmax for both the caffeine (273 nm) and carbohydrate (489 nm) in the sample with those of the standard caffeine and carbohydrate, they were identified. From the calibration curves, the amount of caffeine and carbohydrate present in the samples was calculated using the formula y = mx+c, where y =absorbance, x =amount of caffeine or carbohydrate, m = slope of calibration curve, and c = intercept on the Y-axis. In this study, the standard deviation (S) and relative standard deviation (RSD) were computed to evaluate the determination of caffeine and total carbohydrate content in commercially available energy drink samples in Dhaka city, Bangladesh. Each energy drink sample was analyzed in triplicate. Microsoft Excel was employed for these calculations, utilizing standard mathematical formulas to determine the SD and RSD. The RSD values were instrumental in assessing the analytical method's consistency, thereby ensuring the reliability of the UV-Visible spectrophotometric technique used in this research. The following statistical equations are used to calculate S (Eq. 1) and RSD (Eq. 2).

$$S = \sqrt{\frac{\Sigma(x-\bar{x})^2}{n-1}} \quad \text{---------- (Eq.1)}$$

$$\text{RSD (\%)} = \frac{S}{\text{Mean}} \times 100 \quad \text{----------(Eq. 2)}$$

Where x = values of individual data, $\bar{x}$ = Mean value of the data set, and n = number of test values. LOD and LOQ were calculated from the calibration line at low concentrations using the standard deviation of the responses and the slope (Shrivastava and Gupta, 2011). The following equations were used for calculating LOD (Eq. 3) and LOQ (Eq. 4):

$$LOD = \frac{3.3 \times \text{Standard deviation of the response}}{\text{Slope of the calibration curve}} \text{----------(Eq. 3)}$$

$$LOQ = \frac{10 \times \text{Standard deviation of the response}}{\text{Slope of the calibration curve}} \text{----------(Eq. 4)}$$

The SD of the response was also calculated using the SD of the y-intercept of the regression line (y = mx + c), assuming a linear relationship between the response (y) and x over a specified range of concentrations (Suydam, 2000). The equation can be written as y = mx + c.

Results and Discussion

The solid mass of various energy drink samples was determined and is presented in Fig. 5. The solid mass ranged from 10.3 g/100 mL for Power energy drink to 13.13 g/100 mL for Oscar energy drink. This slight variation clearly indicates substantial differences in the values for non-volatile compounds across brands. Braver, Fighter, Speed, and Royal Tiger energy drinks registered values of 12.10 g/100 mL, 11.90 g/100 mL, 12.30 g/100 mL, and 11.30 g/100 mL, respectively. This highlights considerable uniformity within this designated group. It is pertinent to note that the solid mass for Red Bull and Bull Dozer was 11.30 g/100 mL and 11.10 g/100 mL, respectively. This clearly highlights compositional variability in these commercial energy drinks.

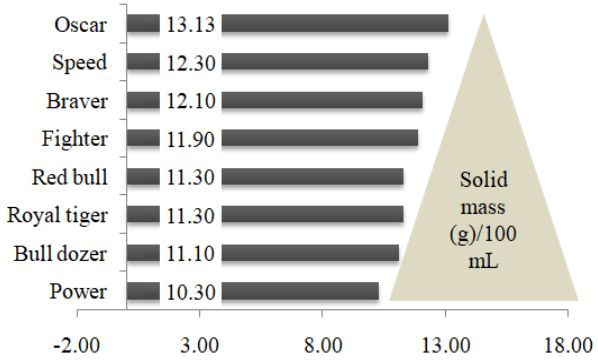

Fig. 5. Amount of total solid mass in the targeted energy drink samples.

The analysis of caffeine and carbohydrate content in energy drink samples from various brands available in Dhaka city, Bangladesh, reveals significant variations in both parameters (Table 1). Caffeine concentrations ranged from 233.30 mgL^{-1} in the Power sample to 546.48 mgL^{-1} in the Oscar sample. The SD and RSD for caffeine content were low, indicating high precision in the measurements. For instance, Oscar exhibited the highest caffeine concentration (546.48 mgL^{-1}) with an SD of 1.42 and an RSD of 0.26%, demonstrating the consistency of the analytical method. Similarly, Braver and Fighter also showed high caffeine contents (418.77 mgL^{-1} and 500.72 mgL^{-1}, respectively) with low RSD values (0.45% and 0.42%, respectively), underscoring the reliability of the data. A recent study from the University of Dhaka showed that the caffeine content in various energy drinks ranged from 147.84 to 846.78 mgL^{-1} (Refat et al., 2022). Hossain et al. analyzed four different energy drinks available in Bangladesh and found caffeine concentrations ranging from 149.41 to 978.28 mgL^{-1} (Hossain et al., 2015). Vuletić et al. (2021 analyzed five energy drink samples from the local markets in Croatia and found caffeine concentration 394.670-173.574 mgL^{-1} (Vuletić et al., 2021). Amos-Tautua et al. (2014 analyzed four energy drink samples from the local markets in Yenagoa, Nigeria, and found caffeine concentration 47.56-58.31 mgL^{-1} (Amos-Tautua et al., 2014). The caffeine levels in the energy drinks determined in this study are consistent with reported research. Compared to previous studies, the caffeine content in the current study's samples is generally higher than that found in Yenagoa, Nigeria, and overlaps with the ranges reported in Dhaka and Croatia.

In terms of carbohydrate content, the values ranged from 7.09 g/100g in Fighter to 11.15 g/100g in Oscar (Table 1). The variability in carbohydrate content is further illustrated by the RSD values, which, although slightly higher than those for caffeine, still indicate acceptable precision. For instance, Power and Bull Dozer exhibited relatively high RSDs for carbohydrate content (2.35% and 2.72%, respectively), suggesting greater variability in these samples. Nonetheless, the overall RSD values remained within acceptable limits, confirming the robustness of the analytical procedures. A recent study in Bangladesh showed that the sugar content in various energy drinks ranged from 16.16 to 338.33 mgL^{-1} (Refat et al., 2022). Hossain et al. analyzed four different energy drinks available in Bangladesh and found carbohydrate concentrations ranging from

Table 1. Caffeine and carbohydrate content in the targeted energy drink samples.

Brand Name	Packing size	Caffeine (mgL^{-1})			Carbohydrate (g/100g)		
		Average	SD	RSD (%)	Average	SD	RSD (%)
Braver	250 mL	418.77	1.88	0.45	11.09	0.08	0.68
Fighter	200 mL	500.72	2.08	0.42	7.09	0.11	0.54
Power	250 mL	233.30	1.04	0.45	8.36	0.20	2.35
Oscar	250 mL	546.48	1.42	0.26	11.15	0.14	1.25
Royal tiger	250 mL	251.27	4.39	1.75	9.12	0.14	1.59
Speed	250 mL	259.12	2.51	0.97	10.64	0.13	1.20
Red bull	250 mL	424.21	3.43	0.81	9.17	0.15	1.37
Bull dozer	250 mL	316.49	2.08	0.66	10.24	0.23	2.72

Note: Three replicates were done for each type of brand

295.20 to 504.00 mgL^{-1} (Hossain et al., 2015). The results of this study are consistent with these published literature values.

The European Food Safety Authority (EFSA) has established that a daily caffeine intake of up to 400 mg for adults, 200 mg for pregnant or lactating women, and 100 mg for children is considered within safe limits (Agostoni et al., 2015; AACAP, 2020). Exceeding these thresholds or abruptly discontinuing caffeine consumption can trigger a spectrum of adverse physiological reactions, including anxiety, insomnia, hallucinations, hypertension, headaches, gastrointestinal disturbances, diuresis, dehydration, tremors, palpitations, and cardiac arrhythmias, attributed to caffeine's stimulant effects (Addicott et al., 2009; Jahrami et al., 2020; Weibel et al., 2021). The EFSA has indicated that data on the safety profile of caffeine for children and adolescents are insufficient (Saraiva et al., 2023). All these sample packs were below the allowable maximum limit for caffeine, which is 400 mg/kg (Agostoni et al., 2015). These rules require that energy drinks contain only safe levels of caffeine, as people may consume them alongside other products or foods containing caffeine, which may result in adverse health consequences if caffeine is consumed at levels above the maximum allowed. Caffeine also finds application in energy drinks for flavoring and for their dependence-forming properties.

The caffeine levels in energy drinks vary among manufacturers, ranging from 10 to 50 mg per serving (Nour et al., 2010). The US Food and Drug Administration (FDA, 2006), however, limits caffeine in beverages to 6 mg per ounce. Consequently, the permissible caffeine content in soft drinks ranges from 30 to 72 mg per 355 mL (NSDA, 1999; Beauty and Oluwasanmi, 2022). According to BSTI (Bangladesh Standards and Testing Institution) regulations, the caffeine concentration in Bangladeshi energy drinks must be between 14.5 mg per 100 mL and 30 mg per 100 mL.

Table 2 provides a comprehensive analysis of the maximum allowable daily intake of eight energy drink brands available in Dhaka, Bangladesh, based on their caffeine content, with permissible consumption levels categorized for adults, pregnant women, and children according to established safe intake limits. For adults, with a maximum caffeine intake capped at 400 mg per day, Braver permits up to 955 mL daily, Fighter allows 799 mL, Power, having the lowest caffeine concentration, enables 1715 mL, Oscar restricts intake to 732 mL, Royal Tiger allows 1592 mL, Speed permits 1544 mL, Red Bull allows 943 mL, and Bull Dozer permits 1264 mL. For pregnant women, the limit on caffeine consumption is 200 mg daily. For Braver, the permitted level is 478 mL; for Fighter, 399 mL; for

Table 2. Maximum consumption levels of the targeted energy drink samples.

Brand Name (n=8)	Caffeine (mg/bottle)	Adult		Pregnant women		Children	
		Daily intake	Maximum Consumption ($mLday^{-1}$)	Daily intake	Maximum Consumption ($mLday^{-1}$)	Daily intake	Maximum Consumption ($mLday^{-1}$)
Braver	104.69	400 mg maximum	955	200 mg maximum	478	100 mg maximum	239
Fighter	100.14		799		399		200
Power	58.32		1715		857		429
Oscar	136.62		732		366		183
Royal tiger	62.82		1592		796		398
Speed	64.78		1544		772		386
Red bull	106.05		943		471		236
Bull dozer	79.12		1264		632		316

Power, 857 mL; and for Oscar, 366 mL. Additionally, Royal Tiger allows 796 mL, Speed 772 mL, Red Bull 471 mL, and, finally, Bull Dozer 632 mL.

Regarding children, with a recommended caffeine intake limit of 100 mg daily, Braver: 239 mL; Fighter: 200 mL; Power: 429 mL; and Oscar: 183 mL. Moreover, Royal Tiger will permit 398 mL, Speed 386 mL, Red Bull 236 mL, and finally Bull Dozer 316 mL. Of course, such varying levels emphasize how different in caffeine content these

products are (Van Dam et al., 2020). Power, with the lowest caffeine content, has the highest intake among all consumer categories. On the contrary, Braver and Oscar, with higher caffeine content, have restricted intake levels so that the concern for cautious consumption, particularly for the vulnerable population of pregnant women and children, is highlighted. This data set underscores the need for consumer awareness of caffeine levels to avoid potential adverse health impacts.

Conclusion

In light of the above discussion, it is essential to conclude that the results obtained have highlighted variation in caffeine and carbohydrate content across different energy drink samples (n = 8) marketed in Dhaka, Bangladesh. Variations in caffeine content were observed in Power to Oscar, while variations in carbohydrates were observed in Fighters to Oscar.

The accurate estimation of both contents in samples by UV-visible spectrophotometry underscores that both instruments exhibit less variability in their results, as indicated by low standard deviation and relative standard deviation values. These outcomes have assumed prime importance for consumer safety, particularly for pregnant women and children, as their estimates would help calculate their recommended safe daily doses. Additionally, such outcomes underscore the need for stringent control measures in the energy drink market to prevent potential health risks from excessive intake of both caffeine and carbohydrates.

Acknowledgment

The authors are grateful to the International Science Programme (ISP), Uppsala University, Sweden, for financial support.

Authors contribution

Othai Saha: Formal analysis, visualization, review and editing; Md. Mazharul Islam: Conceptualization, data curation, investigation, methodology, software, supervision, visualization and writing original draft; and Mohammad Shoeb: Data curation, funding acquisition, project administration, resources, review and editing.

Conflict of interest

The authors declare that they have no competing financial interests or personal relationships that could have influenced the work reported in this paper.

References

AACAP (American Academy of Child and Adeloscent Phychiatry). Caffeine and children. Retrieved on September 18, 2020.

Addicott MA, Yang LL, Peiffer AM, Burnett LR, Burdette JH, Chen MY, Hayasaka S, Kraft RA, Maldjian JA and Laurienti PJ. The effect of daily caffeine use on cerebral blood flow: How much caffeine can we tolerate? *Hum. Brain Mapp.* 2009; 30(10): 3102-3114.

Agostoni C, Canani RB, Fairweather-Tait S, Heinonen M, Korhonen H, La Vieille S and Marchelli R. Scientific opinion on the safety of caffeine. *EFSA J.* 2015; 13(5): 4102.

Albalasmeh AA, Berhe AA and Ghezzehei TA. A new method for rapid determination of carbohydrate and total carbon concentrations using UV spectrophotometry. *Carbohydr. Polym.* 2013; 97(2): 253-261.

Amos-Tautua A, Martin WB and Diepreye E. Ultra-violet spectrophotometric determination of caffeine in soft and energy drinks available in Yenagoa, Nigeria. *Adv. J. Food Sci. Technol.*2014;6(2): 155-158.

Aniţei M, Schuhfried G and Chraif M. The influence of energy drinks and caffeine on time reaction and cognitive processes in young Romanian students. *Procedia: Soc. Behav. Sci.* 2011; 30: 662-670.

Bangladesh Energy Drinks Market Insights. Bangladesh Energy Drinks Market Size and Share Analysis - Growth Trends and Forecasts (2024 - 2029), 2023. Retrieved on June 13, 2024.

Beauty OO and Oluwasanmi AI. Caffeine content in cola and energy drinks commonly consumed in Rufus Giwa polytechnic, Owo, Ondo state, Nigeria. *Int. J. Adv. Engin. Manag.*2022; 4(9): 1579-1583.

Belitz H, Grosch W and Schieberle P. *Food Chemistry*. 4th Edition, Springer-Verlag, Berlin, 2009. p.1070.

Benowitz NL. Clinical pharmacology of caffeine. *Annu. Rev. Med.* 1990; 41(1): 277-288.

Bhawani SA, Fong SS and Ibrahim MNM. Spectrophotometric analysis of caffeine. *Int. J. Analyt. Chem.* 2015; 6: 1-7.

Błaszczyk-Bębenek E, Jagielski P and Schlegel-Zawadzka M. Caffeine consumption in a group of adolescents from South East Poland—A cross sectional study. *Nutrients*, 2021; 13(6): 2084.

Boyle N, Lawton C and Dye L. The effects of carbohydrates, in isolation and combined with caffeine, on cognitive performance and mood—current evidence and future directions. *Nutrients,*2018; 10(2): 192.

Campos V, Tappy L, Bally L, Sievenpiper JL and Lê K. Importance of carbohydrate quality: What does it mean and how to measure it? *J. Nutr.* 2022; 152(5): 1200-1206.

Cappelletti S, Daria P, Sani G and Aromatario M. Caffeine: cognitive and physical performance enhancer or psychoactive drug? *Curr. Neuropharmacol.*2015; 13(1): 71-88.

Childs E and De Wit H. Enhanced mood and psychomotor performance by a caffeine-containing energy capsule in fatigued individuals. *Exp. Clinic. Psychopharm.* 2008; 16(1): 13-21.

Committee on Military Nutrition Research. Caffeine for the sustainment of mental task performance: formulations for military operations. *National Academies Press eBook.*2001.

FDA(Food and Drug Administration). Food additives status list. 2006. Retrieved on June 13, 2024 from www. cfsan.fda.gov/dms/opa-appa.html.

Gerwig GJ. Analytical techniques to study carbohydrates. In: *Techniques in life science and biomedicine for the non-expert*, 2021; pp. 89-126.

Gorby HE, Brownawell AM and Falk MC. Do specific dietary constituents and supplements affect mental energy? Review of the evidence. *Nutr. Rev.*2010; 68(12): 697-718.

Grosch W and Schieberle P. Carbohydrates, *Food Chem.*2008; 248-339.

Habtamu D and Belay A. First order derivative spectra to determine caffeine and chlorogenic acids in defective and nondefective coffee beans. *Food Sci. Nutr.*2020; 8(9): 4757-4762.

Heckman MA, Weil J and De Mejia EG. Caffeine (1, 3, 7-trimethylxanthine) in foods: A comprehensive review on consumption, functionality, safety, and regulatory matters. *J. Food Sci.*2010; 75(3): R77-R87.

Higdon JV and Frei B. Coffee and Health: A review of recent human research. *Critic. Rev. Food Sci. Nutr.* 2006; 46(2): 101-123.

Hossain MDM, Jahan I, Shawan MMaK, Parvin A, Hasan MDM, Uddin KR, Akter S, Banik S, Hasan MDA, Hasan A, Morshed M, Rahman MDN, Rahman N and Rahman SMB. Determination of pH, caffeine and reducing sugar in energy drinks available in Bangladesh. *New York Sci. J.*2015; 8(2): 92-96.

Howard MA and Marczinski CA. Acute effects of a glucose energy drink on behavioral control. *Exp. Clin. Psychopharmacol.* 2010;18(6): 553-561.

Jahrami H, Al-Mutarid M, Penson PE, Faris MA, Saif Z and Hammad L. Intake of caffeine and its association with physical and mental health status among university students in Bahrain. *Foods*, 2020; 9(4): 473.

Kennedy DO and Scholey AB. A glucose-caffeine 'energy drink' ameliorates subjective and performance deficits during prolonged cognitive demand. *Appetite,*2004; 42(3): 331-333.

Menezes EW, de Melo AT, Lima GH and Lajolo FM. Measurement of carbohydrate components and their impact on energy value of foods. *J. Food Comp. Anal.*2004; 17(3-4): 331-338.

Nour V, Trandafir I and Elena M. Chromatographic determination of caffeine contents in soft and energy drinks available on the Romanian market. *Direct. Open Access J*. 2010; 11 (3): 351 – 358.

NSDA: National Soft Drink Association. What's in soft drinks: Caffeine in soft drinks? 1999. Retrieved on June 13, 2024.

O'Brien MC, McCoy TP, Rhodes SD, Wagoner A and Wolfson M. Caffeinated cocktails: Energy drink consumption, high-risk drinking, and alcohol-related consequences among college students. *Academ. Emerg. Med.* 2008; 15(5): 453-460.

Ouhakki H, Elfallah K, Adiba A, Hamid T and Elmejdoub N. Investigation of the water quality in Oum Er Rbia River (Morocco): A multifaceted analysis of physicochemical, undesirable substances, toxic compounds, and bacteriological traits. *Trop. J. Nat. Prod. Res.*2024; 8(4): 6820-6831.

Refat MRA, Nandi P, Shoeb M and Sultana A. Composition of energy drink samples in Bangladesh. *Dhaka Univ. J. Sci.*2022; 70(1): 42-48.

Riksen NP, Rongen GA and Smits P. Acute and long-term cardiovascular effects of coffee: Implications for coronary heart disease. *Pharm. Therapeut.* 2009; 121(2): 185-191.

Saraiva SM, Jacinto TA, Gonçalves AC, Gaspar D and Silva LR. Overview of caffeine effects on human health and emerging delivery strategies. *Pharm.* 2023; 16(8): 1067.

Seifert SM, Schaechter JL, Hershorin ER and Lipshultz SE. Health effects of energy drinks on

children, adolescents, and young adults. *Ped.* 2011; 127(3): 511-528.

Shrivastava A and Gupta V. Methods for the determination of limit of detection and limit of quantitation of the analytical methods. *Chron. Young Sci.* 2011; 2(1): 21-25.

Smit HJ, Grady ML, Finnegan YE, Hughes SC, Cotton JR and Rogers PJ. Role of familiarity on effects of caffeine- and glucose-containing soft drinks. *Physiol. Behav.*2006; 87(2): 287-297.

Smith A. Effects of caffeine on human behavior. *Food Chem. Toxicol.* 2002; 40(9): 1243-1255.

Spaeth AM, Goel N and Dinges DF. Cumulative neurobehavioral and physiological effects of chronic caffeine intake: individual differences and implications for the use of caffeinated energy products. *Nutr. Rev.* 2014;72: 34-47.

Sultana A, Haque MS, Shoeb M, Islam MS, Mamun MIR and Nahar N. Presence of yellow 6, an artificial colour additive in orange juice. *J. Ban. Chem. Soc.*2012; 25(1): 80-86.

Suydam LA. Analytical Procedures and Methods Validation: Chemistry, Manufacturing, and Controls, *Fed. Reg.r (Notices).* 2000; 65(169): 776-7. Retrieved on September 18, 2024.

Temple JL, Bernard C, Lipshultz SE, Czachor JD, Westphal JA and Mestre MA. The safety of ingested caffeine: A comprehensive review. *Front. Psychiatry*, 2017;8:80.

Van Dam RM, Hu FB and Willett WC. Coffee, caffeine, and health. *New Eng. J. Med.*2020; 383(4): 369-378.

Vieira AJ, Gaspar EM and Santos PM. Mechanisms of potential antioxidant activity of caffeine. *Radiat. Phys. Chem.*2020; 174: 108968.

Vuletic N, Bardic L and Odzak R. Spectrophotometric determining of caffeine content in the selection of teas, soft and energy drinks available on the Croatian market. *Food Res.*2021; 5(2): 325-330.

Weibel J, Lin Y, Landolt H, Berthomier C, Brandewinder M, Kistler J, Rehm S, Rentsch KM, Meyer M, Borgwardt S, Cajochen C and Reichert CF. Regular caffeine intake delays REM sleep promotion and attenuates sleep quality in healthy men. *J. Biolog. Rhyth.*2021; 36(4): 384-394.

Wikoff D, Welsh BT, Henderson R, Brorby GP, Britt J, Myers E, Goldberger J, Lieberman HR, O'Brien C, Peck J, Tenenbein M, Weaver C, Harvey S, Urban J and Doepker C. Systematic review of the potential adverse effects of caffeine consumption in healthy adults, pregnant women, adolescents, and children. *Food Chem. Toxicol.*2017; 109: 585-648.

J. Bangladesh Acad. Sci. 49(2); 215-225: December 2025 DOI:https://doi.org/10.3329/jbas.v49i2.81329

Journal of Bangladesh Academy of Sciences

Journal homepage: http://www.bas.org.bd/publications/jbas.html

Research Article

Mobile wave crawler for energy generation: Preliminary feasibility and opportunities for Bangladesh

Md Riad Khan*, Nusrat Sharmin[1] and SM Rashidul Hasan

Department of Naval Architecture and Offshore Engineering, Faculty of Engineering and Technology, Bangladesh Maritime University, Dhaka, Bangladesh

ARTICLE INFO

Article History

Received: 28 April 2025
Revised: 07 July 2025
Accepted: 18 August 2025

Keywords: Mobile wave crawler, Mobile wave energy harvesting system, Wave energy, Island powering.

ABSTRACT

One of the major challenges for a densely populated country like Bangladesh is energy shortage. For electricity generation, the country mostly relies on fossil fuels such as furnace oil, natural gas, and coal. With the environmental problems associated with fossil fuels, the global transition to renewable energy sources is inevitable. Ocean waves represent a promising renewable energy source in this regard. A large area of Bangladesh is covered by the sea, which offer significant potential for wave energy. Wave energy can be converted into electricity using a range of devices, including point absorbers, attenuators, wave surge devices, and oscillating water columns. However, these devices are fixed at specific locations, depend on particular wave profiles, and require expensive underwater cables. Against this background, the Mobile Wave Crawler (MWC), an autonomous wave energy converter, appears to be a promising solution. This work assesses the feasibility of the device, and evaluates its potential energy output. It also demonstrated a levelized cost of energy (LCOE) of USD 0.12 kWh for an energy-producing machine with an hourly rated capacity of 1 MW. Although this cost is higher than of traditional fossil-fuel-based power plants, the technology can be promoted as sustainable and environmentally friendly. This research illustrates that the proposed solution is a feasible source of green energy for the offshore islands of Bangladesh, identifies the major challenges, and suggests possible solutions. In addition, the study estimates the required number of Mobile Wave Crawlers for several example islands. For instance, four MWC units are required for each of Bhashan Char and Shah Porir Dwip, while only one unit is required for each St. Martin's Island and Dublar Char to meet their respective energy demands.

Introduction

One of the most densely populated nations in the world, Bangladesh set a goal in its 2008 renewable energy policy to produce 10% of its energy by 2015. However, the country fell significantly short of this goal, with renewables currently contributing only 2.93% - amounting to 650.14 MW out of a total 22,215 MW of energy produced. In response, the government has revised its objectives, aiming to

*Corresponding author:<riadkhan666@gmail.com>
[1]*Department of Electrical and Electronic Engineering, Ahsanullah University of Science and Technology, Bangladesh*

generate 15% of electricity from renewable sources by 2030, 40% by 2041, and ultimately 100% by 2050 (Uddin and Park, 2021; Mahbub et al., 2023). To achieve this goal, the vast ocean area and its wave energy could play a vital role.

A Mobile Wave Crawler is a portable Wave Energy Conversion Device that can convert wave energy from different ocean locations, store it, and deliver it to the larger grid. It generally comprises a ship with a Wave Energy Converter attached and an onboard energy storage system. This device is a wave energy converter that moves with wave motion, capturing the kinetic and potential energy of the ocean's surface. The wave crawler produces clean, renewable energy and has minimal environmental impact. There are at least three significant disadvantages associated with traditional methods of extracting energy by using waves and currents: 1) the power transmission cables installed in the ocean are costly, 2) the system is vulnerable to storms, and 3) the power cannot be predicted and delivered on demand (Mobile Wave Crawler, 2011). These are things that are translated to higher electricity costs. A Mobile Wave Crawler (MWC) can help overcome these problems. Fraunhofer USA CMI is currently developing an alternative approach to an economically viable ocean wave-harvesting technique, including a boat with an onboard wave energy-harvesting system and energy storage capacity (Mobile Wave Crawler, 2011).

This paper presents a preliminary feasibility analysis of the Mobile Wave Crawler installation in Bangladesh. The results indicate that it may be a viable energy solution for the country's islands and coastal areas. It has also been recommended on the number of devices required and a possible solution to the challenges presented. The paper also provides the procedure fore implementing this system in Bangladesh.

Mobile Wave Crawler Technology

Key Features

a. Mobility: The mobile wave crawler can move across the ocean, unlike stationary converters of wave energy, enabling it to optimize its location to capture energy with peak efficiency depending on the direction and value of the waves.

b. Mechanism of Energy Conversion: Wave motion is converted to electrical energy by the crawler through the use of mechanical devices of levers, buoys, or hydraulic pumps.

c. Modular Design: Wave crawlers do not need underwater cables, which are costly to maintain.

d. Durability: These devices have been constructed to resist the severe marine conditions and are constructed out of corrosion-resistant material.

e. Connection to Energy Grids: The produced electricity is accumulated in onboard batteries and sent to the shore via the underwater cables.

f. Wave-Adaptive Design: The flotation discs are also adjusted in response to the height of the wave to maximize the energy conversion efficiency. This flexibility enables the system to operate even in rough seas, making it more effective as compared to the traditional wave energy buoys.

g. Continuous Power Generation: The Mobile Wave Crawler provides a steady energy supply since ocean waves are continuous and predictable. This makes it a more reliable renewable energy source compared to wind or solar, which can be intermittent.

Main Components and Working Principle

The Mobile Wave Crawler captures wave energy using its large circular flotation discs and converts the kinetic energy of moving waves into mechanical or electrical power. The mechanism is shown in Fig. 1. Below is a detailed breakdown of its working principle:

a. Ship for Transportation: Mobile Wave Crawler is a portable device consisting of a ship (Fig. 1) which travels to the place where the wave energy is the highest. The ship includes all the machinery required for wave energy capture, storage and transmission.

b. Floating Discs as Wave Energy Converters: The wave energy converters are designed to rise and fall with the motion of waves, collecting kinetic and potential energy from ocean swells. The up-and-down movement is transferred to a mechanical system that converts it into electricity.

c. Articulated Arms for Energy Transfer: Support arms connecting the flotation discs to the main hull serve as transmission mechanisms. As the waves push the flotation discs up and down, these arms convert wave motion into mechanical force. This force is then transmitted to an onboard system that drives turbines or hydraulic pumps, generating electricity.

d. Onboard Power Generation System: The mechanical energy from the flotation discs is used to:

- Drive hydraulic pistons that pump fluid to a turbine for electricity generation.
- Spin a generator shaft that converts kinetic energy directly into electrical power. The generated electricity can be stored in batteries, and used for ship operations.

e. Power Transmission: The ship sails back to the shore when the batteries are fully charged. The stored energy is transferred to a shore-based substation. From the substation, the energy is transferred to the national grid through cable.

Table 1. Differentiation between Traditional Wave Energy Devices and Mobile Wave Crawler.

Feature	Traditional Wave Energy Devices	Mobile Wave Crawler
Mobility	Fixed, stationary	Mobile (mounted on moving ships)
Installation	Complex offshore setup	Integrated with ship infrastructure
Underwater Cable Requirement	Yes	No
Maintenance	Offshore, costly and difficult	Onboard, simpler and more accessible
Energy Storage	Not required	Energy storage system needs to be installed onboard
Grid Connection	Directly through cable	Ship travels near the shore and connects with the substation for energy transfer
Environmental Impact	High (permanent marine footprint)	Low (no seabed disturbance)

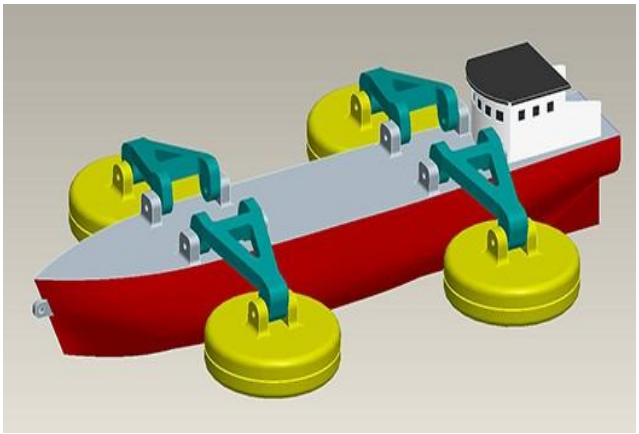

Fig. 1. Mobile Wave Crawler (Briggs et al., 2011).

Traditional Wave Energy Devices vs MWC

The difference between traditional wave energy devices and MWC is shown in Table 1.

Applications of the MWC

a. Offshore Renewable Energy Generation: The device can function as a floating power plant, supplying electricity to coastal areas or offshore facilities. It can be deployed near islands, marine research stations, or offshore oil rigs.
b. Remote & Island Energy Supply: Many remote islands depend on diesel generators for power, which is costly and polluting. The Mobile Wave Crawler can provide a clean and renewable energy source for these communities.
c. Energy to Power Marine Research and Underwater Equipment: Oceanographic sensors, underwater research stations, and underwater vehicles need energy. The crawler can provide green energy to support long-term marine research missions.
d. Military and Defence Applications: The system could be used to power offshore military bases or surveillance equipment. It can serve as a mobile energy station for naval operations.
e. Disaster Response and Emergency Power: After natural disasters, coastal regions often lose access to electricity. A Mobile Wave Crawler can be deployed to provide temporary energy for emergency relief operations.

Power Generation and Cost by MWC

Briggs et al. showed that a typical Mobile Wave Crawler system consists of a 50-meter boat with 1 MW of wave energy-harvesting capacity and 20 MWh of energy storage capability. Operationally, the boat cruises to a favorable offshore location, harvests energy for approximately 20 hours, returns to shore, connects to the electricity grid, and releases the stored energy during high-demand periods. Preliminary calculations promise an electricity cost of US$0.15/kWh (Briggs et al., 2011). For this work, the same type of boat is considered.

Feasibility for Bangladesh

Possible Application

Potential Contribution of MWC to Bangladesh are:

a. Coastal and Island Applications: Mobile crawlers could provide localized power for coastal villages, islands, or fishing operations. It can be a good solution to the electricity problem in Bangladesh’s islands. There are a staggering number of islands (Fig. 2), estimated at 700-1,000 (Chouhan, n.d.). About 60 islands have been identified in the coastal zone (Islam, 2004). Most of the islands are located in the central coastal zone due to the dynamic flow of the Ganges-Brahmaputra-Meghna river system. Hatia, Sandweep, and Maishkhali are three upazilas, and Bhola, an administrative district, is the fourth-largest islands in the zone (Sarwar and Wallman, 2005). Some islands are limited to only a small village. St. Martin is the country's only coral island in the Bay of Bengal, about 9.8 km (Hossain, 2001) to southeast of the mainland. The island has an area of 7.5 km2 and is situated under the Teknaf thana of Cox’s Bazar district. A total number of 177 char lands are also identified in the coastal zone (Islam, 2004). It could support off-grid communities in areas like St. Martin's Island or Kuakata.
b. National Grid Integration: If deployed in larger numbers, mobile crawlers could contribute a modest amount to the national grid, especially during the monsoon season when wave energy is highest. This energy can also be fed into the national grid, ideally near coastal substations like in Cox's Bazar, Chittagong, or Khulna.
c. Powering Offshore Structures: The only offshore gas extraction site of Bangladesh, Sangu, was abandoned in 2013 (Arzu et al., 2024). However, the government has announced plans to initiate oil and gas exploration in the Bay of Bengal. As 90% of the areas are remain unexplored, there is a high possibility of finding new oil and gas exploration sites (Sarker, 2024). MWCs can energize these offshore oil and gas exploration sites.

Fig. 2. Possible Mobile Wave Generation Sites

Technical Requirements

A Mobile Wave Crawler requires a vessel capable of travelling to locations with the highest wave energy potential. The desired electricity generation capacity determines the vessel's size, and the initial cost is directly related to it. Vessel design can follow the methodologies proposed by Khan et al. (2018), Khan et al. (2020) and Kundu et al. (2018). The vessel must be equipped with an appropriate number of wave energy converters and an onboard energy storage system. Additionally, a ground substation is necessary to transfer the collected energy to the national grid.

Energy Generation Probability for Bangladesh

From Fig. 3, it can be seen that the maximum power can be generated when the MWC is positioned at a wave period of approximately 7 seconds.

From Table 2, it can be observed that the mean wave period in Bangladesh is approximately 6s. From Fig. 3, for wave period 6s:

$$\frac{Power}{H\hat{}2} = 20\ kW/m\hat{}2$$

Table 2. Mean Wave Period of Bangladesh (Mansur et al.,2017).

Season	Mean Wave Period (s)	Significant Wave Height (m)
Spring	6.41	1.77
Summer	6.33	3.32
Autumn	6.45	2.01
Winter	5.25	0.99

Assuming the diameter of each Point Absorber attached to the ship is 2 m, the area of each Absorber is 3.1416 m^2. If 4 Point Absorbers are attached to the boat, then the total area is 12.57 m^2, and the mean wave height is 2 m (Table 2).

So, total power = 20 x 4 x12.57 = 1005.3 kW. So, energy per hour = P.t = 1005 kW. 1 hour ~ 1000 kW or 1 MW. So, if it works for 20 hours a day, one device can generate 20 MW of electricity in a day.

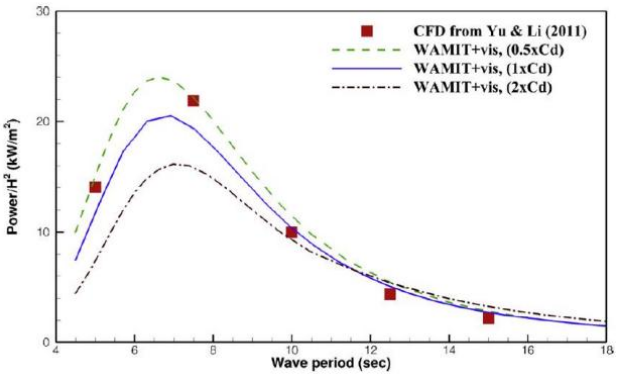

Fig. 3. Captured power of a point absorber WEC vs. wave period calculation using different numerical methods (Li and Yu, 2012)

Techno-Economic Model

A sample techno-economic model is given below:

Technical Parameters:Rated Power Output, P_r = 1000 kWCapacity Factor, CF = 0.35

Annual Operating Hours, H = 7300 hours/year (20 hours/day)

Design Life, N = 20 years

Wave Energy Conversion Efficiency,η=40%

Economic Parameters:

Capital Cost (including WECs + Ship), C_{cap} = 2,500,000 USDO&M Cost per Year, $C_{O\&M}$ = 50,000 USD

Discount Rate, r = 8% (.08)

Inflation Rate, i = 3%

Levelized Cost of Energy (LCOE)

$$LCOE = \frac{\text{Total Lifetime Energy Output (TLE)}}{\text{Total Lifetime Cost (TLC)}}$$

Where,

$TLC = C_{cap} + \sum_{n=1}^{N} (C_{O\&M} / (1+r)^n)$

$TLE = P_r \times CF \times H \times N$

Simplified LCOE Formula (Annuity Method):

$$LCOE = \frac{Ccap \cdot CRF + CO\&M}{Pr \times CF \times H}$$

$CRF = (r(1+r)^N/((1+r)^N - 1)$

So, CRF = 0.1019

and LCOE = 0.12 USD/ kWh

Table 3. Per kWh production cost of electricity from different sources in Bangladesh.

Source of Electricity	Per kWh Cost (USD)	Reference
Furnace oil-Fired electricity	0.14	(Mohiuddin, 2024)
Gas-fired Electricity	0.033	
Coal-fired Electricity	0.049	
Mobile Wave Crawler	0.12	

The production cost of electricity from different sources in Bangladesh is given in Table 3.

The electricity generation cost from MWC is basically due to the boat's operational cost and equipment maintenance costs. The operational cost may vary for the following reasons:

a. Size and shape of the boat.

b. Type of fuel used in the boat.

c. Number of crew on the boat.

d. Efficiency of the equipment used for energy conversion

e. Availability of a position with a sound wave height capable of generating enough electricity.

The energy production cost may be reduced if any of the items stated above are favorable. However, the slightly higher cost for Mobile Wave Crawler can be mitigated for the following reasons:

a. Renewable and Sustainable: Unlike fossil fuels (coal, oil, gas), wave energy is a renewable resource that does not deplete over time. As long as there are ocean waves, electricity can be continuously generated.

b. Environmentally Friendly:

- Zero greenhouse gas emissions: Unlike coal or fuel-powered plants, wave energy does not contribute to air pollution or global warming.
- Less land use: MWCs are based on working in offshore areas, which results in a minimum of

land usage. Thus, it does not disturb land-based habitats.

c. Predictable and Reliable: Ocean waves are more predictable and reliable compared to solar and wind, which are affected by the weather conditions. It is possible to estimate the energy output more accurately, and it can be easily integrated to the grid.

d. Mobility and Accessibility: Mobile wave energy systems can to be installed and transported according to energy requirements. They are applicable for powering remote coastal regions and islands, where there is no conventional power infrastructure.

e. Energy Independence and Security: Reduces dependency on imported fossil fuels, enhancing a country's energy security. It may also help mitigate the impact of fuel price fluctuations.

f. Long-Term Cost Benefits: While the initial cost is higher, maintenance and fuel costs are lower compared to thermal power plants. Again, as technology advances, the cost of wave energy is expected to decline.

g. Good Solution for Islands: Connecting the islands with the national grid requires the installation of a submarine cable system, which is very expensive. To overcome this problem, Mobile Wave Crawler can be a good solution

Required Number of Mobile Wave Crawlers for Some Example Islands of Bangladesh

As of 2023, Bangladesh's per capita electricity consumption was approximately 0.70 megawatt-hours (MWh) annually (Electricity Demand per Capita in MWh in Bangladesh - ChartingTheGlobe, 2024). This translates to about 700 kilowatt-hours (kWh) per person per year, or approximately 1.92 kWh per person per day. Based on this, the required number of Mobile Wave Crawler for some of the islands are given in Table 4. From Table 4, it can be seen that the Mobile Wave Crawler can be used to generate

Table 4. Required No. of Mobile Wave Crawlerfor Some Example Islands of Bangladesh.

Sr No.	Island Name	Population	Current Source of Electricity*	Total Required Electricity per day (MWh)	Required No. of Mobile Wave Crawler as per Briggs et al.
1.	Bhashan Char	35,629 (Bhasan Char," 2024)	Solar Panel	68.41	04
2.	St. Martin	8,000 (Mazumder et al., 2014)	Solar Panel, Stand-alone generators.	15.36	1
3.	Dublar Char	3000 (Saad, 2024)	Solar Panel	5.7	1
4.	Shah PorirDwip	40000 (Islam, 2018)	Solar Panel	76.8	04
5.	Manpura Island	76582 (BBS, 2011)	Solar Panel	147	08

*Currently, small appliances are being run by generated electricity on these Islands.

electricity for the Offshore Islands of Bangladesh instead of expensive Coal or fuel-based electricity.

Steps of Integrating Mobile Wave Crawler in Bangladesh

Adding electricity generated by a mobile wave crawler to Bangladesh's national grid involves several steps and considerations, both technical and regulatory. Here's how it can be done:

Technical Steps

a. Energy Conversion and Stabilization:

- Power Conditioning: The electricity generated by a wave crawler (often variable and inconsistent due to wave conditions) must be converted into a. stable AC (Alternating Current) at standard grid voltage (usually 230V/50Hz in Bangladesh).
- Inverters and Transformers: Use inverters to convert DC (Direct Current) generated by the wave crawler into grid-compatible AC. Transformers may be needed to step up the voltage to match the grid requirements.

b. Grid Connection Infrastructure:

- Shore-Based Connection Hub: Establish an onshore connection point where power from the crawler is aggregated and fed into the national grid.
- Synchronization: Install synchronizing equipment to ensure the crawler's output matches the grid's frequency, phase, and voltage, preventing disruptions.

c. Energy Storage:

Since wave energy is intermittent, installing battery storage systems or other energy storage solutions can help smooth out fluctuations before feeding the electricity into the grid.

Regulatory and Policy Framework

a. Approval and Licensing: Seek approval from the Bangladesh Power Development Board (BPDB) or relevant authorities to feed wave energy into the grid and ensure compliance with grid codes (technical rules for connecting to the grid).

b. Feed-In Tariffs (FiTs) or Power Purchase Agreements (PPAs): Negotiate a feed-in tariff or

PPA with the government or utilities. This determines how much will it be paid per kWh of electricity delivered to the grid.

c. Environmental and Safety Compliance: Conduct an environmental impact assessment (EIA), as Bangladeshi law requires, to ensure minimal ecological disruption and safety measures to handle extreme weather (cyclones, flooding, etc.) in the Bay of Bengal.

Logistics and Deployment

a. Best Site Location: Have the crawler around the available coastal grid infrastructure to reduce the cost of transmission. It is also expected to identify areas of high wave energy in the Bay of Bengal, including around Cox's Bazar, Kuakata, and St. Martin's Island.

b. Scaling the System: A pilot project will be necessary to determine the practicality and the performance of the wave crawler under the actual environment. Increase crawlers and connections gradually, if successful.

c. Maintenance and Monitoring: Have a strong crawler maintenance and periodic performance and grid integration monitoring systems.

Environmental Impact Assessment

When Mobile Wave Crawlers are implemented in the nearshore waters of the Bay of Bengal within Bangladesh's Exclusive Economic Zone (EEZ), specifically at Cox's Bazar, Kuakata, and Saint Martin Island, the possible environmental impacts and mitigation measures are illustrated in Table 5.

Factors Affecting Wave Energy Generation in Bangladesh

a. Wave Potential in Bangladesh: Moderate wave energy potential is available in the Bay of Bengal. Research indicates a range of wave power of 5-15 kW/m along the coastline, with

the highest energy recorded during the monsoon months (June-September). Wave energy availability is seasonal, because when the seas are calmer in winter output is low.

b. MWC Capacity: In general, a small mobile crawler can produce 1-10 kW on its own, depending on the size of the crawler, its efficiency, and the waves. More advanced and bigger MWCs may scale to = 50-100 kW.

c. Deployment Scenario: A single crawler in ideal wave conditions in the Bay of Bengal would yield:

- 5-1 kWh per day on smaller crawlers.
- Larger systems have 50-200 kWh per day, depending on the intensity of the waves.

This production would be scaled by strategically positioning several crawlers.

Key Challenges and Solutions Electricity produced by the mobile wave crawler depends on its design, efficiency and the conditions of the waves in which it has been deployed. These devices utilize wave energy to generate electrical power via mechanical or hydraulic mechanisms. These are the general considerations:

a. Size and Design: A small mobile wave crawler could produce a few kilowatts (kW) that could serve to power small devices, sensors, or communication systems. The larger, more advanced design can produce tens or hundreds of kW, which can be added to a local grid or other larger power requirements.

b. Wave Conditions: The energy production is very much dependent on the height of the wave, the frequency and consistency. Areas that have high and consistent waves (e.g. along the shoreline or the open oceans) will produce more energy.

c. Efficiency: The conversion efficiency of a wave energy device is generally between 20 to 40 percent of the incoming energy.

d. Wave Conditions: Moderate wave power constrains output in areas with greater wave power potential (e.g. the North Sea).

e. Cost and Feasibility: It may be costly to install and maintain on a large scale.

f. Technology Adaptation: The devices should be able to withstand severe weather conditions such as cyclones, which are prevalent in the Bay of Bengal.

Table 6 presents likely solutions to address the issues outlined above in Bangladesh.

Table 6. Key Challenges and Solutions to Implementing MWC in Bangladesh.

Challenge	Solution
High initial investment	Find sources of funds through government subsidies or public- private associations.
Intermittent energy supply	Storing the energy or hybrid (e.g., solar or wind integration).
Cyclones and extreme weather	Install robust crawlers that have weatherproof designs.
Limited grid access in remote areas	Localized microgrids first with crawlers then scaled to national grid.
Transmission losses over long distances	Install offshore substations that are as close to the coast as possible.

Conclusion

To achieve the renewable energy goal, integrating mobile wave crawlers into Bangladesh's grid can be a good solution. Bangladesh can also harness its blue energy potential with this device. Investment case: First-rollout costs are high, but they can lead to energy security and off-grid solutions tailored to coastal areas and islands. So, in other words, we won't have mobile wave crawlers serving as a source of Bangladesh-wide energy by any means. Still, they could potentially be the difference in decentralized coastline or island dependence, especially when

monsoons hit. The number of devices deployed, their efficiency, and the wave energy potential of the Bay of Bengal are some of the variables that determine how much power mobile wave crawlers can contribute to Bangladesh's national grid. The authors of this study outline the Mobile Wave Crawler's viability and operation in Bangladesh. The ship's size, the island's population, and relevant parameters determine how many devices are needed. Keeping these factors in mind, the authors propose a feasible solution for several islands in Bangladesh. The LCOE and energy generation capability presented in this paper can be significantly improved by modifying the other factors related to them. Thus, it can be a good solution for energy in the coastal areas and islands of Bangladesh. The authors plan to conduct detailed technical and economic studies, develop a prototype, and test it in a towing tank shortly.

Acknowledgment

The author received no financial support or external contribution for this work.

Authors contribution

Md Riad Khan: Conceptualisation, literature review, methodology, investigation, analysis, original draft preparation, review and editing

Nusrat Sharmin and SM Rashidul Hasan: Conceptualisation, supervision, review

Conflict of interest

The authors declare that this work has no conflict of interest.

References

Arzu F, Anjum N and Hassan MM. Offshore industry in Bangladesh: Present status and future prospect to contribute for national economy. *Bangladesh Mar. J.* 2024; 7(1): 85-98.

Bangladesh Bureau of Statistics (BBS). Population census - 2011. Preliminary report. Bangladesh Bureau of Statistics, Ministry of Planning, Government of the People's Republic of Bangladesh, Dhaka, 2011.

Bhasan Char Population Factsheet. Report on Rohingya Refugee Response/Bangladesh. GoB - UNHCR Joint Registration Exercise, September 30, 2024.

Briggs J, Sharon A and Wirz H. Mobile wave energy harvesting system.*NSTI-Nanotech*. 2011; 3: 683-686.

Chouhan MS. *How many islands does Bangladesh have? Largest one is...*: www.dnaindia.com/viral August 14, 2024.

Electricity demand per capita in MWh in Bangladesh. ChartingTheGlobe.com, 2024.

Hossain MS. Biological aspects of the coastal and marine environment of Bangladesh, *Ocean & Coastal Managemen*t, 2001; 44: 261-282.

Mobile Wave Crawler. Fraunhofer USA, Electrical Power Generation from Ocean Waves, 2011.

Islam MR. *Where Land Meets the Sea: A Profile of the Coastal Zone of Bangladesh*, The University Press Limited, Dhaka, 2004.

Islam S. *সড়ক পথে যাওয়া যাবে শাহপরীর দ্বীপ* :Bangla Tribune; Nov 9, 2018.

Khan MR, Islam A and Abdullah A. Time and Cost Effective Ship Design Process Using Single Parent Design Approach with Considerable Dimension Difference. In: *12th International Conference on Marine Technology*, 2020; 11–19.

Khan MR, Kundu R, Rahman W, Haque MM and Ullah MR. Efficiency study: Contra-rotating propeller system. In:*International Conference on Mechanical Engineering*, Proceedings of the 12th International Conference on Mechanical Engineering (ICME 2017), 2017 December 20–22; Dhaka, Bangladesh: AIP Conference Proceedings; 2018. vol. 1980. pp.060001-1–060001-7.

Kundu R, Khan MR, Rahman S and Saha GK. Design and structural analysis of a pontoon vessel. In: *International Conference on*

Mechanical Engineering, Proceedings of the 12th International Conference on Mechanical Engineering (ICME 2017), 2017 December 20–22; Dhaka, Bangladesh: AIP Conference Proceedings; 2018. vol. 1980. pp. 030006-1–030006-7.

Mahbub MAL and Islam ARMT. Current status of running renewable energy in Bangladesh and future prospect: A global comparison. *Heliyon*. 2023; 9(3): e14308.

Mansur M, Enam FB and Baree MS. Development of the wave spectrum of the northern region of the Bay of Bengal based on Indian National Centre for Ocean Information Services (INCOIS) moored buoy data. *J. Mech. Eng*. 2017; 47: 22-30.

Mazumder P, Jamil MH, Das CK and Matin MA. Hybrid energy optimization: An ultimate solution to the power crisis of St. Martin Island, Bangladesh. In: 2014 9th International Forum on Strategic Technology (IFOST), Cox's Bazar, Bangladesh; 2014, pp. 363-368

Mohiuddin. *Cost 3 times higher, yet electricity being purchased from oil-run power plants*:Prothomalo; February 28, 2024.

Sarker PK. *Offshore Exploration: Looking back at Bangladesh's historical footprints*: Dhaka Tribune; March12, 2024.

Sarwar GM and Wallman P. *Impacts of Sea Level Rise on the Coastal Zone of Bangladesh*, 2005.

Uddin MM and Park J. Renewable Energy Resources in Bangladesh: Current Status and Future Prospects. In: 2021 IEEE 48th Photovoltaic Specialist Conference (PVSC); 2021. pp. 2180-2186.

J. Bangladesh Acad. Sci. 49(2); 227-242: December 2025 DOI:https://doi.org/10.3329/jbas.v49i2.79820

Journal of Bangladesh Academy of Sciences

Journal homepage: http://www.bas.org.bd/publications/jbas.html

Research Article

A computational analysis of a hypothetical protein from *Acinetobacter nosocomialis* identifies it as a multicopper oxidase linked to the copper resistance system

Nizam Uddin and Anika Tasnim*

Bangladesh Council of Scientific and Industrial Research, Dhaka, Bangladesh

ARTICLE INFO

Article History

Received: 12 Feburay 2025
Revised: 21 August 2025
Accepted: 25 August 205

Keywords: *Acinetobacter nosocomialis*, Hypothetical protein, Homology modeling, Virtual screening.

ABSTRACT

Acinetobacter nosocomialis, a nosocomial pathogen, particularly affecting immunocompromised individuals. This species is retaining multidrug resistance and it is increasing over the time. The organism is dependent on human hosts for survival and exerts several methods to circumvent both innate and adaptive immune response. Some of the defence systems are intrigued by extracellular or intracellular proteins of this pathogen. Hence, characterize the unannotated proteins, also called hypothetical proteins, could play a big role in identifying novel treatment targets. In this study, we focused on the characterization of a hypothetical protein (HP) (accession No. KDM58575.1) derived from *Acinetobacter nosocomialis.* In-silico tools was employed to examine the hypothetical proteins, focusing on physicochemical parameters, subcellular localisation, secondary structure, three-dimensional structure, and functional annotation. To study the active site, protein-protein interactions and molecular docking, the bioinformatics tools CASTp, the STRING server, and PyRx were utilized, respectively. The findings identified this protein as a multicopper oxidase involved in detoxification, transport, and metal binding. The 3D structure derived from the SWISS Model server, and it was matched 89.92% similarity to the AlphaFold DB model A0A0M3ADD5.1, a copper oxidase derived from *Acinetobacter sp*. AG1 (gene: A0A0M3ADD5_9GAMM). This protein also showed considerable biological activity and consists of five functional domains, like cupredoxin. The protein-protein interaction also delineates the essential partners required for bacterial viability, whereas KEGG suggested the protein associated with the bacterial two-component signalling system. In docking analysis, the ligand exhibited significant binding activities and suggesting a potential target for treating nosocomials infection. This study highlights the bioinformatics tools for protein characterization and understanding molecular pathways for *Acinetobacter nosocomialis.* Furthermore, it offers significant insights into the development of innovative therapeutic procedures.

Introduction

Acinetobacter spp., a nosocomial pathogen, is accountable for a variety of infections, especially in Immunocompromised individuals or those who have experienced prolonged hospitalisation. These infections are linked to considerable morbidity and mortality rates. (Ainsworth et al., 2017; McConnell and Pachón, 2010). Most Acinetobacter species are widely distributed in the environment and can survive and persist in harsh, desiccated environments (Williams et al., 2016). Acinetobacter species are presently widespread in healthcare environments, especially within intensive care units (ICUs). Anton et al. (2008) say Acinetobacter species can cause pneumonia, urinary tract infections, bacteremia, skin

*Corresponding author:<anika-2016514146@bmb.du.ac>

and soft tissue infections, osteomyelitis, and meningitis. Antibiotic-resistant bacteria can cause more serious sickness and death without proper treatment (Metan et al., 2009). The incidence of extensively drug-resistant (XDR) and multidrug-resistant (MDR) strains makes Acinetobacter species a "serious" concern for the CDC.

The National Cancer Institute of Mexico conducted a study of ICU infections. Acinetobacter species caused 6% of nosocomial infections. These infections were strongly associated with pneumonia (60% of cases) and bloodstream (25% of cases) (Cornejo-Juárez et al., 2015). The rise of drug-resistant Acinetobacter species and other highly resistant bacteria has highlighted the need for alternative antibacterial methods to address broad antibiotic resistance (Williams et al., 2016). Maintaining metal homeostasis is essential and offers many unique targets for bacterial reduction. Copper is needed for cellular processes such as redox balance regulation and enzyme cofactor function (Williams et al., 2016). However, large copper ion concentrations can be hazardous. Fenton chemistry produces hydroxyl radicals that damage important biomolecules when these ions participate (Liochev and Fridovich, 2002).

Iron-sulfur cluster proteins are damaged by copper-sulfur atom interactions and iron ion displacement (Macomber and Imlay, 2009). Copper surfaces damage Escherichia coli and Salmonella spp. outer membranes, according to recent investigations. This process produces hydroxyl radicals, suppresses respiration, and degrades DNA (Warnes et al., 2012). Copper as an antibacterial agent has attracted increased study due to the demand for therapies against antibiotic-resistant organisms. Many diseases have been tested for copper susceptibility in labs. The use of different growth media and experimental techniques makes it impossible to compare these findings.

Hypothetical proteins have been found in *Acinetobacter sp*. Hypothetical proteins (HP) are expressed in organisms but require empirical and chemical validation (Ashrafi et al., 2019; Rahman et al., 2020; Paul et al., 2015). An ORF can predict the creation of these proteins even while there is no evidence for their existence (Paul et al., 2015; Rahman et al., 2020). Putative proteins account for 50% of protein-coding regions in most genomes, and their functions are unknown (Paul et al., 2015; Mazumder et al., 2021). In hypothetical proteins, there are two types: uncharacterized protein families (UPF) and domains of unknown function (DUF) (Rahman et al., 2020). Uncharacterized protein families (UPF) lack a clear relationship with genes but are identified through experimentation. On the other hand, proteins identified empirically lacking functional or structural domains are called DUFs (Rahman et al., 2020). Studying the structural and functional UPF and DUF can reveal domains and motifs, pathways and cascades, and protein networks. This study will identify pharmaceutical targets and help in diagnosis (Ashrafi et al., 2019; Paul et al., 2015). Recently, a number of bioinformatics tools have been used to characterize proteins, including three-dimensional structural conformations, the discovery of novel domains and pathways, phylogenetic profiling, and the provision of functional annotations (Ashrafi et al., 2019; Rahman et al., 2020). This research was used to characterize a hypothetical protein (KDM58575.1) identified in *Acinetobacter nosocomialis*. Multiple bioinformatics tools and databases were used to gain a thorough understanding of the protein's physical and structural characteristics, as well as its possible functions. Furthermore, molecular docking was performed to elucidate the structural features and potential functions of this protein.

Materials and Methods

Sequence Retrieval

At first, the term "Hypothetical proteins AND *Acinetobacter nosocomialis*" was searched in NCBI, and the accession number KDM58575.1 (hypothetical protein) was retrieved in FASTA format. A sequence-based peptide search was also conducted using the UniProt database (https://www.uniprot.org/peptidesearch/) to assess protein redundancy. The sequence was subsequently analyzed using various

computational tools for in-silico characterization and functional analysis (Table 1).

Physicochemical properties

The ProtParam tool on the ExPASy server application (http://web.expasy.org/protparam/) (Gasteiger et al., 2005) was used to analyze various physical and chemical properties of the protein. Among these were the grand average of hydropathicity (GRAVY), instability index, aliphatic index, extinction coefficient, estimated half-life, molecular weight, theoretical pI, amino acid, and atomic composition, and the total number of negatively and positively charged residues (Asp+Glu and Arg+Lys) (Gasteiger et al., 2005).

Identification of Subcellular Localization

Accurate determination of subcellular localization is critical for proper protein function and genetic analysis. Since drug and vaccine targets are situated within cells, understanding this information is crucial for discovering and developing new pharmaceuticals. Subcellular localization and protein topology were analyzed using CELLO v.2.5, which employs a two-level support vector machine (SVM) prediction system (Yu et al., 2006). The localization predictions from CELLO were further cross-validated with results from HMMTOP v.2.0 (Tusnády and Simon, 2001), TMHMM v.2.0 (Krogh et al., 2001; Möller et al., 2001), and PSORTb v3.0 (Yu et al., 2010).

Determining the domain, coil, folding pattern, protein family, and superfamily

The conserved domain was predicted using the NCBI CD tool (Marchler-Bauer et al., 2011) via Reverse Position-Specific BLAST (RPS-BLAST). Evolutionary relationships were analyzed using GenomeNet (Kanehisa et al., 2002), Pfam (Finn et al., 2014), the SuperFamily program (Wilson et al., 2007), and the ScanProsite tool (Sigrist et al., 2012).

Pfam, a database of protein families, uses hidden Markov models (HMMs) for annotation and multiple sequence alignment. Protein sequence motifs were detected using the MOTIF search tool (https://www.genome.jp/tools/motif/) and the InterProScan tool.

Analysis of Multiple Sequence Alignment and Phylogeny

Protein sequences with similar functionalities were retrieved by querying the NCBI non-redundant protein sequence (nr) database using BLASTp with default settings. Multiple sequence alignment was performed using EBI's MUSCLE server (https://www.ebi.ac.uk/Tools/msa/muscle/) (Edgar, 2004) and visualized using CLC Sequence Viewer 7.0.2 (http://www.clcbio.com). Phylogenetic analysis was performed utilizing the Phylogeny online platform (http://phylogeny.lirmm.fr/).

Secondary structural assessment

The SOPMA program was used with default parameters, including a window width of 17, a similarity threshold of 8, and 4 states (Combet et al., 2000). The PSIPRED version 4.0 (Buchan and Jones, 2019) is used to determine additional secondary structure and protein topology.

Three-dimensional structure prediction and assessment of Model quality

The tertiary structure of the uncharacterized protein was modelled to examine its three-dimensional configuration and folding characteristics. The Swiss Model program (Bitencourt-Ferreira and de Azevedo, 2019) and the D-I-TASSER servers were used to generate the protein's tertiary structure. The HHpred tool was used to search for the best template, including the SWISS model template, for further analysis (Biegert et al., 2006; Gabler et al., 2020; Zimmermann et al., 2018).

PROCHECK and Verify3D programs within the SAVES (v.6.0) platform were used to validate the protein structure (Bowie et al., 1991). Using the ProSA-web application, Z-score and modelled 3D-structure validation were performed (Wiederstein and Sippl, 2007).

Table 1. Sequence-Based Function Annotation Databases and Bioinformatics Tools.

Sl no.	Software	Function	Reference
1.	BlastP	Identifies similar sequences within protein databases	Altschul et al., 1997
2.	MUSCLE	Performs multiple sequence alignment	Edgar, 2004
3.	ExPASy-Protparam tool	Calculates physical and chemical properties of proteins	Gasteiger et al., 2003
4.	CELLO	Predicts localization of proteins in prokaryotic and eukaryotic cells	Yu et al., 2004
5.	PSLpred	Predicts subcellular localization for proteins in Gram-negative bacteria	Bhasin et al., 2005
6.	PSORTb	Predicts the subcellular localization of bacterial proteins	Yu et al., 2010
7.	SOPMA	Predicts the secondary structure of proteins	Mazumder et al., 2021
8.	PSIPRED	Analyzes protein secondary structure using PSI-blast	Jones, 1999
9.	HHpred	Detects protein homology using HMM-HMM comparison	Zimmermann et al., 2018
10.	PyMOL	Facilitates structural analysis and generation of model figures	Mazumder et al., 2021
11.	YASARA	Enhances the stability of 3D protein models	Krieger et al., 2009
12.	PROCHECK's Ramachandran plot analysis	Evaluates the quality and accuracy of predicted 3D protein structures	Laskowski et al., 1993
13.	Verify3D	Assesses protein models using 3D profiles	Eisenberg et al., 1997
14.	ERRAT	Analyzes nonbonded atomic interactions to validate protein structures	Colovos andYeates, 1993
15.	CD Search	Identifies conserved structural and functional domains within sequences	Marchler-Bauer et al., 2011
16.	InterProScan	Searches InterPro for motif and domain discovery	Jones et al., 2014
17.	STRING	Predicts protein-protein interactions	Szklarczyk et al., 2019
18.	CASTp	Identifies and measures surface regions within 3D protein structures	Tian et al., 2018

Energy minimization of the model structure

The 3D structure was energy-minimized using YASARA (Krieger et al., 2009). The PDB format of the hypothetical protein was submitted to the server, which optimizes the protein structure and provides an accurate, stable 3D conformation.

Active Sites Determination

Active Sites were determined by the Computed Atlas of Surface Topography of Proteins (CASTp) algorithm (http://sts.bioengr.uic.edu/castp/) (Tian et al., 2018). The CASTp results were subsequently visualised using PyMOL software (Mazumder et al., 2021).

Analysis of Protein-protein interaction

A computational software, STRING (version 11.5), was used to elucidate protein-protein interactions (Szklarczyk et al., 2018).

Analysis of Molecular Docking

Molecular Docking was performed to investigate the interactions between the protein and two distinct ligands. Previous research has not identified the ligands association with this potential protein. Ligand selection was based on the most structurally similar protein in the Protein Data Bank (PDB). This study investigated the compounds that are agonists or antagonists of multicopper oxidases (MCOs). MCOs, a redox enzymes, helps convert molecular oxygen into water by transferring four electrons.

Based on their expected high-affinity binding to the protein, two ligands were chosen: NAG (2-acetamido-2-deoxy-beta-D-glucopyranose) and beta-D-Mannopyranose. The ligands structure were obtained from PubChem and later converted to PDB format using Discovery Studio software. Docking was performed using PyRx, and interactions were visualized using PyMOL and Discovery Studio. Chimaera was also used to examine hydrophobic and hydrogen-bond interactions within 5 Å of the receptor and ligands. Fig.1. illustrates the workflow of the study.

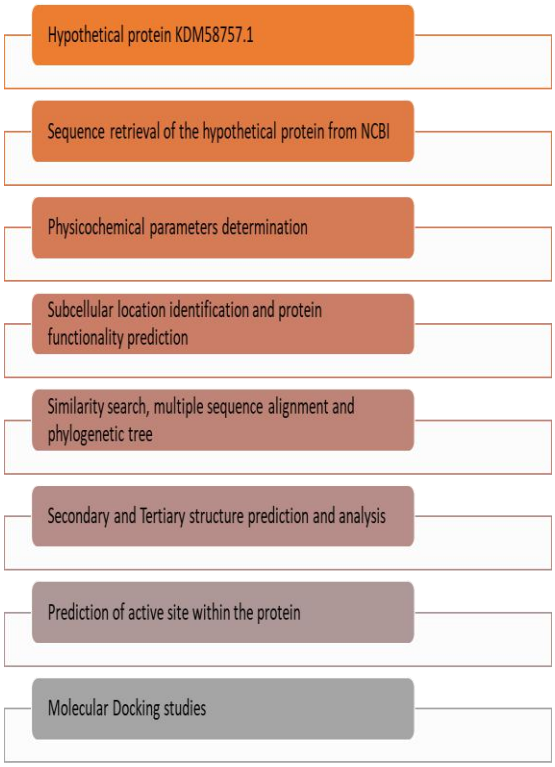

Fig. 1. A comprehensive study workflow.

Results and Discussion

Information about sequence retrieval and similarity

The protein's amino acid sequence of 645 residues was obtained in FASTA format from the National Centre for Biotechnology Information (NCBI) database. The sequence was subsequently analyzed using UniProt. The UniProt database entries confirmed that the protein is non-redundant, which suggests its potential significance. Additional details retrieved from the NCBI database are presented in Table 2.

The ProtParam tool was used to obtain a full picture of its physicochemical properties. There are 645 amino acids in the protein. The most common ones are serine (n=56, 8.7%) and methionine (n=55, 8.5%). It is important to note that the sequence does not include selenocysteine or pyrrolysine.

Table 2. Protein distinctiveness and protein data.

Parameters	Protein Information
Locus	KDM58575
Amino Acid	645 aa
Definition	hypothetical protein AE32_00579 [*Acinetobacter nosocomialis*]
Accession	KDM58575
Version	KDM58575.1
GenBank ID	KDM58575.1
Source	*Acinetobacter nosocomialis*
Organism	*Acinetobacter nosocomialis*

Determination of Physicochemical Parameters

The half-life of the protein, which is the time it takes for the concentration of a radiolabeled protein to drop by 50% during the chase phase (Zhou, 2004), was about 30 hours in vitro in mammalian reticulocytes, over 20 hours in vivo in yeast, and more than 10 hours in vivo in Escherichia coli. The isoelectric point (pI), total atom count, and molecular weight were found to be 6.34, 10,041, and 72,740.88 Daltons, respectively (Table 3).

The protein comprises 72 positively charged residues (Arg + Lys) and 81 negatively charged residues (Asp + Glu). The instability index (40.61) indicates the protein's stability, whereas the aliphatic index (63.60) denotes its structural robustness over a wide spectrum of temperatures. Furthermore, the overall average hydropathicity (GRAVY) value of -0.576 indicates an improvement in thermostability (Pawel et al., 2007).

Subcellular location determination and protein topology prediction

The classification of the proteome, identification of potential therapeutic targets, and development of vaccines all depend on automated prediction of bacterial protein subcellular localization. In recent years, researchers have developed seversl subcellular localisation predictors, including both generalized and feature-based predictors (Restrepo-Montoya et al., 2009; Schneider and Fechner, 2004). Using the CELLO (v.2.5) and PSORTb (v3.0) computational methods, it was anticipated that the protein would be found outside of the cell (Yu et al., 2004).

Table 3. Protein Physicochemical parameters determination.

Parameter	Value
Molecular Weight	72740.88
Formula	C3159H4966N884O976S56
Total number of atoms	10041
Theoretical pI	6.34
The total number of positively charged residues (Arg + Lys)	72
The total number of negatively charged residues (Asp + Glu)	81
The measured half-life	30 hours (mammalian reticulocytes, in vitro) over 20 hours (yeast, in vivo) over 10 hours (Escherichia coli, in vivo)
Aliphatic index	63.60
Instability index (II)	40.61
Grand average of hydropathicity	-0.576

Moreover, one of the most important aspects of bioinformatics is the detection of transmembrane helices in integral membrane proteins. Furthermore, the most successful current methodologies aim to predict the comprehensive topology of proteins, encompassing the total number of transmembrane helices and their orientation with respect to the membrane (Krogh et al., 2001; Möller et al., 2001). A single transmembrane helix was predicted to be present in the protein by the TMHMM version 2.0 and HMMTOP version 2.0 software programs (Table 4).

Forecasting the domain, coil, folding pattern, protein family, and superfamily

The preliminary objective of the Conserved Domain Database (CDD) is to provide annotations for

Table 4. Subcellular location Identification.

Web Tools Analysis	Result
CELLO v2.5	Periplasmic
PSORTb v3.0	Periplasmic
HMMTOP v.2.0	one transmembrane helix
TMHMM v.2.0	one transmembrane helix
CCTOP	one transmembrane helix

molecular sequences by identifying and assigning evolutionarily conserved protein domains. NCBI's Entrez database maintains a collection of pre-computed domain identification for proteins, along with real-time search capabilities. The protein was categorized by the CDD tools as a multicopper oxidase belonging to the copper resistance system. This protein, with a domain architectural ID of 1001039, exhibits significant similarity to the copper resistance protein A found in Escherichia coli. The latter is known to play a crucial role in the copper-inducible production of copper resistance and is believed to possess oxidase function. The GenomeNet program has successfully identified five motifs in the given dataset. These motifs include multicopper oxidase, which is located between positions 32 and 146, with an independent E-value of 1.1*10-34. Another instance of multicopper oxidase is found between positions 159 and 317, with an independent E-value of 3.8*10-26. Additionally, there is a multicopper oxidase motif between positions 505 and 617, with an independent E-value of 2.9*10-27. Another motif identified is the cupredoxin-like domain, spanning positions 529-610, with an independent E-value of 0.92. Lastly, a motif corresponding to a protein of unknown function is located between positions 206 and 233, with an independent E-value of 0.2. The five motifs, namely multicopper oxidase (accession id PF07732), multicopper oxidase (accession id PF00394), multicopper oxidase (accession id PF07731), cupredoxin-like domain (accession id PF13473), and protein of unknown function (accession id PF05339), were validated by both the Pfam program (Finn et al., 2014) and the ScanProsite tool.

Examination of alignment, phylogenetic tree, and sequence similarity

The hypothetical protein's (HP) BLASTp analysis against non-redundant databases revealed a high degree of homology with other copper oxidase proteins from different species. Table 5 lists the copper oxidase proteins extracted from the multiple sequence alignment (MSA) generated by BLASTp. The hypothetical protein's sequence matched that of other copper oxidases, as indicated by the MSA (Fig. 2). A phylogenetic analysis was performed to further validate the homology and to investigate the evolutionary relationship among the aligned oxidases and the target protein. Based on the MSA and BLASTp results, the phylogenetic tree confirmed the hypothetical protein's homology and provided additional information on evolutionary distance (Figs. 2 and 3).

Table 5. A protein BLASTp search analysis was used to find homologs of KDM58575.1.

Accession	Description	Scientific Name	Total Score	E value	Per. ident
WP_050488919.1	copper resistance system multicopper oxidase	*Acinetobacter nosocomialis*	1340	0	100
WP_086376332.1	copper resistance system multicopper oxidase	*Gammaproteobacteria*	1333	0	99.38
MCT9255433.1	copper resistance system multicopper oxidase	*Acinetobacter baumannii*	1325	0	98.6
WP_006582181.1	multicopper oxidase domain-containing protein	*Acinetobacter nosocomialis*	1324	0	95.56
WP_098715181.1	copper resistance system multicopper oxidase	*Acinetobacter baumannii*	1323	0	98.45

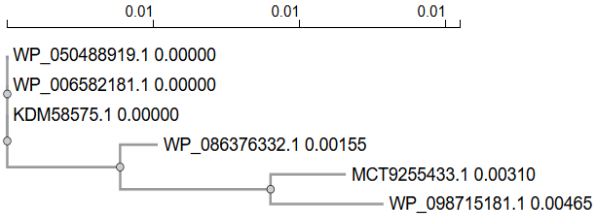

Fig. 2. Phylogenetic trees depicting the true distances between various oxidase proteins are shown. The scale bar in the tree estimates sequence divergence, while the line segments, labeled with the number (0.01), represent the degree of genetic change.

prediction using SOPMA and PSI PRED produced consistent results. The SOPMA analysis identified alpha-helices (n=51, 7.91%), extended strands (n=142, 22.02%), and random coils (n=452, 70.02%) (Fig. 4), emphasizing the predominance of random coil structures.

Tertiary Structure Analysis, Energy minimization, and assessment of Model quality

The Swiss-Model server was used to analyze the query sequence in order to predict the structure and determine protein homology; the Alpha Fold DBmodel of

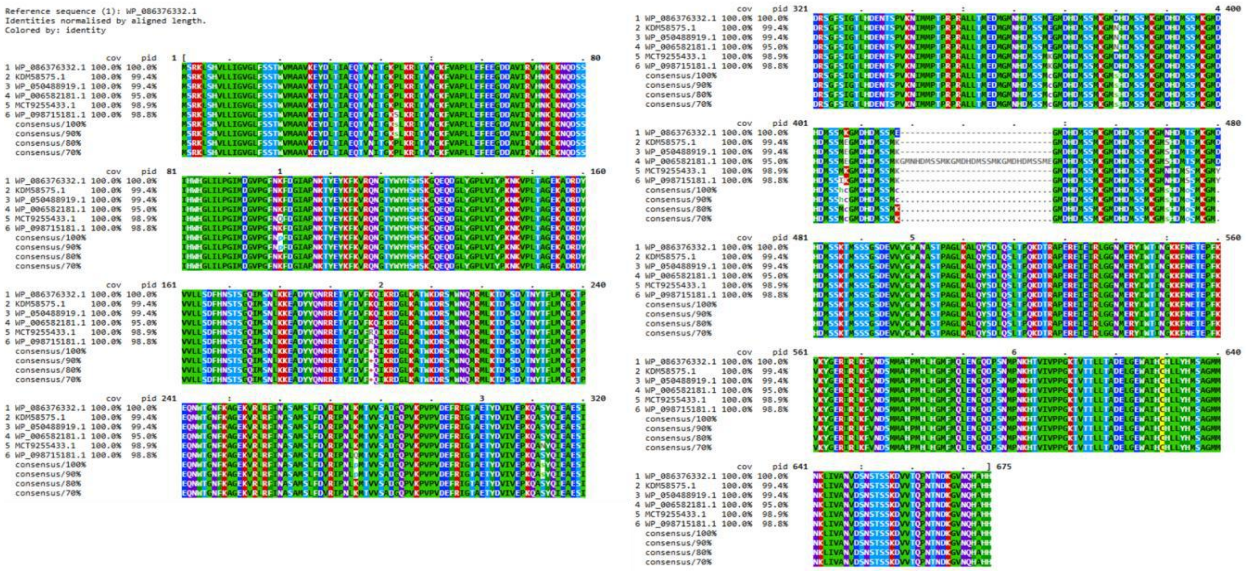

Fig. 3. MSA analysis among the different types of copper resistance system multicopper oxidase with the KDM58575.1 (generated by Mview Version 8).

Assessment of Secondary Structure

Static high-resolution structures have greatly enhanced our understanding of protein architecture and molecular mechanisms. However, developments in structural biology have shown that the molecular basis of protein structure and function in solution cannot be fully understood by high-resolution structures alone (Hodge et al., 2020; Hu et al., 2018; Uversky, 2019). Protein functionality, structural organization, and intermolecular interactions are all significantly influenced by secondary structural elements like helices, sheets, coils, and turns (Hegyi and Gerstein, 1999; Hodge et al., 2020). Secondary structure

A0A0M3ADD5.1, a copper oxidase from *Acinetobacter* sp. AG1 (gene: A0A0M3ADD5_9GAMM), as illustrated in Fig. 5A.

Additionally, 3D structures were generated using the D-I-TASSER server (Fig. 5B).

The quality of the predicted three-dimensional models was assessed using PROCHECK, which analyzed φ and ψ angle distributions using Ramachandran plot. For the Swiss-Model prediction, 85.7% of residues were found in the most favored regions (Table 6, Fig. 6A), indicating a high-quality model. In contrast, the model generated by D-I-TASSER demonstrated lower quality and was excluded from further analysis.

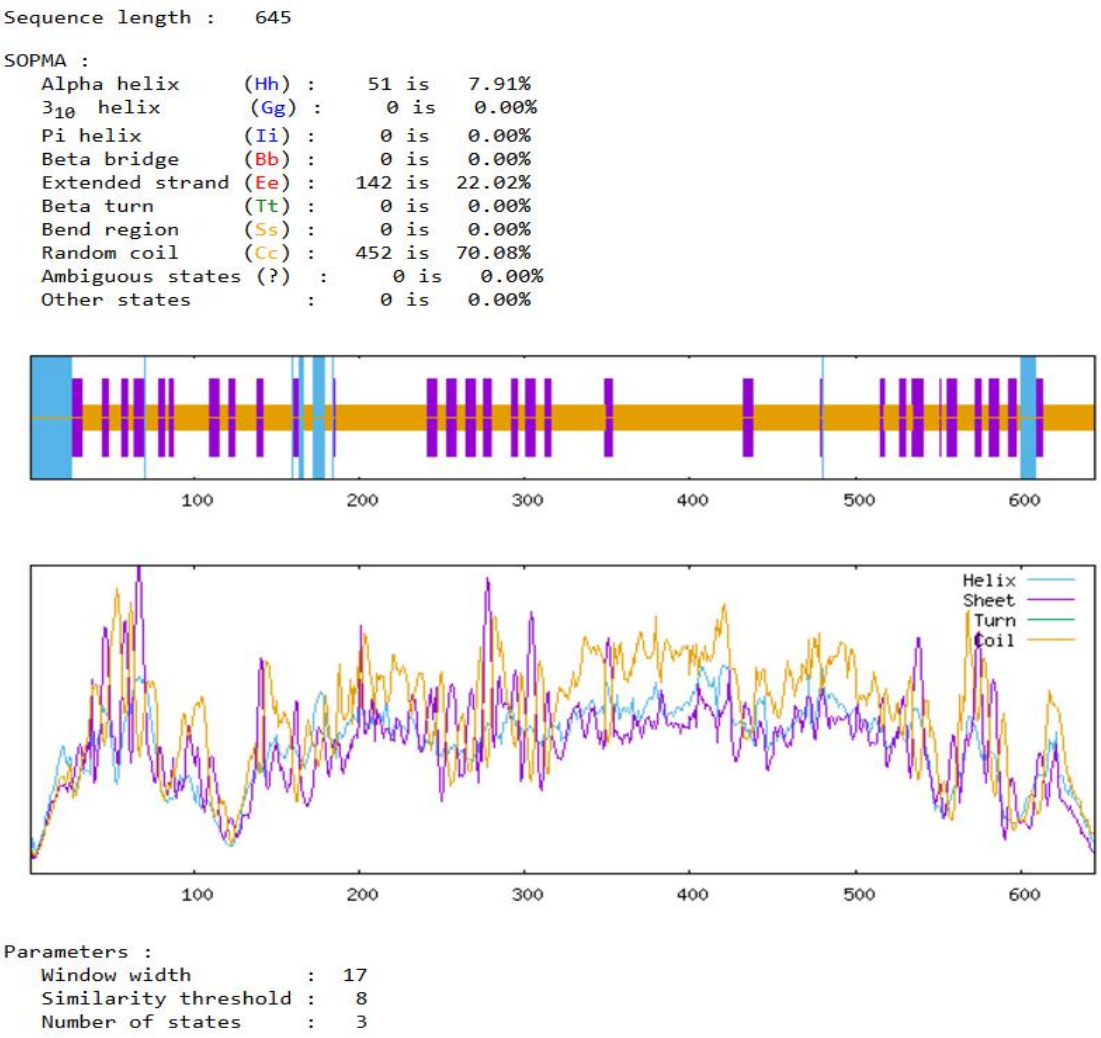

Fig. 4. The predicted secondary structure is visualized by the SOPMA server, which gives information about the coils, sheets, and helices that the protein is expected to contain based on its amino acid sequence.

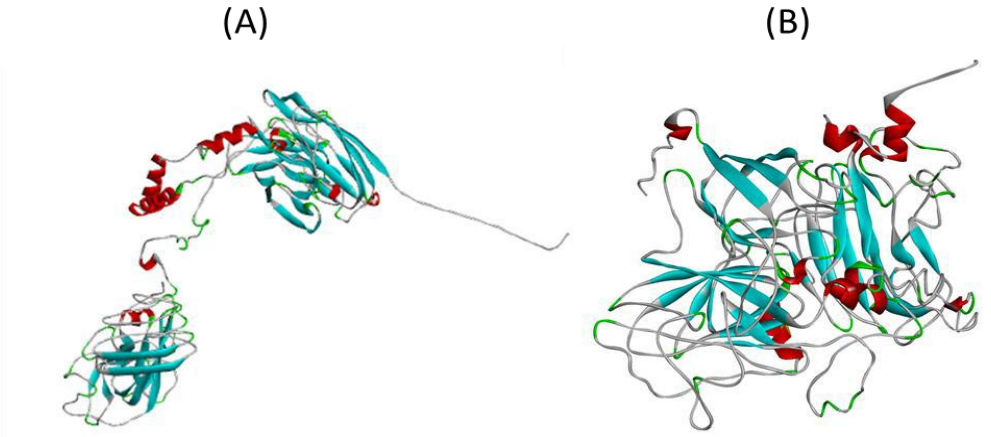

Fig. 5. Predicted three-dimensional structure of the KDM58575.1 by Swiss model (A) and I-TASSER (B) (visualized by Discovery Studio).

Table 6. The hypothetical protein's Ramachandran plot statistics

Statistics for Ramachandran plots	No. (%)
The most preferred regions' residues ⌊A, B, L⌋ 487	85.7
Residues in the additional allowed regions ⌊a, b, l, p⌋ 64	11.3
Residues in the generously allowed regions ⌊a, b, l, p⌋ 9	1.6
residues in the prohibited areas: 8	1.4
Number of non-glycine and non-proline residues: 568	100
Number of end-residues (excl. Gly and Pro): 2	
Number of glycine residues (shown in triangles): 47	
Number of proline residues: 28	
Total Number of residues: 645	

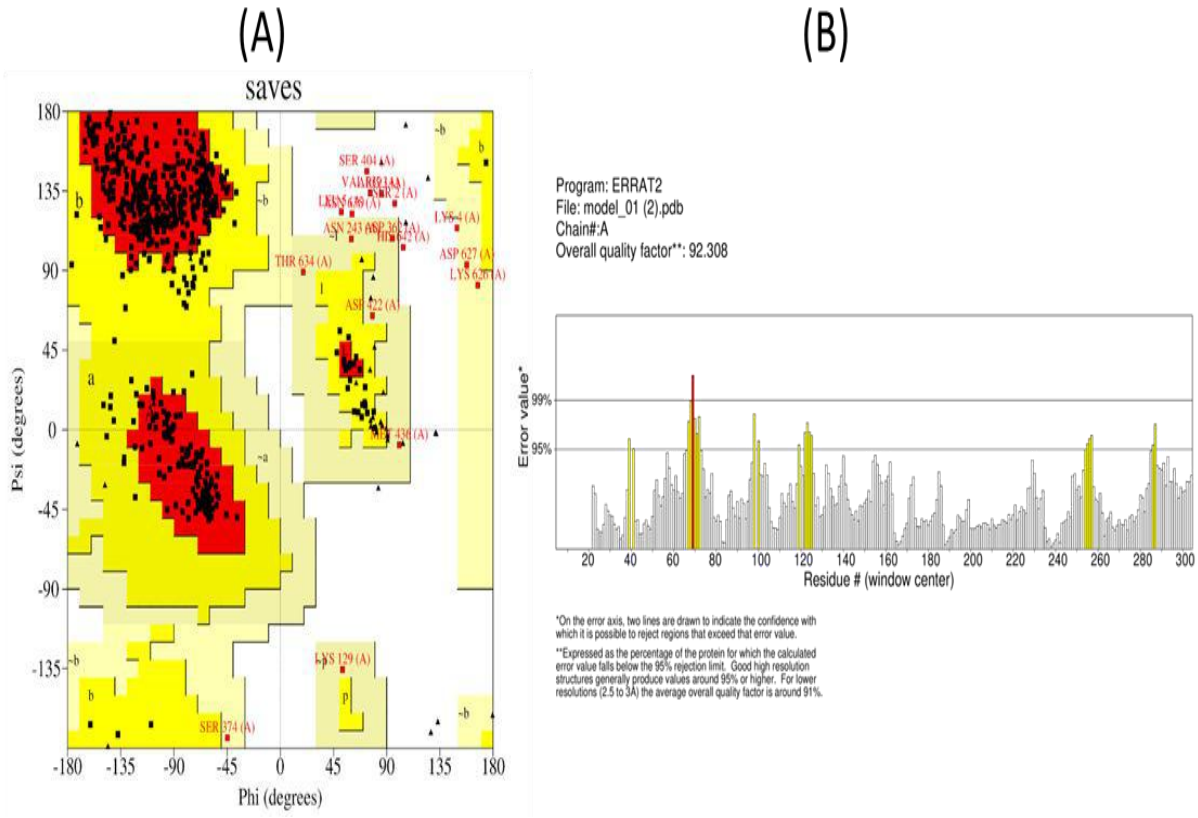

Fig. 6. (A) The Ramachandran plot of the predicted model through the Swiss Model, validated using the PROCHECK server, illustrates the tertiary structure of the hypothetical protein (HP). The beta-sheet region is represented in the first quadrant, while the right-handed and left-handed alpha-helix regions are depicted in the second and third quadrants, respectively. The plot's color-coded regions indicate residue distribution: red represents the most favored regions, yellow denotes additional allowed regions, gray indicates generously allowed regions, and white corresponds to disallowed regions. (B) The ERRAT server, which supplied the model's quality factor, was used to evaluate the target model's overall quality.

Verify3D and ERRAT were employed to verify 3D structures. The SWISS model's strong environmental profile was validated by the Verify3D analysis, which revealed that 92.73% of residues had an average 3D-1D score ≥ 0.2. The ERRAT analysis produced an overall quality factor of 92.308, signifying a reliable model (Fig. 6B).

The YASARA energy minimization server was used to fine-tune the protein. The energy of the structure prior to minimization was -238,197.1 kJ/mol, which improved significantly to -327,989.1 kJ/mol after three rounds of steepest descent energy minimization. Finally, the ProSA-web tool was employed to evaluate the model, yielding a Z-score of -6.76, consistent with a high-quality structural prediction.

Active site of the hypothetical protein

Identifying and characterizing active site residues are crucial steps in designing drugs or inhibitors. The CASTp server was used to analyze the active site of the modeled protein structure and identify the active-site amino acid residues. With a volume of 2779.748 and an area of 906.501, one of the largest pockets contained the main active sites. The active residues of the model protein as predicted by CASTp are shown in Fig. 7.

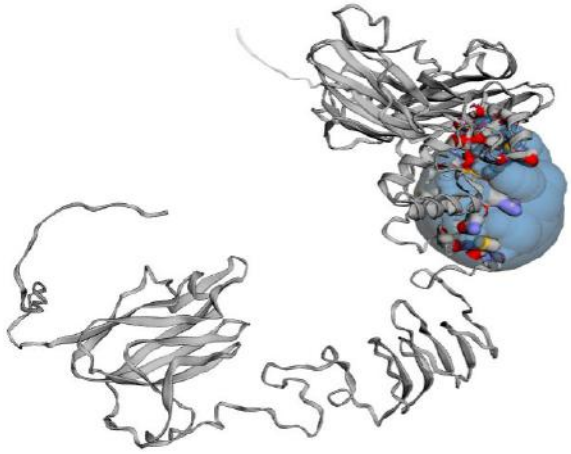

Fig. 7: The active site of KDM58575.1 was located using the CASTp server. The regions containing 906.501 and 2779.748 amino acid volumes had some of the largest active sites.

Protein-protein interaction

To attain a comprehensive understanding of biological phenomena, it is essential to consider proteins and their interrelationships with other proteins. However, current knowledge regarding protein-protein interactions is inadequate. The aim of the STRING database is to compile, assess, and integrate all publicly accessible sources of information on protein-protein interactions, while including computational predictions to improve its comprehensiveness. The purpose of this initiative is to construct a comprehensive and unbiased global network, encompassing both main (physical) and secondary (functional) connections (Marsh and Teichmann, 2014; Sowmya and Ranganathan, 2013; M. Wang et al., 2015). The protein-protein (pr-pr) interaction was identified using the STRING software (v.11.5). The program involving strings showcased the performance of various functional colleagues, as indicated by their respective scores: ARG18227.1 (0.489), ARG18228.1 (0.484), ARG18229.1 (0.506), ARG18230.1 (0.980), ARG18232.1 (0.749), ARG18233.1 (0.579), ARG18234.1 (0.622), ARG18235.1 (0.697), ARG18892.1 (0.916), ARG18900.1 (0.542) (Figure 8). Gene Ontology analysis indicates that this hypothetical protein plays a role in cellular copper ion homeostasis and copper ion binding (Table 7). Additionally, KEGG pathway analysis reveals its involvement in the bacterial two-component system of *Acinetobacter nosocomialis* (Table 7). These two-component signal transduction systems allow bacteria to detect, respond to, and adapt to environmental or intracellular changes. Each system typically comprises a sensor histidine kinase (HK) and a corresponding response regulator (RR).

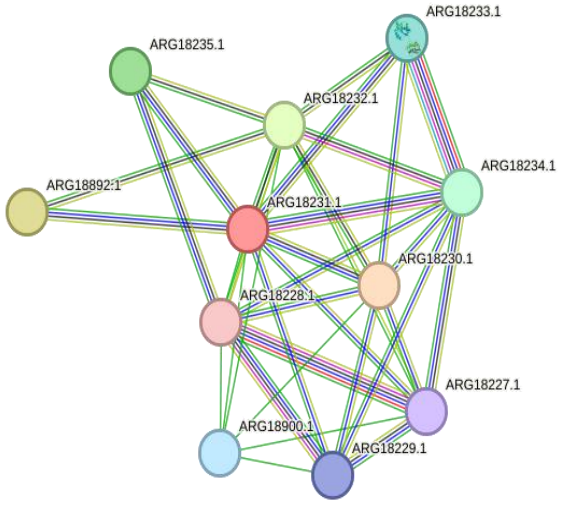

Fig. 8. Proteins with known or predicted 3D structures are represented as filled nodes, while unknown proteins are shown as empty nodes in a string network analysis of the hypothetical protein ARG18231.1.

Table 7. Functional Enrichment Analysis of the Hypothetical Protein.

Category of the function	Term ID	Description	Strength	Signal	False Discovery Rate(FDR)
GO Process	GO:0006878	Cellular copper ion homeostasis	2.54	1.77	0.00054
GO Function	GO:0005507	Copper ion binding	2.03	2.05	7.22E-05
STRING clusters	CL:5237	Mixed, incl. Copper binding periplasmic protein CusF, and Cellular copper ion homeostasis	2.24	5.01	1.46E-11
STRING clusters	CL:5164	Mixed, incl. Efflux transmembrane transporter activity, and HlyD family secretion protein	1.42	2.37	8.87E-10
STRING clusters	CL:5239	Copper binding periplasmic protein CusF, and AcrB/AcrD/AcrF family	2.44	3.2	6.94E-07
KEGG	ano02020	Two-component system	1.29	0.94	0.0046

Table 8. The summary provides information about the range and precision of interactions involving proteins.

Ligand	Binding Affinity	rmsd/ub	rmsd/lb	Interacting Molecules
2-acetamido-2-deoxy-beta-D-glucopyranose	-5.3	0	0	ARG255, GLU154, ALA15
beta-D-Mannopyranose	-5.7	0	0	GLN559, LEU556, PHE55 ASP590, ASN571

Molecular Docking Analysis

A structure-based approach to drug design, the molecular docking method predicts the mechanisms by which ligands and receptors bind by simulating molecular interactions. Docking analyses were used to investigate the interactions between a host protein and potential inhibitors using two ligands: NAG (2-acetamido-2-deoxy-beta-D-glucopyranose) and beta-D-mannopyranose. NAG is frequently used in computational docking studies as a representative sugar moiety due to its prevalence in bacterial cell walls and in host–pathogen interactions. We chose β-D-mannopyranose because sugars containing mannose are often used in studies of how microbes recognise and bind to substrates. We used Autodock Vina for docking studies and a targeted docking method to test substrate specificity. After the docking process, Discovery Studio was used to examine the interactions in more detail.

This study showed several interactions between the ligands and the protein. Beta-D-mannopyranose showed a significant propensity for binding affinity for the protein, with a docking score of -5.7 kcal/mol. NAG had a somewhat lower binding affinity, as shown by a docking score of -5.3 kcal/mol (Table 8 and Fig. 9). The compounds with the lowest docking scores were considered to have significant affinities,

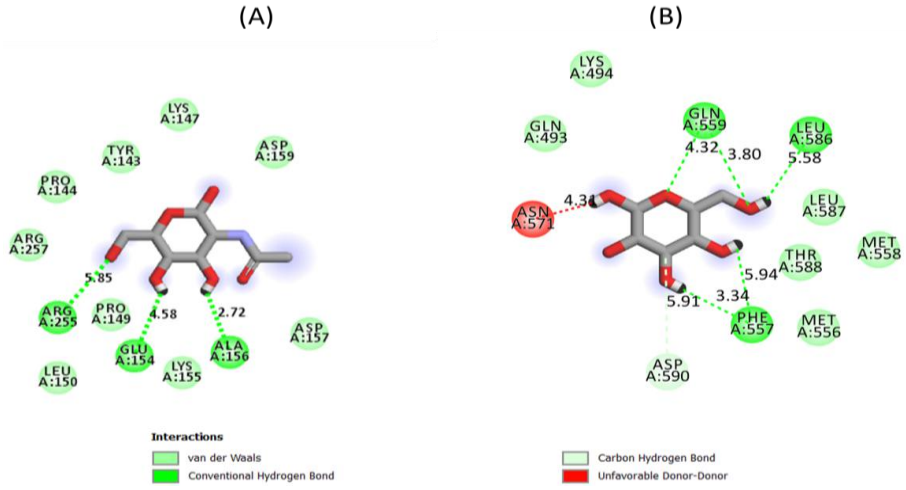

Fig. 9. The target protein's (HP) and putative ligands' intermolecular interactions are depicted as follows: (A) The target protein interacts with the ligand NAG (2-acetamido-2-deoxy-beta-D-glucopyranose); (B) the target protein interacts with the ligand beta-D-Mannopyranose.

suggesting they could be good inhibitors. This research provides valuable insights into where ligands are located and how they fit within the protein's binding site. This information is important for the design and improvement of therapeutic drugs targeting this protein.

Docking results indicated that 3-4 amino acid residues of the protein form hydrogen bonds with the bound complexes of NAG and beta-D-mannopyranose. Specifically, these interactions pertain to the residues ARG255, GLU154, and ALA156. Furthermore, complexes containing beta-D-mannopyranose ligands engage with residues GLN559, LEU556, and PHE557 (Fig. 9). These interactions, especially the hydrogen bonds within the active site residues, offer crucial insights into the mechanisms of residue-ligand binding, conformational architecture, and function, clarifying significant aspects of the protein's bilogical structure and function.

Conclusion

This study focused on the characterization of a hypothetical protein from *Acinetobacter nosocomialis*. The findings revealed that it is a multicopper oxidase involved in the copper resistance system. Through in silico analysis, the physicochemical characteristics, subcellular localisation, and structural and functional features of the protein were thoroughly characterised. The multicopper oxidase, which detoxifies, transports, and binds metal ions, indicates its involvement in bacterial survival. The SWISS-modeled protein's 3D structure confirmed its functional domain by identifying copper oxidase. The findings also revealed protein-protein interaction partners for essential bacterial pathways and KEGG pathways with respect to the bacterial two-component system. In a molecular docking study, high-binding ligands were identified as having therapeutic target potential. This examined protein may enable the pathogen *Acinetobacter nosocomialis* to be less resistant to copper toxicity, making it a possible diagnostic target for multidrug-esistant infections. Finally, these findings suggest that experimental validation and drug development are needed to address emerging diseases caused by *Acinetobacter nosocomialis.*

Acknowledgment

The authors acknowledge the Bangladesh Council of Scientific and Industrial Research for funding the study.

Authors contribution

Anika Tasnim: Conceptualization, formal analysis, methodology, review and editing; Nizam Uddin: Data curation, formal analysis, methodology.

Conflict of interest

We hereby declare that we have no conflict of interest regarding this paper.

References

Ainsworth S, Ketter PM, Yu JJ, Grimm RC, May HC, Cap AP, Chambers JP, Guentzel MN and Arulanandam BP. Vaccination with a live attenuated Acinetobacter baumannii deficient in thioredoxin provides protection against systemic Acinetobacter infection. *Vaccine*, 2017; 35(26): 3387-3394.

Altschul SF, Madden TL, Schäffer AA, Zhang J, Zhang Z, Miller W and Lipman DJ. Gapped BLAST and PSI-BLAST: A new generation of protein database search programs. *Nucleic Acids Res.*1997; 25(17): 3389-3402.

Anton Y, Peleg HS and David LP. Acinetobacter baumannii: Emergence of a Successful Pathogen Clinical Microbiology Reviews, 2008; 21(3): 538-582.

Ashrafi H, Siraji MI, Showva NN, Hossain MM, Hossan T, Hasan MA, Shohael AM and Shawan MMAK. Structure to function analysis with antigenic characterization of a hypothetical protein, HPAG1_0576 from Helicobacter pylori HPAG1. *Bioinform.* 2019; 15(7): 456-466.

Bhasin M, Garg A and Raghava GPS. PSLpred: Prediction of subcellular localization of bacterial proteins. *Bioinform.* 2005; 21(10): 2522-2524.

Biegert A, Mayer C, Remmert M, Söding J and Lupas A. The MPI Toolkit for protein sequence analysis. *Nucleic Acids Res.* 2006; 34: W335-W339.

Bitencourt-Ferreira G and de Azevedo WF. Homology modeling of protein targets with MODELLER. *Methods Mol. Biol.* 2019; 2053: 231-249.

Bowie J, Luethy R and Eisenberg D. A Method to Identify Protein Sequences That Fold into a Known Three-Dimensional Structure. *Science*, 1991; 253: 164-170.

Buchan D and Jones D. The PSIPRED Protein Analysis Workbench: 20 years on. *Nucleic Acids Res.*2019; 47: W402-W407.

Colovos C and Yeates TO. Verification of protein structures: Patterns of nonbonded atomic interactions. *Protein Sci.* 1993; 2(9): 1511-1519.

Combet C, Blanchet C, Geourjon C and Deleage G. NPS@: Network protein sequence analysis. *Trends Biochem. Sci.* 2000; 25(3): 147-150.

Cornejo-Juárez P, Vilar-Compte D, Pérez-Jiménez C, Ñamendys-Silva SA, Sandoval-Hernández Sand Volkow-Fernández P. The impact of hospital-acquired infections with multidrug-resistant bacteria in an oncology intensive care unit. *Int. J. Infect. Dis.* 2015; 31: 31-34.

Edgar RC. MUSCLE: Multiple sequence alignment with high accuracy and high throughput. *Nucleic Acids Res.*2004; 32(5): 1792-1797.

Eisenberg D, Lüthy R and Bowie JU. VERIFY3D: Assessment of protein models with three-dimensional profiles. *Methods Enzymol.* 1997; 277: 396-404.

Finn RD, Bateman A, Clements J, Coggill P, Eberhardt RY, Eddy SR, Heger A, Hetherington K, Holm L, Mistry J, Sonnhammer ELL, Tate Jand Punta M. Pfam: The protein families database. *Nucleic Acids Res.* 2014; 42(D1): D222-D230.

Gabler F, Nam SZ, Till S, Mirdita M, Steinegger M, Söding J, Lupas A and Alva V. Protein sequence analysis using the MPI bioinformatics toolkit. *Curr.Protoc. Bioinform.* 2020;72(1):e108.

Gasteiger E, Gattiker A, Hoogland C, Ivanyi I, Appel RD and Bairoch A. ExPASy: The proteomics server for in-depth protein knowledge and analysis. *Nucleic Acids Res.* 2003; 31(13): 3784-3788.

Gasteiger E, Hoogland C, Gattiker A, Duvaud S, Wilkins M, Appel RD and Bairoch AM. Protein identification and analysis tools on the ExPASy server. In: *The Proteomics Protocols Handbook*, 2005; pp. 571-607.

Hegyi H and Gerstein M. The relationship between protein structure and function: A comprehensive survey with application to the yeast genome. *J. Mol. Biol.*1999; 288: 147-164.

Hodge EA, Benhaim MA and Lee KK. Bridging protein structure, dynamics, and function using

hydrogen/deuterium-exchange mass spectrometry. *Protein Sci.* 2020; 29(4): 843-855.

Hu J, Han J, Li H, Zhang X, Liu LL, Chen F and Zeng B. Human embryonic kidney 293 cells: A vehicle for biopharmaceutical manufacturing, structural biology, and electrophysiology. *Cells Tissues Organs*, 2018; 205(1): 1-8.

Jones DT. Protein secondary structure prediction based on position-specific scoring matrices. *J. Mol. Biol.*1999; 292(2): 195-202.

Jones P, Binns D, Chang HY, Fraser M, Li W, McAnulla C, McWilliam H, Maslen J, Mitchell A, Nuka G, Pesseat S, Quinn AF, Sangrador-Vegas A, Scheremetjew M, Yong SY, Lopez R and Hunter S. InterProScan 5: Genome-scale protein function classification. *Bioinform*. 2014; 30(9): 1236-1240.

Kanehisa M, Goto S, Kawashima S and Nakaya A. The KEGG databases at genomenet. *Nucleic Acids Res.* 2002; 30: 42-46.

Krieger E, Joo K, Lee J, Lee J, Raman S, Thompson, J, Tyka M, Baker D and Karplus K. Improving physical realism, stereochemistry, and side-chain accuracy in homology modeling: Four approaches that performed well in CASP8. *Proteins Struct. Funct. Bioinf.* 2009; 77(S9): 114-122.

Krogh A, Larsson B, von Heijne Gand Sonnhammer ELL. Predicting transmembrane protein topology with a hidden markov model: Application to complete genomes11Edited by F. Cohen. *J. Mol. Biol.*2001; 305(3): 567-580.

Laskowski RA, MacArthur MW, Moss DS and Thornton JM. PROCHECK: A program to check the stereochemical quality of protein structures. *J. Appl. Crystallogr.* 1993; 26(2): 283-291.

Liochev S and Fridovich I. The Haber-Weiss cycle—70 years later: An alternative view. Redox Report : *Communications in Free Radical Research*, 2002; 7: 55-57.

Macomber L and Imlay J. The iron-sulfur clusters of dehydratases are primary targets of copper toxicity. *Proc. Natl. Acad. Sci. USA*. 2009; 106: 8344-8349.

Marchler-Bauer A, Lu S, Anderson JB, Chitsaz F, Derbyshire MK, DeWeese-Scott C, Fong JH, Geer LY, Geer RC, Gonzales NR, Gwadz M, Hurwitz DI, Jackson JD, Ke Z, Lanczycki CJ, Lu F, Marchler GH, Mullokandov M, Omelchenko MV and Bryant SH. CDD: A conserved domain database for the functional annotation of proteins. *Nucleic Acids Res.* 2011; 39(suppl_1): D225-D229.

Marsh J, Teichmann S. Structure, dynamics, assembly, and evolution of protein complexes. *Annu. Rev. Biochem.* 2014; 84: 551-575.

Mazumder L, Hasan M, Abu Rus'd Aand Islam M. In-silico characterization and structure-based functional annotation of a hypothetical protein from Campylobacter jejuni involved in propionate catabolism. *Genomics Inform.* 2021;19: e43.

McConnell MJ and Pachón J. Active and passive immunization against Acinetobacter baumannii using an inactivated whole cell vaccine. *Vaccine*, 2010; 29(1): 1-5.

Metan G, Sariguzel F and Sumerkan B. Factors influencing survival in patients with multi-drug-resistant Acinetobacter bacteraemia. *Euro.J. Int. Medi.*,2009; 20(5): 540-544.

Möller S, Croning MD and Apweiler R. Valuation of methods for the prediction of membrane spanning regions. *Bioinform.* 2001; 17(7): 646-653.

Paul S, Saha M, Bhoumik N and Talukdar S. In silico structural and functional annotation of mycoplasma genitalium hypothetical protein MG_377. *Int. J. Biol.* 2015;19: 15-24.

Pawel S, Martin-Galiano AJ, Mikolajka A, Girschick T, Holak T and Frishman D. Protein solubility: Sequence based prediction and experimental verification. *Bioinform.* 2007;23: 2536-2542.

Rahman A, Susmi TF, Karim ME and Hossain MU. Functional annotation of an ecologically important protein from Chloroflexusaurantiacus involved in polyhydroxyalkanoates (PHA) biosynthetic pathway. *SN Appl. Sci.* 2020; 2(11): 1810.

Restrepo-Montoya D, Vizcaíno C, Niño LF, Ocampo M, Patarroyo ME and Patarroyo MA. Validating subcellular localization prediction tools with

mycobacterial proteins. *BMC Bioinform.* 2009; 10(1): 134.

Schneider G and Fechner U. Advances in the prediction of protein targeting signals. *Proteomics*, 2004; 4(6): 1571-1580.

Sigrist C, Castro E, Cerutti L, Cuche B, Hulo N, Bridge A, Bougueleret L and Xenarios I. New and continuing developments at PROSITE. *Nucleic Acids Res.*2012; 41: D344-D347.

Sowmya G and Ranganathan S. Protein-protein interactions and prediction: A Comprehensive overview. *Protein Pept. Lett.* 2013; 21(8): 779-789.

Szklarczyk D, Gable AL, Lyon D, Junge A, Wyder S, Huerta-Cepas J, Simonovic M, Doncheva NT, Morris JH, Bork P, Jensen LJ and Mering C. von. STRING v11: Protein–protein association networks with increased coverage, supporting functional discovery in genome-wide experimental datasets. *Nucleic Acids Res.* 2019; 47(D1): D607-D613.

Szklarczyk D, Gable A, Lyon D, Junge A, Wyder S, Huerta-Cepas J, Simonovic M, Doncheva N, Morris J, Bork P, Jensen Land von Mering C. STRING v11: Protein-protein association networks with increased coverage, supporting functional discovery in genome-wide experimental datasets. *Nucleic Acids Res.* 2018; 47(D1): D607-D613.

Tian W, Chen C, Lei X, Zhao J and Liang J. CASTp 3.0: Computed atlas of surface topography of proteins. *Nucleic Acids Res.* 2018; 46(W1): W363-W367.

Tusnady G and Simon I. The HMMTOP transmembrane topology prediction server. *Bioinform.* 2001;17: 849-850.

Uversky VN. Protein intrinsic disorder and structure-function continuum. *Prog. Mol. Biol. Transl. Sci.* 2019; 166: 1-17.

Wang M, Herrmann C, Simonovic M, Szklarczyk Dand von Mering C. Version 4.0 of PaxDb: Protein abundance data, integrated across model organisms, tissues and cell-lines. *Proteomics*, 2015;15(18): 3163-3168.

Warnes SL, Caves V and Keevil CW. Mechanism of copper surface toxicity in Escherichia coli O157:H7 and Salmonella involves immediate membrane depolarization followed by slower rate of DNA destruction which differs from that observed for Gram-positive bacteria: Rapid death of Gram-negative bacteria on dry copper surfaces. *Environ. Microbiol.* 2012; 14(7): 1730-1743.

Wiederstein M and Sippl M. ProSA-web: Interactive web service for the recognition of errors in three-dimensional structures of proteins. *Nucleic Acids Res.* 2007; 35: W407-W410.

Williams CL, Neu HM, Gilbreath JJ, Michel SLJ, Zurawski DV and Merrell DS. Copper resistance of the emerging pathogen acinetobacter-baumannii. *Appl. Environ. Microbiol.* 2016; 82(20): 6174-6188.

Wilson D, Madera M, Vogel C, Chothia C and Gough J. The superfamily database in 2007: Families and functions. *Nucleic Acids Res.*2007; 35: D308-D313.

Yu CS, Chen YC, Lu CH and Hwang JK. Prediction of protein subcellular localization. *Proteins: Struct. Funct. Bioinf.* 2006; 64(3): 643-651.

Yu CS, Lin CJ and Hwang JK. Predicting subcellular localization of proteins for Gram-negative bacteria by support vector machines based on n-peptide compositions. *Protein Sci.* 2004; 13(5): 1402-1406.

Yu NY, Wagner JR, Laird MR, Melli G, Rey S, LoR, Dao P, Sahinalp SC, Ester M, Foster LJ and Brinkman FSL. PSORTb 3.0: Improved protein subcellular localization prediction with refined localization subcategories and predictive capabilities for all prokaryotes. *Bioinform.* 2010); 26(13): 1608-1615.

Zhou P. Determining protein half-lives. *Methods Mol. Biol.* 2004; 284: 67-77.

Zimmermann L, Stephens A, Nam SZ, Rau D, Kübler J, Lozajic M, Gabler F, Söding J, Lupas AN and Alva V. A Completely reimplemented MPI bioinformatics toolkit with a new HHpredserver at its core. *J. Mol. Biol. 2018*; 430(15): 2237-2243.

J. Bangladesh Acad. Sci. 49(2); 243-253: December 2025 DOI:https://doi.org/10.3329/jbas.v49i2.80644

Journal of Bangladesh Academy of Sciences

Journal homepage: http://www.bas.org.bd/publications/jbas.html

Research Article

Phytochemical and antibacterial properties of clove from India, Sri Lanka, and Indonesia available in Bangladesh

Sharmin Hossen, Irin Hossain[1], Shamim Akhtar[1], Arpita Chowdhury[*],
Mohammed Tanvir Ahamed, Susmita Chowdhury and Monsur Ahmad

Department of Applied Chemistry & Chemical Technology, Faculty of Food Science and Technology
Chattogram Veterinary and Animal Sciences University, Chittagong, Bangladesh

ARTICLE INFO

Article History

Received: 19 March 2025
Revised: 19 May 2025
Accepted: 25 August 2025

Keywords: *Syzygium aromaticum*, Clove, Essential oil, Phytocomponent, GC-MS profiling, Antibacterial activity, Antioxidant activity.

ABSTRACT

Cloves (*Syzygium aromaticum*) are aromatic flower buds that have been extensively studied for their culinary, medicinal, and economic value. Bangladesh has Indonesian (CIS), Indian (CID) and Sri Lankan (CSI) cloves. This study investigates the bioactive compounds, proximate analysis, physicochemical properties, and antibacterial efficacy of clove essential oils from three commercially available brands in Chattogram. Using Gas Chromatography-Mass Spectrometry (GC-MS), the primary bioactive compounds identified were eugenol, eugenol acetate, and β-caryophyllene, with significant variations in their concentrations across brands. Proximate analysis revealed differences in moisture, ash, and volatile content, highlighting disparities in quality and purity. Physicochemical properties were assessed. Antibacterial efficacy was evaluated using the agar disc diffusion method against *Escherichia coli* and *Staphylococcus aureus* and *Pseudomonas aeruginosa*, as indicated by its minimal inhibitory concentration (MIC) values. These findings underscore the importance of brand selection in ensuring the therapeutic and functional efficacy of clove essential oil, emphasizing the need for stringent quality control in the market.

Introduction

Cloves (*Syzygium aromaticum*) are the fragrant desiccated flower buds of a tree belonging to the Myrtaceae family (Srivastava and Malhotra, 1991). Exotic goods imported from Asia were particularly appealing to the Greeks and Romans. The Portuguese, Dutch, Spanish, and British were driven to expand into countries such as India, Sri Lanka, and Indonesia by their ambition to control sources of spices. Every country fought with others to gain monopolistic control over main trade routes and areas of spice production (Takeda et al., 2008). For the reason that cloves from all these three locations are abundant in essential oils, predominantly comprising eugenol. Eugenol, which comprises 72-90% of the essential oil derived from cloves, is responsible for their distinctive fragrance and numerous biological functions (Alma et al., 2007). Clove essential oil (CEO) extracted from all parts of clove tree are a rich source of bioactive compounds with potential antioxidant, antimicrobial and

[*]Corresponding author:<arpitachy23@gmail.com>

[1]*Department of Chemistry, University of Chittagong, Chittagong, Bangladesh;*

[*]*Department of Food Processing and Engineering, Chattogram Veterinary and Animal Sciences University, Bangladesh*

anti-inflammatory properties. The CEO also combats dental pain and oxidative stress. Principal health advantages comprise: antioxidant properties (Jirovetz et al., 2006), antibacterial and antifungal effects (Nzeako et al., 2006), blood sugar regulation (Mohan et al., 2019), cancer prevention (Liu et al., 2014). Researchers have been investigating the potential health advantages of clove oil and its constituents, similar to other EOs (Haro-González et al., 2021). In a prior study, researchers identified the components of EO derived from the leaves and buds (Bhuiyan et al., 2010). Cloves, particularly their bioactive compounds like eugenol, may offer natural alternatives to synthetic antibiotics, against *E. coli*, *Staph. aureus*, and *P. aeruginosa*, helping combat antibiotic resistance (Jayarathne et al., 2020). As these bacteria are often resistant to conventional antibiotics, cloves could provide a natural solution, potentially reducing reliance on synthetic drugs and slowing the development of resistance. To summarize, this study has the potential to provide natural remedies for health problems, make food more secure, and bolster long-term health and food industry sustainability of the food industry.

Materials and methods

Collection and processing of cloves

Cloves were procured from the Khatunganj market in Chittagong City. The samples were purified, dust particles removed, and dried. The dried cloves were ultimately pulverized using a Fritsch mortar grinder (Germany) for 1 hour.

Extraction of Essential Oil (EO)

Plant essential oil extraction uses several methods. In this investigation, steam distillation using the Clevenger apparatus (Germany) was performed according to the steps described by Shavisi et al. (2017), with slight moderations.

Determination of physicochemical properties of EO

The physical parameters of the extracted EO, including refractive index, density, optical rotation, and alcohol solubility, were assessed following established methods (Pharmacopoeia Commission, 2011) with three replications.

Determination of acid value

The Acid value was estimated using the following equation mentioned in Paez et al. (2016):

$$\text{Acid value} = \frac{\text{N of alkali (0.1) x ml of alkali}}{\text{Wt. of sample (gm)}}$$

Determination of saponification value

The saponification value was estimated using the following equation mentioned in Paez et al. (2016):

$$\text{Saponification value} = \frac{\text{N x (b-a) x 56.1}}{\text{Wt. of sample (gm)}}$$

Where, b = blank titer value, a = sample titer value and N = 0.5 (Normality) of HCl.

Determination of peroxide value

Peroxide value was determined using the formula described by Paez et al. (2016) incorporating $Na_2S_2O_3$.

Determination of Iodine value

Iodine value was determined using methods mentioned in Paez et al. (2016).

Identification of unidentified chemicals in clove oil via GC-MS analysis

The analysis was conducted using GC-MS electron impact ionization (EI) on a GC-17A gas chromatograph (Shimadzu, Japan) coupled to a GC/MS-QP 5050A mass spectrometer (Shimadzu). The column temperature was programmed from 40°C (for 2 minutes) to 250°C at a rate of 5°C/min (Aziz et al., 2012).

Extract Preparation

Making of an Extract by adding 10 ml of 100% ethanol + acetone to 1g of material in a Falcon tube and then letting it sit for 72 hours. After 72 hours, filtered the solvent and collected the filtrates. Then, the extract was analyzed.

Determination of antioxidant activity (AOA) by DPPH scavenging method

Antioxidant mobility of the extracts was determined using DPPH assay described by Akther et al. (2023) with slight modifications. The absorbance was measured at 517 nm using a UV-VIS spectrophotometer (UV-2600, Shimadzu Corporation, USA).

Determination of Bioactive Compounds

Extract Preparation

The extraction process involves combining 10 ml of pure ethanol (100%) with 1 g of the substance in a Falcon tube, then allowing it to rest undisturbed for a duration of 72 hours. After 72 hours, strain the solvent and collect the resulting filtrates. Subsequently, the ethanoic extract was identified.

Total Flavonoid Content (TFC)

The total flavonoids content (TFC) of the clove oil samples was determined using the aluminum chloride colorimetric method reported by Chang et al. (2002) with slight modifications. A suitable volume of extract stock solution (1 mg/mL) was prepared for the calibration curve. Quercetin (Sigma, USA) was dissolved in 80% ethanol to generate standard solutions at concentrations of 0.025, 0.050, 0.075, and 0.100 mg/ml. In the cuvette, 0.5 mL aliquots of the standard solution (diluted extract) were mixed with 1.5 mL of 95% ethanol, 0.1 mL of 10% aluminium chloride (QualiChem, India), 0.1 mL of 1 mol/L potassium acetate (Merck, Germany), and 2.8 mL of distilled water. The obtained mixture was allowed to cool to room temperature (25.5 ± 1°C) for 30 minutes prior to use. The absorbance at 415 nm was subsequently measured via a UV-visible spectrophotometer. In the blank preparation, 10% aluminium chloride was substituted with an equivalent volume of distilled water. Total flavonoid content (TFC) was quantified in milligrammes of quercetin equivalents (QE) per 100 grammes of extract.

Measurement of Polyphenols (TPC)

The total polyphenol content (TPC) of the CEO was determined using the Folin-Ciocalteu method reported by Al-Owaisi et al. (2014) with slight modifications. Appropriate stock solutions (1 mg/mL) of extracts and standard solutions (0.02, 0.04, 0.06, 0.08, and 0.10 mg/mL) of gallic acid (Sigma, USA) were formulated for the experiment. Subsequently, 0.3 mL of gallic acid standard solution or extracts was pipetted into a cuvette. Subsequently, 1.5 mL of the diluted Folin-Ciocalteu reagent was added, and the mixture was mixed. After a 3-minute pause, 1.5 mL of sodium carbonate solution (75 g/L) was added, and the mixture was allowed to stand for 60 minutes. Ethanol served as the blank for absorbance measurement at 765 nm utilising a UV spectrophotometer. Total phenolic content (TPC) was quantified in milligrammes of gallic acid equivalents (GAE) per 100 grammes of extracts.

Quantification of Anthocyanins (TAC)

Total anthocyanin content (TAC) of clove oil extracts was determined colorimetrically following the process expressed with slight modifications (Akther et al., 2023). A precise 10 mg/mL stock solution of extracts was formulated for the experiment. Furthermore, 3 mL aliquots of the extract solution were transferred into a cuvette. The colour concentration was measured at 520 nm using a UV-vis spectrophotometer (UV-2600, Shimadzu). Ethanol (Merck, Germany) served as the control sample. TAC was measured in mg/100 g with the subsequent equation:

TAC = (Absorbance of sample) x (DF) x (100) / (m) x (E)

Where, DF denotes the dilution factor, m signifies the weight of the sample utilised to make a stock solution, and E indicates the extinction coefficient, valued at 55.9.

Determination of antibacterial activity of clove oil

The antibacterial activity was evaluated using the disc diffusion method, commonly referred to as the Kirby-Bauer test, as stated in Drew et al. (1972). Sterile saline silution was used as nagative control.

Statistical Analysis

The obtained data were stored in Microsoft Excel 2013 spreadsheet to evaluate statistical analysis, and significant differences were determined using one-way analysis of variance (ANOVA). All samples were in three replicates. Data were sorted, coded and recorded in IBM SPSS Statistics 25. The statistical analysis was conducted for at 5% level of significant ($p \leq 0.05$).

Results and Discussions

Physicochemical properties of clove essential oil

Table 1 and 2 represent the physicochemical properties of CEO, which were found to be as follows: the acid value, saponification value, peroxide value, Iodine value, Density and Viscosity.

The acid value (AV) is an important determinant of oil quality (Gharby et al., 2017). The acid values were determined to be 5.213 mg KOH/g oil, 6.09 mg KOH/g oil, and 6.457 mg KOH/g oil for the CIS, CID, and CSI clove essential oils, respectively. In this investigation, the acid values of all clove essential oil samples exceeded the maximum limit. The principal mechanism resulting in rancidity is lipid oxidation. Heat can expedite this process, as seen by essential oils such as nutmeg, which exhibit enhanced free radical-scavenging activity, leading to the production of aldehydes and other chemicals that promote rancidity and alterations in chemical composition upon heating (Tomaino et al., 2005).

The saponification values (SV) were determined to be 37.257 mg/g oil, 40.670 mg/g oil, and 38.056 mg/g oil with regard to CIS, CID, and CSI clove essential oils, respectively. This value closely aligned with those reported by numerous studies (Alanazi et al., 2022; Sulieman et al., 2007). The Peroxide value was found to be 4.61, 6.667 and 5.127 meq O_2/kg oil of the CIS, CID and CSI clove essential oil respectively. The peroxide value serves as an indicator of the stability and quality of oils and fats (Zahir et al., 2017). In this investigation, the PV of clove essential oil samples from CIS was lower than that of the other two samples. The unsaturation of fats and oils is shown by the iodine value. Higher unsaturated fats and oils have higher iodine values.

For the oil sample used in this investigation, the iodine value was 51.457 g I_2/100 g of oil for CIS, 49.507 g I_2/100 g of oil for CID, and 50.157 g I_2/100 g of oil for CSI clove essential oil, respectively. Kyriakidis and Katsiloulis (2000) state that the recommended range for semi-drying oils is between 100 and 300, which is far lower than this amount. The iodine value (IV) of CIS clove essential oil samples was lower than that of the other two samples in this study.

The density (ρ) and viscosity (η) of three brands of clove essential oil were determined at 6 distinct temperatures ranging from 25°C to 50°C, with 5°C intervals. All density (ρ) results are presented in Table 2. It can be observed regarding density that at a specific temperature, the density (ρ) of clove essential oil falls in the following order: CID > CSI > CIS. The ρ vs T comparison of 3 brands of clove essential oil exhibits a comparable tendency, with p falling nearly linearly as temperature increases. This result is in accordance with Porter and Lammerink (1994). As the temperature rises, the kinetic energy of the molecules in the essential oil increases, leading to their separation. This expansion results in reduced density (Gandova et al., 2024).

The subsequent observations regarding viscosity (η) are - at a specific temperature, the viscosity (η) of clove essential oil diminishes in the following sequence: CSI > CID > CIS. The η vs T comparison for 3 brands of clove essential oil exhibits a comparable tendency, with η gradually dropping as the temperature rises. This results from increased heat energy, which diminishes the intermolecular interactions within the oil, allowing the molecules to move more freely. At elevated temperatures, the kinetic energy of the molecules

in the essential oil escalates. This energy exceeds the intermolecular forces binding the molecules, resulting a reduced viscosity (Gandova et al., 2024).

Phytocomponents identified in clove bud essential oils by GC-MS analysis

Table 3 presents the phytocomponents identified in CEOs, primarily Aniline, Eugenol, Phenol, Caryophyllene oxide etc. CEO demonstrates significant antioxidant and antibacterial properties, principally due to its Eugenol content. Therefore, this oil is widely used in the food industry as a preservative and flavoring agent due to its antibacterial and antioxidant characteristics. It is employed in cosmetics for its aroma and medicinal properties (Liñán-Atero et al., 2024). Eugenyl acetate, another important ingredient, adds to the oil's scent and possible health advantages

Table 1. Physicochemical properties of clove essential oil.

Country of origin	Acid value (mg KOH /g oil)	Saponification value (mg /g oil)	Peroxide value (meq O_2/kg oil)	Iodine value (g I_2/100 g of oil)
CIS	5.213±0.01^{c}	37.257±0.01^{c}	4.610±0.01^{c}	51.457±0.01^{a}
CID	6.087±0.01^{b}	40.670±0.01^{a}	6.667±0.01^{a}	49.507±0.01^{c}
CSI	6.457±0.01^{a}	38.056±0.01^{b}	5.127±0.01^{b}	50.157±0.01^{b}

Mean ± S.D. for three replicates (n=3) and different superseripts indicate differences among orgin of clove. CIS = Indonesian origin; CID = Indian origin; CSI = Sri Lanka origin

Table 2. Density and viscosity of clove essential oil.

Temperature (^{o}C)	Density (ρ)			Viscosity (η)		
	CIS	CID	CSI	CIS	CID	CSI
25	1.02±0.005^{c}	1.03±0.005^{a}	1.03±0.005^{ab}	10.32±0.005^{c}	14.43±0.005^{b}	16.35±0.005^{a}
30	1.01±0.005^{c}	1.03±0.005^{a}	1.02±0.00^{b}	8.36±0.005^{c}	11.34±0.005^{b}	12.94±0.005^{a}
35	1.01±0.005^{c}	1.02±0.005^{a}	1.02±0.005^{ab}	6.66±0.005^{c}	9.12±0.001^{b}	10.53±0.005^{a}
40	1.00±0.005^{c}	1.02±0.005^{a}	1.02±0.005^{ab}	5.63±0.005^{c}	7.56±0.005^{b}	8.67±0.005^{a}
45	1.00±0.005^{c}	1.01±0.005^{a}	1.01±0.005^{ab}	4.82±0.005^{c}	6.36±0.005^{b}	7.31±0.005^{a}
50	0.99±0.00^{c}	1.01±0.005^{a}	1.01±0.057^{ab}	4.17±0.005^{c}	5.44±0.005^{b}	6.26±0.005^{a}

Mean ± S.D. for three replicates (n=3) and different superseripts indicate differences among orgin of clove. CIS = Indonesian origin; CID = Indian origin; CSI = Sri Lanka origin

Table 3. Phytocomponent commponents identified in clove essential oils by GC-MS analysis.

Country of origin		Compounds name	Chemical formula	MW	Retention Index (RI)
CIS	1.	2,5-Diethylideneoctahydropentalene	$C_{12}H_{18}$	162	1229
	2.	3,5-Methanocyclopentapyrazole, 3,3a,4,5,6,6a-hexahydro-3a,4,4-trimethyl-	$C_{10}H_{16}N_2$	164	0
	3.	P-Picoline (Methylpyridine)	C_6H_7N	93	787
	4.	Alpha-picoline (Methylpyridine)	C_6H_7N	93	787
	5.	Aniline (Phenylamine)	C_6H_7N	93	992
	6.	Chavicol (Hydroxyallylbenzene)	$C_9H_{10}O$	134	1203
	7.	Eugenol (2-methoxy-4-(2-propenyl)	$C_{10}H_{12}O_2$	164	1392
			$C_{12}H_{14}O_3$	206	1552
CID	8.	Trans-Z-alpha. Bisabolene epoxide	$C_{15}H_{24}O$	220	1531
	9.	Spiro[androst- 5-ene-17,1cyclobutan] -2'-one,3-hydroxy-,(3β, 17β)-	$C_{22}H_{32}O_2$	328	2413
	10.	Caryophyllene oxide	$C_{15}H_{24}O$	220	1507
	11.	1, 7, 7-Trimethylbicyclo [2.2.l] heptane-2, 5-diol	$C_{10}H_{18}O_2$	170	1326
	12.	Eugenol (2-methoxy-4-(2-propenyl)	$C_{10}H_{12}O_2$	164	1392
	13.	Phenol, 2-rnethoxy-3-(2-propenyl)-	$C_{10}H_{12}O_2$	164	1392
	14.	Phenol, 2-Allyl-4-propenyl	$C_{10}H_{12}O_2$	164	1392
	15.	Ylangene	$C_{15}H_{24}$	204	1221
	16.	Eugenyl acetate	$C_{12}H_{14}O_3$	206	1552
CSI	17.	Ethanone,1-(2,3,4-Trimethoxyphenyl)	$C_{11}H_{14}O_4$	210	1596
	18.	4-(2,6,6-Trimethyl-1-cyclohexen-l-yl) butanoic acid	$C_{13}H_{22}O_2$	210	1670
	19.	2-Arnino-5-ethyl-3-nitro-benzoic acid	$C_9H_{10}N_2O_4$	210	2070
	20.	Eugenyl acetate	$C_{12}H_{14}O_3$	206	1552
	21.	3-Allyl-6-methoxyphenyl acetate	$C_{12}H_{14}O_3$	206	1552
	22.	Eugenol (2-methoxy-4-(2-propenyl)	$C_{10}H_{12}O_2$	164	1392
	23.	Caryophyllene oxide	$C_{15}H_{24}O$	220	1507

(Hemalatha et al., 2016). Eugenyl acetate was present in the CID sample. The samples also included beta-caryophyllene, a sesquiterpene that is frequently present in clove oil and is well-known for its analgesic and anti-inflammatory effects (Amelia et al., 2017). The oil also contains minor amounts of sesquiterpene hydrocarbons, oxygenated monoterpenes, and other phenolic chemicals (Oliveira et al., 2016). In this study, phenolic chemicals are only identified in CID. For certain phenolic compounds, GC-MS may not always provide adequate sensitivity and specificity, particularly when they are present in complex mixes or in low levels (Proestos et al., 2006).

Concentration (ppm) of TFC, TPC and TAC in three brands cloves

CEO is acknowledged for its potent antioxidant capabilities. The principal constituent responsible for this activity is eugenol, which comprises approximately 76.8% in clove essential oil (Jirovetz et al., 2006). The antioxidant activity of the clove powder sample was measured as 70.66 ppm, 70.14 ppm, and 69.74 ppm for the CIS, CID, and CSI clove essential oils, respectively, as presented in Table 4. The contents are consistent with prior research (Alfikri et al., 2020). Besides eugenol, other constituents including β-caryophyllene and α-humulene further enhance the oil's antioxidant properties. The oil's capacity to mitigate oxidation reactions and diminish free radicals renders it a significant potential for pharmaceutical formulations targeting oxidative stress and associated disorders (Kiki, 2023). The TFC of the clove essential oil was measured as 244.36 ppm, 161.13 ppm, and 321.95 ppm for the CIS, CID, and CSI varieties, respectively. Although comprehensive quantitative data on the total flavonoid concentration of clove essential oil is limited in the existing literature, clove is recognized as a significant source of bioactive constituents, encompassing flavonoids and phenolic compounds (Pandey et al., 2023). The TPC of the clove essential oils was measured as 159.44 ppm, 142.82 ppm, and 135.11 ppm for the CIS, CID, and CSI varieties, respectively. A robust association frequently exists between the total phenolic content (TPC) of a plant extract and its antioxidant activity. Elevated concentrations of phenolic compounds generally signify enhanced antioxidant (Zargoosh et al., 2019). The average TAC values were determined to be 16.07 mg/100 g, 18.156 mg/100 g, and 17.94 mg/100 g for the CIS, CID, and CSI clove essential oils, respectively. The CEO is not recognized for its anthocyanin content. The oil is predominantly derived from the flower buds and leaves of the clove plant, resulting in a minimal anthocyanin concentration.

Zone of inhibition (mm) showing the antibacterial activity of CEO

The results obtained for *E. coli*, *Staphylococcus aureus* and *Pseudomonus aeruginosa* observed using the Kirby-Bauer disk diffusion method are illustrated in Table 5. In all experiments, the negative controls showed no zone of inhibition.

Table 4. Concentration (ppm) of TFC, TPC, TAC, and AOA in cloves.

Sample ID	TFC	TPC	TAC	AOA
CIS	244.36±0.01^{b}	159.44±0.01^{a}	16.071±0.01^{c}	70.66 ±0.01^{a}
CID	161.13±0.01^{c}	142.82±0.01^{b}	18.156±0.01^{a}	70.14±0.01^{b}
CSI	321.95±0.01^{a}	135.11±0.01^{c}	17.942±0.01^{b}	69.74±0.01^{c}

Mean ± S.D. for three replicates (n=3) and different superseripts indicate differences among orgin of clove. TFC= total flavonoid content; TPC= total phenolic content; TAC= total antioxidant capacity; AOA= antioxidant activity.

Table 5: Antibacterial activity of clove essential oil extract (100 µg/ml)

Country of origin	*Escherichia coli*		*Staphylococcus aureus*		*Pseudomonus aeruginosa*	
	Essential Oil (mL)	Positive Control (mm)	Essential Oil (mL)	Positive Control (mm)	Essential Oil (mL)	Positive Control (mm)
CIS	25	Nz	26	30	26	36
CID	24	Nz	25	28	25	27
CSI	27	Nz	24	29	24	33

CIS = Indonesian origin; CID = Indian origin; CSI = Sri Lanka origin; Nz = No zone of inhibition; Positive control: Ciprofloxacin

Eugenol is a phenolic substance. Phenols possess antibacterial characteristics (Nuñez and Aquino, 2012). Findings indicate that *S. aromaticum* contains bioactive compounds, underscoring its significance as a therapeutic plant. The results indicate that *S. aromaticum* extracts impede bacterial proliferation. The most substantial inhibitory zone measured 27 mm against *E. coli* by CSI. The clove oil extract showed antibacterial activity against all tested Gram-positive and Gram-negative pathogens. Previous studies demonstrate a comparable pattern

obstructing the proliferation of several pathogens,

such as *Staph. aureus, E. coli*, and *P. aeruginosa* (Kovács et al., 2016). No significant difference was seen among CIS, CID, and CSI regarding their bactericidal efficacy. All of them possessed the capacity to limit the proliferation of subsequent infections. Nonetheless, the clove oil extract exhibited greater efficacy against the *Staph. aureus* isolate at doses of 100 µg/ml. Ciprofloxacin exhibited no effect against *E. coli*, whereas the clove oil extract showed significant efficacy against *E. coli*. The antibacterial efficacy is affected by variables including oil content, temperature, and the presence of organic materials (Nuñez and Aquino, 2012).

Conclusion

Lower acid and peroxide value in CIS, CID, and CSI indicate enhanced stability and extended shelf-life. The viscosity (η) of the CEOs exhibited a linear correlation with temperature. The GC-MS analysis of the oil extract identified eugenol, caryophyllene, and eugenol acetate as the principal constituents. The antibacterial properties of clove oil extract can be attributed to the discovered components. Eugenol and caryophyllene are well-known for their antibacterial effects. Consequently, impeding the advancement and proliferation of all examined pathogens and indicator organisms, particularly *E. coli, Staph. aureus*, and *P. aeruginosa*. The most significant inhibitory impact of clove oil was observed against *E. coli* by CSI. However, some asymmetry was also observed due to environmental factors such as temperature, photosynthetic rate, and heat, which influence the carbohydrate and protein levels in cloves. All three varieties of cloves exhibited no significant differences among them. The study suggested that clove and clove oils may serve as antibacterial and antiseptic agents. Subsequent research may involve developing goods including clove essential oil to enhance their longevity.

Acknowledgment

Department of Applied Chemistry and Chemical Technology, CVASU for technical assistance and material support.

Authors contribution

S.H. and I.H. performed the experiments and collected data. S.A. and A.C. analyzed the results and prepared the manuscript draft. M.T.A. and S.C. contributed to data interpretation and literature review. M.A. supervised the study, provided critical insights, and approved the final manuscript.

Conflict of interest

The authors declare no conflicts of interest.

References

Akther S, Jothi JS, Badsha MR., Rahman MM, Das GB and Alim MA. Drying methods effect on bioactive compounds, phenolic profile, and antioxidant capacity of mango powder. *J. King Saud Univ. Sci.*, 2023; 35(1): 102370.

Alanazi AK, Alqasmi MH, Alrouji M, Kuriri FA, Almuhanna Y, Joseph B and Asad M. Antibacterial activity of syzygium aromaticum (Clove) bud oil and its interaction with imipenem in controlling wound infections in rats caused by methicillin-resistant staphylococcus aureus. *Molecules*, 2022; 27(23): 8551.

Alfikri FN, Pujiarti R, Wibisono MG and Hardiyanto EB. Yield, quality, and antioxidant activity of clove (*Syzygium aromaticum* L.) bud oil at the different phenological stages in young and mature trees. *Scientifica*, 2020; 2020: 9701701.

Alma MH, Ertaş M, Nitz S and Kollmannsberger H. Chemical composition and content of essential oil from the bud of cultivated Turkish clove (*Syzygium aromaticum* L.). *Bio Resou.*, 2007; 2(2): 265-269.

Al-Owaisi M, Al-Hadiwi N and Khan SA. GC-MS analysis, determination of total phenolics, flavonoid content and free radical scavenging activities of various crude extracts of *Moringa peregrina* (Forssk.) Fiori leaves. *Asian Pac. J. Trop. Biomed.* 2014; 4(12): 964-970.

Amelia B, Saepudin E, Cahyana AH, Rahayu DU, Sulistyoningrum AS and Haib J. GC-MS analysis of clove (Syzygium aromaticum) bud essential oil from Java and Manado: 2nd International symposium on current progress in mathematics and sciences 2016, ISCPMS 2016. *International Symposium on Current Progress in Mathematics and Sciences*. 2017; 2016: ISCPMS 2016.

Aziz S, Naher S, Abukawsar M and Roy SKB. Comparative studies on physicochemical properties and GC-MS analysis of essential oil of the two varieties of the black pepper (Piper nigrum Linn.). *Int. J. Pharm. Phytopharm. Res.* 2012; 2(2): 67-70.

Bhuiyan MNI, Begum J, Ch N, NR I and Akter F. Constituents of the essential oil from leaves and buds of clove (Syzigium caryophyllatum (L.) Alston). *Afr. J. Plant Sci.* 2010; 4(11): 451-454.

Chang CC, Yang MH, Wen HM and Chern JC. Estimation of total flavonoid content in propolis by two complementary colometric methods. *J. Food Drug Anal.* 2002; 10(3): 178-182.

Drew WL, Barry ALO, Toole R and Sherris JC. Reliability of the kirby-bauer disc diffusion method for detecting methicillin-resistant strains of staphylococcus aureus. *Appl. Microbiol.* 1972; 24(2): 240-247.

Gandova V, Lazarov A, Petkova N and Stoyanova A. Physicochemical parameters and antioxidant activity of summer savory essential oil (*Satureja hortensis* L.)-Consensus. *BIO Web of Conferences*, 2024; 102: 01017.

Gharby S, Harhar H, Bouzoubaa Z, Asdadi AEl, Yadini A and Charrouf Z. Chemical characterization and oxidative stability of seeds and oil of sesame grown in Morocco. *J. Saudi Soc. Agric. Sci.* 2017; 16(2): 105-111.

Haro-González JN, Castillo-Herrera GA, Martínez-Velázquez M and Espinosa-Andrews H. Clove essential oil (*Syzygium aromaticum* L. Myrtaceae): extraction, chemical composition, food applications, and essential bioactivity for human health. *Molecules*, 2021; 26(21): 6387.

Hemalatha R, Nivetha P, Mohanapriya C, Sharmila G, Muthukumaran C and Gopinath M. Phytochemical composition, GC-MS analysis, in vitro antioxidant and antibacterial potential of clove flower bud (*Eugenia caryophyllus*) methanolic extract. *J. Food Sci. Technol.*, 2016; 53(2): 1189-1198.

Jayarathne SK, Liyanage T and Kumari DWMMM. Physical, chemical and morphological characterization of Sri Lankan origin dried clove (*Syzygium aromuticum* L.) BUDS. 2020.

Jirovetz L, Buchbauer G, Stoilova I, Stoyanova A, Krastanov A and Schmidt E. Chemical composition and antioxidant properties of clove

leaf essential oil. *J. Agri. Food Chem.,* 2006; 54(17): 6303-6307.

Kiki MJ. In Vitro antiviral potential, antioxidant, and chemical composition of clove (*Syzygium aromaticum*) essential oil. *Molecules*, 2023; 28(6): 2421.

Kovács JK, Felső P, Makszin L, Pápai Z, Horváth G, Ábrahám H, Palkovics T, Böszörményi A, Emődy L and Schneider G. Antimicrobial and virulence-modulating effects of clove essential oil on the foodborne pathogen *campylobacter jejuni*. *Appl. Environ. Microbiol.* 2016; 82(20): 6158-6166.

Kyriakidis NB and Katsiloulis T. Calculation of iodine value from measurements of fatty acid methyl esters of some oils: Comparison with the relevant American Oil Chemists Society method. *J. Am. Oil Chem. Soc.*, 2000; 77(12): 1235-1238.

Liñán-Atero R, Aghababaei F, García SR, Hasiri Z, Ziogkas D, Moreno A and Hadidi M. Clove essential oil: chemical profile, biological activities, encapsulation strategies, and food applications - consensus. *Antioxidants*, 2024; 13(4): 488.

Liu H, Schmitz JC, Wei J, Cao S, Beumer JH, Strychor S, Cheng L, Liu M, Wang C, Wu N, Zhao X, Zhang Y, Liao J, Chu E and Lin X. Clove extract inhibits tumor growth and promotes cell cycle arrest and apoptosis. *Oncol. Res.* 2014; 21(5): 247-259.

Mohan R, Jose S, Mulakkal J, Karpinsky-Semper D, Swick AG and Krishnakumar IM. Water-soluble polyphenol-rich clove extract lowers pre- and post-prandial blood glucose levels in healthy and prediabetic volunteers: An open label pilot study. *BMC Complement. Altern. Med.* 2019; 19(1): 99.

Nuñez L and Aquino MD. Microbicide activity of clove essential oil (*Eugenia caryophyllata*). *Brazilian J. Micro.*, 2012; 43(4): 1255-1260.

Nzeako BC, Al-Kharousi ZSN and Al-Mahrooqui Z. Antimicrobial activities of clove and thyme extracts. *Sultan Qaboos Univ. Med. J.* 2006; 6(1): 33-39.

Oliveira M, Costa WA, Pereira DS, Botelho JRS, Menezes TO, Andrade E, Silva SEM, Filho AP da SS and Junior RC. Chemical composition and phytotoxic activity of clove (*Syzygium aromaticum*) essential oil obtained with supercritical CO2—Consensus. *J. Supercrit. Fluids*, 2016; 118: 185-193.

Paez V, Barrett WB, Deng X, Diaz-Amigo C, Fiedler K, Fuerer C, Hostetler GL, Johnson P, Joseph G, Konings EJM, Lacorn M, Lawry J, Liu H, Marceau E, Mastovska K, Monteroso L, Pan SJ, Parker C, Phillips MM and Coates SG. AOAC SMPR® 2016.002. *J. AOAC Inter.*, 2016; 99(4): 1122-1124.

Pandey VK, Srivastava S, Ashish Dash KK, Singh R, Dar AH, Singh T, Farooqui A, Shaikh AM and Kovacs B. Bioactive properties of clove (Syzygium aromaticum) essential oil nanoemulsion: A comprehensive review. *Heliyon*, 2023; 10(1): e22437.

MHPRA (Medicines and Healthcare products Regulatory Agency). Pharmacopoeia Commission: New arrangements for human medicines in line with the Windsor Framework, 2011.

Porter NG and Lammerink JP. Effect of temperature on the relative densities of essential oils and water—consensus. *J. Essent. Oil Res*. 1994; 6: 269-277.

Proestos C, Sereli D and Komaitis M. Determination of phenolic compounds in aromatic plants by RP-HPLC and GC-MS. *Food Chem.* 2006; 95(1): 44-52.

Shavisi N, Akhondzadeh Basti A, Khanjari A, Misaghi A, Shahbazi Y, Hajjar Bargh A and Vanaki E. In Vitro antibacterial activity of polylactic acid film incorporated with ethanolic propolis extract and ziziphora clinopodioides essential oil. *J. Food Qual. Hazards Control*, 2017: 4: 3-8.

Srivastava K and Malhotra N. Acetyl eugenol, a component of oil of cloves (Syzygium aromaticum L.) inhibits aggregation and alters arachidonic acid metabolism in human blood platelets. *Prostaglandins Leukot. Essent. Fat. Acids*. 1991; 42(1): 73-81.

Sulieman EA, El Boshra I and El Khalifa EA. Nutritive value of clove (*Syzygium aromaticum*) and detection of antimicrobial effect of its bud oil. *Res. J. Microbiol.* 2007; 2(3): 266-271.

Takeda J, Silva S, Kawet L and Lanka S. Spices in Sri Lanka, India and Bangladesh with special reference to the usages and consumptions. *Bull. Fac. Agr. Saga Univ.* 2008; 93: 1-25.

Tomaino A, Cimino F, Zimbalatti V, Venuti V, Sulfaro V, Pasquale A and Saija A. Influence of heating on antioxidant activity and the chemical composition of some spice essential oils—Consensus. *Food Chem.* 2005; 89: 549-554.

Zahir E, Saeed R, Hameed MA and Yousuf A. Study of physicochemical properties of edible oil and evaluation of frying oil quality by Fourier Transform-Infrared (FT-IR) Spectroscopy. *Arabian J. Chem.*, 2017; 10: S3870-S3876.

Zargoosh Z, Ghavam M, Bacchetta G and Tavili A. Effects of ecological factors on the antioxidant potential and total phenol content of Scrophularia striata Boiss. *Sci. Rep.* 2019; 9(1): 16021.

J. Bangladesh Acad. Sci. 49(2); 255-269: December 2025 DOI:https://doi.org/10.3329/jbas.v49i2.86721

Journal of Bangladesh Academy of Sciences

Journal homepage: http://www.bas.org.bd/publications/jbas.html

Research Article

Genetic variability and trait associations pertaining to agronomic, post-harvest, and nutritional characteristics of the parents and hybrids of tomato (*Solanum lycopersicum* L)

Niloy Gain, Mahbuba Fatema and Jamilur Rahman*

Department of Genetics and Plant Breeding, Faculty of Agriculture, Sher-e-Bangla Agricultural University, Dhaka, Bangladesh

ARTICLE INFO

Article History

Received: 24 August 2025
Revised: 18 September 2025
Accepted: 19 September 2025

Keywords: Tomato fruit qualities, Agronomic performance, Genetic variability, Trait relationship.

ABSTRACT

In the current study, ten F_1 hybrids and their five parents were evaluated for agronomic, post-harvest, and nutritional traits. Significant genetic variation was observed among the traits, which grouped the planting materials into four phylogenetic clades. High heritability, coupled with high genetic advance was recorded for fruits per plant (99.61% and 170.55%), single fruit weight (99.06% and 102.09%), and vitamin C content (99.98% and 177.53%), suggesting that these traits are governed predominantly by additive gene action. Pearson's correlation and path coefficient analyses identified fruit diameter, number of secondary branches, single-fruit weight, and skin thickness as key traits positively associated with fruit yield, while increased skin thickness also contributed to enhanced shelf-life. Based on mean performance, the hybrids BT-15 × BT-3, BT-8 × BT-15, and BT-8 × BT-14 emerged as promising candidates for high yield. In addition, BT-8 × BT-11 and BT-8 × BT-15 exhibited superior shelf life and nutritional quality. Overall, the findings highlight the potential of integrating yield, post-harvest, and nutritional traits into selection indices for the development of superior tomato hybrids.

Introduction

Tomato (*Solanum lycopersicum* L.) is one of the most widely cultivated vegetable crops worldwide, valued for its economic significance and rich nutritional composition. It is an important source of vitamin C, provitamin A, lycopene, and essential minerals, which contribute to dietary health and help prevent chronic diseases (Gonzalez-Vega et al., 2021). Beyond its nutritional profile, farmers prefer tomato cultivation for its relatively short life cycle, higher yields, and broad adaptability to varying agro-climatic conditions (Lin et al., 2014). Despite its broad adaptability and short life cycle, Bangladesh faces a substantial yield gap in tomato production, averaging 14.05 t/ha compared with the global mean of 33 t/ha (FAOSTAT, 2023). This gap underscores the need for breeding early-maturing, high-yielding tomato hybrids that also possess superior post-harvest and nutritional qualities to meet the growing demand from both producers and consumers.

Moreover, tomato is a fleshy vegetable, particularly vulnerable to post-harvest deterioration due to poor shelf life, skin thickness, storability, and resistance to mechanical damage, which are essential for preserving quality during transport and storage (Sinha et al., 2019). However, many existing commercial hybrids in Bangladesh fail to combine these attributes, often exhibiting either late maturity, poor shelf life, or suboptimal yield (Islam et al., 2021). To overcome these constraints, tomato-

*Corresponding author:<jamilursau@sau.edu.bd>

breeding strategies must integrate multiple trait targets, including earliness, productivity, storability, and nutritional quality, thereby minimizing reliance on tomato imports.

Effective tomato improvement relies on the analysis of genetic variability and trait interrelationships, which provide the basis for informed selection of superior genotypes (Johnson et al., 1955). Correlation analysis helps identify the degree and direction of associations among traits, facilitating indirect selection for complex targets such as yield and quality (Dewey and Lu, 1959). While previous studies have often evaluated agronomic, post-harvest, or nutritional traits individually, integrated assessments of these traits in early-maturing, high-yielding hybrids are limited. The present study evaluates diverse early-maturing tomato hybrids for agronomic performance, post-harvest quality, and nutritional composition, alongside assessments of genetic variability and trait associations. By integrating these dimensions, the study provides a robust framework for selecting superior hybrids that combine productivity, early maturity, post-harvest performance, and nutritional enhancement, contributing to sustainable tomato breeding and improved food security in Bangladesh.

Materials and Methods

Ten hybrids with five parents and a check variety were evaluated for quantitative, post-harvest, and nutritional traits in the research field of Sher-e-Bangla Agricultural University during the 2018-19 rabi season. A Randomized Complete Block Design (RCBD) with three replications was used, with row-to-row spacing of 60 cm, and plant-to-plant spacing of 40 cm. All intercultural operations and fertilizer doses were carried out according to the BARI handbook (2017). The complete list of sixteen planting materials employed in this study is presented in Table 1. The planting materials were assessed by recording various agronomic parameters, including days to 50% flowering, plant height (cm), number of secondary branches, number of fruits per cluster, number of fruits per plant, single fruit weight (g), fruit diameter (mm), fruit length (mm), days to first harvesting, and yield per plant (kg); and post-harvest parameters viz., number of locules per fruit, shelf life, skin thickness, and nutritional qualities including vitamin C content, brix percentage (%), titrable acidity (%). Data collection was performed from thirty random plants per planting material. Considering these data, Statistix 10 was used to perform the analysis of variance and the least significant difference (LSD) test. Additionally, the genetic variability components, correlation coefficient, and clustering analysis using the Euclidean complete method were performed with the aid of R software (version 4.3.1), whereas the clustering dendrogram was constructed using ggrplot2. Moreover, the remaining visual presentations were prepared using Origin (2023b) software.

The brix percentages or total soluble solid content were evaluated by using a portable refractometer (ERMA, Tokyo, Japan), whilst an oxidation-reduction titration procedure suggested by Tee et al. (1988) was followed to assess the vitamin C contents.

$$\text{Vitamin-C} = \frac{0.5 \text{ dye required for tomato juice} \times 100 \times 100}{\text{dye required for L – ascorbic acid x 5 weight for fruit}}$$

and according to Panse and Sukhatme (1967), titrable acidity was assessed following the formula below:

$$\text{Titrable acidity (\%)} = \frac{\text{titrate} \times \text{normality of alkali} \times \text{volume made up} \times \text{equivalent wt. of acid} \times 100}{\text{volume of sample} \times \text{weight of sample} \times 100}$$

Table 1. List of planting materials used for the experiment.

Sl. no.	Designation	Name
	Parents	
1.	BT-8	BARI Tomato-8
2.	BT-15	BARI Tomato-15
3.	BT-14	BARI Tomato-14
4.	BT-11	BARI Tomato-11
5.	BT-3	BARI Tomato-3
	F_1 cross combinations	
6.	BT-8 × BT-15	BARI Tomato-8 × BARI Tomato-15
7.	BT-8 × BT-14	BARI Tomato-8 × BARI Tomato-14
8.	BT-8 × BT-11	BARI Tomato-8 × BARI Tomato-11
9.	BT-8 × BT-3	BARI Tomato-8 × BARI Tomato-3
10.	BT-15 × BT-14	BARI Tomato-15 × BARI Tomato-14
11.	BT-15 × BT-11	BARI Tomato-15 × BARI Tomato-11
12.	BT-15 × BT-3	BARI Tomato-15 × BARI Tomato-3
13.	BT-14 × BT-11	BARI Tomato-14 × BARI Tomato-11
14.	BT-14 × BT-3	BARI Tomato-14 × BARI Tomato-3
15.	BT-11 × BT-3	BARI Tomato-11 × BARI Tomato-3
16.	BHT-4 (Check variety)	BARI Hybrid Tomato-4

Note: BARI: Bangladesh Agricultural Research Institute

Results and Discussion

Mean performance of hybrids and their parents

In a breeding program, the breeders' primary objective is to identify genetic variations among the traits of interest, thereby accumulating favorable genes into new cultivars. In the current study, we observed significant genetic differences between F_1 hybrids and their parents, suggesting ample opportunities for varietal development (Table 2). The mean performance for yield-contributing traits and post-harvest traits was presented in Table 3. Among the hybrids, the highest fruit yield performance was found in BT-15 × BT-3 followed by BT-8 × BT-15 and BT-8 × BT-14, surpassing the better parent BT-3. Furthermore, for single fruit weight per plant, the hybrids BT-15 × BT-14 produced the highest fruit weight, possibly due to the accumulation of genes from the parental line, as BT-15 yielded the highest individual fruit weight among the parents. Variations in fruit yield performance among tomato cultivars were also reported by Meena et al. (2017) and Kumar et al.

Table 2. Analysis of variances (MS values) of eighteen quantitative, post-harvest and nutritional traits of tomato.

Sources	df	D50%F	PH	NSB	NFC	NFP	SFW	FD	FL	DFH	YPP	NL	ST	SL	VC	BRIX	TA
Replications	2	2.69	2.83	0.01	0.13	2.34	2.28	11.89	7.35	1.58	0.01	1.90	0.07	14.65	16.46	0.15	0.01
Genotypes	15	19.42**	381.83*	8.06**	10.86**	8968.69**	3181.72**	589.35**	355.24**	202.92	1.02**	3.51**	4.53**	137.71**	5161.06*	1.54*	0.03**
Error	30	1.29	4.75	0.02	0.14	12.62	10.53	8.40	4.08	6.58	0.02	0.65	0.03	2.20	16.56	0.02	0.01

Note: D50%F=Days of 50% flowering; PH=Plant height (cm); NSB=Number of secondary branches, NFC= Number of fruits per cluster; NFP= Number of fruits per plant; SFW=Single fruit weight (g); FD=Fruit diameter (mm); FL=Fruit length (mm); DFH=Days of first harvesting; YPP= Yield per plant (kg), NL = Number of locules per fruit, ST = Skin thickness (mm), SL = Shelf-life duration (Days after harvesting), VC = Vitamin C (mg/100g), Brix content and TA = Titrable acidity (%).

(2020). It is found that the number of fruits per cluster and per plant is a reliable indicator of the yield potential of tomato hybrids. In this experiment, the F_1 hybrids BT-8 × BT-11 and BT-15 × BT-11 demonstrated the highest number at both pre- and post-flowering, while the parent BT-11exhibited the maximum number of fruits per cluster and fruit per plant, indicating the additive gene action in controlling the inheritance of these traits, which suggested that an early selection from these combinations would be advantageous. Furthermore, the superior short stature and early maturity were observed in the hybrids BT-8 × BT-11 and BT-15 × BT-11 compared with the parent BT-15, the earliest-maturing genotype among the parental lines. Therefore, selecting these promising hybrids would be advantageous and would expand the scope for isolating potential early-maturing, high-yielding recombinant lines in the future.

In the current study, the post-harvest and nutritional qualities of the hybrids, parents, and check variety were also assessed (Fig. 1). For tomato cultivars, thicker flesh for prolonged preservation is a prerequisite. The hybrid BT-8 × BT-15, followed by BT-8 × BT-11, which showed the highest shelf-life, and skin thickness, had higher values than the corresponding better parent in the cross combinations. Hosen et al. (2022) and Rasheed et al. (2022) are consistent with the experimental findings. In terms of nutritional quality, the hybrid BT-8 × BT-11 showed higher values for vitamin C and Brix percentage than the parental lines used in the crosses. Additionally, the highest titrable acidity was found in hybrid BT-11 × BT-3. Kumar (2021) and Farwah et al. (2023) reported that vitamin C and Brix percentages were within the ranges observed in tomato accessions. Therefore, these findings suggest that the selected hybrids could serve as preferred genetic resources for developing improved tomato hybrids.

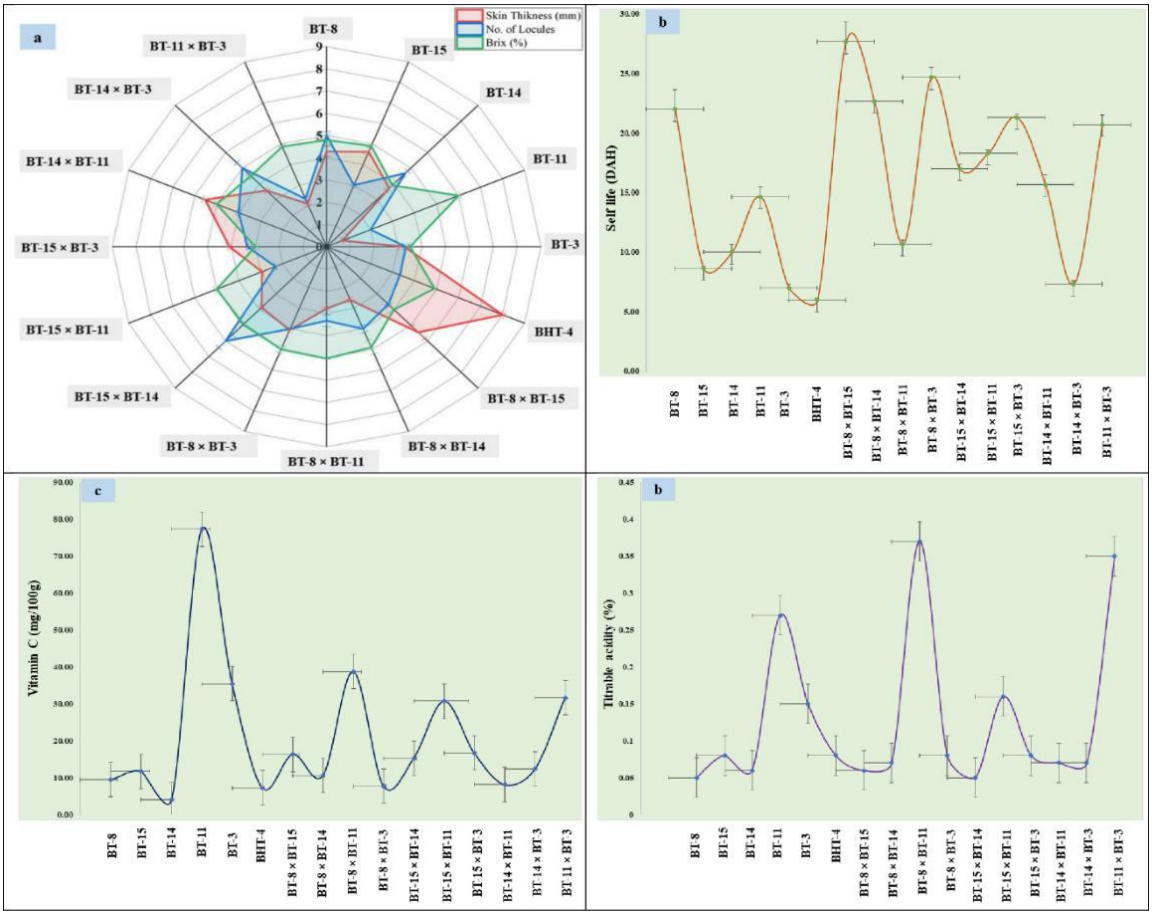

Fig. 1.Mean performance of ten hybrids, five parents and check variety for (a) skin thickness (mm), number of locules per fruit and brix content; (b) shelf-life duration (days after harvesting); (c) vitamin C contents (mg/100 g) and (d) titrable acidity (%).

Table 3. Mean performance of ten quantitative characteristics of five parents and their 10 F_1 lines of tomato.

Genotypes	D50%F	PH	NSB	NFC	NFP	SFW	FD	FL	DFH	YPP
Parents										
BT-8	25.67 b	92.40ef	7.67g	4.98gh	27.00 h	91.74cd	63.60ab	56.83ab	83.00 c	1.34f
BT-15	23.00cd	89.40fg	6.07 h	5.84d	27.27 h	100.18a	53.68ef	59.34a	76.67d	1.92e
BT-14	27.00ab	117.47a	5.60i	5.61de	32.68gh	89.56cde	54.96def	49.89cd	82.67c	2.16cde
BT-11	21.33de	97.66c	7.67g	11.67a	217.25a	8.00k	21.40i	25.25f	72.00e	1.08g
BT-3	27.67a	90.27efg	8.74c	5.17efgh	31.20gh	92.08cd	56.25def	49.92cd	84.00c	2.30c
F_1 Hybrids										
BT-8 × BT-15	22.33cd	96.80cd	8.50d	4.87gh	47.87f	67.55g	52.78f	47.06d	66.33f	2.97ab
BT-8 × BT-14	23.67c	111.53b	7.70g	5.55def	62.47d	84.17ef	67.35a	57.79ab	80.33cd	2.84b
BT-8 × BT-11	21.67de	87.93g	9.10b	8.50b	155.95b	18.70ij	33.12g	32.73e	66.33f	2.16cde
BT-8 × BT-3	26.33ab	87.67g	9.00b	5.32defg	29.96h	55.55h	53.82ef	51.50c	80.67cd	1.20fg
BT-15 × BT-14	22.67cd	111.73b	7.93f	5.31defg	36.13g	97.70ab	59.61bcd	55.81b	82.00c	2.24cd
BT-15 × BT-11	20.00e	98.33c	11.00a	7.63c	114.43c	17.60j	26.53h	31.28e	66.33f	2.07cde
BT-15 × BT-3	23.00cd	93.60de	7.93f	4.58h	48.97f	83.48f	59.43bcd	50.57c	88.33b	3.18a
BT-14 × BT-11	28.00a	111.30b	8.24e	5.54def	43.60f	93.62bc	63.20abc	60.12a	92.67a	2.31c
BT-14 × BT-3	27.00ab	120.32a	5.61i	5.07efgh	36.53g	87.30def	58.41cde	50.86c	81.00c	2.29c
BT-11 × BT-3	22.00cd	98.87c	11.03a	8.61b	109.77c	23.04i	34.81g	33.62e	67.00f	1.99de
CV (BHT-4)	25.67b	86.67g	6.12h	5.80d	55.67e	56.45h	58.32de	48.62cd	80.33cd	2.12cde
Mean	24.19	99.48	7.80	6.25	67.30	66.67	51.08	47.51	78.10	2.14
Maximum	28.00	120.32	11.03	8.50	217.25	100.18	67.35	60.12	92.67	3.18
Minimum	20.00	86.67	5.61	4.58	27.00	8.00	21.40	25.25	66.33	1.08
LSD	1.89	3.63	0.21	0.61	5.92	5.41	4.83	3.37	4.28	0.26
CV%	4.69	2.19	1.56	5.90	5.28	4.87	5.67	4.25	3.29	7.28
SE (±)	0.655	1.258	0.072	0.213	2.051	1.873	1.674	1.166	1.481	0.089

Note: D50%F=Days of 50% flowering; PH=Plant height (cm); NSB=Number of secondary branches, NFC=Number of fruits per cluster; NFP=Number of fruits per plant; SFW=Single fruit weight (g); FD=Fruit diameter (mm); FL=Fruit length (mm); DFH=Days of first harvesting; YPP= Yield per plant (kg).

Cluster analysis

The genetic improvement of yield and other agronomic traits largely depends on the genetic distance between the parental lines, as more diverse parents produce vigorous hybrids and subsequent generations (Snehi et al., 2023). The constructed dendrogram visualized that the 10 hybrids and their 5 respective parents were separated into four distinct clusters (Fig. 2). Within the clusters, three hybrids BT-15 × BT-14, BT-14 × BT-11, BT-14 × BT-3, BT-8 × BT-14 and one parent BT-14 were included in cluster I, and the accessions included in this cluster exhibited the maximum number of secondary branches, number of fruits per cluster, number of fruits per plant, vitamin C, brix content, titrable acidity, and also showed short duration for 50% flower initiation and days to first fruit harvest (Table 4). Again, cluster II contained three parents, BT-3, BT-8, BT-15, and three hybrids, BT-8 × BT-15, BT-8 × BT-3, BT-15 × BT-3, which showed promising agronomic characters, viz., single fruit weight, fruit diameter, fruit length, and number of locules per fruit. However, cluster III included only one parent BT-11 due to its distinct features, such as shorter plant height, higher yield per plant, thick skin, and longer shelf-life. Furthermore, three hybrids, BT-8 × BT-11, BT-11 × BT-3, and BT-15 × BT-11 were clubbed in cluster IV, which had moderate performance in terms of single fruit weight, fruit diameter, fruit length, and skin thickness. Similarly, Rahimi et al. (2022) and Verma et al. (2023) employed clustering analysis to determine genetic distances among tomato accessions and suggested that genetic distances obtained through clustering can be used to exploit high-heterotic groups in hybridization programs. In the current study, the cluster distance demonstrated that cluster I had the maximum intra-cluster distances, suggesting that populations included in this cluster were highly heterogeneous (Fig. 3). However, the highest inter-cluster distances were noted between cluster I and cluster II, preceded by cluster II and cluster III, indicating that populations under these clusters had the highest genetic variability among themselves. This may be due to the involvement of diverse parents in the hybrid combinations. Therefore, it is expected that segregating populations can be obtained from these hybrids through recurrent selection in future breeding programs to develop superior tomato varieties.

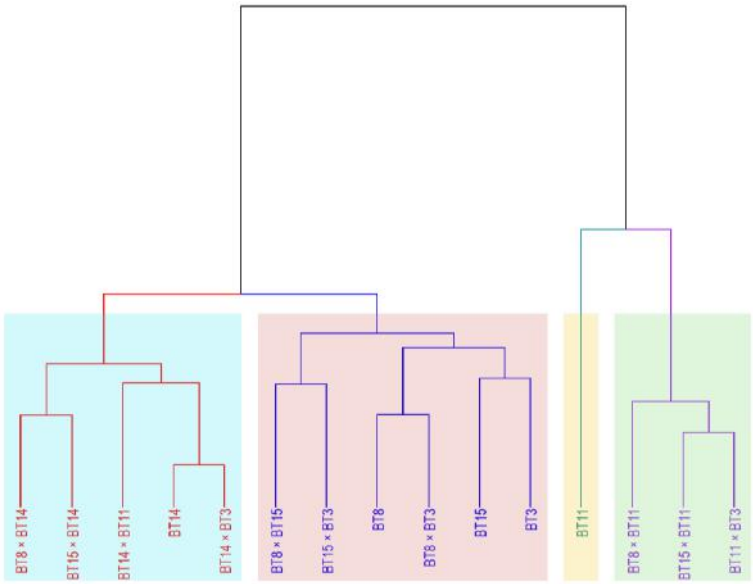

Fig. 2. Dendrogram showing the genetic relationships among hybrids and their parental lines, grouped into four distinct clusters based on their similarity. Here, light blue color indicated cluster I, light pink indicated cluster II, light yellow indicated cluster III and light green indicated cluster IV.

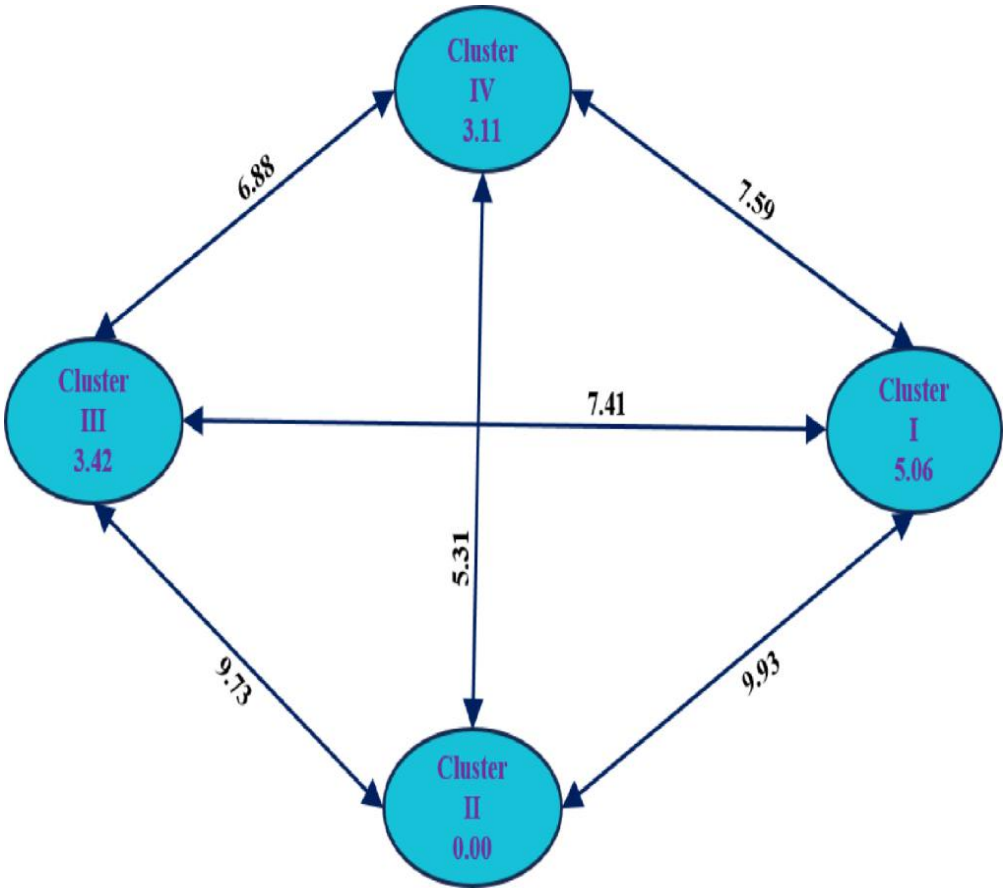

Fig. 3. Intra- and inter-cluster distances among the four clusters derived from hierarchical cluster analysis.The ellipses represent the four clusters (I–IV), with values inside each ellipse indicatingintra-cluster distances(within-cluster genetic divergence), and the arrows showing inter-cluster distances (genetic divergence between clusters).

Table 4. Average cluster mean values for the sixteen traits of four clusters.

Clusters	D50%F	PH	NSB	NFC	NFP	SFW	FD	FL	DFH	YPP	NL	ST	SL	VC	BRIX	TA
Cluster I	21.25	95.70	9.70	9.10	149.35	16.84	28.97	30.72	67.92	1.83	2.50	2.13	16.09	44.69	5.23	0.29
Cluster II	25.67	114.47	7.02	5.41	42.25	90.47	60.71	54.89	83.73	2.37	4.73	3.85	14.53	10.24	4.65	0.06
Cluster III	22.67	95.20	8.22	4.73	48.42	75.52	56.11	48.82	77.33	3.08	3.50	4.77	24.50	16.64	3.50	0.07
Cluster IV	25.67	89.94	7.87	7.87	28.86	84.89	56.84	54.40	81.09	1.69	3.83	4.06	15.59	16.23	4.55	0.09

Note: D50%F=Days of 50% flowering; PH=Plant height (cm); NSB=Number of secondary branches, NFC= Number of fruits per cluster; NFP= Number of fruits per plant; SFW=Single fruit weight (g); FD=Fruit diameter (mm); FL=Fruit length (mm); DFH=Days of first harvesting; YPP= Yield per plant (kg), NL = Number of locules per fruit, ST = Skin thickness (mm), SL = Shelf-life duration (Days after harvesting), VC = Vitamin C (mg/100g), Brix content and TA = Titrable acidity (%).

Genetic parameters among the variables

In crop improvement programs, genetic variation determination is a crucial step for estimating breeding values, aiding in selecting important yield-contributing traits. Regarding these, variability components viz. phenotypic and genotypic coefficient of variance, heritability, and genetic advance (%) provide reliable selection methods in breeding programs (Rasheed et al., 2022). In the present study, all the studied traits possessed a higher phenotypic coefficient of variance than their genotypic counterparts (GCV). In contrast, the minimal fluctuation between PCV and GCV implied that genes that regulated the heredity of these traits were greatly influenced by genetic factors (Fig. 4a). Moreover, the major percentage of the traits, excluding days to 50% flowering, plant height, number of secondary branches, days to first fruiting, and brix percentage, had a higher genotypic coefficient variation (variance> 20), indicating the existing variance among these traits facilitated an enormous scope to develop improved tomato cultivars by selecting these traits. Previously, Singh et al. (2017) and Hussain et al. (2021) also reported similar ranges of variability across different tomato accessions.

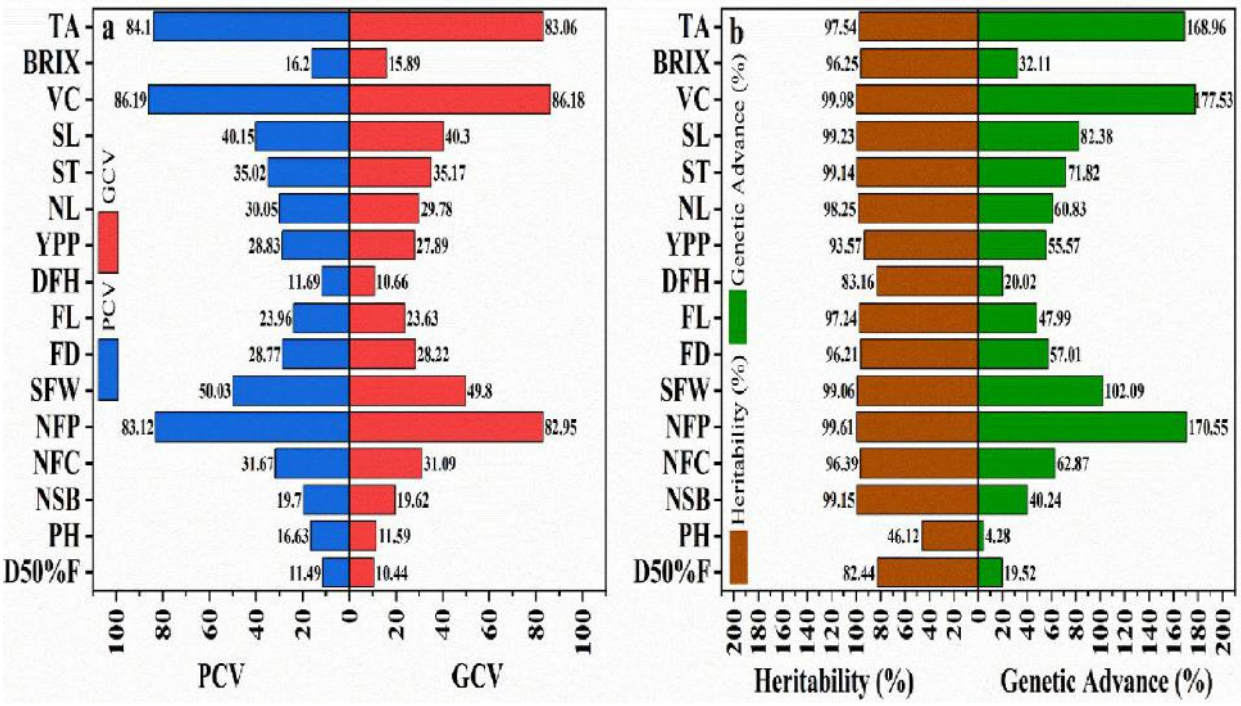

Fig. 4. (a) Phenotypic and genotypic coefficient of variance, (b) broad sense heritability (%) and genetic advancement (%) for the selected eighteen variables among the hybrids and parents.

Note: D50%F=Days of 50% flowering; PH=Plant height (cm); NSB=Number of secondary branches, NFC= Number of fruits per cluster; NFP= Number of fruits per plant; SFW=Single fruit weight (g); FD=Fruit diameter (mm); FL=Fruit length (mm); DFH=Days of first harvesting; YPP= Yield per plant (kg), NL = Number of locules per fruit, ST = Skin thickness (mm), SL = Shelf-life duration (Days after harvesting), VC = Vitamin C (mg/100g), Brix content and TA = Titrable acidity (%).

In tomato breeding programs, selecting traits to formulate feasible breeding strategies based on heritability and genetic advance is a well-recognized biometric tool. Heritability defines the degree of inheritance from the progenitors to the offspring, whereas genetic advance determines the effectiveness of selection (Pooja et al., 2022). Therefore, selecting suitable traits based on heritability and genetic advance is more predictable than heritability alone. Interestingly, all the studied traits except plant height (46.12 and 4.28%) showed a higher broad sense heritability accompanied by a higher genetic advance in percentage of mean (Fig. 4b). However, traits viz. the number of fruits per plant (99.61 and 170.55), single fruit weight (99.06 and 102.09), vitamin C content (99.98 and 177.53) and titrable acidity (97.54 and 168.96) exhibited the highest percentage of heritability and genetic advance. Similarly, the preponderance of high heritability and genetic advance for yield-attributing and nutritional traits was also reported by Anuradha et al. (2020) and Zannat et al. (2023). Therefore, consideration of these traits will be effective in selecting appropriate breeding lines to develop high-yielding tomato cultivars.

Linear relationship among the pairwise traits with fruit yield

Tomato fruit yield is a complicated trait reflecting the interaction of multiple genes that also govern the expression of other traits. Therefore, the association between the traits and fruit yields needs to be assessed in fabricating an efficient selection strategy. Correlation analysis aids breeding programs by identifying pairwise relationships among traits, enabling breeders to select the most important traits for future genetic improvement and to enhance yield performance. Falconer (1981) stated that the changes in one trait can significantly alter the performance of other traits. In the current study, Pearson correlation analysis among the yield-attributing traits with fruit yield was estimated (Fig. 5). The association among the pairwise traits revealed that fruit yields had a positive and strong interrelationship with fruit diameter (0.39**), number of secondary branches (0.44**), single fruit weight (0.34*) and skin thickness (0.35*). Therefore, selecting these traits will be rewarded, as their improvement simultaneously increases fruit yield. Furthermore, fruit length (0.26), days to first fruit harvest (0.12), and plant height (0.05) also exerted positive, but weak influences on fruit yield. Similar associations with fruit yield were also suggested by Reddy et al. (2013) and Sushma et al. (2020). Among the yield-contributing traits, days to 50% flowering (-0.06) and number of fruits per plant (-0.30) showed negative correlations with fruit yield, traits that should be improved in the next breeding programs.

As a fleshy vegetable, the preservation capabilities and nutritional properties of tomatoes greatly depend on post-harvest qualities. The current findings revealed that skin thickness exhibited a significant positive association with the number of locules per fruit (0.48***), fruit length (0.71**), fruit diameter (0.65***) and single fruit weight (0.67***). At the same time, skin thickness also showed a positive linear relationship with shelf-life duration (0.18). These associations suggest that thicker skin not only improves the yield of contributing traits but also extends shelf-life. On the other hand, brix content, vitamin C, and titrable acidity similarly showed strong interrelationship with each other and had a positive association with shelf-life, suggesting that longer shelf-life maintains intact nutritional qualities by reducing deterioration in tomato quality after harvesting. However, nutritional qualities such as vitamin C, brix content, and titrable acidity showed strong negative correlations with days to first fruit harvest, indicating that extended harvesting periods greatly decreased the health benefits of the tomato. This may be due to environmental fluctuations that trigger unfavorable conditions, *viz.,* higher transpiration, respiration, and ethylene production, deteriorate nutritional properties (Thole et al., 2021). Considering the above findings, we can conclude that improvements in qualitative traits should also be addressed in tomato breeding programs.

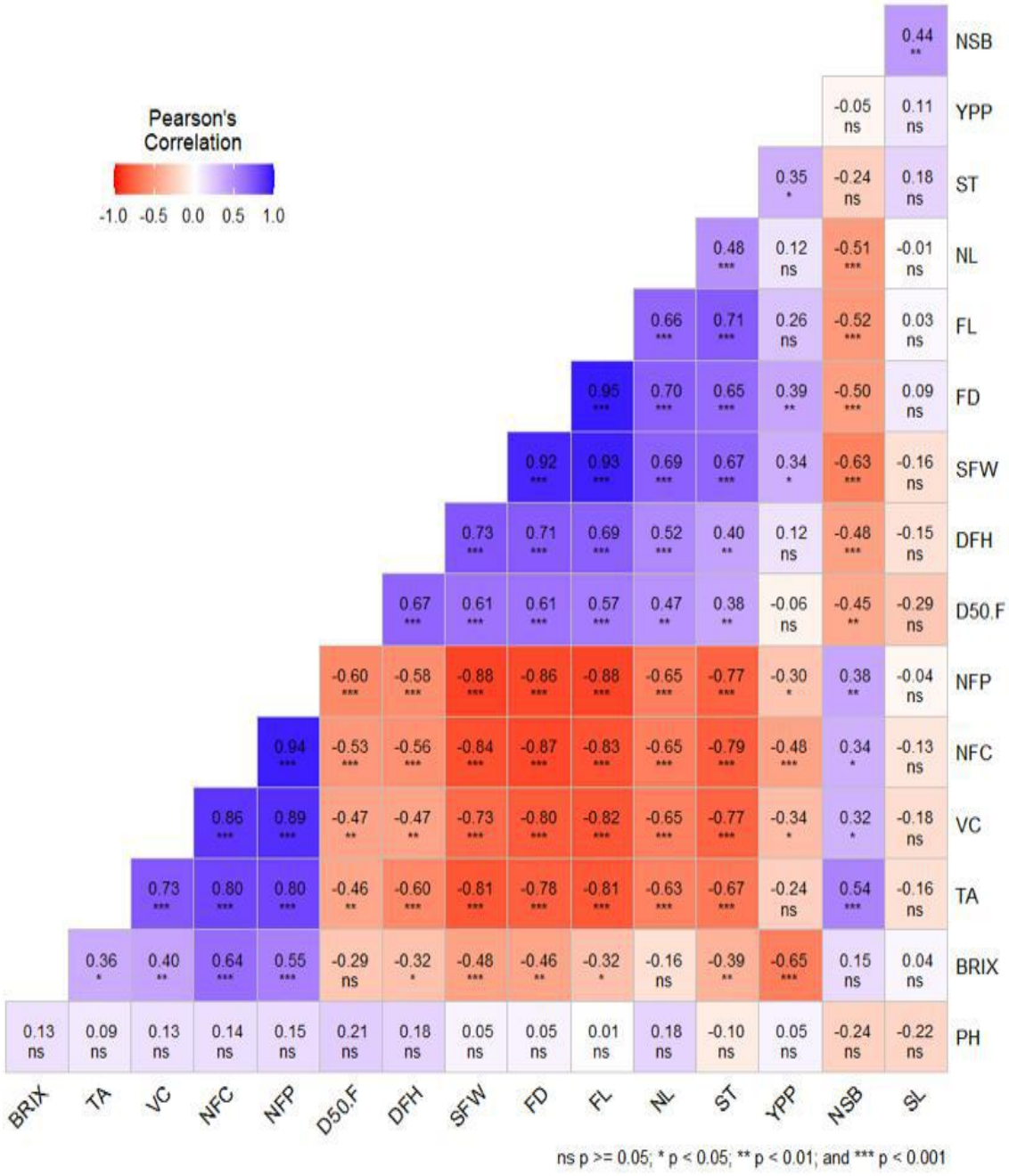

Fig. 5. Correlation coefficient among the different pairs of quantitative traits with fruit yields.

Note: D50%F=Days of 50% flowering; PH=Plant height (cm); NSB=Number of secondary branches, NFC= Number of fruits per cluster; NFP= Number of fruits per plant; SFW=Single fruit weight (g); FD=Fruit diameter (mm); FL=Fruit length (mm); DFH=Days of first harvesting; YPP= Yield per plant (kg), NL = Number of locules per fruit, ST = Skin thickness (mm), SL = Shelf-life duration (Days after harvesting), VC = Vitamin C (mg/100g), Brix content and TA = Titrable acidity (%).

Direct and indirect effects on the fruit yields

Path coefficient analysis partitions the contribution of yield-related traits into direct and indirect effects, enabling breeders to identify the most influential yield components and develop targeted selection strategies for improved productivity. Our current findings indicated that the number of secondary branches (0.59), the number of fruits per plant (0.95), single fruit weight (0.87)**,** fruit diameter (0.94)**,** and skin thickn**ess (**0.10**)** showed the most potent positive direct effects on fruit yield, underscoring that fruit quality related traits exerted significant contribution in overall yield improvement (Table 5). These traits reinforce each other through positive indirect effects; for example, single fruit weight and fruit diameter influence tomato quality via vitamin C content (0.93 and 0.90), BRIX percentage (0.15 and 0.15) and total tritrable acidity (0.28 and 0.27), augmenting its overall correlation with fruit yield (0.34* and 0.39**, respectively) and thereby improving the overall fruit yield production. On the other hand, despite the number of fruits per plant having a negative correlation with fruit yield (-0.30*), this trait indirectly enhances tomato yield production through the positive contribution of fruit length (0.94), days to first fruit harvesting (0.38) and the number of secondary branches (0.23). This indicates a trade-off between fruit number and size, where indirect trait effects can counterbalance direct negative associations and support better fruit development. Similarly, Jogi et al. (2018) and Madhavi et al. (2019) reported that fruit width, fruit length, and average fruit weight are critical yield contributors, as evidenced by correlations and path analysis studies. On the other hand, the number of fruits per cluster (-0.83)**,** fruit length (-0.95), days to first fruit harvest (-0.60), and number of locules (-0.39) manifested strong adverse direct effects. However, these traits can also enhance the fruit yield production through the contribution of other characteristics. For instance, the number of fruits per cluster can indirectly improve the yield performance via the number of secondary branches (0.21), number of fruits per plant (0.91), fruit length (0.94), and number of locules per fruit (0.26). Additionally, fruit length can indirectly improve yield performance via the number of fruits per cluster (0.72), single fruit weight (0.92), and fruit diameter (0.93). Similar trends in enhancing fruit yield via other traits were also reported by Kumar et al. (2014) and Tandel et al. (2023). Conversely, several quality-related characteristics, including higher vitamin C content (-0.98), BRIX content (-0.31), and titratable acidity (-0.34), were found to exert adverse direct effects on yield. This indicates that while these traits enhance fruit quality, they may divert assimilates and metabolic resources away from fruit biomass accumulation, thereby reducing overall yield. Therefore, balancing between yield-contributing and nutritional traits improvement is a critical research area in tomato breeding programs. Similar negative associations between nutritional quality and fruit yield have been reported by Anuradha et al. (2018). Nonetheless, the positive interrelationships among these quality attributes contribute substantially to improving overall fruit quality. These results emphasize that selection strategies in tomato breeding should prioritize traits with strong positive direct or indirect effects on yield, while simultaneously incorporating post-harvest and nutritional quality traits in a balanced manner. Such an integrated approach would enable the development of tomato cultivars that combine high yield potential with superior market and nutritional value.

Table 5.Direct and indirect effects of fifteen traits on the fruit yields.

Traits	D50%F	PH	NSB	NFC	NFP	SFW	FD	FL	DFH	NL	ST	SL	VC	BRIX	TA	Correlation with fruit yield
D50%F	**0.16**	-0.06	-0.29	0.49	-0.67	0.75	0.84	-0.85	-0.50	-0.21	0.04	0.08	0.66	0.11	0.17	-0.06
PH	0.09	**-0.12**	-0.44	-0.30	0.63	0.34	0.27	-0.04	-0.35	-0.17	-0.03	0.16	-0.46	-0.11	-0.09	0.05
NSB	-0.08	0.09	**0.59**	-0.29	0.54	-0.70	-0.73	0.72	0.32	0.20	-0.02	-0.12	-0.41	-0.05	-0.19	-0.05
NFC	-0.09	-0.04	0.21	**-0.83**	0.91	-0.78	-0.88	0.94	0.37	0.26	-0.08	0.04	-0.50	-0.21	-0.28	-0.48***
NFP	-0.10	-0.05	0.23	-0.80	**0.95**	-0.82	-0.87	0.94	0.38	0.26	-0.08	0.01	-0.97	-0.18	-0.28	-0.30*
SFW	0.11	-0.02	-0.38	0.71	-0.88	**0.87**	0.90	-0.94	-0.47	-0.27	0.07	0.04	0.93	0.15	0.28	0.34*
FD	0.11	-0.02	-0.30	0.75	-0.87	0.91	**0.94**	-0.95	-0.47	-0.29	0.07	-0.03	0.90	0.15	0.27	0.39**
FL	0.10	0.00	-0.31	0.72	-0.90	0.92	0.93	**-0.95**	-0.46	-0.27	0.07	-0.01	0.85	0.10	0.28	0.26
DFH	0.13	-0.07	-0.32	0.51	-0.74	0.71	0.85	-0.88	**-0.60**	-0.22	0.04	0.04	0.65	0.12	0.22	0.12
NL	0.08	-0.05	-0.31	0.56	-0.71	0.70	0.84	-0.85	-0.34	**-0.39**	0.05	0.00	0.83	0.06	0.22	0.12
ST	0.07	0.04	-0.15	0.67	-0.73	0.73	0.86	-0.84	-0.26	-0.19	**0.10**	-0.04	0.92	0.13	0.24	0.35*
SL	-0.05	0.07	0.26	0.11	-0.14	-0.38	0.14	-0.06	0.10	0.01	0.02	**-0.26**	0.23	-0.01	0.06	0.11
VC	-0.08	-0.04	0.19	-0.73	0.89	-0.74	-0.87	0.90	0.31	0.26	-0.08	0.05	**-0.98**	0.13	0.25	-0.34*
BRIX	-0.05	-0.04	0.10	-0.56	0.85	-0.69	-0.68	0.57	0.24	0.07	-0.04	-0.01	0.51	**-0.31**	0.12	-0.65***
TA	-0.08	-0.03	0.32	-0.69	0.87	-0.79	-0.87	0.90	0.40	0.25	-0.07	0.04	0.93	0.11	**-0.34**	-0.24
Residual effects 0.09																

Note: Bold indicates the direct effects of traits on the fruit yield

Conclusion

The present study demonstrated substantial genetic variability among tomato hybrids and their parents for agronomic, post-harvest, and nutritional traits, providing a strong foundation for selection. High heritability coupled with high genetic advance in key yield and quality parameters suggests additive gene action, making direct selection effective. Positive correlations between yield and traits such as fruit diameter, single fruit weight, and skin thickness indicate the potential for simultaneous improvement in productivity and shelf-life. Notably, BT-15 × BT-3, BT-8 × BT-15, and BT-8 × BT-14 excelled inyield performance, while BT-8 × BT-11 and BT-8 × BT-15 combined extended storability with enhanced nutritional content. These results underscore the value of integrating agronomic, post-harvest, and nutritional parameters into breeding strategies to develop tomato varieties that meet both producer and consumer demands.

Acknowledgment

The corresponding author acknowledges the Ministry of Science and Technology, Government of the People's Republic of Bangladesh, for funding the research project, and Sher-e-Bangla Agricultural University, Dhaka, for logistical support.

Authors contribution

Mr. Niloy Gain and Ms. Mahbuba Fatema were responsible for conducting the experiments, analyzing the data, and drafting the manuscript. Dr. Jamilur Rahman supervised the research, contributed

to the experimental design, facilitated the required resources, and revised the manuscript.

Conflict of interest

The authors declare no conflicts of interest regarding the publication of this paper.

References

Anuradha B, Saidaiah P, Reddy K, Harikishan S and Geetha A. Genetic variability, heritability and genetic advance for yield and yield attributes in tomato (*Solanum lycopersicum* L.). *Int. J. Curr. Microbiol. Appl. Sci.* 2020; 9: 2385-2391.

Anuradha B, Saidaiah P, Sudini H, Geetha A and Reddy KR. Correlation and path coefficient analysis in tomato (*Solanum lycopersicum* L.). *J. Pharmacogn. Phytochem.* 2018; 7(5): 2748-2751.

BARI Handbook 2017. *Krishi Projukti Hatboi* (Handbook on Agro-technology). 7th edition, Bangladesh Agricultural Research Institute (BARI), 2017.

Dewey DR and Lu KH. A correlation and path-coefficient analysis of components of crested wheatgrass seed production. *Agron. J.* 1959; 51(9): 515-518.

Falconer DS. *Introduction to quantitative genetics*. 2nd ed. Oliver and Boyd, Edinburgh and London. 1981; pp. 164-176.

Farwah S, Afroza B, Rashid R, Dar ZA and Khan I. Mean performance of parents and their crosses in tomato (*Solanum lycopersicum* L.) for qualitative traits. *Pharma Innov. J*. 2023; 12(3): 3697-3701.

FAOSTAT (Food and Agriculture Organization of the United Nations Statistical Database). *Crops and Livestock Products,* Rome, 2023.

Gonzalez-Vega JC, Fougere C, Garcia-Casal MN and Pena-Rosas JP. Nutritional and health benefits of tomatoes: A review. *Food Chem.* 2021; 343: 128547.

Hosen M, Rafii MY, Mazlan N, Jusoh M, Farhana M and Chowdhury N. Estimation of heterosis and combining ability for improving yield, sweetness, carotenoid and antioxidant qualities in pumpkin hybrids (*Cucurbita moschata* Duch. Ex Poir.). *Horticulturae*, 2022; 8(10): 863.

Hussain K, Lone S, Malik A, Masoodi KZ, Dar Z and Nazir N. Genetic variability studies in cherry tomato for growth, yield, and quality traits in open field conditions. *Int. J. Agric. App. Sci.* 2021; 2(2): 60-64.

Islam MT, Hossain MM and Rahman MS. Evaluation of hybrid tomato varieties for yield and shelf life in Bangladesh. *Bangladesh J. Agric. Res.* 2021; 46(3): 517-527.

Jogi M, Lingaiah HB, Indiresh KM, Singh TH, Samuel DK and Ramachandra RK. Studies on correlation and path coefficient analysis in tomato (*Solanum lycopersicum* L.). *Int. J. Chem. Stud.* 2018; 6(5): 1499-1502.

Johnson HW, Robinson HF and Comstock RE. Estimates of genetic and environmental variability in soybeans. *Agron. J.* 1955; 47(7): 314-318.

Kumar P, Ram C, Singh M and Saini S. Studies on analysis of variance and mean performance of parents and their crosses among various quantitative traits in tomato (*Solanum lycopersicum*). *Int. J. Chem. Stud.* 2020; 8(1): 1992-2003.

Kumar R, Ram CN, Yadav GC, Deo C, Vimal C and Bhartiya HD. Studies on correlation and path coefficient analysis in tomato (*Solanum lycopersicum* L.). *Plant Arch.* 2014; 14(1): 443-447.

Kumar R. Performance of tomato (*Solanum lycopersicum* L.) genotypes for growth, yield and quality. *Ann. Plant Soil Res.* 2021; 23(4): 465-468.

Lin T, Zhu G, Zhang J, Xu X, Yu Q, Zheng Z and Huang S. Genomic analyses provide insights into the history of tomato breeding. *Nat. Genet.* 2014; 46(11): 1220-1226.

Madhavi Y, Reddy RVSK, Kumar SS and Reddy CS. Correlation and path analysis studies for yield and quality traits in tomato (*Solanum lycopersicum* L.). *Int. J. Pure App. Biosci.* 2019; 7(1): 306-312.

Meena RK, Sanjay K, Meena ML and Shashank V. Genetic variability, heritability and genetic advance for yield and quality attributes in tomato (*Solanum lycopersicum* L.). *J. Pharmacog. Phytochem*. 2017; 7: 1937–1939.

Panse VG and Sukhatme PV. *Statistical Methods for Agricultural Workers.* 2nd ed., *Indian Council of Agricultural Research, New Delhi*, 1967.

Pooja H, Gasti VD, Bhavidoddi A, Yashavantakumar H, Prashantha A and Srikantaprasad D. Genetic variability, heritability and genetic advance in determinate types of tomato (*Solanum lycopersicum* L.). *Pharm. Innov. J.* 2022; 11(4): 222-225.

Rahimi S, Alam K, Ahmad M, Sharma K, Keshari D and Wamiq M. Assessment of genetic divergence in tomato (*Lycopersicon esculentum* Mill) genotypes. *Int. J. Environ. Clim. Chang.* 2022; 12(3): 1-7.

Rasheed A, Ilyas M, Khan TN, Mahmood A, Riaz U and Chattha MB. Study of genetic variability, heritability, and genetic advance for yield-related traits in tomato (*Solanum lycopersicum* MILL.). *Front. Genet*. 2022; 13: 1-13.

Reddy RB, Reddy MP, Reddy DS and Begum H. Correlation and path analysis studies for yield and quality traits in tomato *(Solanum lycopersicum L.). J. Agri. Vet. Sci.* 2013; 4(4): 56-59.

Singh A, Ram C, Yadav G, Srivastava R, Deo C and Gautam D. Studies on genetic variability, heritability and genetic advance in tomato (*Solanum lycopersicum* L.). *Int. J. Pure App. Biosci.* 2017; 5: 908-912.

Sinha R, Singh R and Singh A. Postharvest management and processing of tomato. *Food Rev. Int.* 2019; 35(4): 375-397.

Snehi S, Prakash NR, Pant U, Singh PK, Kumar S, Jeena AS and Bhajan R. Prediction of heterotic combinations using correlation between genetic distance, heterosis and combining ability in yellow sarson (*Brassica rapa* var. yellow sarson Prain). *Vegetos.* 2023; 37(4): 1552-1564.

Sushma K, Saidaiah P, Reddy RK, Sudini H and Geetha A. Correlation and path coefficient analysis in tomato (*Solanum lycopersicum* L.). *Int. J. Curr. Microbiol. App. Sci.* 2020; 9(11): 2569-2575.

Tandel T, Rathod D, Sarkar M, Emmi S, Chaudhari BN and Tank RV. Studies on correlation and path coefficient analysis in tomato (*Solanum lycopersicum* L.). *Pharma Innov. J.* 2023; 12(12): 2785-2788.

Tee ES, Young SI, Ho SK and Mizura SS. Determination of vitamin C in fresh fruits and vegetables using the dye-titration and microfluorometric methods. Pertanika *J. Trop. Agric. Sci.* 1988; 11(1): 39-44.

Thole V, Vain P and Martin C. Effect of elevated temperature on tomato post-harvest properties. *Plants.* 2021; 10(11): 2359.

Verma B, Sharma D and Patel JK. Assessment of genetic diversity in tomato (*Solanum lycopersicum* L.) genotypes using cluster and principal component analysis. *Pharma Innov. J.* 2023; 12(6): 5014-5019.

Zannat A, Hussain MA, Abdullah AH, Hossain MI, Saifullah AM and Sathi FA. Exploring genotypic variability and interrelationships among growth, yield, and quality characteristics in diverse tomato genotypes. *Heliyon*, 2023; 9(8): e18958.

J. Bangladesh Acad. Sci. 49(2); 271-285: December 2025 DOI:https://doi.org/10.3329/jbas.v49i2.82006

Journal of Bangladesh Academy of Sciences

Journal homepage: http://www.bas.org.bd/publications/jbas.html

Research Article

AC impedance analysis of $Bi_{1-x}Y_xFe_{0.7}Mn_{0.3}O_3$ multiferroic ceramics

Sonet Kumar Saha[1*], Md. Ashraf Ali[2,] and AKM Akther Hossain

Department of Physics, Bangladesh University of Engineering and Technology, Dhaka, Bangladesh

ARTICLE INFO

Article History

Received: 01 June 2025
Revised: 29 September 2025
Accepted: 12 October 2025

Keywords: $Bi_{1-x}Y_xFe_{0.7}Mn_{0.3}O_3$; EDX, Xray diffraction; Dielectric properties; Impedance analysis; AC conductivity.

ABSTRACT

In this paper, the AC impedance properties of $Bi_{1-x}Y_xFe_{0.7}Mn_{0.3}O_3$ (BYFMO) ceramics with x values from 0.00 to 0.20 were studied. It was manufactured via solid-state chemistry, and during manufacturing, sintering at temperatures was at 800, 825, and 850°C, and optimal bulk density was at 825°C. X-ray diffraction investigation verified differences in lattice parameters resulting from doping-induced strain and defect structures, suggesting the presence of a rhombohedral phase along with small secondary phases. Field Emission Scanning Electron Microscopy (FESEM) demonstrated a porous microstructure with grain sizes ranging from 1.22 to 1.89 μm. Energy Dispersive X-ray spectroscopy confirmed the elemental composition. The dielectric constant (ε′) demonstrated a frequency-dependent reduction, stabilizing beyond 10 kHz. At 100Hz, ε′ rose from 65 to 78 at 100 Hz with increasing Y doping due to a reduction in the quantities of oxygen vacancies. Impedance spectroscopy revealed distinct semicircular patterns in undoped material, indicating grain and grain boundary effects, while doped samples mostly demonstrated grain conduction, elucidating multiferroic electrical transport mechanisms. We have gotten the maximum grain resistance 199.02 MΩ for highest doping at x = 0.20.

Introduction

Multiferroic materials are a special kind of material because they simultaneously exhibit at least two ferroic properties. One is ferromagnetism (ordered magnetic moments), and another is ferroelectricity (spontaneous electric polarization), or ferroelasticity (spontaneous strain). And the magneto-electric coupling between the ferroic orders is present in these materials. This coupling can be controlled by an external electric or magnetic field. As a result, they have potential in multifunctional applications, including spintronics, data storage, sensors, energy harvesting, and optoelectronics (Yin and Mi, 2020; Verma, 2020; Muneeswaran et al., 2021; Wang et al., 2020). Bismuth ferrite ($BiFeO_3$, BFO) is a notable single phase multiferroic substance. It is characterized by a rhombohedrally deformed perovskite structure (space group R3c). It demonstrates a significant ferroelectric transition temperature (T_e = 827 °C) and an antiferromagnetic Néel temperature (T_n = 377 °C) (Scott, 2007; Ramesh and Spaldin, 2007; Zatsiupa et al., 2014). These features, along with the simultaneous presence of electric and magnetic ordering at room temperature, make BFO a compelling choice for sensitive device applications. Although it has advantageous properties but BFO faces the major challenges. These are leakage currents at higher levels and inconsistencies in polarization values

*Corresponding author:< sonnet4321@gmail.com, ashrafphy31@cuet.ac.bd>

[1]*Department of Electrical and Electronic Engineering, Z. H. Sikder University of Science and Technology, Shariatpur, Bangladesh*

[2]*Department of Physics, Chittagong University of Engineering and Technology, Chattogram, Bangladesh*

between bulk ceramics and thin films (Teague et al., 1970; Wang et al., 2004). For example, thin films have a polarization of 90–100 μC/cm^{2,} which subjects them to heteroepitaxial constraints; on the other hand, bulk materials exhibit values roughly one-tenth as high. Additionally, structural defects, oxygen vacancies, and non-stoichiometry are present in the material, which impede its practical application (Palkar et al., 2002). To overcome these restrictions, prominent researchers have investigated replacing atoms at both the A- and B-sites of the perovskite lattice. For examples, the substitution of trivalent ions, including La^{3+} (Zhang et al., 2006), Eu^{3+} (Huong et al., 2017), and Gd^{3+} (Singh et al., 2018), as well as divalent ions such as Ca^{2+} (Chen et al., 2010), Sr^{2+} (Varshney and Kumar, 2013), and Ba^{2+} (Chauhan et al., 2013) at the A-site for reducing oxygen vacancies and altering the ferroelectric and magnetic characteristics of a material and also B-site substitutions with ions such as Nb^{5+} (Singh and Yadav, 2012), Ti^{4+} (Minh et al., 2024), and Cr^{3+} (Agrawal et al., 2025) for improving the material's structural, magnetic, and electrical properties. And there are also Co-substitution, such as (Mn, Nb) (Chung et al., 2006), (La, Co) (Gu et al., 2016), (La, V) (Yu et al., 2008), (Pr, Ti) (Wu et al., 2016), and (Na, Ti) (Das Adhikary et al., 2023), at both A- and B-sites for modifying the features of BFO. So, it can be said that the choice of elements for co-substitution at the A- and B-sites in $BiFeO_3$ depends on their influence on the characteristics of the material. Recent studies by Wu et al. (2012) show that the A-site of Bismuth Ferrite (BFO) substituted with Yttrium (Y^{3+}) causes inner lattice stress because its ionic radius is less than that of Bi^{3+}. Consequently, a structural change from rhombohedral (R3c) to orthorhombic (Pnma) symmetry occurred at approximately x = 0.10. This phase transition is related to a ferroelectric-to-paraelectric transformation and significant alterations in magnetization behavior (Wu et al., 2012). Another investigation by Gautam et al. (2012) demonstrates Y-doped $BiFeO_3$ samples exhibit superior dielectric characteristics and increased saturation magnetization, and by Luo et al. (2012) observed a reduction in leakage current with higher Y^{3+} concentration. Another study by Chen et al. (2015) and Chen (2014) illustrated that Mn substitution at the B-site has several effects on BFO. The effects include modifications in ferroelectric and magnetic characteristics, reduced leakage current, and increased dielectric constant. But few studies have examined the dielectric properties, AC conductivity, and impedance characteristics of BFO under the joint effects of Y and Mn co-substitution. This study synthesized $Bi_{1-x}Y_xFe_{0.7}Mn_{0.3}O_3$ ceramics (x=0.00–0.20) using the solid-state reaction technique and investigated the impact of Y^{3+} doping on the dielectric properties, AC conductivity, and impedance characteristics of the material. This study also explores the potential application of Y–Mn co-substituted BFO. It is noted that multiferroic materials need high dielectric properties to enhance their significance for upcoming electronic devices such as memory, sensors, and tunable microwave devices.

Experimental Details

Synthesis of $Bi_{1-x}Y_xFe_{0.7}Mn_{0.3}O_3$ Ceramics

Using high-purity precursors obtained from Sigma-Aldrich (each 99.99% pure) – specifically bismuth (III) oxide (Bi_2O_3), iron(III) oxide (Fe_2O_3), yttrium(III) oxide (Y_2O_3), and manganese carbonate ($MnCO_3$) – $Bi_{1-x}Y_xFe_{0.7}Mn_{0.3}O_3$ ceramic samples (where x=0.00, 0.05, 0.10, 0.15, 0.20) were prepared via a standard solid-state reaction method. The components were accurately weighed to obtain the required stoichiometric ratios using an electronic balance (Shimadzu, AX 120). The initial powders were meticulously combined with acetone in an agate mortar and pestle for 3 hours to achieve a uniform dispersion. Then, the blended powder was calcined at 700°C for 6 hours in an ambient atmosphere using a programmable furnace (Nabertherm P330) to facilitating phase formation. After calcination, the resultant powders were meticulously crushed and reground for 1 hour, then compressed into cylindrical pellets with a diameter of 12 mm using a

uniaxial hydraulic press at 200 MPa. Then, the compacted pellets were sintered at 800°C, 825°C, and 850°C for 12 hours. The heating rate was sustained at 10°C/min, succeeded by a regulated cooling rate of 5°C/min in ambient air. The sintered pellets were carefully polished to prepare the samples for future characterization. This entailed employing silicon carbide abrasive sheets with ever finer grit sizes until a uniformly smooth and even surface was attained across all samples.

Characterizations

Crystal and Microstructural Characterization

The crystal structure was analyzed using an X-ray diffractometer (Philips PANalytical X'PERT-PRO). Where Cu-Kα radiation is an X-ray source with λ=1.5406 Å. The operation setup was set to 40 kV and 30 mA. The X-ray scan for data collection was performeed over a 2θ range of 20° to 60° at a rate of 1°/min. Here, the instrument was calibrated time-to-time using a standard silicon sample. It ensures the accuracy and reliability of the measurements.

A FESEM with model JEOL JSM 7600F was employed to examine the microstructural properties of the samples. And, EDX spectroscopy was conducted to determine the elemental composition and also verify the chemical consistency of the materials.

Density and Dielectric Properties

The following formula was used to measure the bulk density (ρ_B) of all samples:

$$\rho_B = \frac{m}{\pi r^2 t}$$

where m = mass, r = radius, and t = the thickness of the pellet. To assess the dielectric property, two metallic conductors were connected to the opposing faces of the prepared samples by using silver paste as electrodes. The samples were then heated in an oven for 1 hour. Consequently, it ensures the complete curing of the silver paste and establishes a robust electrical contact without affecting the properties of the materials. The dielectric constant ε' was calculated using the equation:

$$\varepsilon' = \frac{Ct}{\varepsilon_o A}$$

where C, t, ε_o and A are the capacitance, the sample thickness, the permittivity of free space, and electrode area, respectively. AC conductivity σ_{ac} was determined using the relation: $\sigma_{ac} = \omega\varepsilon'\varepsilon_o \tan\delta_{AC}$ where ω, tanδ, ε' are angular frequency, dielectric loss, and the dielectric constant, respectively. All dielectric properties were measured using a Wayne Kerr Impedance Analyzer (Model 6500B) over a frequency range of 100 Hz to 120 MHz.

Result and Discussion

Structural Analysis with XRD

Fig. 1 presents the X-ray diffraction (XRD) patterns. The patterns are drawn from X-ray diffraction data collected on a series of $Bi_{1-x}Y_xFe_{0.7}Mn_{0.3}O_3$ samples using an X-ray diffractometer. From these patterns, the crystalline structures for Y-doping concentrations at x=0.00, 0.05, 0.10, 0.15, and 0.20 can be evaluated. Systematic variations in the XRD profiles are observed across different x values, revealing the structural evolution and phase purity of these materials. Here, the observed diffraction peaks exhibit a pattern similar to that of $BiFeO_3$ (JCPDS Card No. 71-2494). Although secondary phase peaks corresponding to Bi- or Fe-rich phases, specifically $Bi_2Fe_4O_9$ and $Bi_{25}FeO_{40}$, were detected across all samples. Those are denoted by asterisk (*) in Fig. 1. That kind of finding is consistent with previous studies by Dao et al. (2013) and Xu et al. (2009). Despite these secondary phases, all primary diffraction peaks for various x align with the rhombohedral R3c crystal structure, characteristic of $BiFeO_3$.

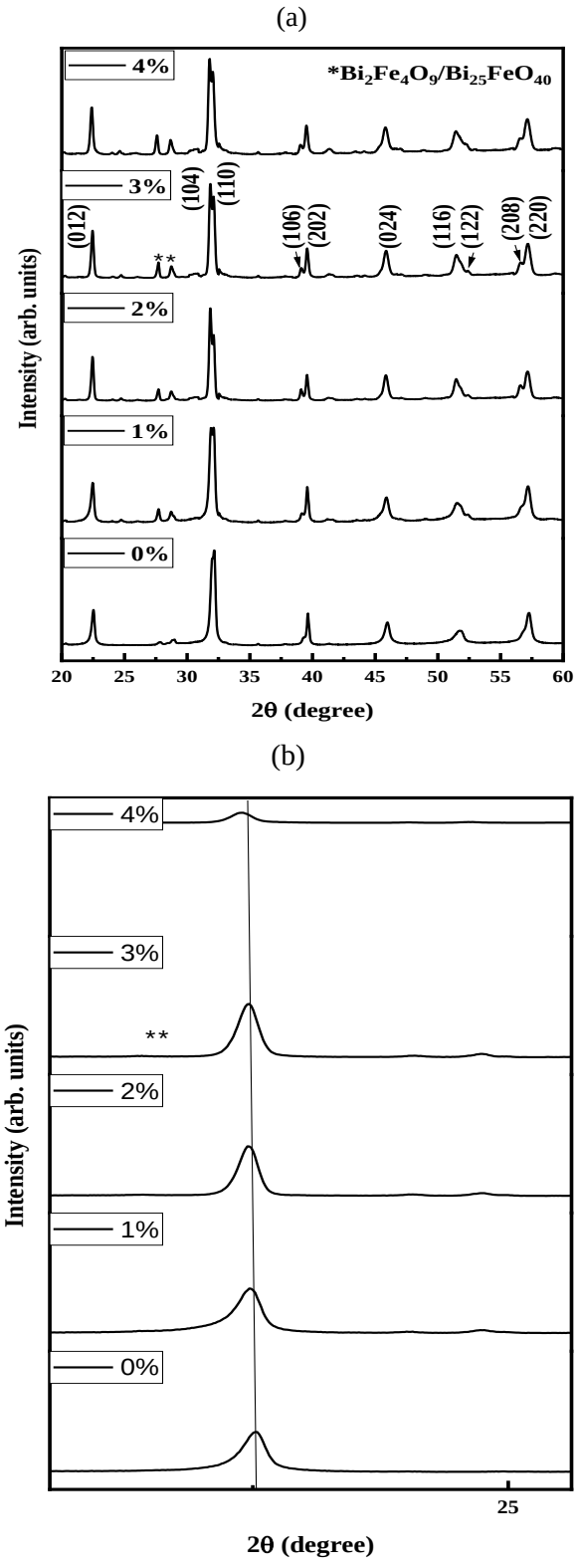

Fig. 1 (a) XRD patterns of $Bi_{1-x}Y_xFe_{0.7}Mn_{0.3}O_3$ (x=0.00, 0.05, 0.10, 0.15, and 0.20) compositions sintered at 825 ºC (b) enlarged view.

Notably, increasing Y doping concentration in our samples shifted the diffraction peaks to lower Bragg angles Fig. 1(b)) indicating the successful incorporation of Y ions into the parent lattice and their influence on its structure. This structure was further confirmed by performing a Rietveld refinement analysis using the FullProf software package, which provided impurity phases for composition as shown in Fig. 1(c).

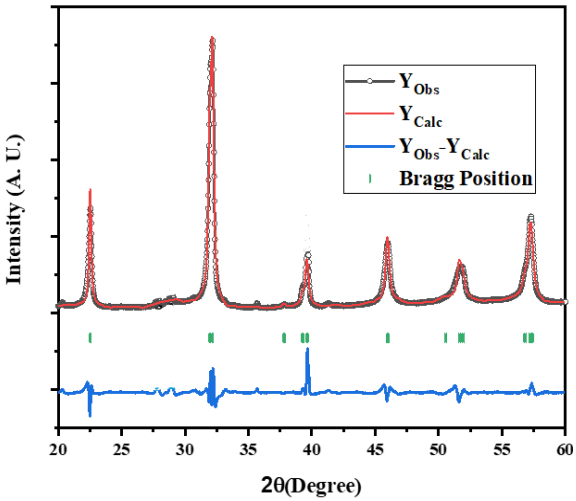

Fig. 1 (c) XRD refinement patterns of $Bi_{1-x}Y_xFe_{0.7}Mn_{0.3}O_3$ (x=0.00) compositions sintered at 825 ºC.

The tolerance factor (t) is a useful tool for determining the stability of perovskite compounds. This factor is calculated as follows: $t = (r_A + r_O)/\sqrt{2}(r_B+r_O)$, where r_A is the average ionic radius of Bi^{3+} and Y^{3+} ions, r_O for O^{2-} ion, and r_B for Fe^{3+}, Fe^{4+}, and Mn^{3+} ions. In this investigation, a decreasing trend in the tolerance factor was observed with increasing Yttrium (Y) doping concentration, specifically from t = 0.84023 for the undoped (x= 0.0) composition to t = 0.83124 for the x = 0.20 doped sample. This reduction inherently expresses that a mismatch between the ionic radii of the constituent cations and the oxygen anions has increased. So, it enhances the thermodynamic driving force for cooperative octahedral tilting or rotation. Consequently, a structural distortion occurs in doped samples (Karimi et al., 2009).

Density of the compositions

Fig. 2 illustrates the influence of sintering temperature on the bulk density for various Y-doping samples. At first, there is a clear correlation between bulk density and sintering temperatures; it increases with rising temperature and reaches a maximum at 825°C.

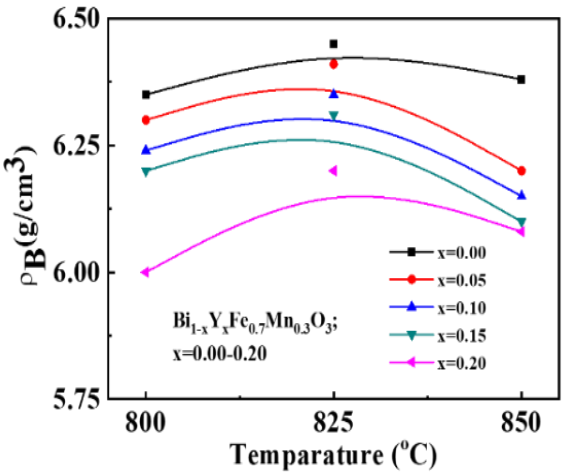

Fig. 2 Dependence of bulk density, ρ_B on sintering temperature for various $Bi_{1-x}Y_xFe_{0.7}Mn_{0.3}O_3$.

Nevertheless, additional increases in temperature result in a reduction of bulk density. This pattern can be ascribed to the interaction and the correlation between grain expansion and the loss of Bi_2O_3. Initially, thermal energy during sintering facilitates grain growth. As a result, grain boundaries expand into pores, reducing pore volume and enhancing material densification. On the other hand, an opposite behavior is observed above 825°C. It may occur because Bi_2O_3 evaporation becomes significant, counteracting the densification effect. Moreover, its melting point at approximately 825°C contributes to the observed density reduction. Based on these findings, an optimal sintering temperature for our samples is 825°C. It recommends that subsequent characterization studies of the samples be carried out at this temperature.

Microstructure of $Bi_{1-x}Y_xFe_{0.7}Mn_{0.3}O_3$ (BYFMO)

Fig. 3 presents FESEM micrographs of the studied samples. From micrographs, randomly oriented microstructure and non-uniform grains with intergranular porosity are observed. The factors influencing this grain growth depend on the interplay between the thermodynamic driving forces promoting grain boundary migration and the kinetic hindering imposed by pervasive porosity. When driving forces are inhomogeneous, non-uniform grain growth occurs, whereas when forces are homogeneous, uniform grain sizes are available (Miah et al., 2016). The average grain size (D) was quantified from FESEM micrographs using ImageJ. The corresponding grain size distribution histograms, fitted to a Gaussian distribution, are shown in the right panel of each image. The calculated D values range from 1.22 to 1.89 μm. This anomalous value suggests that the sintering temperature may not have been optimal for this composition. But, to study the effect of variation in Y contents, the sintering temperature was kept fixed for all compositions. A correlation with D and elevated Y content. This relation can arise from the role of fine particles as high-diffusion pathways, which promote grain expansion (Basiri et al., 2014).

EDX Analysis

EDX spectroscopy is an effective technique for determining the elemental composition of the samples. Analysis of various points across the samples (Fig. 4) revealed the experimental and calculated mass percentages of elements. EDX spectra ensured that all raw compositions are present in the sample. The details of elemental compositions are tabulated in the accompanying EDX spectra.

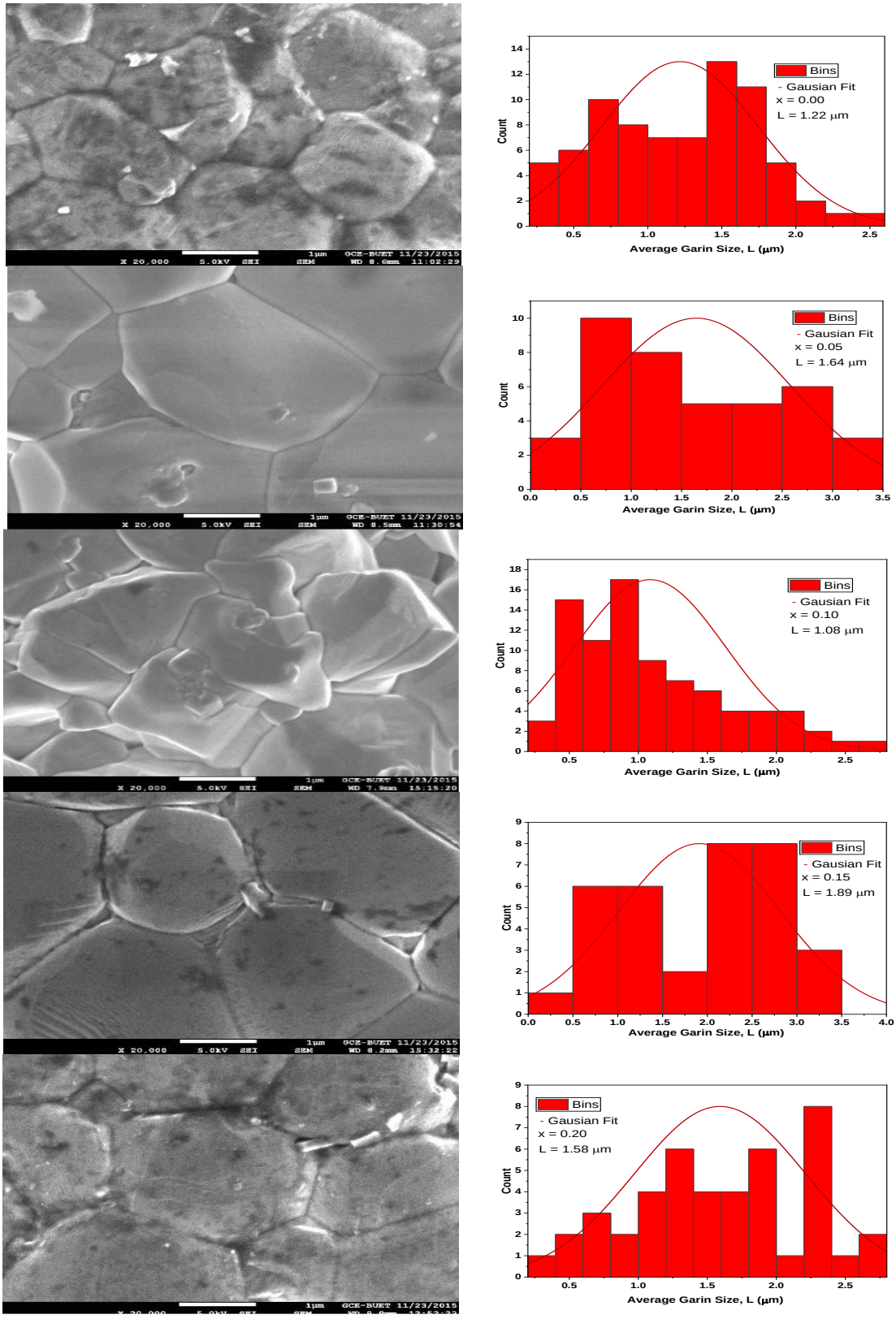

Fig. 3 FESEM micrographs of various $Bi_{1-x}Y_xFe_{0.7}Mn_{0.7}O_3$ ceramics sintered at 825 °C.

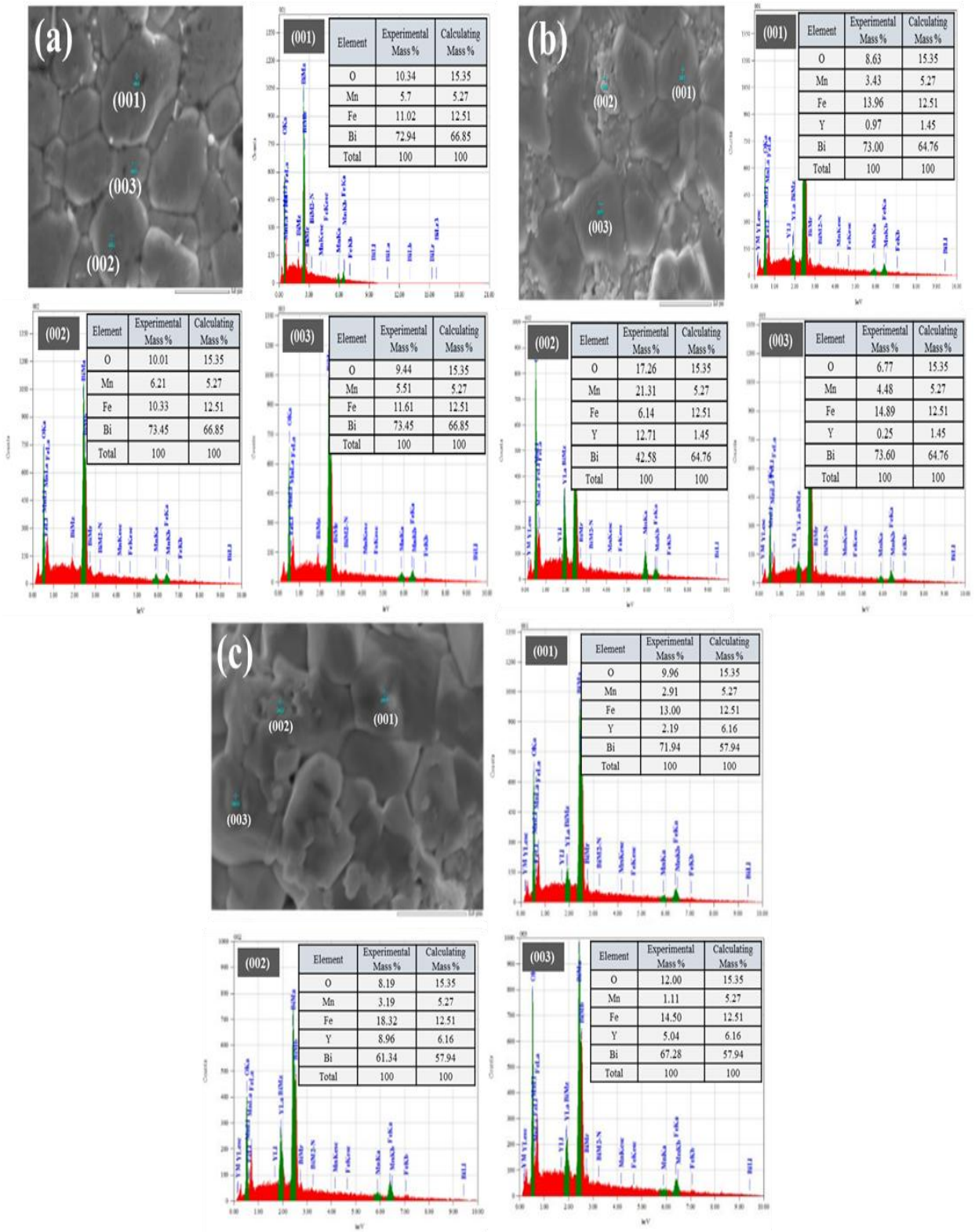

Fig. 4 EDX spectrum for $Bi_{1-x}Y_xFe_{0.7}Mn_{0.3}O_3$ samples sintered at 825°C with (a) x = 0.01 (b) x = 0.05 (a) x = 0.2.

Dielectric Properties at Room Temperature

In Fig. 5 (a), the graph shows how ε′ changes with frequency. From the graph, it appears that the dielectric constant initially decreases with increasing frequency up to 10 kHz for both undoped and doped samples, then becomes nearly constant up to 1 MHz. This behavior can be explained by the polarization model of Maxwell (Fiebig et al., 2002) and Wagner (Maxwell, 1973), consistent with Koop's phenomenon theory (Koops, 1951). Now the effect of yttrium doping on the dielectric properties of $Bi_{1-x}Y_xFe_{0.7}Mn_{0.3}O_3$ ceramics can be interpreted based on oxygen vacancies and Fe^{3+} ions (Pattanayak et al., 2014; Jonscher, 1977). Fig. 5(a) demonstrates that there is a direct correlation between the Y content and an increase in ε′. This increase arises from the isovalent substitution of volatile Bi^{3+} ions by non-volatile Y^{3+} ions.

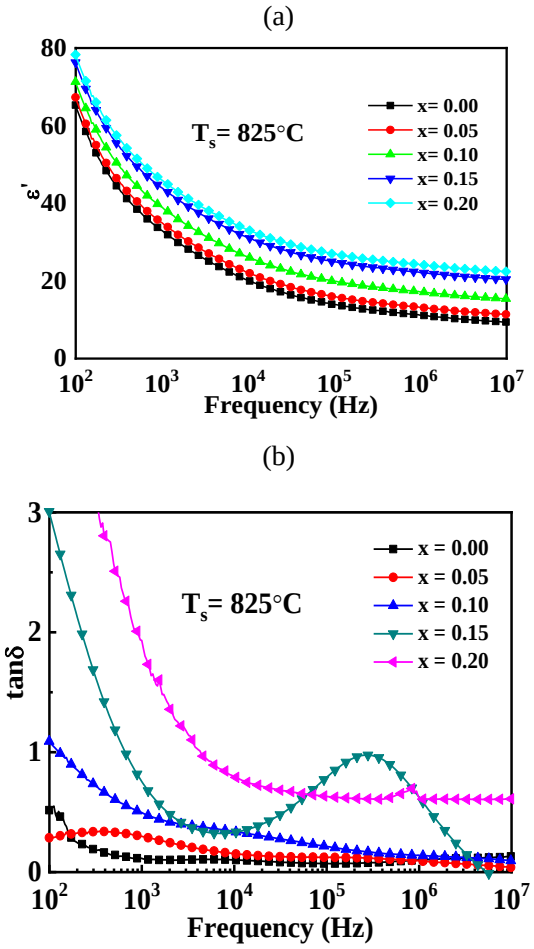

Fig. 5 Variation of (a) dielectric constant ε′ and (b) dielectric loss with frequency for various $Bi_{1-x}Y_xFe_{0.7}Mn_{0.3}O_3$ sintered at 825 °C.

That kind of substitution attenuates the formation of oxygen vacancies. The presence of Y^{3+} ions is believed to stabilize the valence states of Fe^{3+} and Fe^{2+}, thereby mitigation of oxygen vacancy concentration. This reduction in oxygen vacancies directly correlates with the observed improvement in dielectric properties, as shown in Fig. 5(a). Fig. 5(b) illustrates how the dielectric loss (tan δ) changes as a function of frequency. Its value is high at low frequencies, then its value decreases as the frequency increases. However, there is an upward trend at high frequencies for the x = 0.15 sample, which may be attributed to polarization relaxation (Barick et al., 2011).

AC conductivity

Conductivity is a fundamental property of a material, as it provides insight into the material's electrical behaviour. Understanding the conduction mechanisms in multiferroic compounds like BYFMO is crucial, as their conductivity is governed by a combination of electronic and ionic (Mukherjee, 2014). Fig. 6(a) illustrates the frequency-dependent AC conductivity (σ_{ac}) of $Bi_{1-x}Y_xFe_{0.7}Mn_{0.3}O_3$ multiferroic ceramics with two distinct conductive regions at room temperature. One region stays at a low frequency. In which σac remains relatively constant and reflects the intrinsic DC conductivity (σ_{dc}). And another region stays at a high frequency. In that case, σac rapidly increases, indicates enhanced charge-carrier hopping between localized sites. This hopping phenomenon can be explained by an increase in the conductive grain at higher frequencies (Macdonald, 1992). There is Jonscher's power law (Jonscher, 1977), shown in the following equation below. It can explain the frequency dependence of σ_{ac}.

$$\sigma_{ac}(\omega) = \sigma_{dc} + B\omega^n$$

where the exponent 'n' quantifies the interaction between mobile ions and the surrounding lattice, with values ranging from 0 to 1. The observed increase in conductivity with frequency, as shown in Fig. 6(b), suggests a small polaron hopping mechanism in the conduction process. Further, it

is supported by the frequency exponent 'n' values, determined from the slope of log(σac) vs. logω curves shown in Fig. 6(b), which stay less than unity ($0.433 \leq n \leq 0.916$). This trend is consistent with previous reports on doped BFO (Das et al., 2012; Khandekar et al., 2011).

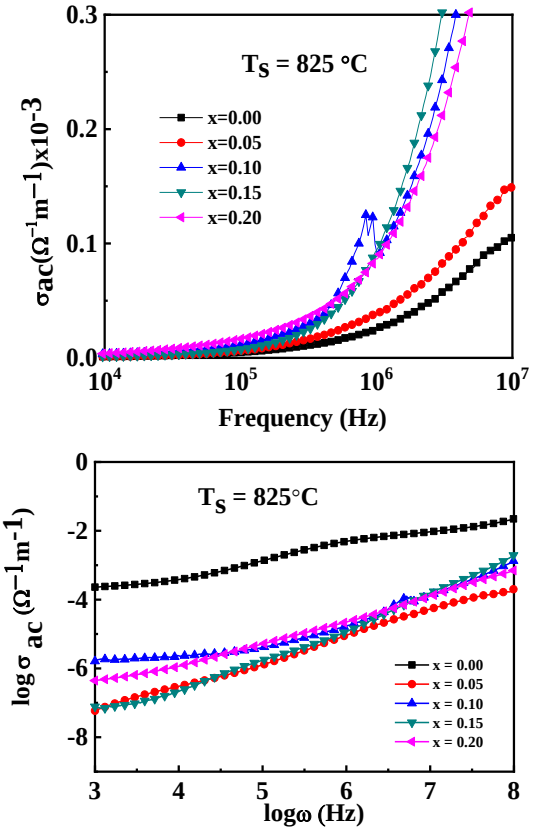

Fig. 6(a) Variation of ac conductivity with frequency and (b) *logσ$_{ac}$* as *logω* for various $Bi_{1-x}YxFe_{0.7}Mn_{0.3}O_3$ sintered at 825 ºC.

Additionally, it is observed that σ_{ac} increases with increasing Y content. This improvement is ascribed to an increased number of charge carriers.

Complex Impedance Spectra Analysis

Fig. 7(a) displays the change in the real part of impedance ($Z^{/}$) with frequency at room temperature for different $Bi_{1-x}Y_xFe_{0.7}Mn_{0.3}O_3$ samples sintered at 825°C with x values of 0.00, 0.05, 0.10, 0.15, and 0.20. As shown in this figure, the $Z^{/}$ value gradually decreases as the frequency increases up to a certain limit, 10 kHz, after which its frequency dependence becomes negligible. At higher frequencies, a constant $Z^{/}$ ensures higher conductivity. At lower frequencies, the observation of higher impedance ($Z^{/}$) values indicates that the materials exhibit greater polarization effects. This effect is likely due to the presence of all types of polarization mechanisms, including dipolar, interfacial, and electronic polarization, at lower frequencies. All compositions exhibited similar impedance values ($Z^{/}$) at higher frequencies. This convergence indicates the potential for space charge polarization to be released (Behera et al., 2008). Moreover, the undoped sample displayed lower impedance compared to its doped counterparts. Fig. 7(b) illustrates how the imaginary part of the complex impedance ($Z^{//}$) changes with frequency for $Bi_{1-x}Y_xFe_{0.7}Mn_{0.3}O_3$ compositions sintered at 825°C for 2 hours each. The behavior observed in Fig. 7(b) with respect to frequency is similar to that of $Z^{/}$.

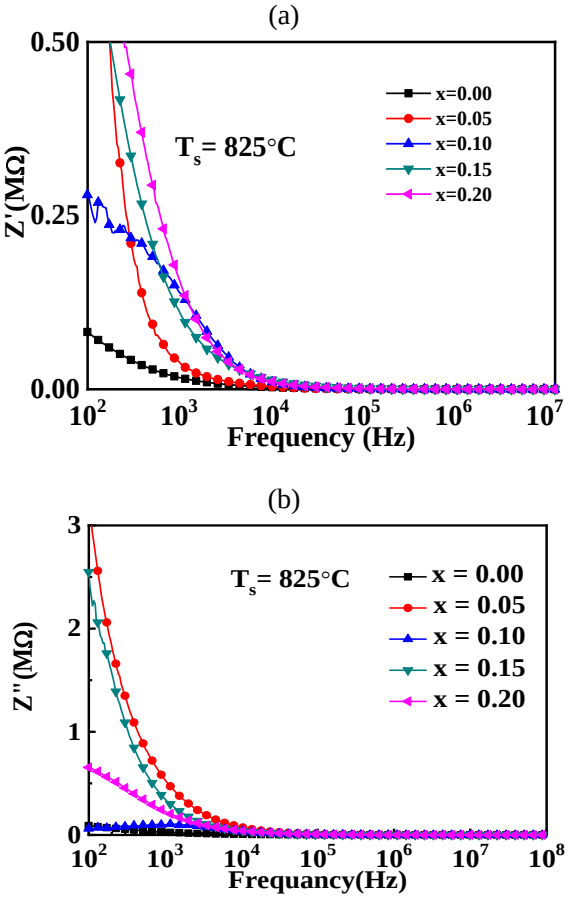

Fig. 7(a) Variation of (a) Z′ and (b) Z″ with the frequency for $Bi_{1-x}Y_xFe_{0.7}Mn_{0.3}O_3$ samples.

Table 1. Grain and grain boundary resistance of various $Bi_{1-x}Y_xFe_{0.7}Mn_{0.3}O_3$ compositions.

Composition, x	0.00	0.05	0.10	0.15	0.20
R_g (MΩ)	0.28	41.28	99.99	190.7	199.02
R_{gb} (MΩ)	37.00				

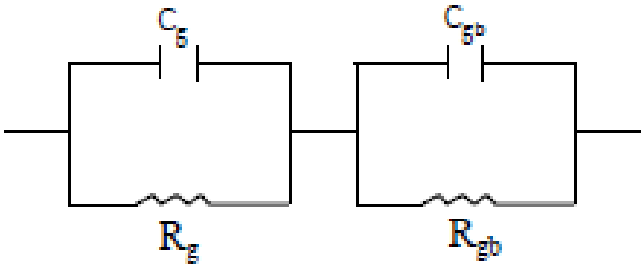

Fig. 8(a) Electrical equivalent circuit of CIS.

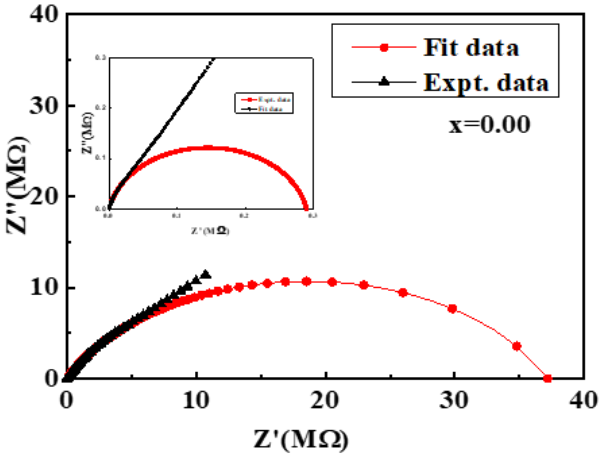

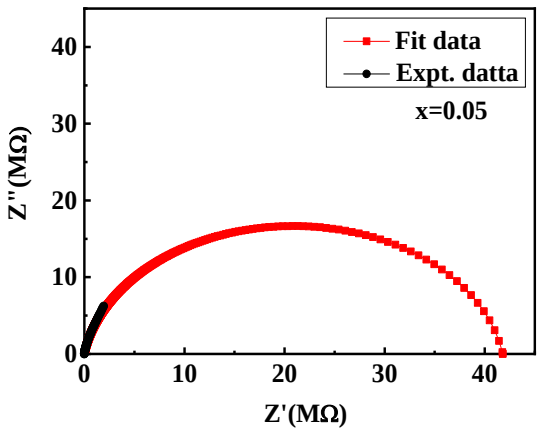

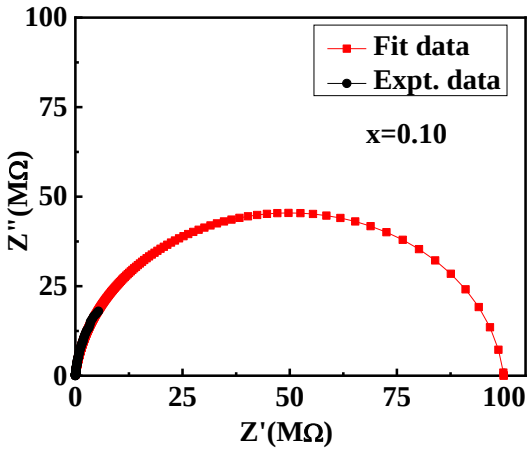

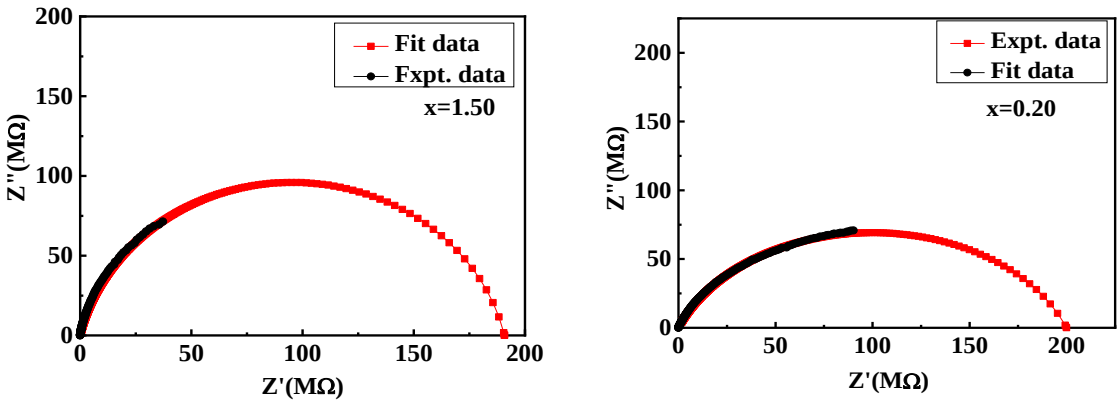

Fig. 8(b) Cole–Cole plots of Z/ and Z// at room temperature for various $Bi_{1-x}Y_xFe_{0.7}Mn_{0.3}O_3$ samples.

Cole-Cole Plot Analysis

Here, impedance is measured for all samples. Impedance spectroscopy is used to measure impedance. It analyzes all contributions to impedance for the bulk grain, grain boundary, and electrode interface of a material. These contributions characterized by plotting successive semicircles in the complex plane, known as Cole-Cole plots, in the complex plane. This plot is the imaginary part plotted against the real part (Macdonald et al., 2018; Zhu et al., 2001). An ideal Cole-Cole plot consists of perfect semicircles, and its centers sit on the real axis. But when a pot is drawn using experimental data, it often deviates from the ideal plot due to various factors (Kumar et al., 2000). In the plot, a high-frequency semicircle is attributed to grain/bulk resistance, a low-frequency semicircle to ion and electron transfers at the electrode-sample interface, and an intermediate-frequency semicircle to grain boundary resistance (Pattanayak et al., 2014). These contributions can vary with temperature, and not all may be observed within a given frequency range. To analyze the impedance data, an equivalent circuit consisting of two parallel RC circuits connected in series was employed in Fig. 8(a). In the present study, the impedance spectrum, which features two overlapping semicircular arcs, was modeled using an equivalent circuit. This circuit consists of two parallel resistor-capacitor (RC) elements: one representing the grain (Rg and Cg), and the other representing the grain boundary (Rgb and Cgb).

Each RC element represents a grain and a grain boundary and corresponds to a semicircle in the Cole-Cole plot. Fig. 8(b) shows the Cole-Cole plots for different $Bi_{1-x}Y_xFe_{0.7}Mn_{0.3}O_3$ compositions measured at room temperature. The distorted semicircular arcs are observed in both high- and low-frequency regions and indicate non-Debye-type relaxation (West et al., 1997) for all the samples. By fitting the simulated data to depressed/distorted semicircles as shown in Fig. 8(b), it was found that the sample with x = 0.00 exhibited two semicircles, samples with $0.05 < x < 2.00$ showed only one semicircle, and all semicircles originated from the origin of the axis. This suggests that, at room temperature, the dominant conductivity mechanism in the majority of samples is primarily grain-boundary-related. When a Cole-Cole plot shows only a single semicircle after doping, it typically means the grain boundary resistance has become negligible compared to the grain resistance, so the two responses are no longer distinct. The increasing arc diameter with higher Y content indicates an increase in grain resistance (R_g). The higher R_g values with increasing Y content can be explained by the observed microstructural changes and the decrease in oxygen vacancy defects. The values of R_g and grain boundary resistance (R_{gb}) were calculated from the intercepts on the Z' axis and are listed in Table 1.

Conclusions

In this study, $Bi_{1-x}Y_xFe_{0.7}Mn_{0.3}O_3$ ceramics were successfully synthesized using the conventional solid-state reaction method. All samples were sintered at 800°C, 825°C, and 850°C. Investigation of the influence of sintering temperature on the bulk density of the samples

showed that bulk density increased, peaked at 825°C, and then declined. Therefore, 825°C is the optimal sintering temperature for all samples. XRD patterns confirmed a rhombohedral R3c crystal structure for all samples. And its primary peaks aligned closely with BiFeO3 (JCPDS Card No. 71-2494). Secondary phases such as $Bi_2Fe_4O_9$ and $Bi_{25}FeO_{40}$ were present. The decreasing trend in tolerance factor (t) from 0.84023 to 0.83124 with increasing Y doping led to a structural distortion in the perovskite lattice. FESEM analysis confirmed that randomly oriented microstructures, unevenly sized grains, and significant intergranular porosity were present in all samples. Average grain sizes **(**D) measured by ImageJ software were found in the range of 1.22 to 1.89 μm. EDX spectroscopy analysis confirmed the presence of raw elements in the samples, although slight variations in composition ratios were visible across the surfaces. The dielectric properties of all samples ensured a decrease in ε′ with increasing frequency up to 10 kHz, after which it stabilized up to 1 MHz. The effect of Yttrium on the dielectric properties of the samples also showed that ε′ was enhanced due to a reduction in oxygen vacancies. The frequency-dependent behaviour of σ_{ac} of all samples followed Jonscher's power law. σ_{ac} enhanced with increasing Y content due to a greater number of charge carriers, provided insights into the electrical conduction mechanisms in these multiferroic ceramics. Impedance analysis of all samples made sure that a frequency-dependent decrease in the real part of impedance (Z') up to 10 kHz, which indicates enhanced conductivity at higher frequencies. Impedance spectroscopy of all samples revealed non-Debye-type relaxation with conductivity dominated by grain effects in Y-doped samples. From Cole-Cole plots, a transition from two semicircles (x = 0.00) to a single semicircle (x = 0.05–0.20) was observed, indicated reduced grain boundary contributions to resistance. The increase in grain resistance (Rg) with higher Y content verified the decrease in oxygen vacancy defects and microstructural changes confirmed by equivalent circuit modelling. Finally, increased AC conductivity and optimized dielectric properties make $Bi_{1-x}Y_xFe_{0.7}Mn_{0.3}O_3$ ceramics promising for multiferroic devices, including capacitors, spintronic devices, and high-frequency applications.

Acknowledgment

The authors thank the Committee for Advanced Studies & Research (CASR) at BUET for their financial support. They also express their gratitude to the Microstructural Analysis Unit at the University of Technology Sydney, Australia, for granting access to the X-ray diffractometer facility.

Authors contribution

Sonet Kumar Saha conducted all experimental investigations and prepare samples, acquired data, and performed subsequent analysis. He also drafted the conceptual framework and the initial manuscript version. Md. Ashraf Ali performed a critical review of the manuscript and provided editorial contributions. A. K. M. Akther Hossain provided overall project supervision and intellectual guidance.

Conflict of interest

The authors declare that they have no competing interests.

References

Agrawal AK, Kumari A, Kumar B, Kumar P, Jena LK, Asthana S, Singh RK and Jaiswal SK. Structural, optical absorption and electrical characteristics of sol-gel synthesized chromium-doped bismuth ferrites. *Phys. B: Condens. Matter* 2025; 696: 416639.

Barick BK, Mishra KK, Arora AK, Choudhary RNP and Pradhan DK. Impedance and Raman spectroscopic studies of $(Na_{0.5}Bi_{0.5})TiO_3$. *J. Phys. D: Appl. Phys.* 2011; 44(35): 355402.

Basiri MH, Shokrollahi H and Isapour G. Effects of La content on the magnetic, electric and structural properties of $BiFeO_3$. *J. Magn. Magn. Mater.* 2014; 354: 184-189.

Behera B, Nayak P and Choudhary RNP. Structural and electrical properties of $KCa_2Nb_5O_{15}$ ceramics. *Cent. Eur. J. Phys.* 2008; 6: 289-295.

Chauhan S, Arora M, Sati PC, Chhoker S, Katyal SC and Kumar M. Structural, vibrational, optical, magnetic and dielectric properties of $Bi_{1-x}Ba_xFeO_3$ nanoparticles. *Ceram. Int.* 2013; 39(6): 6399-6405.

Chen CC. Study on the ferroelectric and magnetic properties of $BiFe_{1-x}Mn_xO_3$ polycrystalline ceramics dependence on the Mn content. *J. Ceramic Process. Res.* 2014; 15(6): 424-427.

Chen J, Dai H, Li T, Liu D, Xue R, Xiang H and Chen Z. Role of Mn substitution in the multiferroic properties of $BiFeO_3$ ceramics. *J. Supercond. Novel Magn.* 2015; 28: 2751-2754.

Chen SY, Wang L, Xuan H, Zheng Y, Wang D, Wu J, Du Y and Huang Z. Multiferroic properties and converse magnetoelectric effect in $Bi_{1-x}Ca_xFeO_3$ ceramics. *J. Alloys Compd.* 2010; 506(2): 537-540.

Chung CF, Lin JP and Wu JM. Influence of Mn and Nb dopants on electric properties of chemical-solution-deposited $BiFeO_3$ films. *Appl. Phys. Lett.* 2006; 88: 242909.

Dao VT, Du Thi XT and Nguyen VM. Structural and physical properties of Y-doped $BiFeO_3$ material prepared by sol-gel method. *VNU J. Sci. Math.-Phys.* 2013; 29(3): 63-69.

Das Adhikary G, Muleta GJ, Tina GA, Sharma D, Mahale B, Silva LL, Hinterstein M, Senyshyn A and Ranjan R. Structural insights into electric field induced polarization and strain responses in $K_{0.5}Na_{0.5}NbO_3$ modified morphotropic phase boundary compositions of $Na_{0.5}Bi_{0.5}TiO_3$-based lead-free piezoelectrics. *Phys. Rev. B,* 2023; 107(13): 134108.

Das R, Sarkar T and Mandal K. Multiferroic properties of Ba^{2+} and Gd^{3+} co-doped bismuth ferrite: magnetic, ferroelectric and impedance spectroscopic analysis. *J. Phys. D: Appl. Phys.* 2012; 45(45): 455002.

Fiebig M, Lottermoser T, Fröhlich D, Goltsev AV and Pisarev RV. Observation of coupled magnetic and electric domains. *Nature* 2002; 419(6909): 818-820.

Gautam A, Uniyal P, Yadav KL and Rangra VS. Dielectric and magnetic properties of $Bi_{1-x}Y_xFeO_3$ ceramics. *J. Phys. Chem. Solids* 2012; 73(2): 188-192.

Gu Y, Zhao J, Zhang W, Liu S, Ge S, Chen W and Zhang Y. Improved ferromagnetism and ferroelectricity of La and Co co-doped $BiFeO_3$ ceramics with Fe vacancies. *Ceram. Int.* 2016; 42(7): 8863-8868.

Huong TN, Luu Thu HA, Nguyen Long N and Nguyen Hong H. Crystal structure and magnetic properties for $Bi_{1-x}Eu_xFeO_3$ compounds. *VNU J. Sci. Math.-Phys.* 2017; 33(1): 35-40.

Jonscher AK. The universal dielectric response. *Nature* 1977; 267(5613): 673-679.

Karimi S, Reaney IM, Levin I and Sterianou I. Nd-doped $BiFeO_3$ ceramics with antipolar order. *Appl. Phys. Lett.* 2009; 94(11): 112903.

Khandekar MS, Kambale RC, Patil JY, Kolekar YD and Suryavanshi SS. Effect of calcination temperature on the structural and electrical properties of cobalt ferrite synthesized by combustion method. *J. Alloys Compd.* 2011; 509(5): 1861-1865.

Koops CG. On the dispersion of resistivity and dielectric constant of some semiconductors at audio frequencies. *Phys. Rev.* 1951; 83(1): 121.

Kumar MM, Srinivas A and Suryanarayana SV. Structure property relations in $BiFeO_3$/$BaTiO_3$ solid solutions. *J. Appl. Phys.* 2000; 87(2): 855-862.

Luo L, Wei W, Yuan X, Shen K, Xu M and Xu Q. Multiferroic properties of Y-doped $BiFeO_3$. *J. Alloys Compd.* 2012; 540: 36-38.

Macdonald JR, Johnson WB, Raistrick ID, Franceschetti DR, Wagner N, McKubre MCH, Macdonald DD, Sayers B, Bonanos N, Steele BCH and Butler EP. *Impedance spectroscopy:*

theory, experiment, and applications. Hoboken, NJ: John Wiley & Sons; 2018. p. 424-458.

Macdonald JR. Impedance spectroscopy. *Ann. Biomed. Eng.* 1992; 20: 289-305.

Maxwell JC. *Electricity and Magnetism, Vol. 2*. New York: Oxford University Press; 1973. p. 828.

Miah MJ, Khan MNI and Hossain AKMA. Synthesis and enhancement of multiferroic properties of (x) $Ba_{0.95}Sr_{0.05}TiO_3$–(1−x) $BiFe_{0.90}Dy_{0.10}O_3$ ceramics. *J. Magn. Magn. Mat.* 2016; 397: 39-50.

Minh NNN, Hue VT, Thu NT, Hien VT, Dung DD and Quan ND. Augmentation of optical and magnetic characteristics at ambient temperature in bismuth ferrite-titanium ($BiFe_{1-x}Ti_xO_3$) multiferroic compounds. *Mater. Res. Express* 2024; 11(4): 045702.

Mukherjee A, Banerjee M, Basu S, Thanh NTK, Green LAW and Pal M. Enhanced magnetic and electrical properties of Y and Mn co-doped BiFeO3 nanoparticles. *Phys. B: Condens. Matter*, 2014; 448:199-203.

Muneeswaran M, Gopiraman M, Dhanabalan SS, Giridharan NV and Akbari-Fakhrabadi A. Multiferroic properties of rare earth-doped $BiFeO_3$ and their spintronic applications. In: *Metal and Metal Oxides for Energy and Electronics*, springer, 2021: pp. 375-395.

Palkar VR, John J and Pinto R. Observation of saturated polarization and dielectric anomaly in magnetoelectric $BiFeO_3$ thin films. *Appl. Phys. Lett.* 2002; 80(9): 1628-1630.

Pattanayak S, Choudhary RNP, Das PR and Shannigrahi SR. Effect of Dy-substitution on structural, electrical and magnetic properties of multiferroic $BiFeO_3$ ceramics. *Ceram. Int.* 2014; 40(6): 7983-7991.

Ramesh R and Spaldin NA. Multiferroics: progress and prospects in thin films. *Nat. Mater.* 2007; 6(1): 21-29.

Scott JF. Applications of modern ferroelectrics. *Science* 2007; 315(5814): 954-959.

Singh AK, Mani AD and Soibam I. Low temperature synthesis and structural, dielectric and optical studies of $Bi_{1-x}Gd_xFeO_3$ (x=0–0.15) nanoceramics. *Integr. Ferroelectrics* 2018; 193(1): 134-141.

Singh H and Yadav KL. Effect of Nb substitution on the structural, dielectric and magnetic properties of multiferroic $BiFe_{1-x}Nb_xO_3$ ceramics. *Mater. Chem. Phys.* 2012; 132(1): 17-21.

Teague JR, Gerson R and James WJ. Dielectric hysteresis in single crystal $BiFeO_3$. *Solid State Commun.* 1970; 8(13): 1073-1074.

Varshney D and Kumar A. Structural, Raman and dielectric behavior in $Bi_{1-x}Sr_xFeO_3$ multiferroic. *J. Mol. Struct.* 2013; 1038: 242-249.

Verma KC. Synthesis and characterization of multiferroic $BiFeO_3$ for data storage. In: *Bismuth-Fundamentals and Optoelectronic Applications*. *Intech Open*, 2020: 94049.

Wang N, Luo X, Han L, Zhang Z, Zhang R, Olin H and Yang Y. Structure, performance, and application of $BiFeO_3$ nanomaterials. *Nano-Micro Lett.* 2020; 12 (1): 81.

Wang YP, Zhou L, Zhang MF, Chen XY, Liu JM and Liu ZG. Room-temperature saturated ferroelectric polarization in $BiFeO_3$ ceramics synthesized by rapid liquid phase sintering. *Appl. Phys. Lett.* 2004; 84(10): 1731-1733.

West AR, Sinclair DC and Hirose N. Characterization of electrical materials, especially ferroelectrics, by impedance spectroscopy. *J. Electroceram.* 1997; 1(1): 65-71.

Wu M, Wang W, Jiao X, Wei G, He L, Han S, Liu Y and Chen D. Structural and multiferroic properties of Pr and Ti co-doped $BiFeO_3$ ceramics. *Ceram. Int.* 2016; 42(13): 14675-14678.

Wu YJ, Chen XK, Zhang J and Chen XJ. Structural transition and enhanced magnetization in $Bi_{1-x}Y_xFeO_3$. *J. Magn. Magn. Mat.* 2012; 324(7): 1348-1352.

Xu JM, Wang GM, Wang HX, Ding DF and He Y. Synthesis and weak ferromagnetism of Dy-doped $BiFeO_3$ powders. *Mater. Lett.* 2009; 63(11): 855-857.

Yin L and Mi W. Progress in $BiFeO_3$- based heterostructures: materials, properties and applications. *Nanoscale* 2020; 12(2): 477-523.

Yu B, Li M, Wang J, Pei L, Guo D and Zhao X. Enhanced electrical properties in multiferroic $BiFeO_3$ ceramics co-doped by La^{3+} and V^{5+}. *J. Phys. D: Appl. Phys.* 2008; 41(18): 185401.

Zatsiupa AA, Bashkirov LA, Troyanchuk IO, Petrov GS, Galyas AI, Lobanovsky LS and Truhanov SV. Magnetization, magnetic susceptibility, effective magnetic moment of Fe^{3+} ions in $Bi_{25}FeO_{39}$ ferrite. *J. Solid State Chem.* 2014; 212: 147-150.

Zhang ST, Zhang Y, Lu MH, Du CL, Chen YF, Liu ZG, Zhu YY, Ming NB and Pan XQ. Substitution-induced phase transition and enhanced multiferroic properties of $Bi_{1-x}La_xFeO_3$ ceramics. *Appl. Phys. Lett.* 2006; 88(16): 162901.

Zhu M, Xie H, Guo J, Bai W and Xu Z. Impedance spectroscopy analysis on electrical properties of serpentine at high pressure and high temperature. *Sci. China Ser. D: Earth Sci.* 2001; 44: 336-345.

J. Bangladesh Acad. Sci. 49(2); 287-293: December 2025 DOI:https://doi.org/10.3329/jbas.v49i2.77709

Journal of Bangladesh Academy of Sciences

Journal homepage: http://www.bas.org.bd/publications/jbas.html

Research Article

Intuitionistic set and its relations

Nasrin Ifnath Nithun, Tahmina Tasnim Trisha*, Md. Sahadat Hossain, Shahriar Kobir and Israt Jahan Swarna

Department of Mathematics, University of Rajshahi, Rajshahi, Bangladesh

ARTICLE INFO

Article History

Received: 28 January 2025
Revised: 07 Jurly 2025
Accepted: 22 December 2025

Keywords: Set, Relation, Intuitionistic set, Intuitionistic function, Intuitionistic relation.

ABSTRACT

We present a brief overview on Intuitionistic sets and its relations which cuts across some definitions, operations, relations and functions on intuitionistic set. In this article, we have shown various operations and their applications using intuitionistic set. We have also seen that relationships can be established using intuitionistic sets, which work similarly to usual relations. Reflexive, Symmetric, Antisymmetric and Transitive relations can be described using intuitionistic set theory, which demonstrated better results than the previous classical set.

Introduction

Since the introduction of intuitionistic sets, numerous researchers have made significant contributions to the field. By exploring various properties of classical sets, they have also introduced new concepts to broaden its generalization.

Intuitionistic set is the generalization of classical set and intuitionistic logic is the generalization of classical logic. Many researchers have worked on intuitionistic set. Atanassov (Atanassov 1986,1988,2001) is one of them who firstly gave the knowledge about it.

After that, many mathematicians also worked on it. Following Zadeh's (Zadeh 1965) introduction of fuzzy sets, classical topological spaces evolved into a new dimension known as "Fuzzy Topological Spaces," as defined by Chang (Chang 1968). Subsequently, Atanassov introduced intuitionistic fuzzy sets, which serve as a generalization of fuzzy sets. Later, Coker (Coker 1996) and colleagues defined intuitionistic fuzzy topological spaces, along with the concepts of intuitionistic sets and intuitionistic topological spaces.

In this paper, we investigate different types of intuitionistic set operations like De Morgan's law, Associative law, Commutative law, Distributive law and relation like Reflexive relation, Symmetric relation, Antisymmetric relation and Transitive relations.

Preliminaries

Brief introduction of intuitionistic sets and relations

Definition (Atanassov, 1986; Islam et. al., 2018): An intuitionistic set A defined on a non-empty set X can be expressed as follows:

An intuitionistic set A takes the form $= (A_1, A_2)$, where:A_1 is a subset of X, representing the members of the intuitionistic set A.$A_2$is a subset of X. representing the non-members of the intuitionistic set A. The defining condition is that.$A_1 \cap A_2 = \emptyset$. This ensures that an element cannot belong to both the members and non-members of A. For the purposes of this discussion, we simplify the notation by using $A = (A_1, A_2)$, omitting X from the expression. This means that the focus is on the classification of elements into members and non-members without explicitly referencing the underlying set X.

Remark (Atanassov, 1986; Prova and Hossain, 2022): Every subset A of a non-empty set X can be considered as an intuitionistic set in the following

*Corresponding author:<roufmollah1970@gmail.com>

way: We define A as an intuitionistic set with the form $A = (A, A^C)$, where: A is the subset itself, representing the members of the intuitionistic set.A^c (the complement of A in X) consists of all elements in X that are not in A, representing the non-members. This means that the intuitionistic set A effectively classifies elements of X into those that belong to A and those that do not. The notation emphasizes the dual nature of A as both a member set and its complement, encapsulating the full structure of the intuitionistic set.

Definition: Universal set is an intuitionistic set which contains all the elements or objects of other intuitionistic sets, including its own elements. It is usually denoted by the symbol "$U_{\sim}$"

$U_{\sim} = (U, \emptyset)$

Where,U is considered as interior point and $\emptyset$ is considered as exterior point.

Definition: Null set is a set which contains no value or element. It is denoted by $\emptyset = (\emptyset, U)$ .Where,$\emptyset$ is considered as interior point and U is considered as exterior point.

Definition: (Bayhan and Coker, 2001; Ahmed et. al., 2014): Null the intuitionistic sets M and N in P be of the forms

$M = (M_1, M_2)$and $N = (N_1, N_2)$ respectively. Furthermore, let $\{M_j, j \in J\}$ be an arbitrary family of intuitionistic sets in P, where $M_j = \left(M_j^{(1)}, M_j^{(2)}\right)$

Then:

a. $M \subseteq N$ if and only if $M_1 \subseteq N_1$ and $M_2 \supseteq N_2$;

b. $M = N$ if and only if $M \subseteq N$ and $N \supseteq M$;

c. $\overline{M} = (M_1, M_2)$ denotes the complement of A;

d. $\cap M_j = \left(\cap M_j^{(1)}, \cup M_j^{(2)}\right)$;

e. $\cup M_j = \left(\cup M_j^{(1)}, \cap M_j^{(2)}\right)$;

f. $\emptyset_{\sim} = (\emptyset, P)$ and $X_{\sim} = (P, \emptyset)$.

Intuitionistic set function and its relation

Definition: A function f is an intuitionistic function if for every $p \in P$, there exists a unique $q \in Q$ such that $f(p) = q$. This means that each element of P is associated with exactly one element of , ensuring the well-defined nature of the function.

Mathematically,$f: P \longrightarrow Q$

If M is an intuitionistic set in P then,

$f(M) = \left(f(M_1), f(M_2) - f(M_1)\right)$

Example 1: $f: R \longrightarrow R$ be a function defined by

$f(x) = x^2 + 3x + 1$

If, M is an intuitionistic set

$M = (\{2,3,8\}, \{1,4,7\})$ then

$f(M_1) = \{11,19,89\}$

$f(M_2) = \{5,29,71\}$

$f(M_2) - f(M_1) = \{5,29,71\}$

$f(M) = (f(M_1), f(M_2) - f(M_1))$

$f(M) = (\{11,19,89\}, \{5,29,71\})$

$f : R \to R$ be a function defined by

$f(x) = x^2$

If N is an intuitionistic set then,

$N = (\{1,2,3\}, \{-1, -3,4\})$

$$f(N_1) = \{1,4,9\}$$

$$f(N_2) = \{1,9,16\}$$

$$f(N_2) - f(N_1) = \{16\}$$

$$f(N) = (f(N_1), f(N_2) - f(N_1))$$

$f(N) = (\{1,4,9\}, \{16\})$

Definition: Intuitionistic relations can represent data mappings where a value in one set is transformed into a value in another set based on defined functions. This is akin to functional programming, where the relationship is constructed through function definitions.

Visualizing the relation as a directed graph can help. Each element in the domain (P) connects to one or more elements in the range (Q), illustrating how relationships are formed based on constructive criteria.

R be an intuitionistic relation from intuitionistic set M to N then $R \subseteq M \times N$

$M \times N = \{(p, q) : p \in M, q \in N\}$

Example 2: Let, $M = (M_1, M_2)$ and $N = (N_1, N_2)$ be two intuitionistic set where,

$$M = (\{1,2\}, \{a, b\})$$

$$N = (\{3,4\}, \{c, d\})$$

Then a relation, $R = (\{(1,4), (2,3)\}, \{(a, d)\})$

Theorem: De-Morgan's Law for intuitionistic set:

$$(M \cap N)^c = M^c \cup N^c$$

Proof:

Let $M = (M_1, M_2)$ and $N = (N_1, N_2)$ be two intuitionistic set then,

$M \cap N = (M_1 \cap N_1, M_2 \cup N_2)$

$$(M \cap N)^C = (M_2 \cup N_2, M_1 \cap N_1)^c$$

Again,

$$M^c = (M_2, M_1) \; and \; N^c = (N_2, N_1)$$

$$M^c \cup N^C = (M_2 \cup N_2, M_1 \cap N_1)$$

$= (M \cap N)^C$ (proved)

Theorem: Commutative law for intuitionistic set:

For all intuitionistic sets M, N

$M = (M_1, \; M_2)$

$N = (N_1, \; N_2)$

$M \cup N = N \cup M$ and

$M \cap N = N \cap M$

Proof:

For interior points p_1 and q_1,

$Let, p_1 \in (M_1 \cup N_1)$

$\Rightarrow p_1 \in M_1$ or $p_1 \in N_1$

$\Rightarrow p_1 \in N_1$ or $p_1 \in M_1$

$\Rightarrow p_1 \in (N_1 \cup M_1)$

$\therefore (M_1 \cup N_1) \subseteq (N_1 \cup M_1)$

Again let,$q_1 \in (N_1 \cup M_1)$

$\Rightarrow q_1 \in N_1 \; or \; q_1 \in M_1$

$\Rightarrow q_1 \in M_1 \; or \; q_1 \in N_1$

$\Rightarrow q_1 \in (M_1 \cup N_1)$

$\therefore (N_1 \cup M_1) \subseteq (M_1 \cup N_1)$

$(M_1 \cup N_1) = (N_1 \cup M_1)$

For exterior points p_2 and q_2,

Let, $p_2 \in (M_2 \cap N_2)$

$\Rightarrow p_2 \in M_2 \; and \; p_2 \in N_2$

$\Rightarrow p_2 \in N_2 \; and \; p_2 \in M_2$

$\Rightarrow p_2 \in (N_2 \cap M_2)$

$\therefore (M_2 \cap N_2) \subseteq (N_2 \cap M_2)$

Again let,$q_2 \in (N_2 \cap M_2)$

$\Rightarrow q_2 \in N_2 \; and \; q_2 \in M_2$

$\Rightarrow q_2 \in M_2 \; and \; q_2 \in N_2$

$\Rightarrow q_2 \in (M_2 \cap N_2)$

$\therefore (N_2 \cap M_2) \subseteq (M_2 \cap N_2)$

$(M_2 \cap N_2) = (N_2 \cap M_2)$

Hence, $(M \cup N) = (N \cup M)$ (proved)

Similarly,$(M \cap N) = (N \cap M)$

Theorem: Associative Law for intuitionistic set:

For all intuitionistic sets M, N, O

$M = (M_1, M_2)$

$N = (N_1, N_2)$

$O = (O_1, O_2)$

$(M \cup N) \cup O = M \cup (N \cup O)$ and

$(M \cap N) \cap O = M \cap (N \cap O)$

Proof:

For interior points x_1 and y_1,

Let, $p_1 \in (M_1 \cup N_1) \cup O_1$

$\Rightarrow p_1 \in (M_1 \cup N_1) \; or \; p_1 \in O_1$

$\Rightarrow p_1 \in M_1 \; or \; p_1 \in N_1 \; or \; p_1 \in O_1$

$\Rightarrow p_1 \in M_1 \; or \; p_1 \in (N_1 \cup O_1)$

$\Rightarrow p_1 \in M_1 \cup (N_1 \cup O_1)$

$\therefore (M_1 \cup N_1) \cup O_1 \subseteq M_1 \cup (N_1 \cup O_1)$

Again let,$q_1 \in M_1 \cup (N_1 \cup O_1)$

$\Rightarrow q_1 \in M_1 \; or \; q_1 \in (N_1 \cup O_1)$

$\Rightarrow q_1 \in M_1 \; or \; q_1 \in N_1 \; or \; q_1 \in O_1$

$\Rightarrow q_1 \in (M_1 \cup N_1) \; or \; q_1 \in O_1$

$\Rightarrow q_1 \in (M_1 \cup N_1) \cup O_1$

$\therefore M_1 \cup (N_1 \cup O_1) \subseteq (M_1 \cup N_1) \cup O_1$

$(M_1 \cup N_1) \cup O_1 = M_1 \cup (N_1 \cup O_1)$

For exterior points p_2 and q_2,

Let,$p_2 \in (M_2 \cap N_2) \cap O_2$

$\Rightarrow p_2 \in (M_2 \cap N_2)$ and $P_2 \in O_2$

$\Rightarrow p_2 \in M_2$ and $p_2 \in N_2$ and $p_2 \in O_2$

$\Rightarrow p_2 \in M_2$ and $p_2 \in (N_2 \cap O_2)$

$\Rightarrow p_2 \in M_2 \cap (N_2 \cap O_2)$

$\therefore (M_2 \cap N_2) \cap O_2 \subseteq M_2 \cap (N_2 \cap O_2)$

Again let, $q_2 \in M_2 \cap (N_2 \cap O_2)$

$\Rightarrow q_2 \in M_2$ and $q_2 \in (N_2 \cap O_2)$

$\Rightarrow q_2 \in M_2$ and $q_2 \in N_2$ and $q_2 \in O_2$

$\Rightarrow q_2 \in (M_2 \cap N_2)$ and $q_2 \in O_2$

$\Rightarrow q_2 \in (M_2 \cap N_2) \cap O_2$

$\therefore M_2 \cap (N_2 \cap O_2) \subseteq (M_2 \cap N_2) \cap O_2$

$(M_2 \cap N_2) \cap O_2 = M_2 \cap (N_2 \cap O_2)$

Hence,$(M \cup N) \cup O = M \cup (N \cup O)$ (proved)

Similarly,$(M \cap N) \cap O = M \cap (N \cap O)$

Theorem: Distributive law for intuitionistic set:

For all intuitionistic sets M , N , O

$M = (M_1 , M_2)$, $N = (N_1 , N_2)$

$O = (O_1 , O_2)$

$M \cap (N \cup O) = (M \cap N) \cup (M \cap O)$and

$M \cup (N \cap O) = (M \cup N) \cap (M \cup O)$

Proof:

For interior points p_1 and q_1,

Let,$p_1 \in M_1 \cap (N_1 \cup O_1)$

$\Rightarrow p_1 \in M_1$ and $p_1 \in (N_1 \cup O_1)$

$\Rightarrow p_1 \in M_1$ and $(p_1 \in N_1 \; or \; p_1 \in O_1)$

$\Rightarrow (p_1 \in M_1$ and $p_1 \in N_1)$ or $(p_1 \in M_1$ and $p_1 \in O_1)$

$\Rightarrow p_1 \in (M_1 \cap N_1) \cup (M_1 \cap O_1)$

$\therefore M_1 \cap (N_1 \cup O_1) \subseteq (M_1 \cap N_1) \cup (M_1 \cap O_1)$

Again let,$q_1 \in (M_1 \cap N_1) \cup (M_1 \cap O_1)$

$\Rightarrow (q_1 \in M_1$ and $q_1 \in N_1)$ or $(q_1 \in M_1$ and $q_1 \in O_1)$

$\Rightarrow q_1 \in M_1$ and $(q_1 \in N_1$ or $q_1 \in O_1)$

$\Rightarrow q_1 \in M_1$ and $q_1 \in (N_1 \cup O_1)$

$\Rightarrow q_1 \in M_1 \cap (N_1 \cup O_1)$

$\therefore (M_1 \cap N_1) \cup (M_1 \cap O_1) \subseteq M_1 \cap (N_1 \cup O_1)$

$M_1 \cap (N_1 \cup O_1) = (M_1 \cap N_1) \cup (M_1 \cap O_1)$

For exterior points p_2 and q_2 ,

Let,$p_2 \in M_2 \cup (N_2 \cap O_2)$

$\Rightarrow p_2 \in M_2$ or $p_2 \in (N_2 \cap O_2)$

$\Rightarrow p_2 \in M_2$ or $(p_2 \in N_2 \; and \; p_2 \in O_2)$

$\Rightarrow (p_2 \in M_2$ or $p_2 \in N_2)$ and $(p_2 \in M_2$ or $p_2 \in O_2)$

$\Rightarrow p_2 \in (M_2 \cup N_2) \cap (M_2 \cup O_2)$

$\therefore M_2 \cup (N_2 \cap O_2) \subseteq (M_2 \cup N_2) \cap (M_2 \cup O_2)$

Let,$q_2 \in (M_2 \cup N_2) \cap (M_2 \cup O_2)$

$\Rightarrow (q_2 \in M_2 \; or \; q_2 \in N_2) \; and \; (q_2 \in M_2 \; or \; q_2 \in O_2)$

$\Rightarrow q_2 \in M_2$ or $(q_2 \in N_2 \; and \; q_2 \in O_2)$

$\Rightarrow q_2 \in M_2$ or $q_2 \in (N_2 \cap O_2)$

$\Rightarrow q_2 \in M_2 \cup (N_2 \cap O_2)$

$\therefore (M_2 \cup N_2) \cap (M_2 \cup O_2) \subseteq M_2 \cup (N_2 \cap O_2)$

$M_2 \cup (N_2 \cap O_2) = (M_2 \cup N_2) \cap (M_2 \cup O_2)$

Hence,

$M \cap (N \cup O) = (M \cap N) \cup (M \cap O)$ (proved)

Similarly,$M \cup (N \cap O) = (M \cup N) \cap (M \cup O)$

Concept of domain and range of intuitionistic function:

Let, $M = (M_1 , M_2) , N = (N_1 , N_2)$ be two intuitionistic sets where, M_1 and N_1 are interior point and M_2 , N_2 are exterior point of the set M and N respectively.

Let, $R = (R_1, R_2)$ be a relation from intuitionistic set M to N is defined as a subset of $M \times N = (M_1 \times N_1, M_2 \times N_2)$.

Example 3:

Let, M and N be two intuitionistic sets where $M = (\{1,2,3\}, \{5,6\})$ and $N = (\{p, q, r\}, \{a, b, c\})$. Here, $M_1 = \{1,2,3\}$, $M_2 = \{5,6\}$, $N_1 = \{p, q, r\}$, $N_2 = \{a, b, c\}$.

Let,$R = (R_1, R_2) \subseteq (M \times N) = (M_1 \times N_1, M_2 \times N_2)$ where, $R = (\{(1, p), (3, p), (3, r)\}, \{(5, b), (5, c)\})$.

When the exterior point is fixed:

Domain of $R = (I_1 , M_2) \subseteq (M_1 , M_2)$

where, $I_1 = \{i_1 \in M_1 : \exists\, j_1 \in N_1 \; and \; (i_1, j_1) \in R_1\}$

Range of $R = (J_1, N_2) \subseteq (N_1, N_2)$

where, $J_1 = \{j_1 \in N_1 : \exists\, i_1 \in M_1 \; and \; (i_1, j_1) \in R_1\}$

$$I_1 = \{1,3\}$$

$$D_R = (\{1,3\}, \{5,6\})$$

$$J_1 = \{p, r\}$$

$$R_R = (\{p, r\}, \{a, b, c\})$$

When interior point is fixed:

Domain of $R = (M_1, I_2) \subseteq (M_1, M_2)$

where, $I_2 = \{i_2 \in M_2 : \exists\, j_2 \in N_2 \; and \; (i_2, j_2) \in R_2\}$

Range of $R = (N_1, J_2) \subseteq (N_1, N_2)$

$J_2 = \{j_2 \in N_2 : \exists\, i_2 \in M_2 \; and \; (i_2, j_2) \in R_2\}$

$$I_2 = \{5\}$$

$$D_R = (\{1,2,3\}, \{5\})$$

$$J_2 = \{b, c\}$$

$$R_R = (\{p, q, r\}, \{b, c\})$$

When interior and exterior both are changeable:

Domain of $R = (I_1, I_2) \subseteq (M_1, M_2)$

where, $I_1 = \{i_1 \in M_1 : \exists\, j_1 \in N_1 \; and \; (i_1, j_1) \in R_1\}$

$I_2 = \{i_2 \in M_2 : \exists\, j_2 \in N_2 \; and \; (i_2, j_2) \in R_2\}$

Range of $R = (J_1, J_2) \subseteq (N_1, N_2)$

where, $J_1 = \{j_1 \in N_1 : \exists\, i_1 \in M_1 \; and \; (i_1, j_1) \in R_1\}$

$J_2 = \{j_2 \in N_2 : \exists\, i_2 \in M_2 \; and \; (i_2, j_2) \in R_2\}$

$$I_1 = \{1,3\}$$

$$I_2 = \{5\}$$

$$D_R = (\{1,3\}, \{5\})$$

$$J_1 = \{p, r\}$$

$$J_2 = \{b, c\}$$

$$R_R = (\{p, r\}, \{b, c\})$$

Intuitionistic relations

Definition: Here we define four types of special intuitionistic relations. Such as Reflexive, Symmetric, Anti-symmetric, Transitive

Interior Point (M_1): This is a point within the set M where you can find a neighbourhood around M_1 that is completely contained in M.

Exterior Point (M_2): This is a point outside the set M such that you can find a neighbourhood around M_2 that does not intersect .

$$R \subseteq M \times M$$

$$R = (R_1, R_2) \subseteq (M_1 \times M_1 \,,\, M_2 \times M_2)$$

Reflexive Relation

Let $R = (R_1, R_2)$ be a binary relation on a set $M = (M_1, M_2)$ which can be define as $(R_1, R_2) \subseteq (M_1 \times M_1, M_2 \times M_2)$.Then the relation$(R_1, R_2)$ is called strongly reflexive if $(a, a) \in R_1 \,, \forall\, a \in M_1$ and $(b, b) \notin R_2 \,, \forall\, b \in M_2$

And for weakly reflexive $(a, a) \in R_1, \forall\, a \in M_1$

Example 4: Let, $M = (M_1, M_2) = (\{a, b\}, \{x, y, z\})$ be an intuitionistic set and $R = (R_1, R_2) = (\{(a, a), (a, b), (b, b)\}, \{(x, x), (x, y), (x, z)\})$ be a relation on the set M.

The relation is weakly reflexive since $(a, a), (b, b) \in R_1, \forall\, a, b \in M_1$.But it is not strongly reflexive since $(x, x) \in R_1, \forall\, x \in M_2$

Another relation $R = (\{(a, a), (a, b), (b, b)\}, \{(x, y), (x, z)\})$ is defined on the set M.The relation is strongly and weakly reflexive relation since $(a, a), (b, b) \in R_1, \forall\, a, b \in M_1$ and $(x, x), (y, y), (z, z) \notin R_2, \forall\, x, y, z \in M_2$

Symmetric relation

Let, (R_1, R_2) be a subset of $(M_1 \times M_1, M_2 \times M_2)$ i.e. $R = (R_1, R_2)$ be a relation on an intuitionistic set $M = (M_1, M_2)$.Then the relation R is called a strongly symmetric relation if

$$(a_1, b_1) \in R_1 \Rightarrow (b_1, a_1) \in R_1$$

$$(a_2, b_2) \in R_2 \Rightarrow (b_2, a_2) \notin R_2$$

On the contrary, the symmetric relation is called weakly symmetric relation if it satisfies the condition,

$$(a_1, b_1) \in R_1 \Rightarrow (b_1, a_1) \in R_1$$

Example 5: Let, $M = (M_1, M_2) = (\{a, b\}, \{x, y\})$ be an intuitionistic set and $R = (R_1, R_2) = (\{(a, a), (a, b), (b, a)\}, \{(x, y)\})$ be a relation on the set M.The relation is strongly and weakly symmetric relation since $(a, a), (a, b), (b, a) \in R_1$ and $(x, y) \in R_2$ but $(y, x) \notin R_2$.

Another relation $R = (R_1, R_2) = (\{(a, a), (a, b), (b, a)\}, \{(x, y), (y, x)\})$ is defined on the set M.It is weakly symmetric relation since $(a, a), (a, b), (b, a) \in R_1$.But it is not strongly symmetric relation since $(y, x) \in R_2$.

Anti-symmetric relation

Let, (R_1, R_2) be a relation on an intuitionistic set (M_1, M_2) i.e. (R_1, R_2) be a subset of $(M_1 \times M_1, M_2 \times M_2)$.Then the relation$(R_1, R_2)$ is called a strongly anti-symmetric relation if

$(a_1, b_1) \in R_1$ and $(b_1, a_1) \in R_1 \Rightarrow a_1 = b_1$

$(a_2, b_2) \in R_2$ *and* $(b_2, a_2) \in R_2 \Rightarrow a_2 \neq b_2$

On the contrary, it is called a weakly anti-symmetric relation if it satisfies the condition,

$(a_1, b_1) \in R_1$ and $(b_1, a_1) \in R_1 \Rightarrow a_1 = b_1$

Example 6: Let, $M = (M_1, M_2) = (\{1,2\}, \{b, c\})$ be an intuitionistic set and $R = (R_1, R_2) = (\{(1,1), (1,2), (2,2)\}, \{(b, c), (c, b)\})$ be a relation on the set M.The relation is strongly and weakly anti-symmetric relation since $(1,1), (2,2) \in R_1$ *and* $1 = 1$ *and* $2 = 2$ and $(b, c), (c, b) \in R_2$ but $b \neq c$.

Another relation $R = (R_1, R_2) = (\{(1,1), (1,2), (2,2)\}, \{(b, b), (c, c)\})$ is defined on the set M.It is weakly anti-symmetric relation since $(1,1), (2,2) \in R_1$ *and* $1 = 1$ *and* $2 = 2$. But it is not strongly anti-symmetric relation since $(b, b), (c, c) \in R_1$ *because* $b = b$ *and* $c = c$.

Transitive relation

Let, $R = (R_1, R_2)$ be a relation on an intuitionistic set $M = (M_1, M_2)$ i.e. $R = (R_1, R_2)$ be a subset of $(M_1 \times M_1, M_2 \times M_2)$.The relation (R_1, R_2) is called a strongly transitive relation if

$(a_1, b_1) \in R_1$ and $(b_1, c_1) \in R_1 \Rightarrow (a_1, c_1) \in R_1$

$(a_2, b_2) \in R_2$ *and* $(b_2, c_2) \in R_2 \Rightarrow (a_2, c_2) \notin R_2$

On the other hand, it is called a weakly transitive relation if it satisfies the condition,

$(a_1, b_1) \in R_1$ and $(b_1, c_1) \in R_1 \Rightarrow (a_1, c_1) \in R_1$

Example 7: Let, $M = (M_1, M_2) = (\{5,6,7\}, \{p, q, r\})$ be an intuitionistic set and $R = (R_1, R_2) = (\{(5,6), (5,7), (6,7)\}, \{(p, q), (q, r)\})$ be a relation on the set M.The relation is strongly and weakly transitive relation since $(5,6), (6,7) \in R_1$ *and* $(5,7) \in R_1$ and $(p, q), (q, r) \in R_2$ but $(p, r) \notin R_2$.

Another relation $R = (R_1, R_2) = (\{(5,6), (5,7), (6,7)\}, \{(p, q), (p, r), (q, r)\})$ is defined on the set M.It is weakly transitive relation since $(5,6), (5,7), (6,7) \in R_1$.But it is not strongly transitive relation since $(p, q), (p, r), (q, r) \in R_2$.

Acknowledgment

The authors express their sincere gratitude to the respected supervisor, Dr. Md. Sahadat Hossain sir, for his valuable guidance, insightful suggestions and continuous support throughout this work.We also acknowledge the foundational contributions of researchers in intuitionistic set theory that informed this study, as well as institutional resources that facilitated its completion.Finally,we thank the reviewers for their constructive feedback which enhanced the quality of this manuscript.

Authors contribution

All authors contributed equally to the collection of relevant information, interpretation of the data and preparation of the manuscript.

Conflict of interest

The authors declare that there is no financial or personal relationships that could have influenced the work reported in this paper.

References

Ahmed E, Hossain MS and Ali MM. On intuitionistic fuzzy T_0- spaces. *J. Bangladesh Acad. Sci.* 2014; 38(2): 197-207.

Atanassov KT. Intuitionistic fuzzy sets. *Fuzzy Sets Syst.* 1986; 20: 87-96.

Atanassov KT. On four intuitionistic fuzzy topological operators. *Math-ware Soft Comput.* 2001; 8: 65-70.

Atanassov KT. Review and new results on intuitionistic fuzzy sets. *Preprint IM-MFAIS*-1. 1988; 88: 1-8, Sofia.

Bayhan S and Coker D. On Separation axioms in intuitionistic topological space. *Int. J. Math. Sci.* 2001; 27(10): 621-630.

Chang CL. Fuzzy topological space. *J. Math. Anal. Appl*. 1968; 24: 182-190.

Coker D. A note on intuitionistic sets and intuitionistic points. *Tu J. Math*. 1996; 20(3): 343-351.

Islam MS, Hossain MS and Asaduzzaman M. Level separation on intuitionistic fuzzyT_1 spaces. *J. Bangladesh Acad. Sci*. 2018; 42: 73-85.

Prova TT and Hossain MS. Separation axioms in intuitionistic topological spaces. *Italian J. of Pure and Applied Mathematics*. 2022; 48: 986-995.

Zadeh LA. Fuzzy Sets. *Information and Control*. 1965; 8: 338-353..

J. Bangladesh Acad. Sci. 49(2); 295-298: December 2025 DOI:https://doi.org/10.3329/jbas.v49i2.75551

Journal of Bangladesh Academy of Sciences

Journal homepage: http://www.bas.org.bd/publications/jbas.html

Short Communication

Effect of antidepressant drug Flupentixol-Melitracen on locomotory behaviors of *Drosophila*

Azizul Islam Barkat, Rabeya Bosri Mehe Jabin, Farhin Momtaz Riana, Sumaiya Akter, Md Shamsudduha and Mohammad Shamimul Alam*

Genetics and Molecular Biology branch, Department of Zoology, University of Dhaka, Dhaka, Bangladesh

ARTICLE INFO

Article History

Received: 20 August 2024
Revised: 17 February 2025
Accepted: 08 May 2025

Keywords: Depression, Fruit fly, Crawling, Negative geotaxis, Behavioral assays, Motor function, Gene expression.

ABSTRACT

Antidepressant drugs are frequently used in the treatment of depression. Their effects on locomotory behavior have been poorly studied in human and *Drosophila* models. In this study, the effects of an antidepressant drug on larval crawling, negative geotaxis, and TOR gene expression were investigated in a *Drosophila* model. Drug-treated flies showed significantly higher activity in the negative geotaxis assay. However, no statistically significant differences were observed in the other behavioral assays or in TOR gene expression.

Introduction

Depression, a mental disorder, is characterized by despair, pessimism, and a loss of interest in once-enjoyed pursuits. The prevalence of depression is increasing worldwide (Liu et al., 2020). The combination of flupentixol (0.5 mg) and melitracen (10 mg) drug is widely used as an antidepressant to treat clinical depression. Flupentixol acts as an inhibitor of D2 receptors, limiting dopamine activity in the brain, while melitracen blocks the reuptake of serotonin and norepinephrine at presynaptic terminals in neurons (Wang et al., 2015). The pathophysiology of depression might be influenced by the dysregulated TOR (Target of Rapamycin) pathway. It is found that the antidepressant increases the expression of the TOR gene, suggesting its involvement in regulating the TOR pathway (Réus et al., 2015). Antidepressant drugs have been associated with movement disorders (Revet et al., 2020). Therefore, it has the potential to disrupt motor function. *Drosophila* is regularly used to study motor function through larval crawling and negative geotaxis tests. The negative geotaxis assay utilizes the innate escape response of flies to move against gravity when agitated (Ali et al., 2011). Although Flupentixol-Melitracen is widely prescribed, its role in motor function remains poorly studied. In this study, we investigated the effects of antidepressant drugs on larval crawling, negative geotaxis, and TOR gene expression in the *Drosophila* model.

Wild fruit flies were collected from the local environment and reared on a standard food medium at 25°C under a 12:12 light:dark photoperiod. Morphological and molecular analyses (NCBI accession no. PQ198554) confirmed the species as *Drosophila ananassae*. The flies were then grouped into control and treatment. The control group was reared in standard food, while the treatment flies were cultured in drug-treated food. The antidepressant drug Frenxit (Beximco Pharmaceuticals Ltd., Bangladesh), was added to the treatment food following a previous study (Kruger and Denton, 2020). The dose applied in this experiment was 400 mg/L food, which is the LC_{50} (Lethal Concentration 50%) of the drug for the fly (Riana, 2024).

*Corresponding author:<shamimul@du.ac.bd>

For the larval crawling assay, the 3rd instar larvae from the two groups were gently transferred from the vials and washed off the food material from their bodies using a 5% sugar solution. A 2% agar plate was prepared to provide a smooth surface for crawling, and the larva was placed in the center. The agar plate was placed on a grid (1x1 cm) of paper (Fig.1), and a video camera was placed above the plate. One larva was placed on the agar plate at a time, and a 30-seconds video was recorded. For both groups, ten videos were taken (10 biological replicates). Three data types were taken for the crawling assay: bending, turning, and distance. A larva was regarded as turning when it moved less than 30 degrees and bending when it moved more than 30 degrees. The distance was determined by the number of grids it passed.

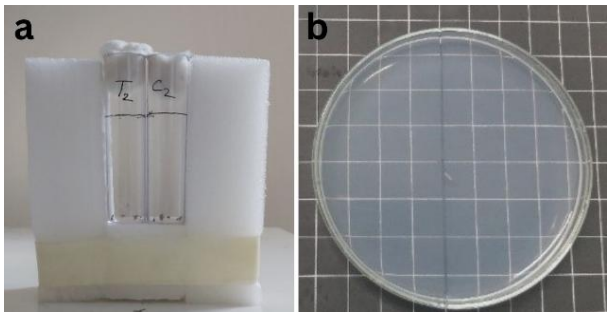

Fig. 1. *Drosophila* behavioral assay setup. a) Negative geotaxis: the number of flies crossed the mark from the bottom was observed. b) Larval crawling assay: an individual larva is dropped at the center of the plate to observe and image the locomotion.

To conduct the negative geotaxis assay, adult virgin flies were collected via cold anaesthetization on the day of emergence before they fully developed to mate. The assay was performed 1 hour after anaesthetization to ensure the flies had fully recovered from the anesthesia stress. The flies were sorted into control and treatment groups, with 10 flies per vial. Two vials for the two groups were marked at a vertical distance of 6 cm from the bottom (Fig. 1). The flies were tapped down, and the number of flies that climbed above the mark by 10 seconds was counted. The assay was repeated ten times, and the number of flies passing the mark was recorded as a percentage of the total number of flies.

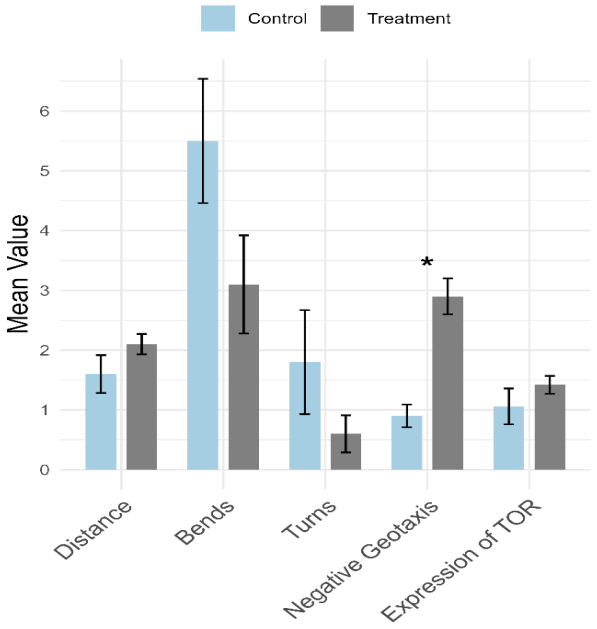

Fig. 2. Effect of antidepressant on *Drosophila*'s behavioral phenotypes and gene expression. Only the negative geotaxis behavior was statistically significant (p=0.0001) between the control and treatment flies. The other behavioral assays, i.e. distance, bends, turns and gene expression levels, were not statistically significant difference (p<0.05).

To measure TOR gene expression, a dye-based qPCR was used. After RNA extraction (Tiangen, China) from 10 3rd - instar larvae of *Drosophila melanogaster* Hikon-H strain, cDNA was synthesized according to the manufacturer's instructions (ABclonal, USA). Three biological replicates were used from each group, and each reaction was run in triplicate in qPCR. The total reaction cycle was 35 with the thermal conditions of denaturation at 95°C for 30 s, annealing at 60°C for 30 s, and extension at 60°C for 20 s. The RPL11 (Ribosomal Protein Loci 11) was taken as a housekeeping gene. The sequence of the primer was 5´-ACTTCGGTTTCGGCATCCA-3' (forward) and 5'- TTGCGCTTCCTGTGGTTCA-3' (reverse). The sequences of primers for the amplification of the TOR gene used in this study were 5´-CGAAAGCGTGATGCTGGTG-3' (forward) and 5'-

TTGCACTTGACCCGCTTGAT-3' (reverse). The $2^{-\Delta\Delta CT}$ Method was followed to analyze the expression of the targeted gene (Livak and Schmittgen, 2001).

To identify the significant differences between the groups, the t-test was used in this study. All the statistical analyses were conducted in excel and the graph was produced in R.

The larvae in both groups showed no significant difference in the larval crawling assay. The average distance the drug-treated and control group larvae crossed was 2.10 and 1.562 cm, respectively (p=0.1907). The average number of bends and turns in the control and treatment groups were 5.5 and 3.1 (p=0.086) and 1.8 and 0.6 (p=0.21) (Fig. 2).

Significant differences in the negative geotaxis assay were observed between the groups. The average number of individuals (n=10) crossing the '6 cm' mark in 10 seconds was 0.9 (9%) in the control group and 2.9 (29%) in the treatment group. The p-value is 0.0001. The flies of the treatment group exhibited a greater capacity to respond to a stimulus than those of the control group.

The TOR gene was expressed slightly higher in the treatment group. TOR The expression was 1.42- and 1.06-fold higher in the treatment and control groups, respectively. Though the expression of TOR was higher in treatment, it was not statistically significant (p=0.722) (Fig. 2).

According to this study, antidepressant drugs cause changes in the negative geotaxis behavior of *Drosophila*. The drug-treated flies show high locomotion activity. The TOR gene was expressed at a higher level in the treatment group's larvae, though the difference was not statistically significant. When the TOR gene is downregulated, behavioral deficits are observed (Potter et al., 2019). Based on the present findings, we hypothesize that higher expression of the TOR gene may potentially enhance geotaxis activity. However, the current study, with its small sample size, is not sufficient to establish a definitive hypothesis. Further study is required to analyze the expression pattern of TOR in drug-treated pupae and adult fruit flies with a large sample size.

Acknowledgment

We gratefully acknowledge the financial support of the University Grants Commission of Bangladesh (Biological Science, 2020-21).

Authors contribution

Azizul Islam Barkat: concept development, laboratory activities, manuscript preparation, review and editing; Rabeya Bosri Mehe Jabin: concept development, laboratory activities; Farhin Momtaz Riana: concept development, laboratory activities; Sumaiya Akter: laboratory activities, manuscript preparation; Md Shamsudduha: laboratory activities, manuscript preparation; Mohammad Shamimul Alam: concept development, review and editing, fund acquisition.

Conflict of interest

There is no conflict of interest regarding the publication.

References

Ali Y, Escala W, Ruana K and Zhai RG. Assaying locomotor, learning, and memory deficits in *Drosophila* models of neurodegeneration. *J. Vis. Exp*. 2011; 49: 2504.

Kruger L and Denton TT. A standardized method for incorporation of drugs into food for use with *Drosophila melanogaster*. *Anal. Biochem*. 2020: 599:113740.

Liu Q, He H, Yang J, Feng X, Zhao F and Lyu J. Changes in the global burden of depression from 1990 to 2017: Findings from the global burden of disease study. *J. Psychiatr. Res*. 2020; 126: 134-140.

Livak KJ and Schmittgen TD. Analysis of relative gene expression data using real-time quantitative PCR and the 2−ΔΔCT method. *Methods*, 2001; 25: 402-408.

Potter S, Sifers J, Yocom E, Blümich SLE, Potter R, Nadolski J, Harrison DA and Cooper RL. Effects of inhibiting mTOR with rapamycin on behavior, development, neuromuscular physiology, and cardiac function in larval Drosophila. *Biol. Open*. 2019; 8(11): bio046508.

Réus GZ, Quevedo J and Rodrigues ALS. mTOR signaling in the neuropathophysiology of depression: Current evidence. *J. Recept. Ligand Channel Res*. 2015; 8: 65-74.

Revet A, Montastruc J, Roussin A, Raynaud J, Lapeyre-Mestre M and Nguyen THO. Antidepressants and movement disorders: a postmarketing study in the world pharmacovigilance database. *BMC Psychiatry*, 2020; 20(1): 308.

Riana FM. *Effect of Antidepressant-Antipsychotic Drug Combination on Motor Function and Semaphorin-2a Gene Expression in Drosophila ananassae*. M.S. Thesis, Department of Zoology, University of Dhaka. 2024.

Wang L, Zhong Z, Hu J, Rong X, Liu J, Xiao S and Liu Z. Sertraline plus deanxit to treat patients with depression and anxiety in chronic somatic diseases: A randomized controlled trial. *BMC Psychiatry*, 2015; 15: 84.

J. Bangladesh Acad. Sci. 49(2); 299-301: December 2025 DOI:https://doi.org/10.3329/jbas.v49i2.82215

Journal of Bangladesh Academy of Sciences

Journal homepage: http://www.bas.org.bd/publications/jbas.html

Short Communication

Amphibian predation by *Lyroderma lyra* (Family: Megadermatidae) in Bangladesh highlights an expanded trophic role

Md Rifat Hasan*, Akash Mojumdar[1], Md. Sabbir Ahammed[2]

Department of Zoology, Govt. Azizul Haque College, National University, Gazipur, Bangladesh

ARTICLE INFO

Article History

Received: 15 June 2025
Revised: 01 September 2025
Accepted: 21 September 2025

Keywords: Bat, *Lyroderma lyra*, Intraguild predation, Trophic level, Bangladesh.

ABSTRACT

We documented amphibian predation by the greater false vampire bat (*Lyroderma lyra*) in Bangladesh, expanding current knowledge of its trophic ecology. This observation highlights the ecological role of this species as both an insectivore and a carnivore, and underscores the need to investigate the frequency and ecological drivers of such predatory behavior.

Introduction

Intraguild predation represents a complex ecological interaction that expands the vertical niche breadth of consumer species, thereby enhancing trophic connectivity and contributing to greater food web complexity (Wang et al., 2019). In terrestrial ecosystems, bats and frogs occupy the same trophic guild and play complementary roles in suppressing arthropod populations (Kunz et al., 2011; Wells, 2007). The greater false vampire bat, *Lyroderma lyra* (family Megadermatidae), previously documented as *Megaderma lyra* (Feng et al., 2024), can be identified by its straight, horizontally rounded noseleaf and body size (Srinivasulu et al., 2010). It is distinct from the closely related *Megaderma spasma* (family: Megadermatidae), with a smaller body size and a short, heart-shaped noseleaf base (Srinivasulu et al., 2010), allowing its identification from the photographs.

The greater false vampire bat (*Lyroderma lyra*, family: Megadermatidae) exhibits a notably broad dietary niche, consuming a wide range of small vertebrates, including birds, rodents, and lizards, in addition to insects (Aitken, 1907; Gleadow, 1907; Mossea, 1931). This trophic generalism, coupled with its use of diverse roosting sites, particularly anthropogenic structures such as buildings, underscores its ecological adaptability and potential resilience in human-modified environments.

Despite this ecological flexibility, the feeding ecology of *L. lyra* remains poorly studied, and no data exist from Bangladesh. Bat research in the country has historically focused on zoonotic disease surveillance, with limited attention to natural history (Ul Hasan and Kingston, 2022). As a result, the ecological roles of predatory bats, such as *L. lyra*, especially in fragmented and human-dominated landscapes, remain poorly understood. In this study, we document an ecological observation of *L. lyra* predation on an amphibian in the Madhutila forest range of north-central Bangladesh.

During our amphibian survey on 31 August 2024 in Madhutila Eco-Park under Madhutila forest range in Bangladesh, we observed a *Lyroderma lyra* flying from the edge of a lake and carrying an Indian bullfrog (*Hoplobatrachus tigerinus*) in its mouth (25°12'20"; 90°8'57"). We followed the bat while it

*Corresponding author:<rifat.hasan2898@gimail.com>

[1]*Department of Computer Science and Information Technology, Shanto-Mariam University of Creative Technology, Dhaka, Bangladesh;* [2]*Department of Zoology, Jagannath University, Dhaka, Bangladesh*

flew approximately 50 meters and entered a nearby tin shed, an abandoned building (Fig. 2). We observed that the bat was hanging from an iron-made rod affixed to the ceiling inside the house. It was continuously chewing the frog's head for approximately 10 minutes (18:55 h to 19:07 h) (Fig. 1). After 12 minutes of irregular chewing (19:19 h), we observed that the bat consumed the frog's head part entirely and then left the place with the frog's body in its mouth and relocated to a nearby (~10 meters from the building) *Ficus indica* tree. We were unable totrack the bats or the frogs later.

This observation broadens our understanding of the trophic ecology of *Lyroderma lyra*, emphasizing its role as both an insectivore and a carnivore. Determining the drivers and frequency of such carnivorous behavior is key to assessing *Lyroderma lyra*'s ecological role and adaptability in changing landscapes.

Fig. 1. *Lyroderma lyra* is holding the head of an Indian Bullfrog (*Hoplobatrachus tigerinus*).

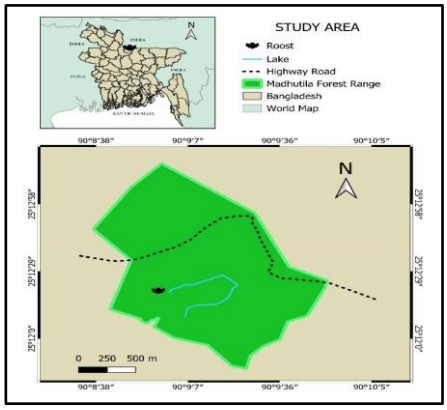

Fig. 2. The map shows the roosting locations of *Lyroderma lyra*. A predation event involving this bat was observed near Lakeshore, within the Madhutila forest range.

Acknowledgment

We sincerely thank Md Ashraf Ul Hasan for his valuable feedback on the manuscript. We gratefully acknowledge the guidance of Sabit Hasan on the project, the support of the Chair of the Department of Zoology, Govt. Azizul Haque College, and the Isabela Foundation for organizational support. We also thank the Bangladesh Forest Department for providing us with the required permission (Permit No: 22.01.0000.101.23.018.23.1260) to conduct the study. Heartfelt appreciation to the volunteers and our local guide for their support. This study was conducted as part of a project funded by SAVE THE FROGS! (California, USA), whose support we deeply appreciate.

Authors contribution

Md Rifat Hasan: Conceptualization, investigation, original draft and project administration. Akash Mojumdar: Conceptualization, review, editing and visualization. Md. Sabbir Ahammed: Review and editing.

Conflicts interest

The authors declare that there are no potential conflicts of interest regarding the publication of this article.

References

Aitken H. Do bats eat birds. *J. Bombay Nat. Hist. Soc.* 1907; 18: 190.

Feng L, Győrössy D, Miguez RP, Kokkini P, Görföl T, Khan SA, Saikia U, Talmale SS, Yu W, Liu S and Jiang T. A reassessment of the taxonomic status and distribution of the subspecies of Lyroderma lyra (Chiroptera: Megadermatidae). *Contrib. Zool.* 2024; 94(2): 121-141.

Gleadow F. Bats feeding on birds. *J. Bombay Nat. Hist. Soc.* 1907; 17: 1020.

Kunz, TH, Torrez, EB, Bauer D, Lobova T and Fleming TH. Ecosystem services provided by bats. *Ann. N. Y. Acad. Sci.* 2011; 1223(1): 1-38.

Mossea HE. On the food of the vampire bat (Lyroderma lyra). *J. Bombay Nat. Hist. Soc.* 1931; 34: pp. 1052-1053.

Srinivasulu C, Racey PA and Mistry S. A key to the bats (Mammalia: Chiroptera) of South Asia. *J. Threat. Taxa.* 2010; 2(7): 1001-1076.

Ul Hasan MA and Kingston T. Bats of Bangladesh—A systematic review of the diversity and distribution with recommendations for future research. *Diversity*, 2022; 14(12): 1042.

Wang S, Brose U and Gravel D. Intraguild predation enhances biodiversity and functioning in complex food webs. *Ecology*. 2019; 100(3): e02616.

Wells KD. *The Ecology and Behavior of Amphibians.* University of Chicago Press; 2007.

INSTRUCTION FOR AUTHORS

The Journal of Bangladesh Academy of Sciences is published four times a year in March, June, September and December. Original research articles, review articles, and short communications of high standards of all branches of Science and Technology are considered for publication in this journal. Review articles are generally by invited authors; however, the Editor welcomes suggestions of potential topics and potential authors.

The following instructions must be followed while preparing the manuscript intended for publication in this journal:

1. **Research Article:** Manuscripts should be concise and consistent with the style of the journal. The manuscript must be typed using Times New Roman font, size 12 on A4 size page, and wide (1 inch) margins on all four sides. The main text must be typed in a two-column format with 1.5 spacing, and for full papers, it should not exceed 10-20 typed pages, including figures, tables, and references. In general, an article may contain the following sub-titles in sequence: **Title, Abstract, Keywords, Introduction, Materials and Methods, Results and Discussion, Acknowledgement (**if any), and **References.**

A. Title: The first page of the paper, the title page, should have the title and the names of the authors. The title should be brief and specific. Abbreviations and formulae should be avoided where possible. The next line in italics should be the authors' affiliation addresses (where the actual work was done) below the names. Indicate all affiliations with a lowercase superscript letter immediately after the author's name and in front of the appropriate address. The corresponding author, along with email address, should be indicated at the footnote with a proper asterisk.

B. The second page should carry the Title of the paper, Abstract, and Keywords. Author(s) name must not be typed on this page.

(i) Abstract: It should not exceed 150 words and should briefly state the purpose of the research, the significant results, and meaningful conclusions. Nonstandard or uncommon abbreviations should be avoided, but if essential, they must be defined at their first mention in the abstract itself.

(ii) Keywords: Immediately after the abstract, provide a maximum of 6 keywords.

C. The next pages (a maximum of 15 printed pages), will contain the main text of the paper.

(i) Introduction: It should be concise and relevant to the objectives of the study. The importance of the research work described should be pointed out. An appropriate review of the current literature should be made to identify the frontier of existing knowledge and point out the need for further work. The knowledge contributed to the study should be mentioned.

(ii) Materials and Methods: Materials used should be mentioned precisely along with their sources and any pre-treatment undertaken.

The description of methods must be brief but clear enough to enable a reader to reproduce the results. References must be considered sufficient for methods described in earlier publications: only relevant modifications should be described.

It is recommended that authors use the nomenclature and symbols adopted by IUPAC document UIFII (S.U.N. 65-3) 1965, symbols, units, and nomenclature in Physics or by IUPAC Manual of Physiochemical symbols,

Terminology and similarly for other disciplines.

(iii) Results and Discussion: This section should include descriptions of results obtained with the help of figures, tables, graphs, and photographs as may be necessary. Tables should have a descriptive title. Large and cumbersome tables should be avoided. Figures and graphs should be prepared and should be properly labelled with bold solid lines such that no further size reduction will be necessary. The paper should contain a minimum number of **Tables, Graphs,** and **Figures.** The same data should not be depicted using both tables and figures. The photographs are to be submitted in JPEG format.

The discussion should include thorough analysis and interpretation of results, and comparison with existing relevant published results, if any, and self-evaluation of the new knowledge contributed, avoiding extensive citations and discussion of published literature.

(iv) Conclusions

The study's main conclusions may be presented in a short Conclusions section, which may stand alone or form a part of the Results and Discussion section.

(v) Acknowledgment: The following support for the research work should be acknowledged:

- Funding by any agency;
- The use of instruments in a laboratory other than those of the authors;
- Individual's help during the research (e.g., providing an interpretation of results, language help, writing assistance, or proofreading, etc.).

(vi) Author contributions

For transparency, we encourage authors to submit an author contribution statement outlining each author's contributions to the paper. The authors should have participated sufficiently in the work to take public responsibility for appropriate portions of the content.

(vii) References and Text Citations:

In the text, references should be cited within brackets quoting the first author's surname followed by et al. if necessary and the year of publication in the appropriate place, e.g. (Bhuiyan, 2020), Khan et al. (2021) or (Khan et al., 2021). In the case of only two authors, surnames of both need to be mentioned, e.g., (Khan and Rahman, 2021). A semi colon should separate two or more references when putting within the same bracket. At the end of the manuscript, references should be listed and arranged alphabetically according to the first author's surname according to the style described below:

(a) Journal article:

In each reference, names of all authors' will have to be given in the same style, e.g., surname followed by initials, lumped together without using a full stop. The names will be followed by the full title of the article and the journal's abbreviated title (in italics). The year of publication will be given next, followed by volume number (issue number) and page ranges. For abbreviations of the names of journals, authors are advised to follow the *World List of Scientific Periodicals.* For online publications, the URL address must be given. Note: Please list ALL authors' names in the list of references, do not use (et al.). **Examples:**

Islam S. The Induced Morphological and Root Anatomical Changes in Lentil. *J. Bangladesh Acad. Sci.* 2019; 43(2):107-112.

James BD and Bennett DA. Causes and Patterns of Dementia: An Update in the Era of Redefining

Alzheimer's Disease. *Annu. Rev. Public Health;* 2019; 40: 65-84.

Moniruzzaman M, Khatoon R and Qamruzzaman AKM. Influence of Plant growth Regulators on Vegetative Growth, Sex Expression and Yield of Summer Bottle Gourd. *Bangladesh J. Agril. Res*. 2019; 44(4): 577-590.

(b) Book or Chapter in a Book:

The place and name of the publisher, year of publication, will have to be given in addition to the name of the author(s), the title of the book (in italics), edition number (if not first), and the number of pages. In the case of an article or chapter in a book or proceedings of a conference, author(s) name and the title of the article or chapter will be followed by the title of the book (in italics), the names of the editors of the book, edition number (if not first), the place and name of the publisher, year of publication and page or page numbers of chapter. **Examples:**

Book:

Carlson BM. *Human Embryology and Developmental Biology*. 4th ed. St. Louis: Mosby; 2009. p. 541.

Cassese A, Acquaviva G, Fan M and Whiting A. *International Criminal Law: Cases and Commentary*. Oxford University Press; 2011, p. 600.

Chapter in an edited book:

Muhammad HFL and Dickinson KM. Nutrients, energy values and health impact of conventional beverages, Chapter 3. In: *The Science of Beverages*, *Volume 12: Nutrients in Beverages*. Grumezescu AM, Holban AM, eds., Elsevier Science; 2019; pp. 77-109.

Balsam KF, Martell CR, Jones KP, Safren SA. Affirmative cognitive behavior therapy with sexual and gender minority people. In: *Culturally Responsible Cognitive Behavior Therapy: Practice and Supervision*. Iwamasa GY, Hays PA, eds., 2nd edition, American Psychological Association. 2019; p. 287-314.

(c) Proceedings of a Conference:

Luca J and Tarricone P. Does emotional intelligence affect successful teamwork? In: *Meeting at the Crossroads*. Kennedy G, Keppell M, McNaught C (eds.), Proceedings of the 18th Annual Conference of the Australasian Society for Computers in Learning in Tertiary Education, 2001 Dec 9-12; Melbourne: Biomedical Multimedia Unit, The University of Melbourne; 2001. pp. 367-376.

(d) Reports:

Bangladesh Bureau of Statistics (BBS). Population census - 2011. Preliminary report. Bangladesh Bureau of Statistics, Ministry of Planning, Government of the People's Republic of Bangladesh, Dhaka, 2011.

Rowe IL and Carson NE. *Medical manpower in Victoria. East Bentleigh (AU)*: Monash University, Department of Community Practice; 1981. p. 35. Report No.: 4.

2. **Short communication:** Important research findings that may initiate further research in the relevant field may be published in the form of a short communication. This should not exceed three printed pages (900 words), including Graphs, Tables, and Figures. The presentation should be continuous and paragraphed, i.e., without headings like Introduction, Materials, and Methods, etc. A short communication paper should have an **Abstract** containing the gist of the article and should not exceed 60 words, followed by **Keywords.**

3. **Declarations:** While submitting, the corresponding **a**uthor will have to make a declaration mentioning the laboratory/laboratories in which the work was carried out and certifying that the contents of the paper were not published before or submitted for publication in any other journal and that all the co-authors have given their consent for the article to be considered by the Editorial Board for publication in the Journal of Bangladesh Academy of Sciences.

Declaration of conflicting interests

The corresponding author must provide a formal conflict of interest statement for all authors disclosing any financial and personal relationships with other people or organizations that could inappropriately influence (bias) their work. If no conflict exists, please state that 'The author(s) declare(s) that they have no conflicts of interest regarding the publication of this article.'

4. The manuscript should be submitted in pdf or MS Word or LaTex files through online at www.bas.org.bd/publications/jbas.html. Equations generated by using Math Type or Math ML should be incorporated in the text.

   Soft copies of manuscripts with tables, graphs, illustrations, and photographs placed correctly in a printable format are to be submitted. Authors wishing to publish coloured schemes/diagrams/ sketches/photographs in their papers need to pay for the printing charges of one format. This will be charged only after the acceptance of the manuscripts for publication in the JBAS.

   The manuscript submitted should also contain a separate list of tables, figures, illustrations, photographs, and sketches with appropriate captions.

5. Electronic versions of final galley proofs will be sent to authors. No alteration in the title or additions in the text is desirable at this stage.

6. All correspondence for publication should be made on www.bas.org.bd/publications/jbas.html to the **Editor, Journal of Bangladesh Academy of Sciences, National Science and Technology Complex, Agargaon, Dhaka 1207.**

N.B.: No paper will be accepted for publication if it does not conform to the style specified for the journal and approved by the Editorial Board, which has the authority to accept or reject the manuscript of a paper submitted without showing any reason.